Catalytic and Adsorbent Properties of Solid Acid Catalysts Studied by Ammonia Adsorption Microcalorimetry

by

Claire Savill-Jowitt M.Chem

A thesis submitted to the University of Huddersfield in partial fulfilment of the requirements for the degree of Doctor of Philosophy.

The University of Huddersfield

June 2007

Abstract

Solid acid catalysts are becoming of great importance within the chemical industry and their acidity is of great interest, as this determines their application, plus many of their catalytic properties can also be directly related with their acidity. There has been a drive towards heterogeneous solid acid catalysts because of the environmental concerns with safe handling and disposal of mineral acid homogeneous catalysts such as H_2SO_4, and their separation from the product.

Objectives of this work have been to study a range of solid acid catalysts and establish a relationship between catalyst strength, activity, and structure, and then identify the influence of solvent and type of reaction on the catalytic properties of the catalysts to be studied. Acid catalysts have been chosen to represent a cross-section of the various types of catalysts in use. The solid acid catalysts being investigated include sulfonated polystyrene ion exchange resins, acid activated clays, zeolites, and heteropoly acid ($H_3PW_{12}O_{40}$) supported on carbon and mesoporous silica. Supported heteropoly acids have been prepared by Dr A Lapkin, University of Bath in the collaborative part of the project.

Catalysts have been characterised in terms of their surface areas, pore diameters, pore volumes, and crystallinity from nitrogen adsorption, powder x-ray diffraction, cation exchange capacity, and elemental analysis. The acidity of these catalysts has been studied by NH_3 adsorption microcalorimetry. NH_3 is assumed to adsorb stoichiometrically on surface acid sites and the molar enthalpy of ammonia adsorption is assumed to reflect the strength of the acid sites. The catalytic activities of the catalysts have been measured using two Brønsted acid catalysed test reactions (rearrangement of α-pinene and the hydrolysis of ethyl acetate). The correlation between characterisation results and catalytic data has been examined with emphasis being placed on the relationship between acidity measurements and the reaction medium or solvent.

Conclusions that can be drawn from this work are that NH_3 adsorption microcalorimetry is a useful technique for studying surface acidity of solid acids and that it does allow for some correlation to be drawn between catalytic activity and acidity, with the aid of additional catalyst characterisation techniques.

Acknowledgements

I would like to thank my supervisor Professor D.R. Brown for his continued encouragement and valuable discussions throughout my Ph.D. I would also like to extend thanks to Dr. A. Lapkin (University of Bath) for the synthesis of supported tungstophosphoric acid catalysts and interpretation of kinetic acidity data, and to members of the Applied Catalysis centre for their help with catalyst characterisation techniques.

I am also very grateful to my family and friends who have encouraged me throughout my Ph.D and have been there to support me.

Contents

Figures

Tables

CHAPTER ONE

INTRODUCTION

Section 1 - Theory

1.1.1 Overview

In recent years environmental pressures have become significant in the scientific community, especially the chemical industry. Within the chemical industry, acid catalyzed liquid phase reactions such as etherification, alkylation, and esterification are amongst the most important industrial reactions, as they provide many useful products and intermediates. The problem is that liquid mineral acid catalysts such as hydrofluoric acid (HF) and sulphuric acid (H_2SO_4) currently used in these processes are detrimental to our environment[1].

Solid acid catalysts have begun to play a larger role due to their becoming more widely available. They provide significant advantages over homogeneous liquid-phase mineral acids. These advantages are mainly concerned with the environment because mineral acids such as HF are associated with handling and disposal problems. This has meant a drive towards non-waste producing alternatives such as solid acid catalysts, which help to reduce equipment corrosion, allow easier product separation, and have less potential for contamination of waste streams that are released into the environment. They can also be designed to give increased activity, selectivity, longer catalyst life, and their repeated use is possible[1, 2].

1.1.2 Overall Objectives of work

The overall object is to study a range of solid acid catalysts and establish a relationship between catalyst structure, strength, and activity, and to identify the influence of solvent and type of reaction on the properties of the catalysts. This work is linked to a study of adsorption properties of solid acids – specifically for ammonia as a model for the removal of basic airborne contaminants. Solid acid catalysts to be investigated include sulfonated polystyrene ion exchange resins, acid activated clays, zeolites, and the heteropoly acid tungstophosphoric acid ($H_3PW_{12}O_{40}$) supported on carbon and porous silica.

1.1.3 General properties of solid acid catalysts

Properties which need to be considered to fully characterise the acidic properties of solid acid catalysts include the nature of their acid sites, Brønsted or Lewis, the concentration of acid sites available, and the strengths and accessibilities of acid sites. Other characteristics which also need to be considered in choosing a solid acid for a catalytic application include its thermal stability, its capacity to be regenerated and its overall lifetime.

1.1.3.1 Nature of Acid sites: Brønsted and/or Lewis sites

Solid acid catalysts are characterised by the presence of Brønsted and/or Lewis acid sites.

a) Brønsted-Lowry Acidity Definition

A Brønsted-Lowry acid is a proton donor.

$$H\text{-}A + :B \longleftrightarrow A^- + H\text{-}B^+$$

A^- is the conjugate base of acid HA, and BH^+ is the conjugate acid of base B.
An example of a Brønsted-Lowry acid is HCl in water:

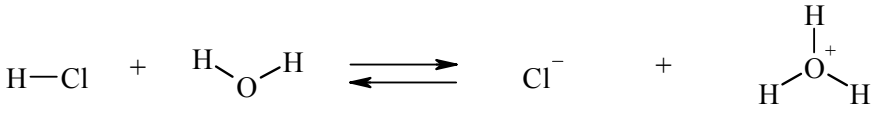

Figure 1: Example of a Brønsted-Lowry acid.[3]

A polar hydrogen chloride molecule donates a proton and a water molecule accepts the proton giving Cl^- and H_3O^+ (see Figure 1 above). The chloride ion produced when HCl loses a proton is the conjugate base, and the product that results when the base (H_2O) gains a proton is the conjugate acid of the base. Brønsted acidity typically arises in solid acids through 1) exchangeable H^+ ions and 2) exchangeable high charge-to-radius metal cations, which under conditions of limited hydration can hydrolyse water producing H^+.[4]

e.g.

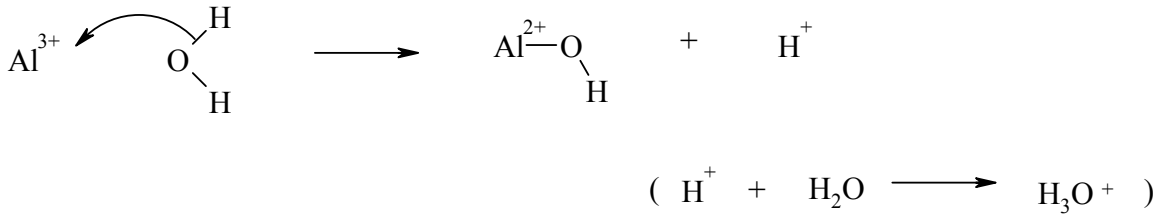

b) Lewis Acidity Definition

A Lewis acid is a substance that accepts an electron pair.

For a Lewis acid to be able to accept an electron pair it must have a vacant, low-energy orbital. This definition is more widely applicable as it can be applied to many other species in addition to H^+. For example, various metal cations including Mg^{2+} are Lewis acids as they can accept a pair of electrons when they form a bond to a base. Elements in Group III such as boron in BF_3 and aluminium in $AlCl_3$ are Lewis acids because they have unfilled valence orbitals and can accept electron pairs from Lewis bases.

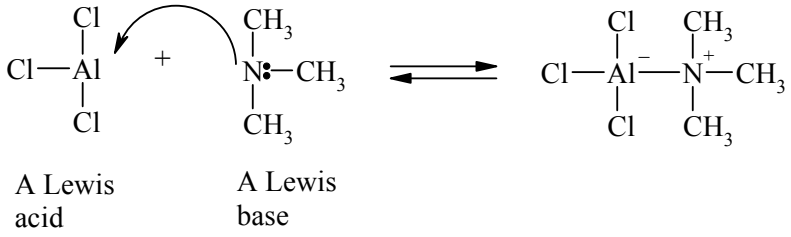

Figure 2: Example of a Lewis acid.[5]

Lewis acidity typically arises in clays and zeolites when they are ion-exchanged with high charge-to-radius metal cations i.e. Fe^{3+} which have been fully dehydrated.

1.1.3.2 Concentration, strength and accessibility of acid sites

Concentration, strength, and accessibility of acid sites on a solid acid catalyst are important and they are the features which need to be controlled when a solid acid catalyst is designed and optimized for a specific catalytic reaction.

A high concentration of acid sites is vital in controlling catalytic activity and, all other things being equal, activity might be expected to be proportional to the concentration of surface acid sites. This is not the case, as the strength and accessibility of available acid sites are also crucial. It is not always the case that increased acid strength will lead to increased activity. One reason for this is that the rate of a reaction will depend on the rate of desorption of products from the acid sites, and in some cases this will be reduced if acid strength is increased. Also for certain reactions, selectivity depends on acid strength being carefully set, as excessively strong acid sites can lead to unwanted side reactions. Acid site accessibility is vital if reaction rates are not to be controlled by the rate of diffusion to and from its sites. This generally means that for reactions in the liquid phase pores must be in the mesopore size range at least. The nature of the solvent in which the catalyst is to be used can also have a dramatic effect on activity because acid strength is often modified by the solvent. Some catalysts change their morphology in different solvents, and access to acid sites can be highly dependent on the type of solvent used. For example, sulfonated polystyrene ion exchange resins have been shown to swell in polar solvents depending on the amount of divinylbenzene (DVB) present, which controls the degree of cross-linking and the rigidity of the structure. Those with less DVB swell more[6].

1.1.4 Solid Acid Catalysts

1.1.4.1 Polyoxometalates

Polyoxometalates are nanosized metal-oxygen cluster anions and form by a self-assembly process typically in acidic aqueous solution. These anions can be balanced by an appropriate counter-cation such as H^+ or NH_4^+ to give solid heteropoly compounds. There are generally two types of polyoxometalates: 1) isopoly anions and 2) heteropoly anions.

$[M_mO_y]^{p-}$ Isopoly anions

$[X_xM_mO_y]^{q-}$ Heteropoly anions

M is known as the *addenda* atom, with the most common addenda atoms being tungsten and molybdenum and less frequently niobium and vanadium. Mo^{6+} and W^{6+} are widely used due to the favourable combination of ionic radius and charge, and the accessibility of empty d orbital's for

metal-oxygen π bonding. X is the *heteroatom* but is also known as the *central atom* as it is located in the centre of the heteropoly anion. A wider range of elements can act as the heteroatom with the most typical being P(V), As(V), Si(IV), Ge(IV) etc. The structures shown below in Figure 3 are adopted by heteropoly anions. The Keggin structure shown in Figure 3a is the most common structure adopted by polyoxometalates as it is the most stable and readily available. Two other parent structures exist, these being the Anderson-Evans structure shown in Figure 3b, based on a central octahedron and the Dexter-Silverton structure (Figure 3c) that forms an icosahedron (a polyhedron with 20 faces)[7].

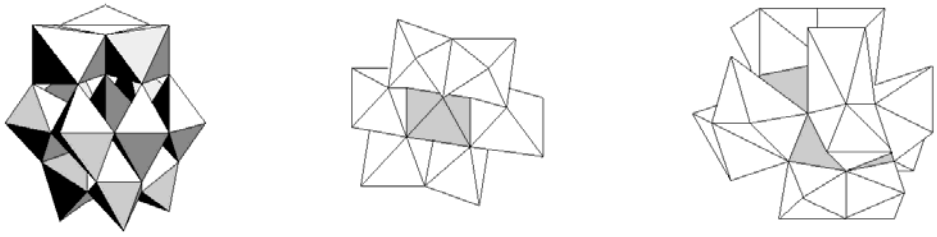

a) Keggin Structure e.g. $[PW_{12}O_{40}]^{3-}$

b) Anderson-Evans Structure e.g. $[TeMo_6O_{24}]^{6-}$

c) Dexter-Silverton Structure e.g. $[CeMo_{12}O_{42}]^{8-}$

Figure 3: Common structures of heteropoly anions.[7]

The Keggin structure is typically represented by the formula $[XM_{12}O_{40}]^{x-8}$ where *x* is the oxidation state of the heteroatom, an example of which is $PW_{12}O_{40}^{3-}$. The Keggin anion has a diameter of ~ 1.2nm and is composed of a central XO_4 tetrahedron surrounded by 12 edge and corner sharing metal-oxygen MO_6 octahedra.

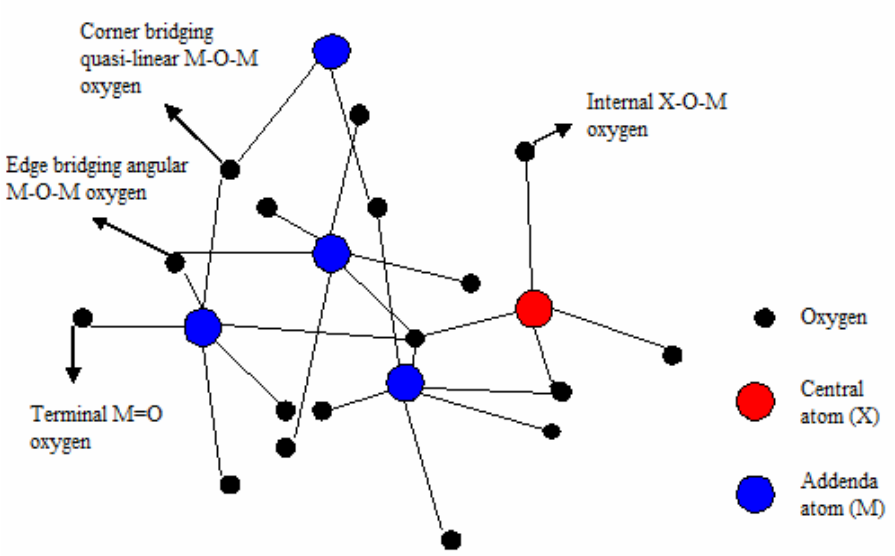

Figure 4: Diagram showing the four types of oxygen atom present in the Keggin structure.

Octahedra are arranged in four (M_3O_{13}) groups with each group sharing edges and having an oxygen atom which is linked to the central XO_4 tetrahedron. The total assemblage contains 40 close packed oxygen atoms of four types: 1) twelve terminal M=O 2) twelve edge-bridging angular M-O-M shared by the octahedra within an M_3O_{13} group 3) twelve corner bridging quasi-linear M-O-M connecting two different M_3O_{13} groups and 4) four internal X-O-M oxygen atoms. Examples of the four types of oxygen present in an M_3O_{13} group are shown in Figure 4 above.

a) Properties of heteropoly acids

Generally solid heteropoly compounds (heteropoly acids and salts) form ionic crystals, which have fairly mobile basic structural units, where waters of crystallization are frequently not in crystographically-defined positions, unlike zeolites and metal oxides[8]. Heteropoly acids consist of the heteropoly anion described above with H^+ as a counter-cation. In the solid state they frequently have large interstices between the large heteropoly anions which can accommodate large amounts of water of crystallization (up to 30 molecules per heteropoly unit and more) as well as the counter-cation. These water molecules are hydrogen bonded together and are often easily and reversibly removed from the solid by heating to 100-150 °C. Depending on the extent of hydration, the crystal structure alters and is frequently accompanied by changes in the crystal cell volume as well as changes in acid strength. This means that not only water but also other polar organic molecules such as alcohols, amines, ethers, ketones, and sulfoxides can enter and leave the

structure, which has important consequences for heterogeneous catalysis by solid heteropoly acids[9].

Many heteropoly acids, for example, those with either Keggin or Wells-Dawson structures, have been shown to be strong Brønsted acids[10, 11]. This is related to the large size of the polyanion having a low delocalized surface charge density which causes a weak interaction between itself and the protons. Acid sites located on the surface and in the bulk of the solid need to be distinguished as the structure of the sites may be different. The bulk proton sites are suggested to play a key role in 'pseudoliquid' catalysis[12], whilst the exact nature of surface acid sites still remains practically unknown.

Two types of proton have been determined in solid heteropoly acids, hydrated protons $[H(H_2O)_n]^+$ and non-hydrated protons. The location of protons in heteropoly anions has been the subject of many studies[13, 14, 15, 16]. The hydrated protons possess a high mobility and they are responsible for the extremely high proton conductivity of crystalline heteropoly acid hydrates. Non-hydrated protons have much less mobility and it has been suggested that they localise on the peripheral oxygens of the polyanion in one of three positions: M=O and bridging oxygens M-O-M (edge sharing and corner sharing)[17], but may also exist as "free protons" without a well-defined location[16]. In solid crystalline heteropoly acids, the protons, hydrated or non-hydrated, take part in the formation of the crystal structure, linking neighbouring heteropoly anions. In the relatively stable crystalline hexahydrate $H_3PW_{12}O_{40}.6H_2O$, bulk proton sites are represented as diaquahydrogen ions, $H_5O_2^+$, which are almost planar, quasi-symmetrical hydrogen bonded species that link four neighbouring heteropoly anions by forming hydrogen bonds with the terminal W=O oxygens (see Figure 5) [18].

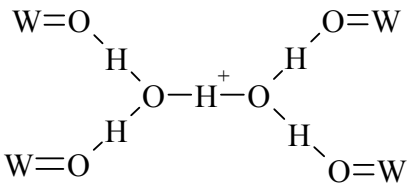

Figure 5: Schematic structure of proposed bulk proton ($H_5O_2^+$) sites in $H_3PW_{12}O_{40}.6H_2O$.

Heteropoly acids possess very low surface areas (1-5 m^2g^{-1}) and low porosity[19]. To increase this surface area they are often supported on inert porous materials such as silica or carbon[20].

1.1.4.2 Montmorillonite Clays

Clay is the general term used to describe naturally occurring silicate minerals that are <2 μm in size[21]. The characteristics common to all clay minerals derive from their chemical composition, layered structure, and size. They are classed as a group of hydrous layered magnesium- or alumino-silicates known as phyllosilicates, and are made up of basic tetrahedral (SiO_4) and octahedral sheets (AlO_6).

Natural montmorillonite has a 2:1 dioctahedral smectite structure, and is one of the most commonly used clays because it is cheap and readily available. It is classed as 2:1 dioctahedral because two tetrahedral sheets are co-ordinated to one octahedral sheet, and two-thirds of the cation positions are filled in the octahedral layer by two Al^{3+} which satisfy the anionic charge of $6OH^-$ anions. The upper and lower layers of the clay consist of bridging oxygen atoms and the montmorillonite laminae are joined with their oxygen layers being adjacent. A structural view is shown below in Figure 6. A 2:1 clay structure's ideal full cell chemical formula would be $Si_8^{IV}Al_4^{VI}O_{20}(OH)_4$ where the superscripts represent four- and sixfold coordination in the tetrahedral and octahedral layers respectively. In montmorillonite a small proportion of the lattice Al ions are replaced by Mg ions, which give the clay an anionic layer charge.

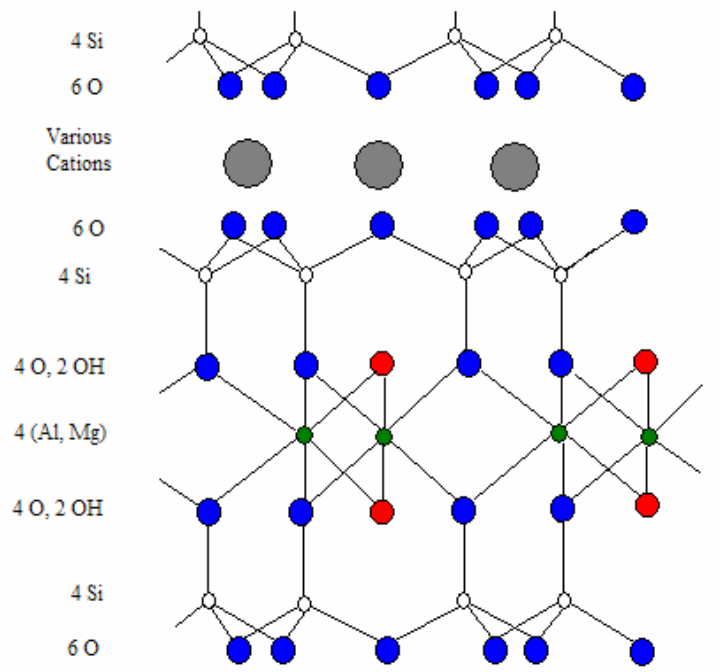

Figure 6: Structure of natural montmorillonite clay $(Si_8)(Al_{3.2}Mg_{0.8})O_{20}(OH)_4$.[22]

The cations present in the interlayer space can easily be exchanged for other cations hence their being called exchangeable cations. This is governed by the cation exchange capacity (C.E.C.), which is usually expressed in milli-equivalents per gram of dry clay. Exchangeable cations attract not only water but also other polar organic molecules, which intercalate between the layers causing the structure to expand. The ability of montmorillonite to swell is provided by this attraction between the cations and water molecules, but may also be related to the relatively small layer charge of montmorillonite when compared to other smectites with high layer charges such as vermiculite. Because montmorillonites possess this ability to swell, surface area can be affected, and depends on whether the clay is in a swollen state or collapsed.

Natural montmorillonites have intrinsic catalytic activity but this can be greatly enhanced by acid activation which converts them into useful catalysts. When treated with strong mineral acids it causes chemical attack of the clay's structure; see Figure 7 below which shows the delamination of the clay structure on acid treatment. This facilitates the development of significant accessible surface area (even when not swollen in water or other polar solvent) and pore volume as well as having catalytically active acid sites of both Brønsted and Lewis types.

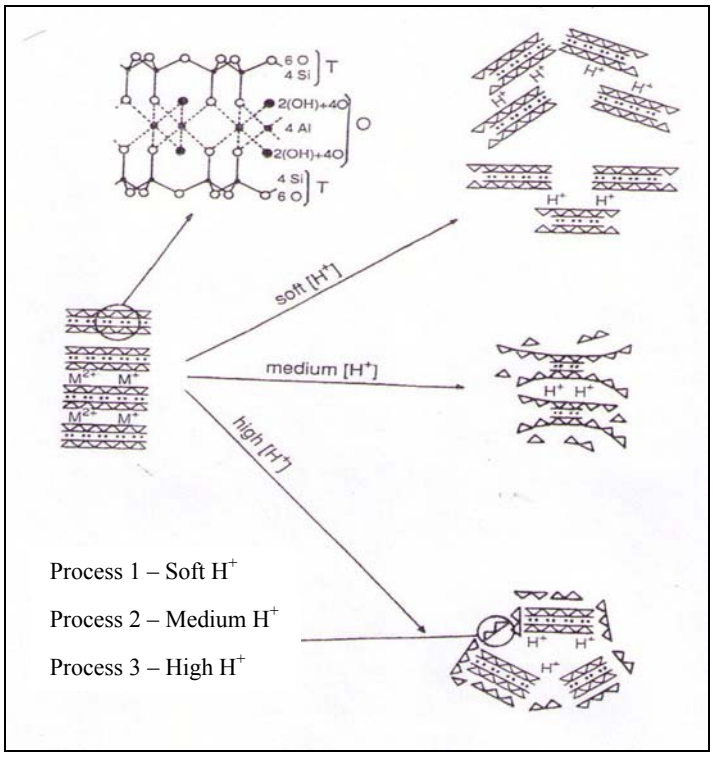

Figure 7: Proposed mechanism of acid leaching (T, tetrahedral sheet; O, octahedral sheet).[23]

Process 1 shown in Figure 7 above shows that on gentle acid treatment, H^+ replaces exchange ions. Moderate acid treatment (Figure 7, process 2) shows the onset of delamination of the clay structure where metallic ions such as aluminium and magnesium associated with the octahedral sheet are removed. It has been determined that removal of one pair of octahedral aluminium ions from montmorillonite removes two hydroxyl groups and leaves the other aluminium of the pair in a four-fold co-ordination. This tetrahedral aluminium has a charge-balancing proton which forms a Brønsted site and is the source of catalytic activity[24]. Under very acidic conditions (8 mol dm^{-3} HCl) (Figure 7, process 3) it has been speculated that some silica that is produced at the beginning of the reaction undergoes polymerization and coats the remaining intact silicate, effectively blocking pores and preventing further reaction[23].

a) Clay as a potential catalyst

In recent years there has been a keen interest in using inorganic solids such as clays in organic reactions as they have been found to be more environmentally friendly than equivalent homogeneous catalysts[25, 26].

In terms of Brønsted and Lewis acidity, it is clear that in most aluminosilicate solids the aluminium in the lattice is the source of the acidic nature of the surface. This is because tetrahedral Al^{3+} gives rise to a net negative charge. To balance this, an H_3O^+ ion is present, associated with the tetrahedral aluminium, which corresponds to a Brønsted acid site. This is not true for montmorillonite as the net negative charge is due to Mg^{2+} substitution for Al^{3+} in the octahedral layer. Lewis acidity in contrast is thought to arise from Al^{3+} ions located at platelet edges in coordinatively unsaturated states – effectively defect sites. This was proposed by Solomon and Rosser (1965) to explain Lewis acidity after thorough dehydration. As water is a Lewis base it will convert the Lewis site into a Brønsted site so this limits studies to relatively anhydrous systems only.

1.1.4.3 Zeolites

Zeolites are perfectly crystalline, ordered materials with open structures and well-defined, extensive pore systems. A number of basic building blocks made up of linked tetrahedra are

combined in various ways to form the different types of zeolite. They are complex materials consisting of linked tetrahedral [SiO_4] and [AlO_4] groups. Tetrahedra are assembled together so that oxygen atoms at each tetrahedral corner are shared with neighbouring tetrahedra to form frameworks that provide cavities/channels of specific pore size. Each AlO_4 unit results in a lattice negative charge which is balanced by an exchangeable cation associated with the structure. Typically these counter-cations are hydrated so by dehydrating the zeolite the cations are forced closer to the framework in order to achieve better coordination to the framework oxygen atoms. This allows the zeolite to adsorb small molecules other than water in their pores. The zeolites to be investigated are H-ZSM-5 and zeolite beta.

The structure of H-ZSM-5 is created through the stacking of layers, in which two pore systems exist (see Figure 8). It effectively has a three dimensional channel system defined by 10 membered ring openings of 0.54 x 0.56 nm when viewed along [010]. Intersecting this channel at right angles is another 10 membered channel with openings of 0.51 x 0.54 nm when viewed along [100]. Diffusion in the [001] direction is achieved by movement between these two channels. These channels are important when it comes to the zeolite's catalytic properties[27]. As water content is low and its framework has hydrophobic tendencies ZSM-5 shows good thermal stability to above 600 ^{o}C. This zeolite has low aluminium content and few cations are present.

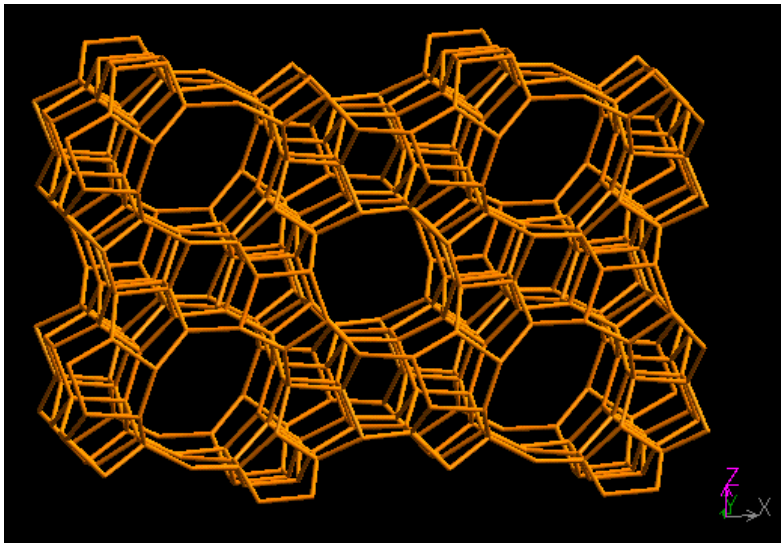

Figure 8: Structure of ZSM-5 (viewed along [010] plane).[28]

Zeolite Beta is a relatively "large pore" zeolite and hence it is one of the most suitable zeolites for liquid phase reactions. It can be regarded as a highly inter-grown hybrid of two distinct, but

closely related structures that both have three dimensional pore systems with 12-rings as the smallest constricting apertures. When viewed along the [100] direction the 12 membered ring has a diameter of 0.66 x 0.67 nm, and 0.56 x 0.56 nm when viewed along the [001] plane. The [100] plane is shown in Figure 9 below[29].

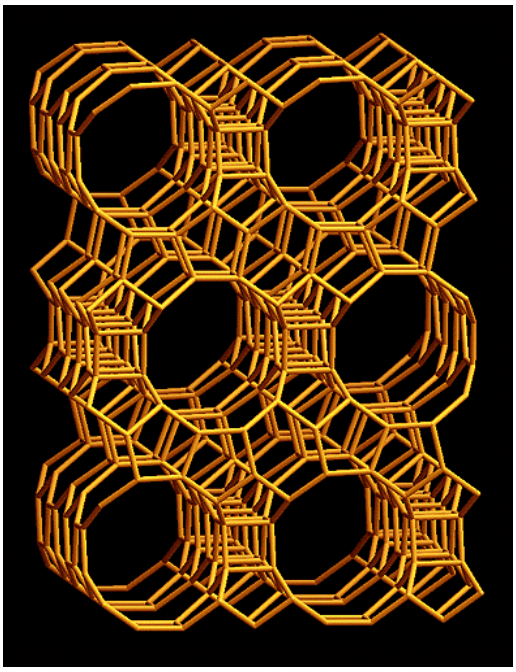

Figure 9: Structure of zeolite beta (viewed along [100] plane).[28]

a) Properties of zeolites

The useful catalytic properties of zeolites depend on a number of factors which include their regular crystalline structure and their pore size. Catalysis takes places largely within the zeolite framework; this therefore means that zeolites have special practical advantages over other solid acid catalysts as they will only admit certain reactant molecules, and can be tailored to give selected products. Acidity and acid strength can be altered by exchanging cations and modifying the Si/Al ratio[30, 31]. However one disadvantage is that zeolite pores are invariably of micropore diameter therefore restricting catalytic application and generating diffusional limitation when used with reactions in the liquid phase.

1.1.4.4 Sulfonated Polystyrene Ion Exchange Resins

Polymers have played an important role in the area of ion exchange resins and have allowed for the development of new and improved resins. Those of interest in the area of solid acid catalysis are the strongly acidic cation exchange resins, especially those of styrenic origin that are synthesized by a free radical induced copolymerisation which is described in the following sections.

a) Free Radical Addition Polymerization

The reaction to form styrenic cation exchange resins depends upon addition/ethenyl (vinyl) polymerization where reactants must carry vinyl double bonds (-CH=CH_2), and one of the reactants must contain at least two vinyl bonds to form cross-linking. Vinyl polymerization reactions are a type of free radical addition polymerization that involve chain reaction processes, and require an initiator to begin the reaction. Peroxides and hydroperoxides are the most widely used initiators as they are thermally unstable and decompose. In the case of forming styrenic resins, the initiator is benzoyl peroxide, which undergoes thermal homolysis to form benzoyloxy radicals, as shown in Figure 10a below.

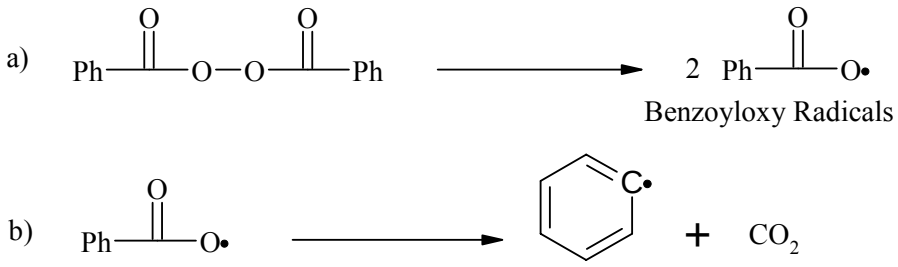

Figure 10: Benzoyl peroxide forming benzoyloxy radicals.[32]

The benzoyloxy radicals can undergo a variety of secondary reactions besides adding to a monomer, such as decomposing to phenyl radicals and carbon dioxide (shown in Figure 10b), and also reforming the peroxide. Secondary reactions such as this occur because of confining effects of solvent molecules. The extents to which side reactions occur depends upon the peroxide structure, the stability of the initially formed radicals, and the reactivity of the monomers. Ideally the polymerisation induction step (shown in Figure 10a) should be relatively stable at room temperature but should decompose at polymer processing temperatures. Benzoyl peroxide has a

half life of 30 minutes at 100°C and the advantage of being stable enough to react with more reactive monomer molecules before eliminating carbon dioxide, thus reducing initiator wastage[32].

b) Sulfonated Polystyrene Ion Exchange Resins

The miscible monomers, ethenylbenzene (styrene) and diethenylbenzene (divinylbenzene) undergo a free radical induced copolymerisation reaction, which is initiated by a benzoyl peroxide catalyst to create poly(styrene-divinylbenzene), which has a semi-rigid structure, see Figure 11, product A below.

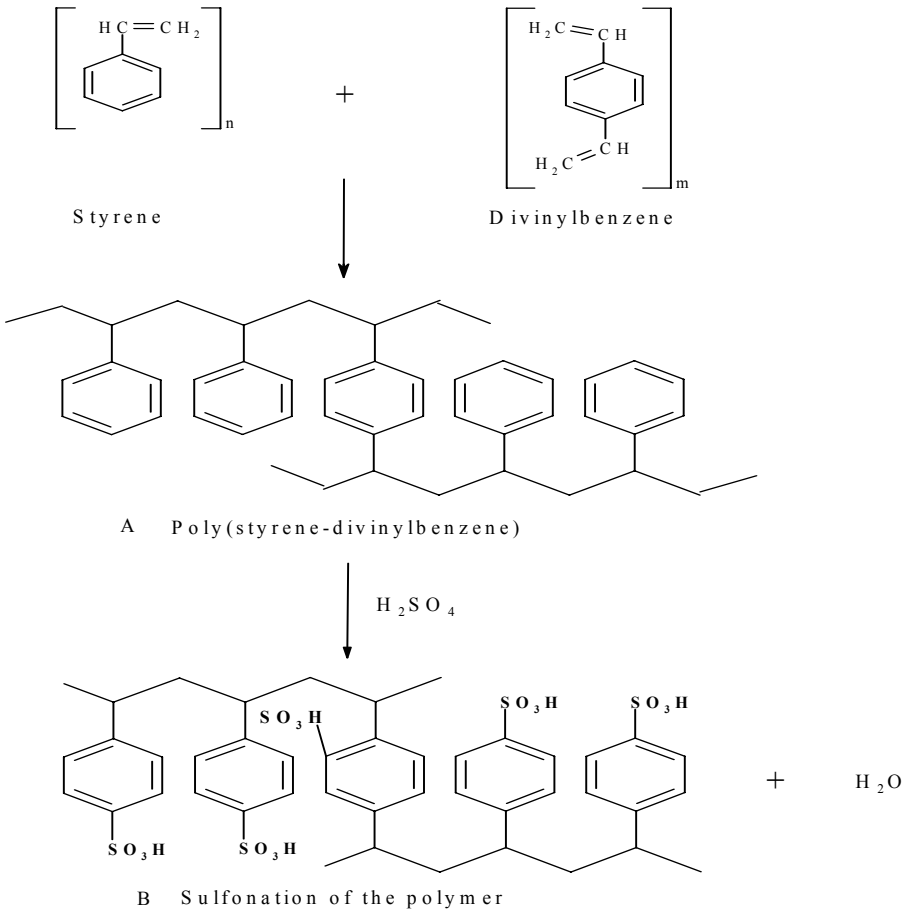

Figure 11: Addition polymerization synthesis of a sulfonated polystyrene ion exchange resin.[33]

The exothermic reaction is carried out in an aqueous suspension whereby the mixed monomers are immiscibly dispersed as spherical droplets throughout the reacting medium, resulting in beads of copolymer being formed. Reaction conditions and the use of suspension stabilizers allow the particle size distribution of the copolymer to be closely controlled. The extent to which the

copolymer is cross linked depends upon the amount of cross linking agent (divinylbenzene) available in the synthesis and has a pronounced impact on both the mechanical and chemical behaviour of the resin (generally for macroporous resins between 15-30 %)[34]. Activation of the copolymer to form the acidic resin is achieved through sulfonation of the matrix with hot sulphuric acid. This introduces sulfonic acid functional groups and forms a strong acidic cation exchange resin (Figure 11b)[33]. Most commercially available sulfonated polystyrene resins are prepared using a one to one mixture of sulfuric acid (H_2SO_4) and polymer based monomer units. This sulfonates the polymer at a level equivalent to one sulfonic acid group per styrene or divinylbenzene monomer unit and is known as 'stoichiometric' sulfonation, which is shown in Figure 11 product B. This method often assumes that every phenyl residue present is sulfonated, but it is important to realise that sulfonation may not occur in this neat manner, resulting in some disulfonation and possibly the formation of sulfone bridges. These are shown below in Figure 12.

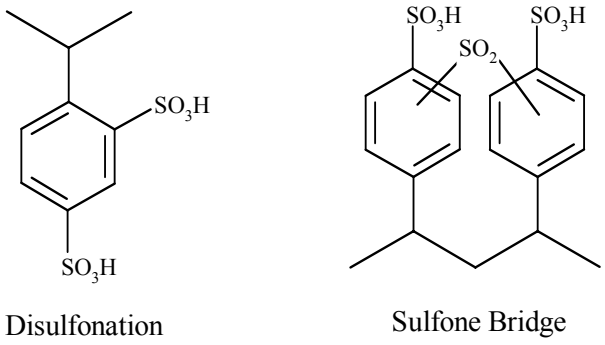

Figure 12: Features that may occur within a sulfonated ion exchange resin.

Certain commercial resins are prepared using more than the stoichiometric amount of sulfuric acid, and are termed 'persulfonated'. The idea behind this is that disulfonation or even trisulfonation of phenyl rings will result in the resin containing stronger acid sites due to the electron withdrawing sulfonic acid group, SO_3H making other SO_3H groups on a phenyl ring better proton donors. It has also been proposed that the formation of sulfone bridges is partially responsible for controlling acid strength and catalytic activity of sulfonic acid groups as some acid catalysed reactions are thought to be facilitated by networks of neighbouring sulfonic acid groups; but the extent to which these networks exist is dependent on the degree of sulfonation[35].

Cross-linkage with divinylbenzene is required to give structural integrity to the sulfonated resin groups, and is also significant in the stability of the resin's sulfonic groups towards hydrolysis, and

in its thermal stability which generally decreases as cross-linkage increases. On average "gel resins" contain 4-10% by weight divinylbenzene, whereas macroporous resins (~ 40 m^2) typically contain 15% or more. The extent to which the resins swell in water (and other swelling solvents) is dictated in part by the divinylbenzene content.

The resulting resins are produced commercially in the form of beads which have diameters usually between 0.5 and 1.0mm, and can be of a simple non-porous gel type or of one that has been suitably manipulated to make it a highly porous 'macroporous resin'. This permanent porosity is achieved by incorporating an inert organic solvent (porogen) at the polymerisation step. An example of a 'porogen' is xylene. This solvent is driven out of the polymer beads following synthesis leaving permanent porosity.

As sulfonated polystyrene ion exchange resins do not exhibit a catalytically active surface in the conventional sense, pore size is an important property as it is directly related to acid site accessibility. Their activity is dependent on reactants diffusing into the polymer bead to access the sites. The ease with which this can occur depends upon the degree to which the solvent solvates and swells the polymer. For example, gel resins are mainly used in water because their internal groups can only be accessed by reactants when the resin structure is swollen. The catalytic process then takes place in what is described as a concentrated 'internal solution' of sulfonic acid[6]. Macroporous resins on the other hand can be produced with a range of porosities and significant surface areas where the transport of reactants occurs through pores and by diffusion through the polymer gel. The development of macroporous resins was driven by the need to use the resin in solvents that would not solvate and swell the resin, so that access to acid groups could be achieved without the need for extensive diffusion through the resin gel.

Commercial catalytic applications of sulfonated polystyrene ion exchange resins have included[2]:

1. The etherification of olefins with alcohols, for example, the coupling of isobutene with methanol to form methyl-t-butyl ether (MTBE). This is currently the largest volume application of acidic ion-exchange resins although it seems likely that it will be phased out due to contamination of ground water sources,
2. Dehydration of alcohols to olefins or ethers e.g. t-butanol dehydration to form isobutene,
3. Alkylation of phenols to alkyl phenols,

4. Condensation reactions such as the manufacturing of bisphenol-A from phenol and acetone,
5. Olefin hydration to form alcohols, for example, propene hydration to form 2-propanol,
6. Purification of the phenol stream after the decomposition of cumene hydroperoxide to phenol and acetone,
7. Ester hydrolysis.

1.1.5 Solid Acids as Adsorbents

The primary requirement for an economic separation process is an adsorbent which has sufficiently high selectivity, capacity, and lifetime. Selectivity may depend on differences in either adsorption kinetics or adsorption equilibrium. Most adsorption processes in current use depend on equilibrium selectivity. Traditional adsorbents such as silica gel, activated alumina, and activated carbon show a distribution in their pore size. The mean pore diameter and the width of the distribution about this mean are controlled by the manufacturing process. Properties of zeolitic adsorbents on the other hand are controlled by the crystal structure and there is virtually no distribution of pore size which leads to significant differences in the adsorptive properties[36].

Solid acids sometimes find application as adsorbents because acid sites can act as strong binding sites for basic adsorbates, and in this way may be regarded as selective adsorbents. If acidic adsorbents are to be effective, they usually need to meet the following criteria: 1) adsorption must be fast even at room temperature so that adsorption can occur from flowing gas streams 2) the adsorption coefficient must be high so that even at low concentration of contaminant, a high proportion of its content can absorb 3) adsorption capacity and rate must not be compromised by the presence of moisture. A high equilibrium capacity isn't normally as important for adsorbents as it is for catalysts.

Further potential applications of acidic adsorbent include the removal of impurities from ultra-pure manufacturing environments, such as use in the manufacture of silicon wafers[37]. At present for this application, acidic adsorbents include mineral acids such as sulphuric or phosphoric acid impregnated on activated carbon and dispersed in a polymer mesh filter. These have a number of drawbacks, one of which is the formation of insoluble salts upon reaction with primary impurities which restrict access to the remaining acid sites. Heteropoly acids have been found to be strong

solid acids in their own right but when supported on inert supports such as silica they have been proposed as good sorbents of gases especially in the area of environmental protection[38].

In the following work, $H_3PW_{12}O_{40}$ supported on carbon and silica are examined in this role as they fulfil the criteria mentioned previously since 1) they possess strong acid sites 2) they have a large surface area, providing rapid adsorption, and 3) the support surface is relatively hydrophobic and is therefore resistant to poisoning by water.

1.1.6 Measuring surface acidity

The characterisation of surface acidity involves measuring acid site concentration, strength, and accessibility. Measuring the acid concentration and acid strength of homogeneous liquid acids is relatively straightforward, but measuring the same properties of a solid acid where acid sites are located on the surface is less so. In dilute aqueous solutions of strong acids the pH scale can be used to measure acid strength, but this is based on the assumption that the strength of individual H_3O^+ ions is fixed. The pH can be expressed as:

$$pH = -\log [H^+] \text{ or more correctly}$$
$$pH = -\log a_{H+},$$

where $[H^+]$ is the concentration and a_{H+} is the activity of H_3O^+ ions. In order to apply this method to highly concentrated aqueous acids it has to be accepted that the acid is fully dissociated and no longer exists in aqueous solution. The same difficulty applies to solid acids for which, again, it is not possible to simply assume that all acid strength is directly related to proton concentration. There are various methods available for determining the acidity.

1.1.6.1 Titration methods – Hammett indicators and acidity function

A quantitative scale that would express acidity of more concentrated acids or non-aqueous systems was suggested by Hammett and Deyrup. The Hammett acidity function (H_o) can be seen as an extension of the pH scale and is related to the degree of transformation of a weakly basic indicator B to its conjugate acid form BH^+ (i.e. the reverse of the reaction following) and defines Brønsted acid strength. The equilibrium for the indicator is shown as follows:

$$BH^+ \rightleftharpoons H^+ + B$$

The thermodynamic equilibrium constant K_{BH+} is given by:

$$K_{BH+} = \frac{a_{H^+}.a_B}{a_{BH^+}} \qquad (\mathbf{1.1})$$

$$K_{BH+} = \frac{a_{H^+}.C_B}{C_{BH^+}}.\frac{\gamma_B}{\gamma_{BH^+}} \qquad (\mathbf{1.2})$$

where a_{H+}, γ_B and γ_{BH+} represent the activity of protons and the activity coefficients in solution of the base and its conjugate acid respectively. C_{BH+} and C_B are the concentrations of the conjugate acid form of the indicator and the indicator. This equation can be rearranged to give:

$$\frac{C_{BH^+}}{C_B} = \frac{1}{K_{BH+}}.a_{H^+}.\frac{\gamma_B}{\gamma_{BH^+}} \qquad (\mathbf{1.3})$$

Hammett defined the acidity function H_o by

$$H_o = -\log\left[a_{H^+}.\frac{\gamma_B}{\gamma_{BH^+}}\right] \qquad (\mathbf{1.4})$$

$$H_o = -\log K_{BH^+} - \log\frac{C_{BH^+}}{C_B} \qquad (\mathbf{1.5})$$

$$H_o = pK_{BH^+} - \log\frac{C_{BH^+}}{C_B} \qquad (\mathbf{1.6})$$

When using pK to express the strength of a base, pK_{BH+} should be used, but it is more commonly written as pK_a which is a measure of the strength of the conjugate acid, BH^+, of base B. It measures the readiness with which BH^+ will lose a proton thus the smaller the numerical value of pK_{BH+}, the stronger the acidity of BH^+ and the weaker B is as a base.

To determine acid strength, titrations are performed where small weighed samples of pre-dried catalyst are covered with an inert solvent such as benzene, and 3-4 drops indicator added. An inert, strong base is then titrated into the sample suspension. It is important that this base is stronger than the indicator; n-butylamine $pK_a \approx 10$ is often used. As the base is added it adsorbs on the acid sites and displaces the indicator from the solid acid, and as Hammett indicators exhibit distinctly different colours in the protonated and unprotonated forms, an end point can be determined. The end point is where $[B]/ [BH^+] = 1$, thus $H_o = pK_a$, so indicates the concentration of acid sites with H_o less than or equal to the pK_{BH+} of the indicator used.

This method has a number of limitations, the first being the difficulty in visually determining the colour change especially when darkly coloured catalysts are used. A second possible limitation is the contamination of an experiment with water as water competes with the indicator for the acid sites. Finally this method gives the sum of the amount of Brønsted and Lewis acid sites, and only if arylcarbinols are used as indicators can Brønsted acid sites be measured separately. The method is also not suitable for all solid acid catalysts as some contain very small pores which the indicator molecules cannot penetrate, such as certain zeolites[4].

1.1.6.2 Vibrational spectroscopy methods

Both Raman and Infrared (IR) spectroscopy have been used to investigate the acidity of solid acids, both with and without adsorbed probe molecules[39, 40]. IR is especially useful as this allows us to look at the hydroxyl groups present either directly (the frequency of –OH bonds falls as acid strength increases) or through adsorbed probe molecules. It is also possible to see if these sites possessing acidity are accessible to various sizes of probe molecule. In principle the concentration of hydroxyl groups and therefore the concentration of potential Brønsted acid sites can be determined from the corresponding IR bands. IR bands for adsorbed pyridine lie in the region 1400 – 1700 cm^{-1}. An important feature is that distinct bands occur for pyridine at Lewis acid and Brønsted acid sites. When IR is combined with temperature programmed desorption (TPD) it provides us with an estimate of the acid strength distribution profile. Pyridine and ammonia have been widely used as probe molecules due to their being relatively stable. A problem with this is that owing to their strong basicity they adsorb strongly so will not distinguish between strong and weak sites. Because of this, weaker bases have also been used, such as carbon monoxide (CO). Adsorption of CO at low temperatures is now largely used as it is a weak soft base, whose small

molecular size excludes steric hindrance. It specifically interacts with hydroxyl acid groups via hydrogen bonding and with cationic Lewis acid sites[41].

Laser Raman spectroscopy can also be used to look at pyridine adsorption on Brønsted and Lewis sites. As Raman bands arise from polarizability changes which accompany skeletal and stretching vibrations, the protonation of pyridine is difficult to detect. This means that it has low sensitivity towards measuring Brønsted acidity. Quinoline is a larger, more basic molecule than pyridine, which can distinguish between Brønsted and Lewis acidity simultaneously, and due to its large size has been used to measure the external number of acid sites in microporous acid materials, with pores smaller than ~0.6 nm[42].

1.1.6.3 Nuclear Magnetic Resonance (NMR) methods

NMR is a powerful technique, and advanced methods such as cross-polarization, magic angle spinning (MAS) of solids, high resolution magnetic resonance etc. have increased the capabilities of this technique to study the acidity of solid acid catalysts[43, 44]. Total numbers of acid sites and strengths have been identified by using MAS NMR techniques. Characteristics of Brønsted acidity have been established based on the intensity and chemical shifts of signals due to acidic protons. The NMR technique can also be used to characterise the interaction of amines with acid sites provided that the spectra of the un-protonated and the protonated forms are significantly different. Good amine probes should have at least one carbon atom that responds differently to Brønsted and Lewis acid sites, and lines should not overlap. When these conditions have been fulfilled the number and strength of OH acidic groups can be directly determined by ^{13}C shifts of the adsorbed molecules[41]. ^{31}P NMR has also been used to study triethylphosphine oxide on solid acids

1.1.6.4 Photoelectron Spectroscopy methods

Photoelectron spectroscopy methods such as X-Ray Photoelectron Spectroscopy (XPS) measure the kinetic energy of photoelectrons emitted from the core of surface atoms upon X-ray irradiation of the uppermost atomic layers of a solid. Therefore they can be used to characterize surface acid sites again through the use of basic probe molecules[45]. It is especially useful for monitoring the acidity of solid acids which are opaque to IR irradiation. Problems with this technique are that due to contamination and charging it is very difficult to obtain accurate measurements, and because a

vacuum is needed conditions are far from "real". It cannot be used to determine total acidity of microporous solid acids.[4]

1.1.6.5 Temperature-programmed desorption of base molecules

Temperature-programmed desorption is based on the adsorption of volatile amines such as pyridine, n-butylamine etc. The principle behind this method is that the higher the temperature required to desorb the base, the stronger the acid site. An excess of base is added, and physically adsorbed base is removed by evacuation at 100-150 °C. Whatever is left is chemically adsorbed and is used to measure the total number of acid sites. Acidity values are determined by desorbing the pre-adsorbed base by heating the sample at a controlled constant rate and measuring the concentration of probes desorbing as a function of temperature. If a peak in the TPD profile can be identified and a temperature of maximum desorption (T_m) identified then the activation energy for desorption of a base (E_d) at that temperature can be determined using the following equation. It is necessary to measure T_m as a function of the heating rate, β to determine E_d.

$$2 \log T_m - \log \beta = E_d/2.303RT_m + \log (E_dA_m/RK_0) \qquad \textbf{(1.7)}$$

In the above equation T_m is the temperature of peak maximum, β is the linear heating rate, A_m is the amount of base adsorbed at saturation, K_0 is the pre-exponential factor in the desorption rate expression, and R is the gas constant.

Limitations of this technique include the restriction to certain basic probe compounds. Ammonia has been most extensively used to measure acidity but even this may be misleading as ammonia can dissociate to give NH_2^- and H^+ especially at high temperatures, so can be adsorbed onto both acidic and basic sites. Amines have been recommended as more appropriate adsorbates. The fact that most basic molecules are adsorbed onto both Brønsted and Lewis acid sites also has to be considered, especially when only one set of sites is catalytically active.

1.1.6.6 Microcalorimetric methods

A method which has gained importance over recent years is adsorption microcalorimetry, and it has become one of the most reliable methods for studying gas-solid interactions[46, 47, 48]. This technique has been used to determine the acidity of solid acids in the work to follow in this thesis.

Base adsorption microcalorimetry allows an insight into both the overall heats of adsorption and any distribution of values of the heat exhibited by a solid acid, and this has been taken as an indicative way of characterizing the surface of acid catalysts. The variation of the differential heats of adsorption as a function of coverage is an indication of the homogeneity or heterogeneity of the adsorption sites, and has been achieved by measuring differential heats of adsorption ($-Q_{diff}$(base)) vs. gas uptake using a basic probe molecule such as ammonia. A Tian-Calvet microcalorimeter is a convenient way of determining heats of adsorption (see Figure 1, Chapter 3.1.3.1) as this allows an experiment to be carried out isothermally throughout. The amount of probe gas is usually determined by gravimetry or more commonly by volumetric glassware attached to the calorimeter cell[49].

Adsorption is generally an exothermic process where $\Delta H_{ads} < 0$ because strong bonds are formed between the base and the acid sites. Differential heats of adsorption are related to the energy of bonds formed between the adsorbent (solid acid) and the adsorbate (probe gas) which allows us to see the strength of interaction when successive small doses of probe gas interact with the solid acid. This is because it is assumed that an acid site can be represented by the following:

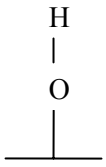

and the acid strength is related to this O-H bond. Strength as may be described by proton affinity of the acid (ΔH_{PA}) or more correctly the negative of the PA ($-\Delta H_{PA}$) is as shown:

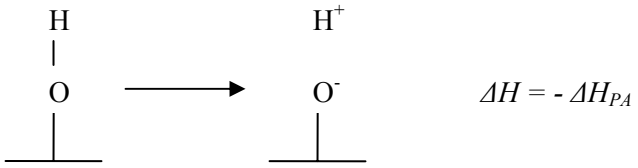

In reaction with NH_3 the following occurs:

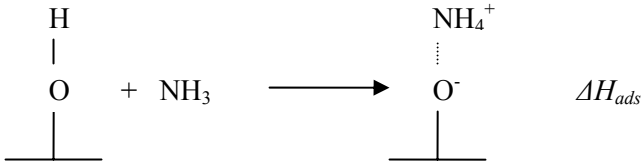

The question is whether ΔH_{ads} varies in the same way as $-\Delta H_{PA}$ as the catalyst is varied. It is possible to express this reaction in hypothetical steps, as shown, so that:

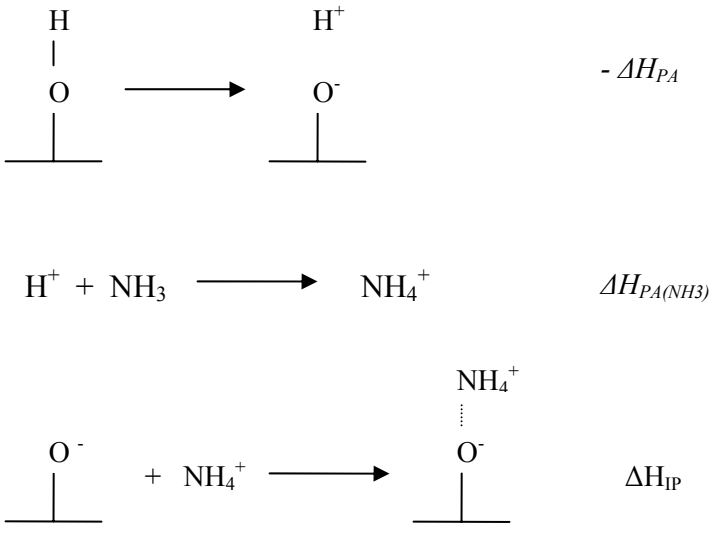

Clearly, $\Delta H_{PA(NH3)}$ is the same for every catalyst so whether or not ΔH_{ads} is a good indicator of $-\Delta H_{PA(acid)}$ depends on how the enthalpy of ion pair formation (ΔH_{IP}) varies between catalysts. It seems unlikely that the enthalpy of ion pair formation is the same for all solid acids. Therefore, in this work it has been assumed that ΔH_{ads} can be used to compare the strengths of solid acid catalysts but only if the catalysts are broadly similar in structure so that the way in which NH_4^+ would be bound to the anionic site and the surrounding catalyst surface would also be similar.

This method is often thought to progressively saturate the acid sites successively with the strongest sites being neutralised first and progressively weaker sites neutralised in order. On this basis, profiles of ΔH^0_{ads} ($-Q_{diff}$(base) versus amount of base adsorbed (progressive acid site coverage) is often interpreted as an indication of the way acid site strength is distributed between the surface acid sites[50]. In reality, neutralisation will not occur in this neat manner even when under thermodynamic control as there will always be a Boltzmann distribution of ammonia adsorption over sites of varying strength.

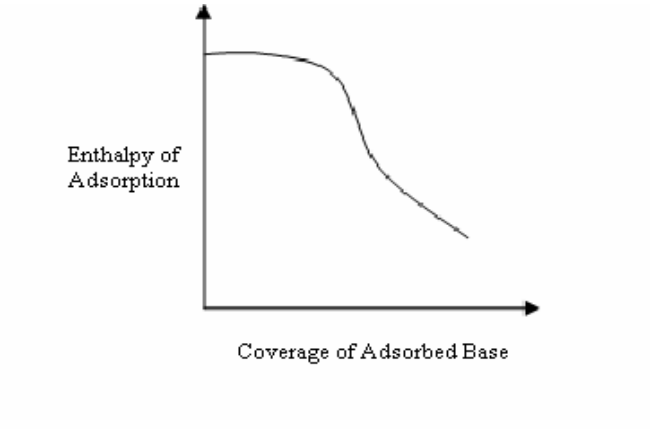

Figure 13: A typical molar enthalpy of base adsorption against coverage plot for a solid acid.

Despite this averaging effect, it is generally assumed that a plot of molar enthalpy adsorption against coverage does indeed give an indication of the distribution in acid strength as well their average strength. A typical plot is shown above in Figure 13. Further details on this technique shall be given in Chapter 3 and the adsorbate selection discussed.

[1] K. Tanabe, W.F. Holderich, App. Catal. A:Gen, 181 (1999) 399-434.

[2] M. A. Harmer, Q. Sun, App. Catal A:Gen., 221 (2001) 45-62.

[3] J. McMurray, "McMurray Organic Chemistry – 4th Edition", Eds; Brooks/Cole (1995) pp50-51.

[4] A. Corma, Chem. Rev., 95 (1995) 559-614.

[5] J. McMurray, "McMurray Organic Chemistry – 4th Edition", Eds; Brooks/Cole pp55-56.

[6] P.K. Paakkonen, A.O.I. Krause, React. Func. Polym., 55 (2003) 139-150.

[7] I.V. Kozhevnikov, "Catalysts for Fine Chemical Synthesis: Catalysis by Polyoxometalates, Vol. 2", Wiley (2002) pp11-13.

[8] L.C.W. Baker, D.C. Glick, Chem. Rev., 98 (1998) 3-49.

[9] M. Misono, Catal. Rev. Sci. Eng., 29 (2-3) (1987) 269-321; 30 (2) (1988) 339-340.

[10] I.V. Kozhevnikov, Russ. Chem. Rev., 56 (1987) 811-825.

[11] T. Okuhara, N. Mizuno, M. Misono, Adv. Catal., 41 (1996) 113-252.

[12] N. Mizuno, M. Misono, Chem. Rev., 98 (1998) 199-217.

[13] M.J. Janik, R.J. Davis, M. Neurock, Catal. Today, 105 (2005) 134-143.

[14] B. B. Bardin, S. V. Bordawekar, M. Neurock, R. J. Davis, J. Phys. Chem. B, 102 (1998) 10817-10825.

[15] G.M. Brown, M.R. Noe-Spirlet, W.R. Busing, H.A. Levy, Acta Crystallogr. B, 33 (1977) 1038.

[16] U.B. Mioc, Ph. Colomban, M. Davidovic, J. Tomkinson, J. Mol. Struct., 326 (1994) 99.

[17] M.J. Janik, R.J. Davis, M. Neurock, J. Phys. Chem. B, 108 (2004) 12292.

[18] I.V. Kozhevnikov, "Catalysts for Fine Chemical Synthesis: Catalysis by Polyoxometalates, Vol. 2", Wiley (2002) p 81.

[19] I. V. Kozhevnikov, Chem. Rev., 98 (1998) 171-198.

[20] L.R. Pizzio, C.V. Cacers, M.N. Blanco, App. Catal. A:Gen., 167 (1998) 283-294.

[21] S. Yariv & K.H. Michaelian: "Structure and surface acidity of clay minerals" in "Organo-clay complexes and interactions", Eds; S. Yariv & H. Cross, Marcel Dekker Inc. (2002) p 1.

[22] Fulcat Catalysts – Technical Bulletin, Rockwood Additives International (2006).

[23] C. Pesquera, F. Gonzalez, C. Blanco, J. Mater. Chem., 2 (9) (1992) 907-911.

[24] A.C.D. Newman, "Chemistry of clays and clay minerals", Mineralogical Society Monograph No.6, Ed; A.C.D. Newman (1987) p 277.

[25] P. E. Dai, Catal. Today, 26 (1995) 3-11.

[26] K. Wilson, J.H. Clark, Pure Appl. Chem., 72 (7) (2000) 1313-1319.

[27] D.H. Olson, G.T. Kokotallo, S.L. Lawton, J. Phys. Chem., 85 (1981) 2238-2243.

[28] http://www.iza-structure.org/databases/ - accessed on 04.09.2006.

[29] J.M. Newsam, M.M.J. Treacy, W.T. Koetsier, C.B. Gruyter, Proc. R. Soc. Lond. A, 420 (1988) 375-405.

[30] N. Cardona-Martinez, J.A. Dumesic, Adv. Catal., 38 (2002) 149-214.

[31] A. Dyer, "An Introduction to Zeolite Molecular Sieves", John Wiley & Sons (1988).

[32] M. P. Stevens, "Polymer Chemistry An Introduction – 3rd Edition", Oxford University Press (1998).

[33] C.E. Harland, "Ion exchange: Theory & Practice – 2nd Edition", RSC Paperbacks (1994) p 26.

[34] C.E. Harland, "Ion exchange: Theory & Practice – 2nd Edition", RSC Paperbacks (1994) p 62.

[35] R. Thornton, B.C. Gates, J. Catal., 34 (1974) 275-287.

[36] D.M. Ruthven, "Principles of Adsorption & Adsorption Processes", Wiley-Interscience (1984) p 4.

[37] A. Lapkin, B. Bozkaya, T. Mays, L. Borello, K. Edler, B. Crittenden, Catal. Today, 81 (2003) 611-621.

[38] D.E. Katsoulis, Chem. Rev., 98 (1998) 359-387.

[39] M. Trombetta, G. Busca, M. Lenarda, L. Storaro, R. Ganzerla, L. Piovesan, A.J. Lopez, M. Alcantara-Rodriguez, E. Rodriguez-Castellon, Appl. Catal. A:Gen., 193 (2000) 55-69.

[40] M. Furuta, K. Sakata, M. Misono, Y. Yoneda, Chem. Lett., 1 (1979) 31-34.

[41] W.E. Farneth, R.J. Gorte, Chem. Rev. 95 (1995) 615-635.

[42] A Corma, V. Fornes, F. Rey, Zeolites, 13 (1993) 56-59.

[43] M.L. Occelli, A. Auroux, G.J. Ray, Micropor. Mesopor. Mater., 39 (2000) 43-56.

[44] A. Ghanbari-Siahkali, A. Philippou, J. Dwyer, M.W. Anderson, App. Catal. A: Gen., 192 (2000) 57-69.

[45] A. Auroux, A. Gervasini, C. Guimon, J. Phys. Chem. B 103 (1999) 7195-7205.

[46] J.M. Guil, J.A. Perdigon-Melon, M.B. de Carvalho, A.P. Carvalho, J. Pires, Micropor. Mesopor. Mater., 51 (2) (2002) 145-154.

[47] V. Rakic, V. Dondur, U. Mioc, D. Jovanovic, Top. Catal., 19 (3-4) (2002) 241 – 247.

[48] D.J. Parrillo, R.J. Gorte, Catal. Lett. 16 (1992) 17-25.

[49] A. Auroux, Top. Catal., 4 (1997) 71-89.

[50] V. Solinas, I. Ferino, Catal. Today, 41 (1998) 179-189.

CHAPTER TWO

SOLID ACID CHARACTERISATION

Section 1 – Theory

2.1.1 Introduction to Studied Solid Acids

The following section will introduce the solid acids to be studied and also the measurement of physical properties such as surface area etc.

2.1.1.1 Supported Heteropoly acids

This section describes the three mesoporous supports (synthetic carbons, Novacarb™ and Sibunit™, and silica SBA-15) used for supporting tungstophosphoric heteropoly acid, $H_3PW_{12}O_{40}$ (HPW). The SBA-15 silica and impregnated HPW samples were prepared by Dr Alexei Lapkin (Department of Chemical Engineering, University of Bath).

Novacarb™, originally from MAST Carbon Ltd (UK), is a mesoporous activated carbon made up of spheres with diameters in the range 50 to 500 μm. These particles were sieved to obtain a fraction 150-212 μm. This sieved fraction contained small amounts of agglomerated finer particles which were placed in cold water and treated ultrasonically for one hour. Following this treatment fines were removed by decanting and repeating washing with demineralised water. The clean sample was then dried in a vacuum oven at 100 °C and sieved again. Prior to impregnation of HPW, Novacarb was washed in water and ethanol and dried under vacuum at 200 °C for 2-3 hours[1].

Sibunit™ is a synthetic mesoporous carbon which was kindly provided by the Boreskov Institute of Catalysis (Novosibirsk, Russia). Sibunit with particles of ca. 2 mm in diameter were washed in water and ethanol, and dried under vacuum at 200 °C for 2-3 hours prior to impregnation. Detailed information on the synthesis and properties of Sibunit is available elsewhere[2].

Pure SBA-15 is a siliceous mesoporous molecular sieve. In a typical synthesis 2 g of Pluronic (P123) polyethylene oxide polypropylene oxide block co-polymer (BASF) is dissolved in a mixture of 45.0 g H_2O and 30 g HCl (4 M) at 40 °C. Tetra-ethoxysilane (TEOS) 3.1 g is then added drop-wise and the mixture stirred for 20 hours at 40 °C. After stirring the mixture is poured into a polypropylene bottle and aged in an oven for 24 hours at 100 °C. Following ageing the

mixture is filtered, washed with demineralised water, and dried under atmospheric conditions for 48 hours. Finally samples are calcined in air with the calcination temperature being increased from ambient to 500 °C at 1 °C/min and kept at that temperature for 6 hours[3]. SBA-15 is characterised by powder XRD, looking specifically for the reflection relating to the [100] planes although reflections from other planes are also seen. Surface areas and pore sizes are determined by nitrogen adsorption at -196 °C [4].

Tungstophosphoric heteropoly acid $H_3PW_{12}O_{40}$ (HPW) was obtained from Fisher and purified by re-crystallisation from methanol prior to impregnation. Supported acid samples were prepared using the two mesoporous carbons, Novacarb™ and Sibunit™, and also the ordered mesoporous silica SBA-15. They were prepared by adsorption from ethanol-water solutions (1:1 volumetric ratio of demineralised water and 96 wt% ethanol) as described elsewhere[5]. These samples were gently stirred and equilibrated for 72 hours at room temperature. The amount of acid adsorbed was determined using a gravimetric technique, and validated by the results of volumetric ammonia chemisorption. Finally samples were dried in air at 150 °C for 2 hours. The following samples were produced in Bath and used in this project in Huddersfield (samples are named as amount of HPW per gram of support):
HPW/Novacarb (100mg/g), HPW /Novacarb (311mg/g), HPW /Sibunit (200mg/g), HPW /Sibunit (254mg/g), HPW/Sibunit (300mg/g), HPW/SBA-15 (174mg/g), HPW/SBA-15 (320 mg/g), HPW/SBA-15 (420mg/g).

2.1.1.2 Montmorillonite Clays

a) *'Fulcat 200 series' acid-activated montmorillonite clays*

Fulcat is a trade name for a series of acid-treated clay catalyst based on Clophill montmorillonite clay used by Rockwood Additives Ltd.

The 'Fulcat 200 series' catalysts have various advantages over mineral acids and some other solid acids in that they are non-corrosive, they have good thermal stability, they have a controlled particle size distribution, and the absence of fine particles allows easy filtration and removal from reaction products. Shown below is the chemical composition table for the 'Fulcat 200 series' (Table 1) and nitrogen adsorption data (Table 2) which has been provided in the company literature[6].

	F200 (Parent Clay)	F220 (Acid Activated)	F230 (Acid Activated)	F240 (Acid Activated)
Chemical Composition (w/w %)				
SiO_2	57.6	61.2	66.2	70.0
Al_2O_3	16.9	13.9	11.9	7.9
Fe_2O_3	8.1	5.9	4.7	4.2
CaO	3.1	1.9	2.6	2.6
MgO	3.6	2.7	2.1	1.3
K_2O	0.7	0.6	0.6	0.6
Na_2O	0.4	0.2	0.2	0.2

Table 1: Elemental composition of 'Fulcat 200 series'.[6]

	F200	F220	F230	F240
Surface Area ($m^2.g^{-1}$)	100	190	400	430
Pore Volume ($ml.g^{-1}$)	0.1	0.3	0.5	0.55
Particle Size				
D10 (µm)	5.0	7.5	7.0	6.0
D50 (µm)	25	40	35	30
D90 (µm)	75	80	75	65

Table 2: Characteristics of 'Fulcat 200 series'.[6]

Particle size is explained by determining the percentage of particles having a particular diameter or less, for example D10 for Fulcat 200 means that 10 % of particles have a diameter of equal to or less than 5.0 µm, D50 means that 50 % of particles have a diameter of 25 µm or less and D90 means that 90 % have a diameter of 75 µm or less.

Fulcat 200

This is a high purity refined montmorillonite clay catalyst in the Ca^{2+} form which has a tightly controlled particle size distribution shown in the manufacturer's information in Table 2. It is claimed to provide both Lewis and Brønsted acidity together with a moderate surface area

although since it is in the Ca^{2+} ion exchange form, only limited surface acidity would be expected. It has received no acid treatment.

Fulcat 220

This is an acid-activated montmorillonite catalyst based on the parent clay Fulcat 200, and again it has a tightly controlled particle size distribution. It is also claimed to provide a combination of Lewis and Brønsted acidity with a high surface area.

Fulcat 230 & 240

These are both acid activated montmorillonite clays, as Fulcat 220 but with increasing relative SiO_2 content, as a result of progressively more extensive acid activation.

Also used in this study were exchanged versions of the parent clay, Fulcat 200 and the acid treated Fulcat 240. Both were exchanged with Al^{3+} and Fulcat 200 was also exchanged with Fe^{3+}. The following ion exchange process was used. A 1 % suspension of the respective clay was stirred with a 1.5 mol dm^{-3} solution of the desired cation in an aqueous solution of either the nitrate or chloride salt overnight at room temperature. The supernatant solution containing the majority of the ion that originally occupied the exchange sites was decanted off and discarded. The exchange process was repeated and the ion-exchanged material was filtered and washed with deionised water and dried in air.

b) *Süd-Chemie acid-activated 'K-series' montmorillonite clays*

Again this is a series of acid-activated montmorillonite clays, but this time produced by Süd-Chemie. In particular, K5, K10, K20, and K30 will be studied. They have been progressively acid activated from K5 to K30. It needs to be mentioned that the parent clay known as Tonsil 13 (Bavarian montmorillonite) for the 'K-series' has not been examined. Shown in Table 3 and Table 4 below are the elemental compositions of the 'K-series' and also the nitrogen adsorption data as shown in the manufacturer's data[7].

	K5 (Acid Activated)	K10 (Acid Activated)	K20 (Acid Activated)	K30 (Acid Activated)
Chemical Composition (w/w %)				
SiO_2	65.0	73.0	75.0	80.0
Al_2O_3	19.0	14.0	12.5	10.0
Fe_2O_3	4.8	2.7	2.4	1.8
CaO	0.2	0.2	0.3	0.2
MgO	2.4	1.1	1.2	1.0
K_2O	1.5	1.9	1.5	0.5
Na_2O	0.3	0.6	0.3	0.3

Table 3: Elemental composition of 'K-series'.[7]

	K5	K10	K20	K30
Surface Area ($m^2.g^{-1}$)	200	240	240	330
Pore Volume ($ml.g^{-1}$)	0.25	0.36	0.39	0.50
Micropore Volume (< 0.2 µm) t-plot value ($ml.g^{-1}$)	0.015	0.010	0.010	0.010

*Table 4: Characteristics of the 'K-series'.*Error! Bookmark not defined.

In general 'K-series' clays are recommended by their manufacturer for reactions such as esterification, etherification, alkylation and acylation of aromatic compounds. They are claimed to possess both Brønsted and Lewis acidity.

Elemental compositions of studied clays from both Rockwood Additives Ltd and Süd-Chemie will be discussed later on in this chapter in Section 2.3.1.

2.1.1.3 Zeolites

H-ZSM-5 zeolites and zeolite β were studied in the following work. H ZSM-5 samples were provided by Catal International and two forms were studied with different Si:Al ratios:

CT 410	$SiO_2:Al_2O_3 = 55$,	Si:Al = 27.5.
CT 434	$SiO_2:Al_2O_3 = 80$,	Si:Al = 40.

Zeolite β with a Si:Al ratio of 37.5 was provided again by Dr Alexei Lapkin from the University of Bath.

2.1.1.4 Sulfonated Polystyrene Ion Exchange Resins

a) Amberlyst Resin Information

Polystyrene sulfonic acid Amberlyst resins are produced by Rohm and Haas for industrial applications including ion exchange and acid catalysis. They generally produce two types of resins, gel and macroporous. Those being studied fall under the macroporous category as they have so called "macroreticular" structure. This allows for the incorporation of permanent porosity for improved selectivity, gives a relatively high surface area, and makes them thermally stable. Table 5 below shows properties of the Amberlyst resins to be studied, data provided by Rohm & Haas.

Amberlyst	Type	Area ($m^2.g^{-1}$)	Pore Diameter (A)	Active Sites ($meq.g^{-1}$)	Moisture (%)	Max temp (^oC)
15	H^+	45	250	4.8	54	120
35	H^+	45	250	5.3	53	140
36	H^+	35	200	5.5	56	150

Table 5: Characteristics of Amberlyst sulfonated ion exchange resins.[8]

b) Purolite Resin Information

The 'CT-series' is produced by Purolite International Ltd. Two members of this series will be investigated, CT-175 and CT-275.

CT-175 is a strong acid ion exchange resin catalyst with a macroporous structure, which has been developed from polystyrene(co-vinylbenzene)sulfonate cation exchangers. It contains a relatively rigid structure and larger pores than Amberlyst 15 resin to allow accessibility to acid sites. This results in a higher concentration of acid sites than Amberlyst 15, as internal acid sites are made

available, and the effect of pore plugging is minimised due to the size of pores. Data provided by Purolite International is provided below in Table 6.

Purolite	Type	Area ($m^2.g^{-1}$)	Pore Diameter (A)	Porosity: Pore Volume ($ml.g^{-1}$)	Active Sites ($meq.g^{-1}$)	Moisture (%)	Max temp (^oC)
CT-175	H^+	30	650	0.5	4.9	54	145
CT-275	H^+	20-35	600-750	0.4-0.6	5.2	53	145

Table 6: Characteristics of CT-175 and CT-275.[9]

CT-275 is also a strong macroporous acidic polymeric catalyst whose properties are claimed to include increased acid strength, a higher concentration of acid sites and also increased thermal stability over CT-175, which results in longer catalyst life.

2.1.2 Nitrogen Adsorption and Adsorption Isotherms

Adsorption isotherms can be used to measure the specific surface area of a solid and also the size of pores in a porous solid and the distribution of pore sizes if they are not of uniform size. Inert gases, primarily nitrogen, are used for this purpose so the technique is often known as nitrogen adsorption. The general principle of the method involves increasing pressure of nitrogen at equilibrium with the adsorbent from zero to its saturated vapour pressure (for N_2 it is done at -196 °C so saturated vapour pressure is 1.0 atm). This allows an adsorption isotherm to be constructed plotting the amount of nitrogen adsorbed vs. relative pressure, p/p_o where p_o is the saturated vapour pressure. It is quite usual to measure the isotherms as the pressure of adsorbate is increased and, in the same experiment, as the pressure is reduced again to zero. Nitrogen and other relatively inert gases are used because adsorption is virtually always physisorption and it is unlikely to show widely varying heats of adsorption on different surface sites. The main types of isotherm for known adsorption systems shall be discussed below.

2.1.2.1 Adsorption systems – Six main types of isotherm

Each adsorption system has its own characteristic adsorption isotherm, most of which can be classified into one of six categories. These are shown below in Figure 14, where the amount of adsorbate adsorbed is expressed as θ, the fraction of surface sites occupied by the adsorbate.

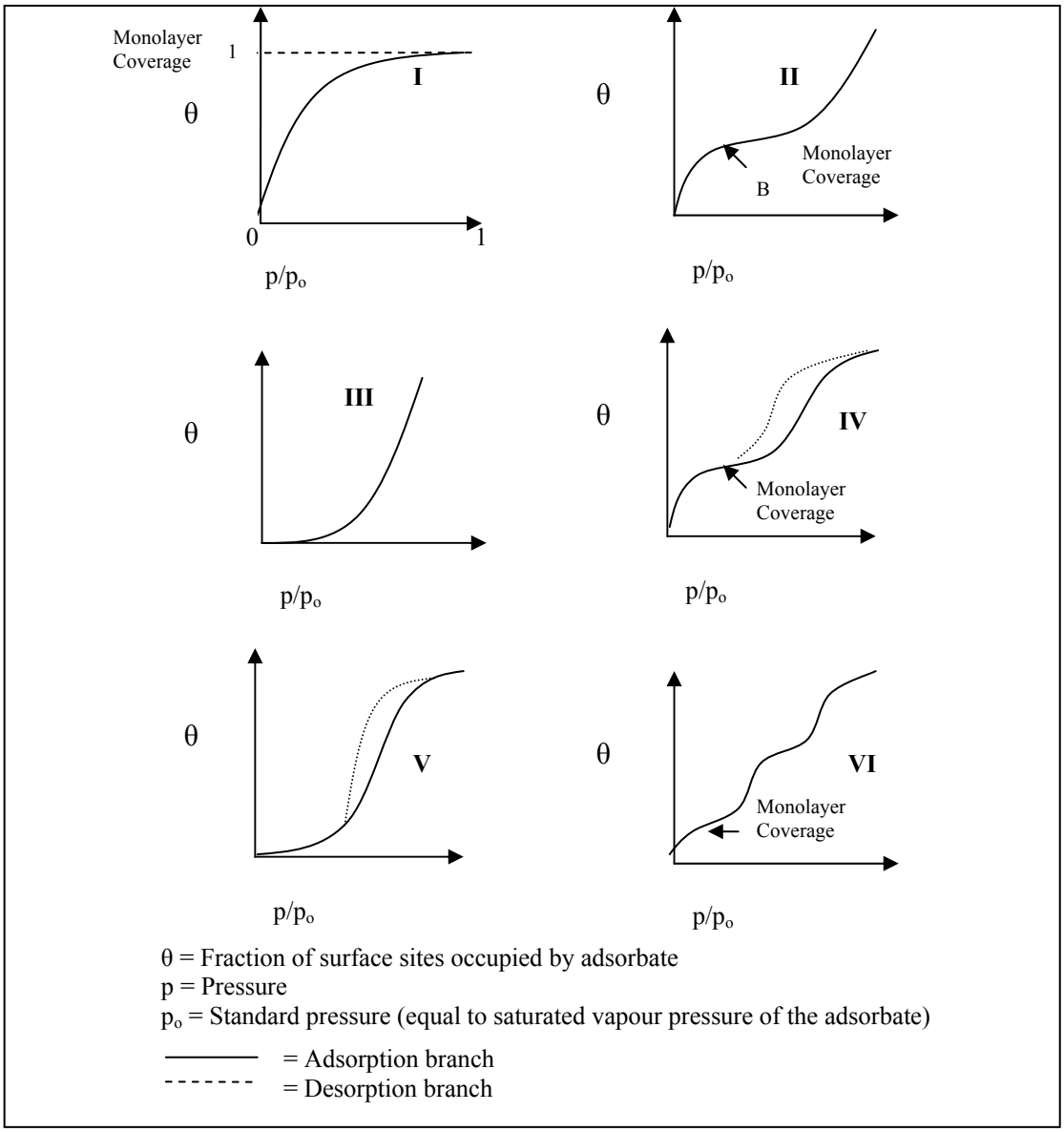

Figure 14: Six main types of physisorption isotherms according to the IUPAC classification.[10]

In type I isotherms the amount adsorbed increases steadily with pressure until a plateau is reached at $\theta = 1$ (where all sites are populated by the adsorbate). At this point no further adsorption occurs. One interpretation of this plateau for physisorption states that the pores are so narrow that they cannot accommodate more than a single molecular layer on their walls, thus the plateau corresponds to the completion of a monolayer of adsorbate. Type I isotherms are given by microporous solids which have relatively small external surfaces i.e. molecular sieve zeolites, activated carbons and certain porous oxides.

In type II isotherms: the monolayer plateau region is reached at point B but there is then a further increase in the amount adsorbed and many layers are ultimately adsorbed as $p/p_o = 1$ is approached. In the majority of cases this type of isotherm is associated with non-porous solids.

Type III isotherms are characteristic of weak gas-solid interactions and are associated with multilayer formation, but are not very common. The isotherm lies convex to the p/p_0 axis over its entire range and does not exhibit a point B. An example of this type of system is given by the adsorption of nitrogen on polyethylene.

The study of pore structure of mesoporous solids is closely connected with the interpretation of Type IV isotherms. A Type IV isotherm follows the same path as the corresponding Type II isotherm in the low-pressure region. At a certain point it begins to deviate upwards until at higher pressures its slope decreases, and as the saturation vapour pressure is approached the amount adsorbed may show little variation. A characteristic feature of a Type IV isotherm is its hysteresis loop as the amount adsorbed is always greater at any given pressure along the desorption branch than along the adsorption branch. This behaviour is usually observed for evaporation and condensation in mesoporous material, and is commonly found in catalysts. The shape of the hysteresis curve can often indicate the size and type of pore in the catalyst. Type IV isotherms are given by many mesoporous adsorbents.

The type V isotherm is uncommon and is related to the type III isotherm in that the adsorbent-adsorbate interaction is weak, but it is obtained with certain porous adsorbents.

Type VI isotherms represent stepwise multilayer adsorption on uniform non-porous surfaces, in which the sharpness of the steps depends upon the system and the temperature. The step height represents the monolayer capacity for each adsorbed layer, and in simplest terms remains nearly constant for two to three adsorbed layers. Examples of type VI systems include those obtained with argon or krypton on graphitised carbon blacks at liquid nitrogen temperature.

The interpretation of adsorption isotherms is based on two main theories, the Langmuir adsorption theory shown in Section 2.1.2.2 below, and the Brunauer-Emmett-Teller (BET) adsorption theory shown in Section 2.1.2.3.

2.1.2.2 Langmuir Adsorption Theory

This is the simplest, most commonly used, model for interpreting adsorption isotherms, and is based on three assumptions:

1. Adsorption of gas on the solid surface cannot proceed beyond monolayer coverage, and only one adsorbate molecule occupies each surface site.
2. The energy for adsorption and the ability of the molecule to adsorb is independent of how many of the surrounding sites are occupied.
3. The surface is uniform and adsorption sites are equivalent.

The dynamic equilibrium of a surface-adsorbate interaction is as follows:

$$A_{(g)} + M(surface) \rightleftharpoons AM\ (surface)$$

This is achieved when the rate of adsorption (R_a) = Rate of desorption (R_d).

When equilibrium is established adsorbed molecules cover a fraction of the surface (θ) and therefore the fraction not covered is (1-θ). The rate of adsorption is proportional to the partial pressure of A, and the number of vacant sites:

$$R_a = \frac{d\theta}{dt} = k_a P_a (1-\theta) \qquad (\mathbf{2.1})$$

The rate of desorption is proportional to the number of adsorbed species which is proportional to the fractional coverage, (θ):

$$R_d = \frac{d\theta}{dt} = k_d \theta \qquad (\mathbf{2.2})$$

At equilibrium the two rates are equal:

$$k_a P_a (1-\theta) = k_d \theta \quad or \quad \frac{\theta}{1-\theta} = \frac{k_a}{k_d} P_a \qquad (\mathbf{2.3})$$

Solving for θ gives the Langmuir isotherm equation:

$$\theta = \frac{KP_a}{1+KP_a} \text{ where adsorption coefficient, } K = \frac{k_a}{k_d} \qquad \textbf{(2.4)}$$

The Langmuir isotherm successfully models type I behaviour for adsorption up to one monolayer (see Figure 14, Section 2.1.2.1).

If V is the volume of gas (at STP) adsorbed on the surface and V_m is the volume to form a monolayer then:

$$\theta = \frac{V}{V_m} = \frac{KP_a}{1+KP_a} \qquad \textbf{(2.5)}$$

This expression can then be arranged to give a linear relationship:

$$\frac{P_a}{V} = \frac{P_a}{V_m} + \frac{1}{KV_m} \qquad \textbf{(2.6)}$$

If the system obeys the Langmuir equation, then a plot of $\frac{P_a}{V}$ against P_a gives a straight line of slope $\frac{1}{V_m}$, and intercept of $\frac{1}{KV_m}$ so giving V_m and K. Surface area of the adsorbent can be calculated by using the determined V_m (the volume of gas to form one monolayer) and the known surface area value associated with an adsorbed gas molecule.

2.1.2.3 The Brunauer-Emmett-Teller (BET) Adsorption Theory

Calculation of surface area based on the Langmuir equation assumes adsorption is limited to one monolayer of adsorbate. A theory is needed that accounts for physisorbed multilayers, where instead of the isotherm levelling off to a saturated value at high pressures, it can be expected to rise beyond this. The most widely used isotherm for dealing with multilayers is the BET isotherm and models type II behaviour (Figure 14, Section 2.1.2.1), and the following assumptions are made:

A. Each layer of adsorbate is treated as a Langmuir monolayer, and each layer must be complete before the next layer starts to form.
B. The adsorption and desorption rates in all layers above the first are identical.
C. ΔH_{ads} in all layers above the first are the same and are equal to the heat of condensation, ΔH_L i.e. $\Delta H_L = \Delta H_2 = \Delta H_3 = \Delta H_4 = \ldots..$

The general form of the BET isotherm is as follows:

$$\theta = \frac{V}{V_m} = \frac{cz}{(1-z)(1+(c-1)/z)} \text{ where } z = \frac{p}{p_0}, \qquad \textbf{(2.7)}$$

p is the equilibrium pressure over the solid and p_0 is the saturated vapour pressure of the gas at the temperature of the experiment, and c is a constant which is large when the enthalpy of desorption from a monolayer is large compared with the enthalpy of vaporization of the liquid adsorbate. This can be re-arranged to give:

$$\frac{p}{V(p_0 - p)} = \frac{1}{V_m c} + \frac{(c-1)}{V_m c} \cdot \frac{p}{p_0}, \qquad \textbf{(2.8)}$$

so that a plot of $\frac{p}{V(p_0 - p)}$ against $\frac{p}{p_0}$ will give a straight line if the system conforms to the BET equation, where the gradient is equal to $\frac{(c-1)}{(cV_m)}$, and the intercept is $\frac{1}{(V_m c)}$. From these, V_m can be calculated.

The BET isotherm is widely used to determine surface areas. An assumption is then made about the packing of adsorbate on the surface and the area each molecule occupies, and the surface area is then acquired from this data. The BET equation is not usually followed at all pressures but is usually obeyed over a pressure range p/p_0 = 0.05 - 0.30 and it is usually from data taken over this range that BET surface areas are determined.

2.1.2.4 Pore Volumes and Pore Size Distributions from Adsorption-Desorption Isotherms

The analysis of mesopores using nitrogen adsorption has become widely accepted as the principle method for determining pore volumes as a function of pore radius[11].

When the vapour pressure of an adsorbate above a flat surface reaches the saturated vapour pressure of the adsorbent, p_o, it condenses. However, when a surface is not flat and contains pores, the liquid condenses at lower pressures because the liquid forms a concave curved surface in the pore. The relationship between the saturated vapour pressure above a curved liquid surface to that above a flat liquid surface is given by the Kelvin equation (equation 2.9),

$$\ln\left(\frac{p_0}{p}\right) = -\frac{2\sigma V}{r_k RT}.\cos\theta \qquad \textbf{(2.9)}$$

where

p_0 = Saturated vapour pressure at STP,

p = Pressure of vapour in equilibrium with the curved liquid surface,

σ = Surface tension of the condensed adsorbate,

V = Adsorbate liquid molar volume, 36.5 ml/mole for liquid N_2 at -195.6 °C,

r_k = Mean radius of curvature of the surface,

R = Gas constant,

T = Absolute temperature,

θ = Contact angle of meniscus with solid, usually assumed to be zero so $cos\theta = 1$.

In the isotherm method for mesopore analysis the basic assumption is that capillary condensation occurs when the vapour pressure of the adsorbate is equal to the saturated vapour pressure that corresponds to the liquid surface with which it is in contact. When adsorbate condenses in mesopores it is assumed that the surface (meniscus) of the liquid in the mesopore is curved, with a radius of curvature dependent on the diameter of the pore. Therefore by measuring the amount of gas condensed at any pressure, the volumes in pores of radius corresponding to that pressure can be calculated from the amount of N_2 that condenses at this pressure. This begins for nitrogen at p/p_0 of ~ 0.4.

Vapour will condense in small pores at relatively low pressures, and large pores at higher pressures. This principle is used to construct a pore volume vs. radius distribution directly from the nitrogen adsorption/desorption isotherm. It is conventional to apply the Kelvin Equation to the desorption branch, rather than the adsorption branch of the isotherm. Pore radii calculated from the desorption isotherm have to be adjusted for the thickness of a film of adsorbate which remains on the pore walls which effectively means the radius of curvature of the liquid surface is less than that of the pores.

One of the most popular methods for obtaining pore size distributions is that of Barrett, Joyner, and Halenda (BJH)[12]. The BJH method uses the Kelvin equation to determine the distribution of mesopores, which have diameters between 2 nm and 50 nm within a solid. It accounts for the pore radius being generally larger than the radius of curvature of the meniscus by the thickness of the film, *t*. Using the desorption branch the BJH method has been used in this study to measure the pore size distribution of catalysts.

Analysis of the volume of micropores (diameter < 2nm) present within an adsorbent can also be determined. This is done using the t-plot method (Lippens, de Boer), and is based on the t-curve which is a plot of *t* (the statistical thickness of the film) against relative pressure (p/p_o) rather than fractional coverage of the adsorbate (θ) versus relative pressure (p/p_0). The isotherm under test is then re-drawn as a t-plot i.e. fractional coverage (θ) is plotted against *t* rather than p/p_o creating a straight-line plot from which a micropore volume (intercept) and surface area (gradient) can be determined.

2.1.3 Powder X-Ray Diffraction

X-rays are part of the electromagnetic spectrum and interact with electrons in matter. When a beam of x-rays comes into contact with a material they are scattered by the electron clouds. A crystal lattice has a regular pattern of atoms and planes of atoms which are all separated by the same distance, and when x-rays are reflected from successive planes of atoms interference can occur. This can be either constructive or destructive. When rays constructively interfere, a diffracted beam is produced as shown below in Figure 15.

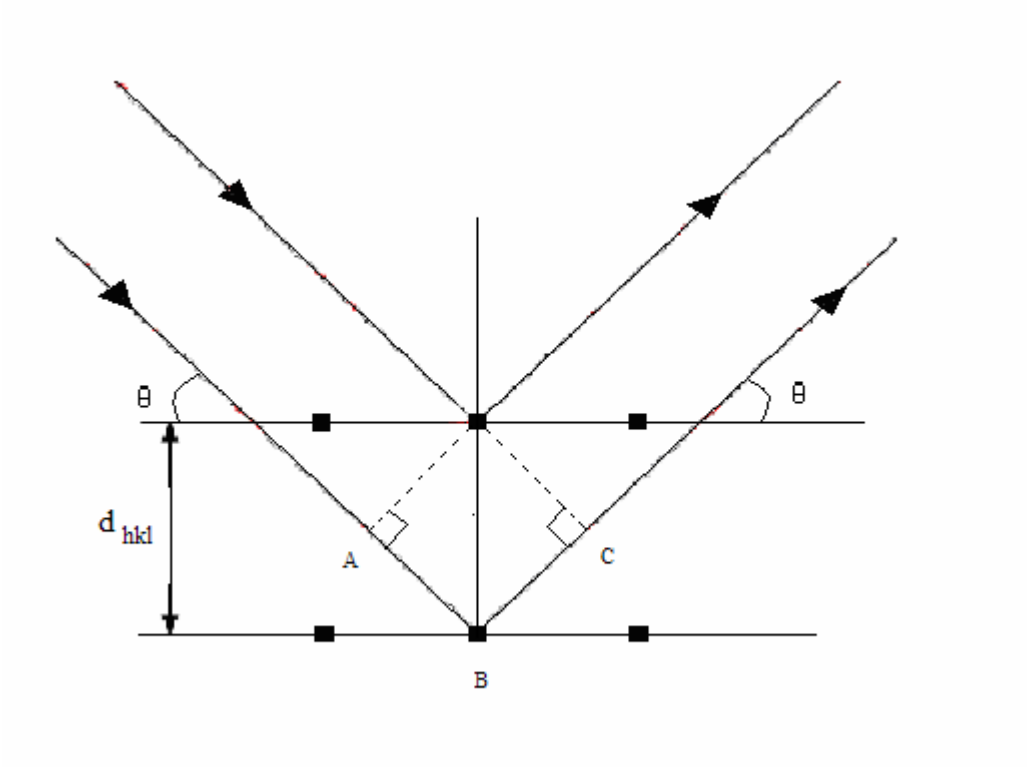

Figure 15: Scattering of x-rays from a parallel set of planes.

The condition for constructive interference of a diffracted beam of x-rays is given by the Bragg equation:

$$n\lambda = 2d\sin\theta . \qquad \textbf{(2.10)}$$

Where n represents the order of diffraction, λ is the wavelength of the x-ray beam, θ is the angle of diffraction, and d is the distance between the atomic planes in the crystal lattice which are causing the diffracted beam. The model makes it easy to calculate the angle the crystal must make to the incoming beam of x-rays for constructive interference to occur i.e. when the path length difference is equal to one wavelength (AB + BC = λ).

As the x-rays interact with the planes of atoms in the three-dimensional lattice, diffraction occurs from parallel sets of equally spaced planes. Each set of planes is described by Miller indices (h, k, and l). The d spacing for the sets of planes differ so that each set gives rise to a reflection at a characteristic angle (θ) according to the Bragg equation above. The overall diffraction pattern is a plot of intensity of reflection against 2θ, and is characteristic of a particular crystalline material.

Powder x-ray diffraction is the simplest technique used to obtain x-ray diffraction patterns, and was developed by Peter Debye and Paul Scherrer. The idea behind this approach is to investigate a powdered sample rather than a single crystal. In a single crystal experiment the alignment of the crystal, source and detector need to be correct to observe any reflections. In contrast, a powdered sample contains an enormous number of very small crystallites which randomly adopt the whole range of possible orientations. Therefore when an x-ray beam strikes a powdered sample, it is diffracted in all directions (as governed by the Bragg equation) simultaneously, giving rise to diffraction cones. Each cone is a set of closely spaced dots, where each dot corresponds to diffraction from a single crystallite within the sample. As x-rays are produced by the x-ray tube, they fall onto the sample through a slit and are scattered in all directions. By scanning the detector around the sample along the circumference of a circle, it cuts through the diffraction cones at various diffraction maxima and produces signals. The x-ray diffraction pattern then displays intensity as a function of the detector angle, 2θ, in a two dimensional plot. This diffraction pattern can be used to fingerprint a sample. In some cases, where the spacing between planes can vary (as with expanding clays), the d-spacing can be calculated and used in structural characterization.

2.1.4 Exchangeable Cations

Cation exchange capacity is an important property of clay minerals and sulfonated polystyrene ion exchange resins especially because the major source of acidity in these materials arises from the exchangeable cation.

In those clay minerals that expand, such as the montmorillonites, the relative ease with which one cation will replace or exchange with another is not always predictable but generally follows the trend below:

$$Na^+ < K^+ < Ca^{2+} < Mg^{2+} < NH_4^+.$$

Measuring the amount of cations freed and replaced by others is a measure of the cation exchange capacity. For catalysts that rely on H^+ or other acidic cations in exchangeable sites the cation exchange capacity is a key property.

In montmorillonite clay exchangeable cations neutralise the negative lattice charge, the source of which is mainly provided by the isomorphous substitution of Mg^{2+} for Al^{3+} in the octahedral layer. The distribution of cations in the interlayer space is most likely controlled by the distribution of charges on the adjacent silicate layers that they neutralize. For example, when there is lattice anionic charge arising from Al^{3+} substitution in the tetrahedral clay layer preferred positions for the location of cations are adjacent to the substituted tetrahedron in the surrounding silica tetrahedral layers[13].

The ion exchange properties of polystyrene sulfonic acid resins are straightforward in comparison. Each sulfonic acid unit – SO_3H is a "strong acid" and readily dissociates to give $-SO_3^-$ and H^+. When hydrated, H^+ exists in "internal solution" in the swollen resin and exchange with other ions can readily occur as diffusion of ions from an external aqueous solution is facile[14].

Section 2 – Experimental

2.2.1 Nitrogen Adsorption

A Beckman Coulter SA3100 sorption analyser was used to record the nitrogen adsorption isotherms at -196 °C, and the adsorption /desorption isotherms were plotted using ~120 data points. Internal commercial software was then used to calculate the BET surface area and pore size distributions were obtained from desorption data and the BJH calculation. Sample (100 mg) was used in its supplied state, and was activated for 2 hours under vacuum of 10^{-5} Torr at 150 °C prior to adsorption for each sample.

2.2.2 Powder X-Ray Diffraction

Powder x-ray diffraction patterns were obtained using a Bruker AXS – D8 Advance diffractometer with Cu K_α radiation with a wavelength of 0.154 nm. Samples were placed in a holder made of inert material, and were scanned from 2θ = 0.6 ° to 5 ° at 0.01 ° steps every 30 seconds for SBA-15 samples, and from 2θ = 2 ° to 50 ° at 0.05 ° steps every 20 seconds for clay and zeolite samples. All diffraction patterns were measured at room temperature.

2.2.3 Cation Exchange Capacity (C.E.C.)

The cation exchange capacities of ion exchange resins were measured using acid-base titration. As supplied resin (0.5 g) under conditions where water content was known was weighed out and 25 ml distilled water added in a conical flask. Sodium chloride (2 g) was added in excess so that sodium ions took the place of hydrogen ions to give an aqueous solution of HCl. This was then titrated with standard 0.1 M NaOH(aq) using phenolphthalein as an indicator. The solution was continuously stirred[15].

Cation exchange capacities for the clays were calculated from their elemental composition (Section 2.1.1.2), on the basis that the cation exchange capacity of montmorillonite is due almost exclusively to Mg substitution for Al in the octahedral layer giving rise to a lattice negative charge.

2.2.4 Elemental Analysis of Montmorillonite Clays

Elemental analyses of the clays were provided by Süd-Chemie and Rockwood Additives Ltd.

2.2.5 Effective Dry Weights of Sulfonated Polystyrene Ion Exchange Resin Catalysts

Sulfonated polystyrene ion exchange resins were hydrated in distilled water overnight and weighed. They were then dried in an oven to constant mass at 105 °C.

Section 3 – Results

In this section characterisation results will be shown for each set of catalysts, and in Section 4 these results will be discussed. The nitrogen adsorption results shall include nitrogen adsorption isotherms as well as a table showing BET surface areas, mesopore volumes, micropore volumes, mean pore diameters, and the percentage of particles having a particular diameter for each catalyst.

2.3.1 Supported Tungstophosphoric Heteropoly Acids

2.3.1.1 SBA-15 Supported Tungstophosphoric Heteropoly Acid (HPW)

a) Nitrogen adsorption isotherms for SBA-15 supported HPW

Isotherms are shown in Figure 16 for pure SBA-15 and for the SBA-15 with supported HPW at two loadings. The data derived from these isotherms appears in Table 7.

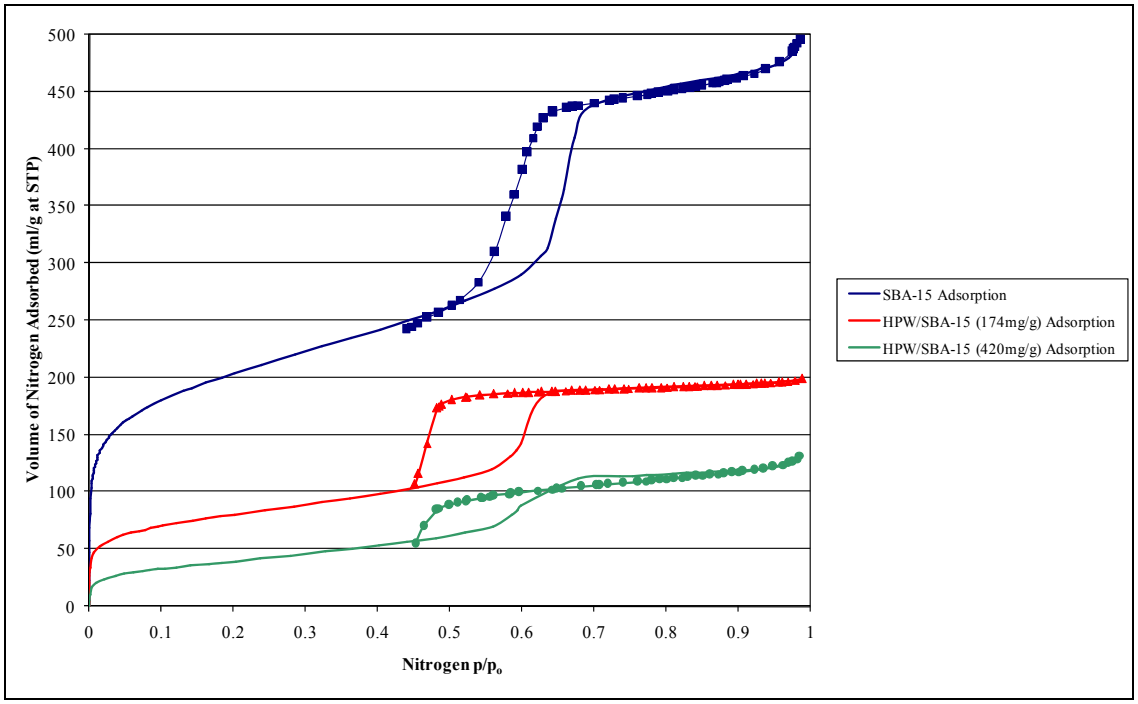

Figure 16: Nitrogen adsorption isotherms (-196 °C) – SBA-15 supported $H_3PW_{12}O_{40}$ (HPW). (Lines with symbols represent the desorption legs).

	N_2 BET Surface Area ($m^2.g^{-1}$)[a]	Mesopore Volume ($ml.g^{-1}$)[b] (>2 nm)	Micropore Volume ($ml.g^{-1}$)[c] (<2 nm)	Mean Pore Diameter (nm)[b]	Particle Size (nm)[b]		
					D_{10}	D_{50}	D_{90}
SBA-15	729	0.63	0.093	10.5	4.34	5.06	17.14
HPW/SBA-15 (174 mg/g)	286	0.065	0.028	12.5	3.87	4.34	32.20
HPW/SBA-15 (420 mg/g)	143	0.11	-	20.1	3.97	6.39	72.01

[a] Measured at -196 °C
[b] Calculated from desorption branch of isotherms using BJH method
[c] Calculated using t-plot method

Table 7: Surface and pore size distribution data for SBA-15 supported $H_3PW_{12}O_{40}$ (HPW).

The BET surface area for SBA-15 was found to be 729 $m^2.g^{-1}$. This is a similar value to that found in the literature[16]. The nitrogen adsorption-desorption hysteresis is characteristic of a narrow pore size distribution in the mesopore region which is also shown by the particle size diameters (Table 7) for pure SBA-15. The mesopore volume for pure SBA-15 is 0.63 $ml.g^{-1}$, and the mean pore diameter found by the Barrat-Joyner-Halenda (BJH) method is 10.5 nm. Nitrogen adsorption data shows that SBA-15 provides very little microporosity.

On the introduction of HPW the surface area decreases dramatically. This is most likely due to pore filling by the heteropoly acid. The mean pore diameter is shifted slightly to 12.5 nm for HPW/SBA-15 (174 mg/g) and to 20.1 nm for HPW/SBA-15 (420 mg/g). As HPW is introduced the mesopore volume decreases, again strongly suggesting that HPW is deposited directly in the pores rather than on the external surface. It is again strange that that the mean pore diameter increases with HPW loading and could possibly be due to some slight restructuring within HPW.

b) Powder x-ray diffraction patterns for SBA-15 supported HPW

Powder XRD patterns are shown below for pure SBA-15 and supported HPW in Figure 17.

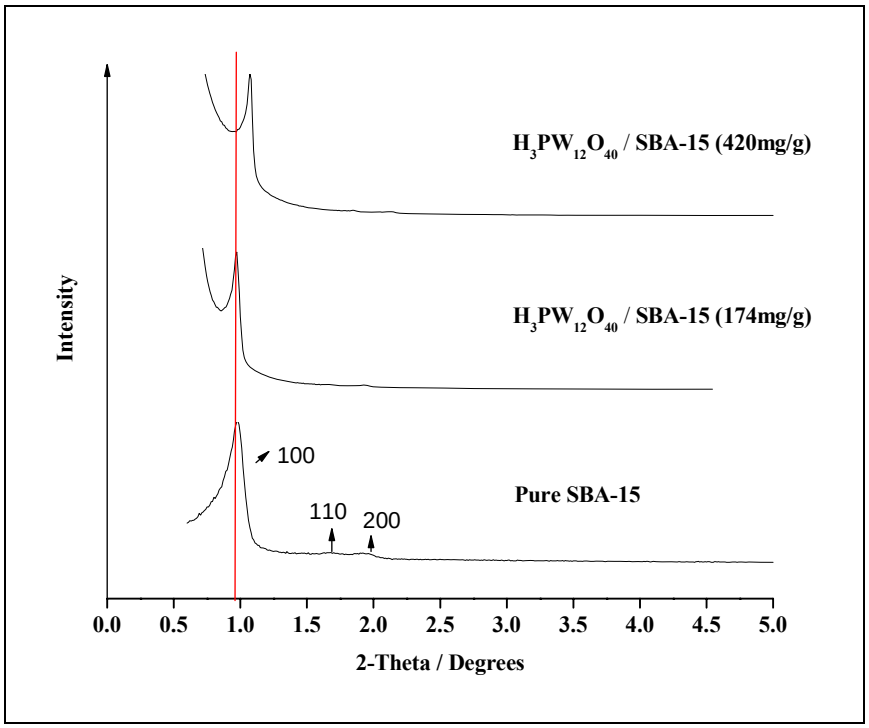

Figure 17: Powder x-ray diffraction patterns for SBA-15 supported $H_3PW_{12}O_{40}$ (HPW).

The powder XRD pattern of supported HPW's show that the long range order in the SBA-15 structure is retained even when high loadings of HPW are supported, but on impregnation diffractions from the (110) and (200) planes are of much lower intensity, possibly due to the dilution effect of HPW or possibly because a real fall in long range order in the structure has accompanied HPW deposition. The major reflections from the (100) plane surprisingly seem sharper for the SBA-15/HPW than for SBA-15 alone. It is not clear why this is the case. However there is also a slight change in 2-theta on depositing HPW from 0.98 ° to 1.07 °. This change together with the sharpened line, might suggest that some slight restructuring in SBA-15 occurs during the adsorption of HPW from water-ethanol solution.

2.3.1.2 Novacarb Carbon Supported Tungstophosphoric Heteropoly Acid

a) Nitrogen adsorption isotherms for Novacarb supported HPW

Isotherms are shown for Novacarb supported HPW in Figure 18 and data derived from them in Table 8.

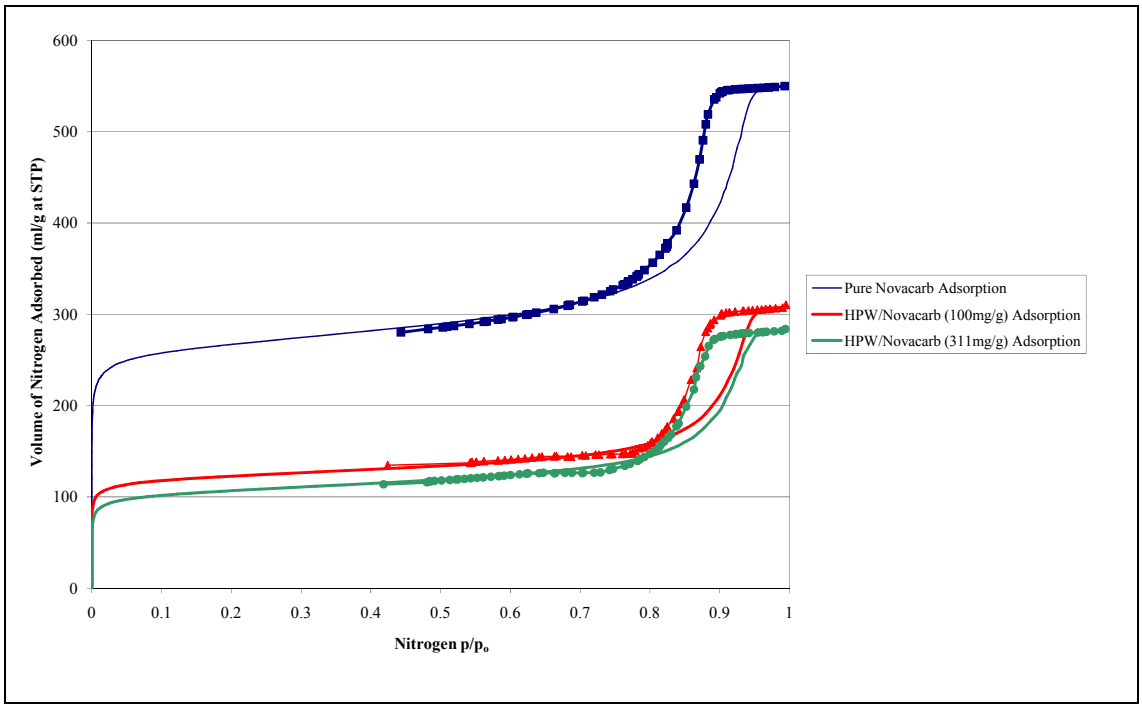

Figure 18: Nitrogen adsorption isotherms (-196 °C) – Novacarb supported $H_3PW_{12}O_{40}$ (HPW).

(Lines with symbols represent the desorption legs).

	N_2 BET Surface Area ($m^2.g^{-1}$)[a]	Mesopore Volume ($ml.g^{-1}$)[b] (>2 nm)	Micropore Volume ($ml.g^{-1}$)[c] (<2 nm)	Mean Pore Diameter (nm)[b]	Particle Size (nm)[b]		
					D_{10}	D_{50}	D_{90}
Novacarb	926	0.53	0.33	14.0	7.41	14.33	18.07
HPW/Novacarb (100 mg/g)	423	0.37	0.15	17.4	9.74	14.46	18.41
HPW/Novacarb (311 mg/g)	369	0.34	0.12	16.0	8.99	14.19	17.88

[a] Measured at -196 °C
[b] Calculated from desorption branch of isotherms using BJH method
[c] Calculated using t-plot method

Table 8: Surface and pore size distribution data for Novacarb supported $H_3PW_{12}O_{40}$ (HPW).

Pure Novacarb has a relatively large BET surface area and exhibits appreciable meso and microporosity. The distinct step in the N_2 isotherm at relative pressures of 0.8 – 0.9, suggests a significant mesopore volume and a relatively narrow pore size distribution for these mesopores (see Figure 18). The mean pore-size diameter for pure Novacarb is 14.0 nm. On impregnation of HPW, surface areas decrease and there is a reduction in both the mesopore and micropore volumes indicating that some HPW is adsorbed in the microporous structure as well as the mesoporous structure.

2.3.1.3 Sibunit Carbon Supported Tungstophosphoric Heteropoly Acid

a) Nitrogen adsorption isotherms for Sibunit supported HPW

Isotherms are shown for Sibunit and supported HPW on Sibunit in Figure 19 and data derived from them shown in Table 9.

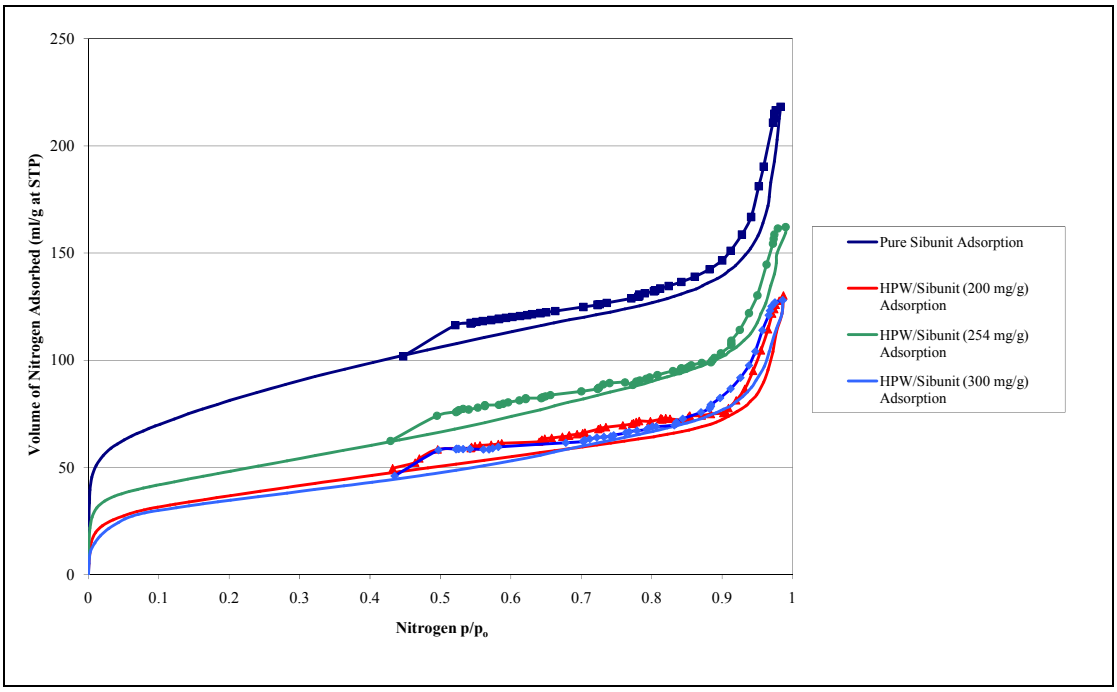

Figure 19: Nitrogen adsorption isotherms (-196 °C) – Sibunit supported $H_3PW_{12}O_{40}$ (HPW).

(Lines with symbols represent the desorption legs).

	N_2 BET Surface Area ($m^2.g^{-1}$)[a]	Mesopore Volume ($ml.g^{-1}$)[b] (>2 nm)	Micropore Volume ($ml.g^{-1}$)[c] (<2 nm)	Mean Pore Diameter (nm)[b]	Particle Size (nm)[b]		
					D_{10}	D_{50}	D_{90}
Sibunit	291	0.18	0.019	35.0	8.07	33.72	65.96
HPW/Sibunit (200 mg/g)	133	0.17	0.0055	31.7	4.45	26.63	66.20
HPW/Sibunit (254 mg/g)	171	0.18	0.013	30.3	5.33	25.22	65.13
HPW/Sibunit (300 mg/g)	125	0.15	0.0083	27.5	6.68	23.46	55.45

[a] Measured at -196 °C
[b] Calculated from desorption branch of isotherms using BJH method
[c] Calculated using t-plot method

Table 9: Surface and pore size distribution data for Sibunit supported $H_3PW_{12}O_{40}$ (HPW).

Compared to the Novacarb carbon, Sibunit has a relatively low BET surface area. It has low mesopore volume and microporosity is virtually zero on the basis of pores < 2 nm. The mean pore size diameter for Sibunit is 35.0 nm, which is much greater than for either Novacarb or SBA-15. Again the surface area and the mesopore volume decrease as HPW is introduced as would be

expected if HPW fills pores. An odd result is given by Sibunit with a loading of 254 mg HPW as the surface area is higher than expected. This possibly suggests that the actual HPW loading on this material is somewhat different to the nominal loading of 254 mg HPW/g. The NH_3 adsorption data detailed later supports the idea that HPW loading in the sample is lower than the nominal value.

Overall when HPW is supported, it dramatically decreases the BET surface areas of the supports, and the pore volume. This suggests that, with all three supports, HPW does, as anticipated deposit in the pores of the support material.

2.3.2 Acid Treated Montmorillonite Clays

2.3.2.1 'Fulcat 200 Series'

a) Nitrogen Adsorption

Figure 20 shows the adsorption/desorption isotherms for the 'Fulcat 200 series' montmorillonite clays and Table 10 shows the BET surface areas, pore volumes and mean pore diameters determined for them.

.

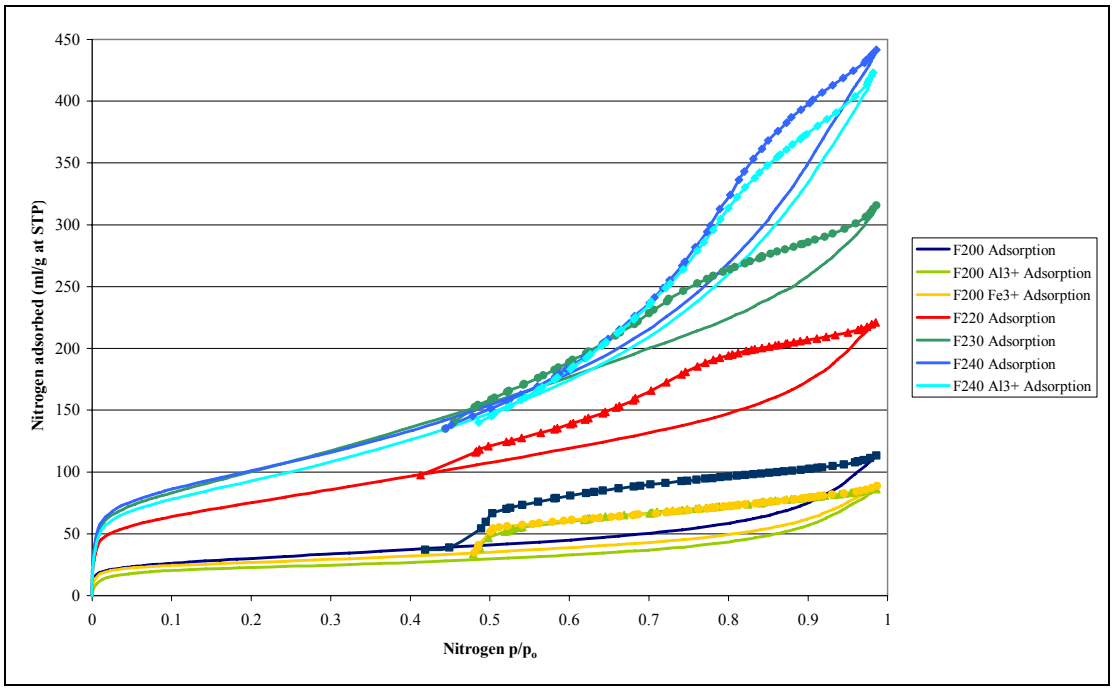

Figure 20: Nitrogen adsorption isotherms (-196 °C) – 'Fulcat 200 Series'.

(Lines with symbols represent the desorption legs)

	Surface Area ($m^2.g^{-1}$) (Rockwood)	Experimental N_2 BET Surface Area ($m^2.g^{-1}$)[a]	Mesopore Volume ($ml.g^{-1}$)[b] (>2 nm)	Micropore Volume ($ml.g^{-1}$)[c] (<2 nm)	Mean Pore Diameter (nm)[b]	Particle Size (nm)[b]		
						D_{10}	D_{50}	D_{90}
F200	100	108	0.145	-	12.0	3.95	4.98	29.13
F200 (Al^{3+})		81	0.134	-		3.88	4.55	19.37
F200 (Fe^{3+})		95	0.163	-	10.7	3.80	4.02	21.02
F220	180	271	0.233	-	12.3	4.45	7.16	22.70
F230	400	363	0.365	-	14.5	4.31	6.95	32.84
F240	430	364	0.635	-	13.5	4.73	8.90	24.01
F240 (Al^{3+})		335	0.605	-	14.1	4.66	8.61	28.75

[a] Measured at -196 °C
[b] Calculated from desorption branch of isotherms using BJH method
[c] Calculated using t-plot method

Table 10: Surface and pore size distribution data for the 'Fulcat 200 series' clays.

It is known that the acid activation is increased in the order F220, F230, and F240. This can be noted in the increase in the surface area, although determined surface area values are slightly lower than those quoted by the manufacturers for the most heavily treated clays. In all cases there is negligible microporosity but appreciable mesoporosity, and throughout the series the mesopore volume increases as would be expected as the clay is progressively delaminated and rendered amorphous.

b) Powder x-ray diffraction patterns for 'Fulcat 200 series'

The powder x-ray diffraction patterns shown below in Figure 21 for the 'Fulcat 200 series' show the parent clay Fulcat 200 to have definite crystallinity, as a broad peak can be seen at 5.8 ° which corresponds to the 001 reflection, and relates to a spacing of 1.53 nm between 001 layers. As the clay is acidified and metal ions are removed this reflection decreases in intensity, suggesting that delamination of the structure is occurring progressively on going from Fulcat 200 to 220 to 230 and to 240. Residual sharp peaks (2θ = 20 ° etc.) are consistent with insoluble and stable impurities such as cristobalite and quartz which are resistant to acid attack[17].

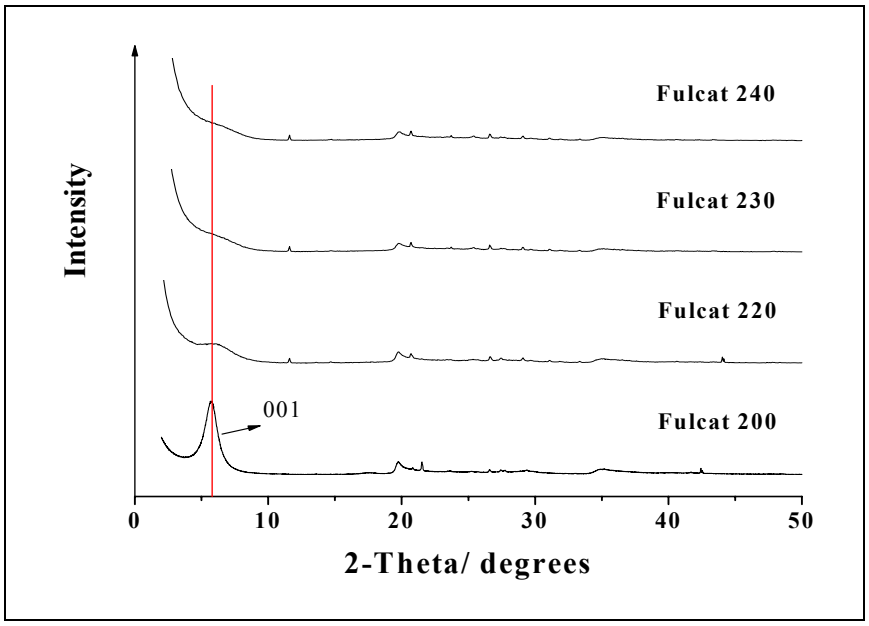

Figure 21: Powder x-ray diffraction patterns for the 'Fulcat 200 series' clays.

c) Elemental Analysis of 'Fulcat 200 series'

The elemental compositions of the 'Fulcat 200 series' clay catalysts are shown below in Table 11.

	F200 (Parent Clay)	F220 (Acid Activated)	F230 (Acid Activated)	F240 (Acid Activated)
Chemical Composition (w/w %)				
SiO_2	57.6	61.2	66.2	70.0
Al_2O_3	16.9	13.9	11.9	7.9
Fe_2O_3	8.1	5.9	4.7	4.2
CaO	3.1	1.9	2.6	2.6
MgO	3.6	2.7	2.1	1.3
K_2O	0.7	0.6	0.6	0.6
Na_2O	0.4	0.2	0.2	0.2

Table 11: Elemental compositions of 'Fulcat 200 series' clays.

In the 'Fulcat 200 series', the effects of progressive acid activation can be seen. As acid treatment progresses, Al_2O_3, Fe_2O_3 and MgO are stripped from the clay all at a similar rate and it becomes richer in SiO_2.

d) Cation exchange capacity (C.E.C.) of 'Fulcat 200 series'

To determine theoretical C.E.C. values for the Fulcats, it was assumed that every lattice Mg is isomorphously substituted for an aluminium atom in the octahedral lattice layer to give one lattice negative charge and therefore one equivalent exchange cation. Values calculated from elemental composition data appear below in Table 12.

Catalyst	MgO (%)	C.E.C. based on Mg content (± 5) meq $100g^{-1}$
Fulcat 200 Parent Clay	3.6	90
Fulcat 220 Acidified	2.7	68
Fulcat 230 Acidified	2.1	53
Fulcat 240 Acidified	1.3	33

Table 12: C.E.C. values for the 'Fulcat 200 series' clays.

Although in montmorillonites isomorphous substitution of Mg for Al is the principle source of cation exchange capacity, it is not unusual for there to be minor amounts of other substitutions which do the same. For instance, there is sometimes a little substitution of Al for Si in the tetrahedral layer. However, when typical compositions of natural montmorillonite are examined such secondary substitution generally accounts for less than 5 % of the exchange capacity[18]. With this is mind, the value for C.E.C. calculated here are generally regarded as minimum values with the possibility that actual values could be a few percent higher, and they are assigned an appropriate confidence limit.

2.3.2.2 'K-series'

a) Nitrogen adsorption data for the 'K-series'

Figure 22 shows the adsorption/desorption isotherms for the 'K-series' clays and Table 13 shows the BET surface areas, pore volumes and mean pore diameters determined for them.

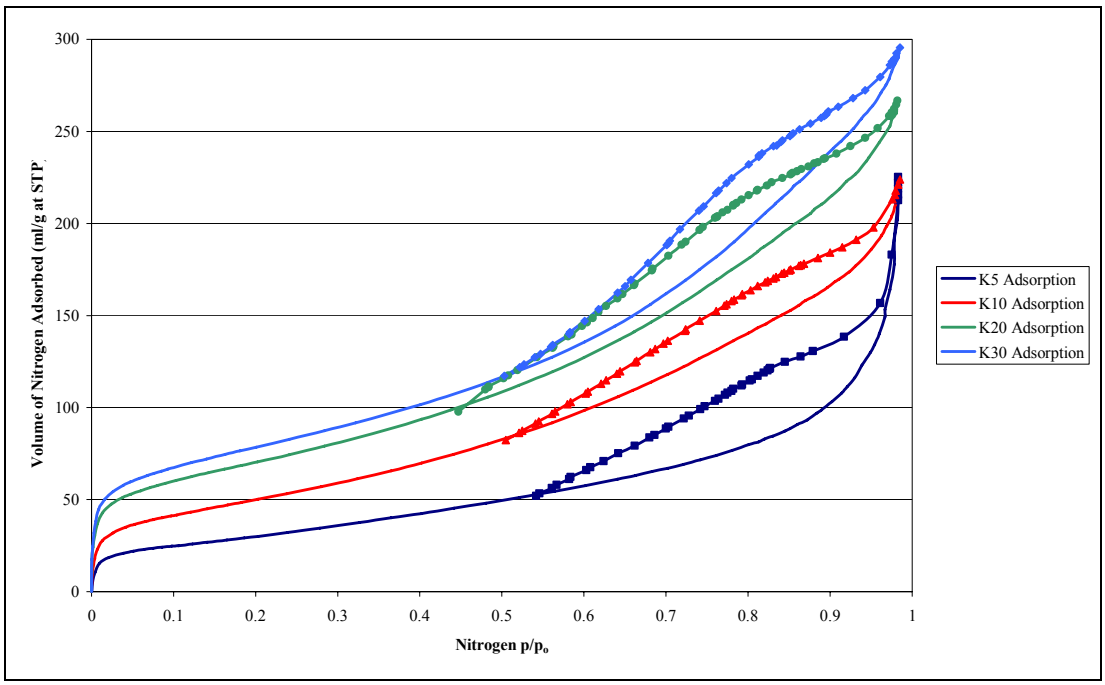

Figure 22: Nitrogen adsorption isotherms (-196 °C) – 'K-series'.

(Lines with symbols represent the desorption legs)

	Surface Area ($m^2.g^{-1}$) (Süd-Chemie)	Experimental N_2 BET Surface Area ($m^2.g^{-1}$)[a]	Mesopore Volume ($ml.g^{-1}$)[b] (>2 nm)	Micropore Volume ($ml.g^{-1}$)[c] (<2 nm)	Mean Pore Diameter (nm)[b]	Particle Size (nm)[b]		
						D_{10}	D_{50}	D_{90}
K5	140	108	0.375	-	34.7	4.36	10.7	101
K10	230	181	0.319	-	18.9	4.32	7.56	60.3
K20	240	253	0.349	-	14.4	4.40	7.03	35.1
K30	230	282	0.402	-	14.7	4.46	7.45	34.8

[a] Measured at -196 °C
[b] Calculated from desorption branch of isotherms using BJH method
[c] Calculated using t-plot method

Table 13: Surface and pore size distribution data for 'K-series' catalysts.

The data shows an increase in surface area throughout the 'K-series', with K30 having the largest BET surface area which is in line with progressive acid treatment and delamination of the structure. The table also shows the acid treated clays to be mesoporous materials with very little microporosity, and as the clay is progressively acid treated the diameter of the pores is significantly reduced. It is not clear why this might occur and it is not seen in the 'Fulcat 200 series'.

Throughout the 'Fulcat 200 series' the BET surface areas increase in line with increasing level of acid treatment to 364 $m^2.g^{-1}$ for Fulcat 240. This is also the case for the 'K-series' but it is not clear if further acid treatment would continue to increase surface area measurements. It has been shown that the surface area of acid treated clays reaches a maximum and then on further acid treatment decreases[19]. This has been explained by the clay delaminating further and increasing surface area, followed by a collapse of the open delaminated structured to form a largely siliceous amorphous material with a lower surface area. Both series show a high degree of mesoporosity though the 'Fulcat 200 series' show lower mean pore diameters than the 'K-series'. It is odd that for the 'K-series' mean pore diameter decreases with acid treatment whereas for the Fulcats the reverse is seen.

b) Powder x-ray diffraction patterns for the 'K-series'

Figure 23 below shows the powder XRD patterns for the 'K-series' clays. It can be seen that as the clay is progressively acidified the peaks in the pattern become less distinct suggesting that the structure is becoming more amorphous, with a dramatic decrease occurring beyond K5 The basal (001) reflection at 2θ of 5.9 ° present for K5 corresponds to a spacing of 1.50 nm. A number of small but relatively sharp peaks are also seen, notably at 2θ of 21.8 ° and 27 ° respectively for all clays in the 'K-series'. These peaks are again consistent with impurities cristobalite and quartz which are resistant to acid attack.

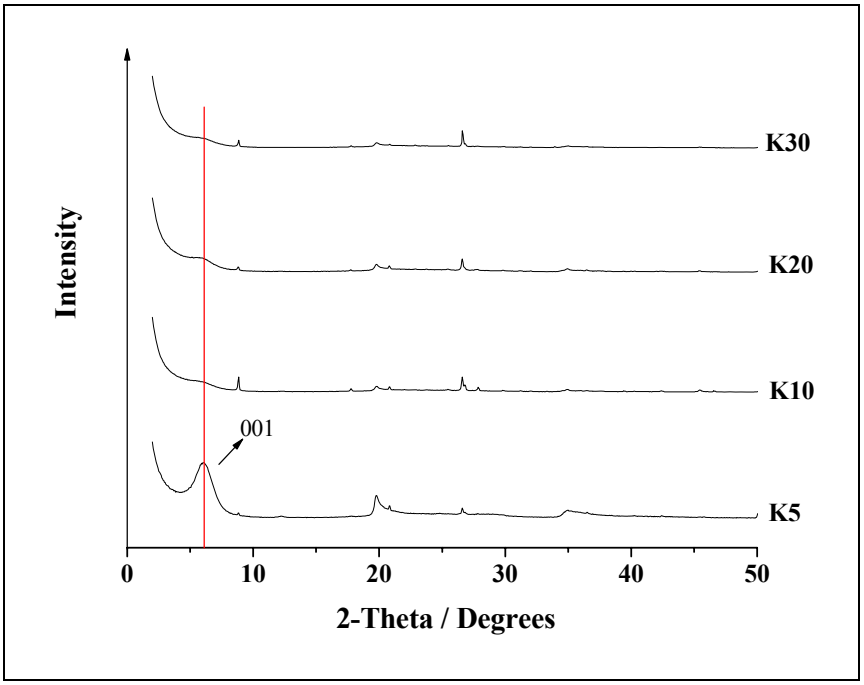

Figure 23: Powder x-ray diffraction patterns for the 'K-series' catalysts.

The powder x-ray diffraction patterns for the 'Fulcat 200 series' (Figure 21) and the 'K-series' above (Figure 23) show the parent clay Fulcat 200 and the first of the activated 'K-series', K5 to have definite crystallinity, as a broad peak can be seen for each clay at 5.8 - 5.9 ° which corresponds to the 001 reflection. As the clay is acidified and metal ions are removed this reflection decreases in intensity, suggesting that delamination of the structure is occurring.

c) Elemental Analysis of 'K-series'

Table 14 below shows that on acidification of the clay the percentage of SiO_2 increases as expected whilst percentages of Al_2O_3 and Fe_2O_3 decrease. Relatively low percentages of CaO, MgO, and Na_2O are maintained throughout. The rate of leaching for Al_2O_3 is also greater than that of Fe_2O_3.

	F200 (Parent Clay)	F220 (Acid Activated)	F230 (Acid Activated)	F240 (Acid Activated)	K5 (Acid Activated)	K10 (Acid Activated)	K20 (Acid Activated)	K30 (Acid Activated)
Chemical Composition (w/w %)								
SiO_2	57.6	61.2	66.2	70.0	65.0	73.0	75.0	80.0
Al_2O_3	16.9	13.9	11.9	7.9	19.0	14.0	12.5	10.0
Fe_2O_3	8.1	5.9	4.7	4.2	4.8	2.7	2.4	1.8
CaO	3.1	1.9	2.6	2.6	0.2	0.2	0.3	0.2
MgO	3.6	2.7	2.1	1.3	2.4	1.1	1.2	1.0
K_2O	0.7	0.6	0.6	0.6	1.5	1.9	1.5	0.5
Na_2O	0.4	0.2	0.2	0.2	0.3	0.6	0.3	0.3

Table 14: Elemental compositions of 'Fulcat 200 series' and 'K-series' clays.

When the elemental compositions shown above in Table 14 are compared, it can be seen that the 'K-series' clays show higher SiO_2 and Al_2O_3 contents than the 'Fulcat 200 series' on acid treatment. This increase in the SiO_2 content would suggest that the structure is more delaminated in the 'K-series' and therefore higher surface areas would be expected. BET surface area measurements in Table 13 do not agree with this expectation and it is unclear why this is the case. On the other hand Fulcat clays retain a much higher percentage of Fe_2O_3 and MgO when acid treated. Therefore it would be expected that the concentration of acid sites might be greater in the Fulcats if it is assumed that acid sites are associated with ion exchange sites and that negative lattice charge is provided when Mg^{2+} replaces Al^{3+} in the lattice.

d) Cation exchange capacity (C.E.C.) of 'K-series'

Again to determine theoretical C.E.C. values for the 'K-series' it was assumed that every lattice Mg is isomorphously substituted for an aluminium atom in the octahedral lattice layer to give one lattice negative charge and therefore one equivalent exchange cation. Values calculated from elemental composition data appear below in Table 15.

Catalyst	MgO (%)	Süd-Chemie C.E.C. meq $100g^{-1}$	C.E.C. based on Mg content (± 5) meq $100g^{-1}$
K5 Acidified	2.4	55	60
K10 Acidified	1.1	30	28
K20 Acidified	1.2	35	30
K30 Acidified	1.0	30	25

Table 15: C.E.C. values for the 'K-series' clays.

The results show reasonably good agreement between the company C.E.C. determined values and the C.E.C. values for the 'K-series' based on the Mg content. On progressive acidification C.E.C. decreases as expected as the structure is leached of metal ions and delamination occurs. The relatively high Mg content and the high C.E.C. suggest that K20 might have received less, rather than more, acid treatment than K10. Indeed the XRD patterns shown in Figure 23 also suggest that K20 may be less severely acid treated as it has a more laminar structure and long-range order than K10. However, contrary evidence is that the BET surface area of K20 is higher than for K10, consistent with K20 having received the longer treatment. These differences are difficult to explain and consequently the explanations for differences between K10 and K20 have to be understood in the context of some uncertainty over how they were prepared.

In comparison between the two clay series, the theoretically determined C.E.C. values (Table 12 and Table 15) show that the 'Fulcat 200 series' have higher C.E.C.'s throughout the series. This is due to the 'Fulcat 200 series' retaining a greater amount of MgO within the lattice. Importantly, with respect to acidity this suggests that there might be a higher concentration of acid sites on the Fulcats than the 'K-series' clays.

It is worth pointing out here that, in acid treated clays, the nature of the Brønsted acid sites is quite well understood. When montmorillonite clays are acid treated, H^+ firstly occupies the exchange sites, but through auto-transformation Al tends to dissolve from the lattice to give the Al^{3+} form, and it is generally accepted that it is this form which is stable and is used as an acid catalyst[20].

2.3.3 Zeolites

a) Nitrogen adsorption isotherms for zeolites

Isotherms are shown for zeolites, H-ZSM-5 with varying Si:Al ratios and also zeolite β in Figure 24 and data derived from this in Table 16.

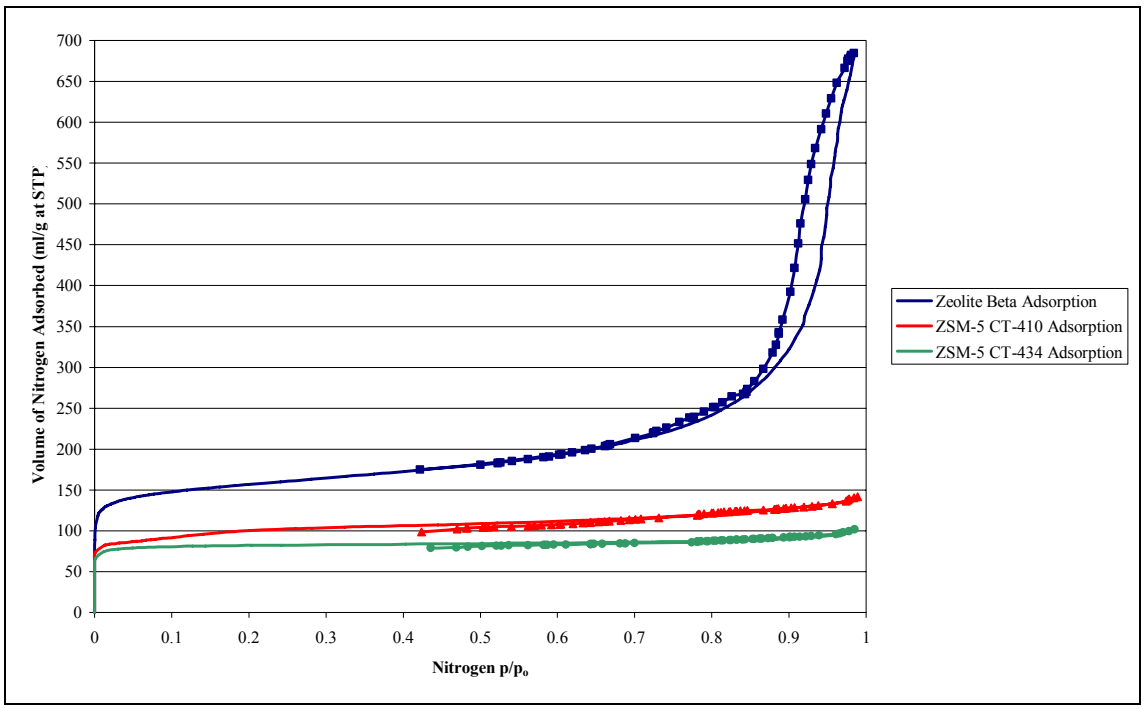

Figure 24: Nitrogen adsorption isotherms (-196 °C) – Zeolite beta and zeolite H-ZSM-5.

(Lines with symbols represent the desorption legs)

	N_2 BET Surface Area ($m^2.g^{-1}$)[a]	Mesopore Volume ($ml.g^{-1}$)[b] (>2 nm)	Micropore Volume ($ml.g^{-1}$)[c] (<2 nm)	Mean Pore Diameter (nm)[b]	Particle Size (nm)[b]		
					D_{10}	D_{50}	D_{90}
Zeolite Beta Si:Al = 37.5	541	0.964	0.156	25.1	9.11	22.1	43.9
CT410 ZSM-5 Si:Al = 27.5	353	0.0781	0.0844	24.7	4.79	9.72	76.9
CT434 ZSM-5 Si:Al = 40	281	0.0418	0.115	28.9	4.60	14.3	84.0

[a] Measured by nitrogen adsorption at -196 °C
[b] Calculated from desorption branch of isotherms using BJH method
[c] Calculated using t-plot method

Table 16: Surface and pore size distribution data for zeolites.

The investigated zeolites have relatively high BET surface areas and contain both microporosity and mesoporosity, though ZSM-5 is essentially microporous. As the Si:Al ratio increases the surface area falls along with the mesopore volume for H-ZSM-5. It is not clear where mesoporosity comes from. One possible explanation for this is that these pores represent inter-particle pores. Zeolite β is shown to have a much higher surface area than either H-ZSM-5 and is essentially mesoporous.

b) Powder x-ray diffraction patterns for zeolites

Powder XRD patterns are shown below for H-ZSM-5 (Si:Al = 40) and zeolite β (Si:Al=37.5) in Figure 17. They show that crystallinity of the zeolite samples was satisfactory and in accordance with literature data[21]. As zeolite β was not calcined beforehand the XRD pattern is not quite as well defined as powder XRD in the literature.

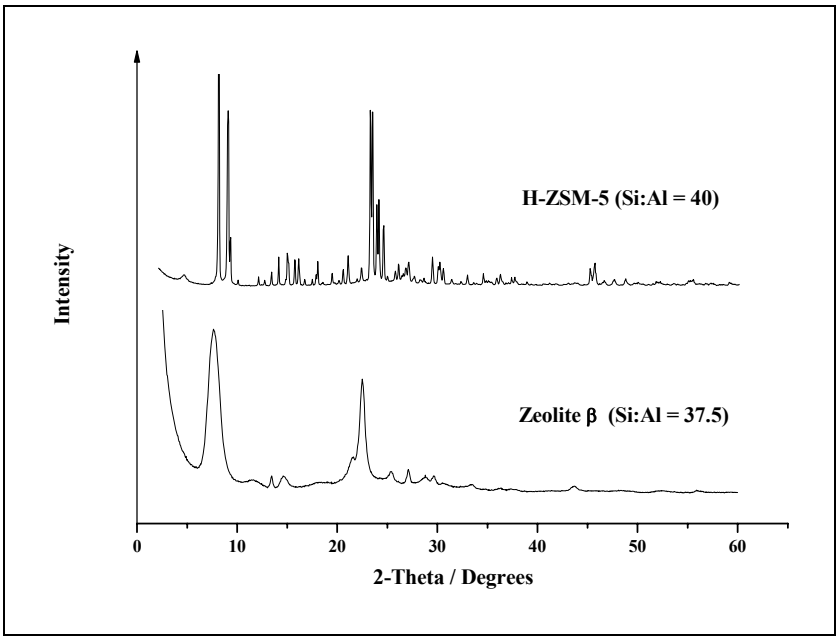

Figure 25: Powder x-ray diffraction patterns for H-ZSM-5 (Si:Al=40) and zeolite β (Si:Al=37.5).

2.3.4 Sulfonated Polystyrene Ion Exchange Resins

a) Cation exchange capacity (C.E.C.) of sulfonated polystyrene ion exchange resins

The cation exchange capacities for sulfonated polystyrene ion exchange resins determined from acid-base titration are shown below in Table 17. These were shown to be reproducible.

Increasing sulfonation ↓

Catalyst	Manufacturers C.E.C. value meq g^{-1}	C.E.C. (± 0.2) meq g^{-1} (by acid-base titration)
Amberlyst 15	4.70	5.30
Amberlyst 35	5.30	5.36
Amberlyst 36	5.50	6.19
CT 175	4.90	4.94
CT 275	5.20 (min)	5.33

Table 17: C.E.C.'s for Purolite and Amberlyst sulfonated ion exchange resins determined from acid base titration based on dry weight.

The results above show a relatively good agreement between the companies' C.E.C. values and the experimental values for the Purolite CT-175 and CT-275 resins, and it can be seen that as sulfonation increases, the cation exchange capacity also increases. For the Amberlyst series a difference can be seen between the measurements. It is not clear why this difference was found. The measured C.E.C.'s are consistently high compared to the manufacturers' claim. One possible explanation is that somehow the water content of the resins was overestimated although this seems unlikely. Another possible explanation is that the resins contained entrained acid not supported on the polymer. Both, however seem unlikely.

b) Effective Dry Weights of Sulfonated Polystyrene Ion Exchange Resins

A summary table of water contents for the Purolite 'CT' range and Rohm & Haas 'Amberlyst' range is shown below in Table 18. The weights of resins after dehydration were successive readings until constant mass was reached.

	Amberlyst 15	Amberlyst 35	Amberlyst 36	CT-175	CT-275
Mass of fully hydrated resin before heating (g)	0.1552	0.1536	0.1555	0.1558	0.1550
Average mass of resin after heating (g)	0.0704 0.0696 0.0694 **0.0694**	0.0712 0.0700 0.0699 **0.0699**	0.0791 0.0759 0.0747 **0.0747**	0.0713 0.07010 0.0707 **0.0707**	0.0721 0.0711 0.0709 **0.0709**
% Resin	44.7 ± 0.3	45.5 ± 0.3	48.0 ± 0.3	45.4 ± 0.3	45.7 ± 0.3
% Water	55.3 ± 0.3	54.5 ± 0.3	52.0 ± 0.3	54.6 ± 0.3	54.3 ± 0.3

Table 18: Percentages of water present in the studied sulfonated polystyrene ion exchange resins.

Ion exchange resins are very hygroscopic as they adsorb roughly their own weight in water. Water contents for all resins were found to be similar.

All resins studied are macroporous resins, which are in the form of spherical beads with mean diameters between 0.5 – 1.2 mm. Due to their open pore "macroreticular" structure based on cross-linked styrene divinylbenzene copolymers, it is not possible to describe them as conventional solids as active sites exist throughout the structure rather than just on the surface. Access to these acid sites depends upon the extent to which the solvent solvates and swells the resin, and the ease

with which probe molecules can diffuse through the resin to the active sites, giving little meaning to quoting BET surface areas.

Data reported in Table 17 and Table 18 show the C.E.C. and water contents of the fully hydrated resins. The C.E.C. is directly related to the degree of sulfonation, and water content is also affected by the degree of sulfonation because the amount of sulfonation controls the hydrophilicity of the resin.

[1] A. Lapkin, B. Bozkaya, T. Mays, Catal. Today, 81 (2003) 611-621.

[2] V.B. Fenelonov, V.A. Likholobov, A.Y. Derevyankin, M.S. Mel'gunov, Catal. Today, 42 (1998) 341-345.

[3] D. Zhao, J. Sun, Q. Li, G.D. Stucky, Chem. Mater., 12 (2000) 275-279.

[4] D. Zhao, Science, 1008, 279, 548-552.

[5] L.R. Pizzio, C.V. Cacers, M.N. Blanco, App. Catal. A:Gen., 167 (1998) 283-294.

[6]Rockwood 'Fulcat 200 series' literature. Retrieved 8th May 2007 from http://www.fulcat.us/product_bulletins.asp.

[7] Süd-Chemie company literature, 2001.

[8]Rohm and Haas 'Amberlyst series' literature. Retrieved 8th May 2007 from http://www.rohmhaas.com/ionexchange/IP/sac.htm.

[9]Purolite 'CT-series' literature. Retrieved 8th May 2007 from http://www.purolite.com/datasheet.php?cat=2.

[10] K.S.W. Sing, D.H. Everett, R.A.W. Haul, L. Moscou, R.A. Pierotti, J. Rouquerol, T. Siemieniewska, Pure Appl. Chem., 57 (4) (1985) 603-619.

[11] D.H. Everett, "The Structure and Properties of Porous Materials", Eds; D.H. Everett & F.S. Stone, Butterworths (1958) p 95.

[12] E.P. Barrett, L.G. Joyner, P.P. Halenda, J. Am. Chem. Soc., 73 (1) (1951) 373-380.

[13] D.M. Moore, R.C. Reynolds, Jr., "X-Ray diffraction and the identification and analysis of clay minerals", Oxford University Press (1989) pp 116-117.

[14] S. Koujout, B.M. Kiernan, D.R. Brown, H.G.M. Edwards, J.A. Dale, S. Plant, Catal. Lett., 85 (1-2) (2003) 33-40.

[15] C.E. Harland, "Ion Exchange: Theory & Practice - 2nd Edition", Royal Society of Chemistry Paperbacks (1994) p.73.

[16] D. Zhao, J. Sun, Q. Li, G.D. Stucky, Chem. Mater., 12 (2000) 275-279.

[17] M.L. Occelli, A. Auroux, G.J. Ray, Micro. Meso. Mat., 39 (2000) 43-56.

[18] A.C.D. Newman, "Chemistry of Clays and Clay Minerals", Ed. A.C.D. Newman, Mineralogical Society Monograph 6, Longman Scientific and Technical (1987) p49.

[19] C.N. Rhodes, J. Massam, D.R. Brown, Acta Universitatis Carolinaes Geologica, 38 (1994) 367-380.

[20] D.R. Brown, C.N. Rhodes, Catal. Lett., 45 (1997) 35-40.

[21] M. M. J. Treacy and J. B. Higgins, "Collection of Simulated XRD Powder Patterns for Zeolites – fourth edition", Elsevier: Amsterdam, 2001, pp 81 & 239.

CHAPTER THREE

MEASUREMENT OF SURFACE ACIDITY USING MICROCALORIMETRY

Section 1 – Theory

3.1.1 Introduction to surface acidity

The concentration of acid sites on a solid surface controls the surface acidity and is commonly expressed as the number of mmol of acid sites per unit weight or per unit of surface area of the solid[1]. It is usually defined relative to a base used in acid-base reactions. A solid acid can therefore be understood as a solid that changes the colour of a basic indicator or a solid which is able to chemically adsorb a base. In terms of Brønsted acidity, the solid acid should donate, or partially donate, a proton to a Brønsted base to generate the conjugate acid, which can become associated with an anion on the surface. In relation to Lewis acidity the acid surface site reacts with a Lewis base and a co-ordinate bond is formed (see Chapter 1, Section 1.1.3.1).

The various techniques used to measure surface acidity have been introduced in Chapter 1, Section 1.1.5 and their relative merits considered. For the work reported in this thesis, base adsorption microcalorimetry has been chosen to measure surface acidity.

3.1.2 Measuring ΔU or ΔH

Calorimetry involves the measurement of heat. A way is needed to keep track of energy changes in a system as energy is transferred in and out, but at the same time acknowledge that heat and work are equivalent. This acknowledgement is provided by a property called the internal energy, U, of the system, which is a measure of the 'energy reserves' of the system. The energy transferred to the system as work is w and q is the energy transferred to it as heat. For calorimetry purposes, it is the change in internal energy, ΔU that is of interest. A change in internal energy is written:

$$\Delta U = w + q. \qquad \textbf{(3.1)}$$

If a system is at constant volume, the system can do no expansion work, so if pressure/volume work is the only type involved $w = 0$ and the equation above can be simplified to:

$$\Delta U = q. \qquad \textbf{(3.2)}$$

However if a system is at constant pressure, and the volume of a system changes, the system can perform expansion work. Therefore

$$w = -p\Delta V$$
$$\text{so: } \Delta U = q - p\,\Delta V \qquad \textbf{(3.3)}$$

where p is pressure and ΔV is the change in volume. To avoid the complication of having to take into account the work of expansion, the idea of enthalpy of a system, H, is introduced, where:

$$H = U + pV$$
$$\textit{Therefore } \Delta H = \Delta U + p\Delta V + V\Delta p. \qquad \textbf{(3.4)}$$

So if pressure is constant then $V\Delta p = 0$, so

$$\Delta H = \Delta U + p\Delta V$$
$$\textit{And } \therefore\ \Delta H = (-p\Delta V + q) + p\Delta V$$
$$\textit{And } \therefore\ \Delta H = q. \qquad \textbf{(3.5)}$$

We can therefore conclude that the change in enthalpy is equal to the heat absorbed by the system at constant pressure. The calorimeter measures heat entering the calorimeter and we assume that $q_{cal} = -q_{sys} = -\Delta H_{sys}$. As this reported study has been undertaken at constant pressure, the molar enthalpy of adsorption, $\Delta H°$, has been used rather than $\Delta U°$.[2] In this work $\Delta H°_{ads}$ will be referred to as $-Q_{diff}$ as heats produced are exothermic.

Since heterogeneous catalysts require adsorption of a reactant as a step of the reaction mechanism, a correlation exists between the amount of chemisorbed reactant and the adsorption heats (see Chapter One, section 1.1.6.6). Therefore the basic principle of this work is that the enthalpy of adsorption/reaction of a base on an acid site is a measure of the strength of that acid site[3].

3.1.3 Chemisorption and Physisorption

3.1.3.1 Chemisorption

Chemisorption is an abbreviation of 'chemical adsorption' and describes the process by which a strong chemical bond is formed between a surface and an adsorbate. It is usually formed by a covalent or ionic bond and involves the exchange of electrons between the adsorbing molecule and the surface. The enthalpy of chemisorption is generally greater than that for physisorption with the distance between the surface and adsorbate being typically shorter. There is also usually a large degree of specificity in the interactions of different adsorbates with different substrate surfaces[4,5].

3.1.3.2 Physisorption

Physisorption is an abbreviation of 'physical adsorption' and involves the balancing of weak attractive forces, for example Van Der Waals forces, between the adsorbate and the surface. The process is always exothermic, though the energy given out is low, typically in the region of -10 to -80 $kJ.mol^{-1}$. Physisorption tends to be non-specific and any atom or molecule can adsorb onto the surface under the right conditions[4, 5]. Physisorption typically occurs below -80 $kJ\ mol^{-1}$ when using ammonia as a base probe[6]. An important characteristic of physisorption is that this type of adsorption is often easily reversed and physisorbed adsorbate can frequently be forced to desorb from a surface by raising the temperature of the surface a moderate amount. This is largely not the case for chemisorption since the chemical bond formed between surface and adsorbate frequently cannot be broken without a very substantial temperature rise, often of hundreds of degrees i.e. the adsorbate is irreversibly adsorbed. Throughout this work the terms chemisorbed and physisorbed will be used interchangeably with irreversibly and reversibly adsorbed respectively.

3.1.3.3 Effects of Temperature on Adsorption

When performing a base adsorption experiment on a typical solid acid catalyst both physisorption and chemisorption (on acid sites) occur simultaneously. The contribution of physisorption increases as the temperature is reduced, so typically experiments are performed at temperatures in excess of 100 °C when measurement of chemisorbed ammonia is required. There will however always be a significant contribution from physisorbed adsorbate to the total amount of base adsorbed at equilibrium. It is possible to differentiate between physisorption and chemisorption by

recording a typical adsorption isotherm followed by application of a vacuum and then a repeat adsorption isotherm[7]. The isotherms are both recorded until essentially surface saturation is achieved. The idea is that only physisorbed adsorbate is removed after the first adsorption experiment so the second adsorption isotherm corresponds only to physisorbed adsorbate re-adsorbing[8]. This is shown below in Figure 26.

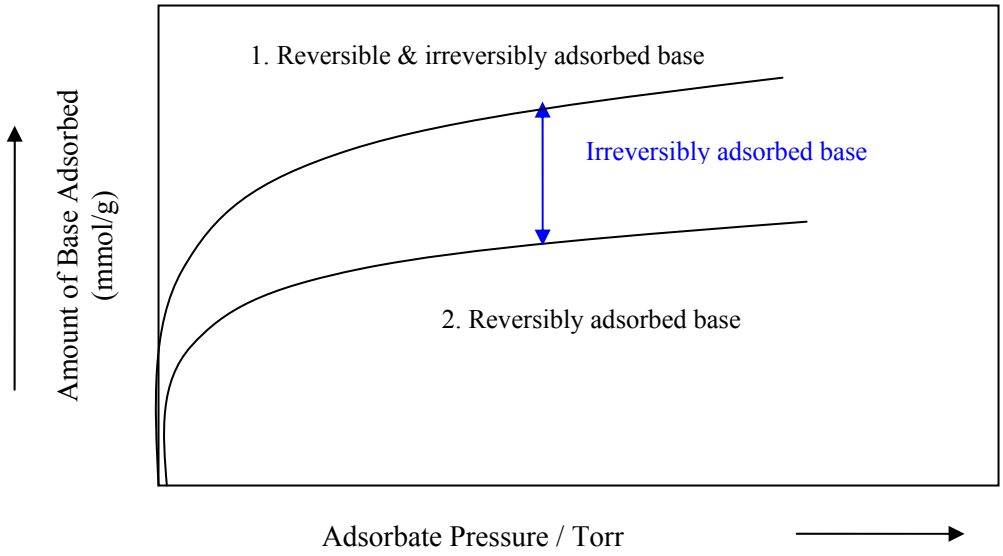

Figure 26: Two-cycle base adsorption isotherms.

3.1.4 Introduction to Base Adsorption Microcalorimetry

3.1.4.1 Types of Calorimeter

Depending on the measuring principle there are three types of calorimeter:

a) *Heat Accumulation Calorimeters*

These types of calorimeter allow for a rise in temperature of the reaction system for an exothermic reaction and a decrease in temperature for endothermic reactions. The quantity of heat absorbed or evolved can be calculated from this change in temperature as a function of time. An adiabatic solution calorimeter is typical of this type.

b) *Heat Exchange Calorimeters*

These calorimeters actively exchange heat between the sample and surroundings, often during a temperature scanning experiment. When an event occurs in the calorimeter, which absorbs or emits heat, the heat flow rate can be determined by the temperature difference along the thermal resistance between the sample and surroundings and is recorded. Heat flux DSC uses this principle.

c) *Heat Conduction (Isothermal) Calorimeters*

These operate at constant temperature, and measure the conduction of heat between the sample and the surroundings required for this. Because the temperature must remain constant, evolved or absorbed heat must be compensated for by either bringing in heat or by pumping it out. Sometimes this is achieved by using a relatively large heat sink as the surroundings for the system (sample). They often have a high degree of sensitivity.

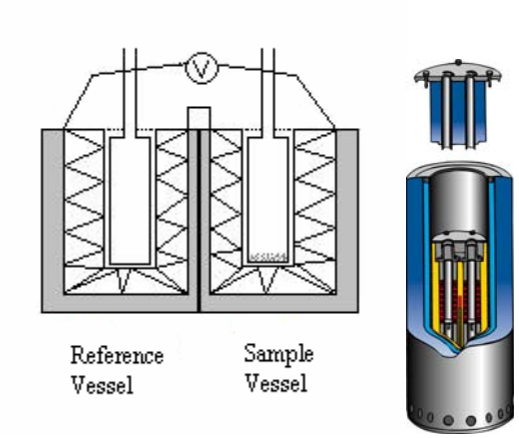

Figure 27: Schematic of a Setaram C80 microcalorimeter.[9]

A Setaram C80 Tian-Calvet microcalorimeter as shown above in Figure 27, which has been used in the reported study, follows this principle. The principle behind heat flow measurement in a Tian-Calvet microcalorimeter is the use of thermocouples which are used to measure the temperature difference between the system and the surroundings as a function of time. A thermocouple consists of a closed circuit of two dissimilar metals with two junctions that are connected to the sample and the surroundings. A potential difference is generated when a temperature difference exists between the junctions. Thermocouples can be arranged in a series called a thermopile allowing heat flow to be determined with much greater sensitivity. These thermopiles are represented above in Figure 27. There is an identical assembly of two vessels situated in the same calorimetric block, which are set-up as sample and reference vessels where

thermopiles are connected "back-to-back". Voltage is therefore only detected if the heat flow from the sample cell is different from the reference cell. This differential mode compensates for fluctuations occurring in the calorimeter temperature, resulting in high stability[10].

3.1.4.2 Types of Basic Probe Gases

The adsorption of basic molecules i.e. ammonia, pyridine, n-butylamine has been extensively studied using adsorption microcalorimetry[11, 12]. Ammonia is almost certainly the most widely studied[13, 14, 15].

Ammonia is a reliable basic probe molecule for surface acidity due to its small size (diameter 3Å). Also it does not usually undergo any chemical decomposition or reaction other than to form NH_4^+. It is a medium strength base in water and has a pK_B of 4.75 (at 25 °C) at atmospheric pressure which lies between pyridine a weaker base (8.75) and ethylamine a stronger base (3.19).[16] In the gas phase, proton affinity (PA) is a better measure of basicity, and for ammonia PA is 846 $kJ.mol^{-1}$. Pyridine which is a stronger base in the gas phase has a PA of 912 $kJ.mol^{-1}$.[17] Ammonia has been used as the base probe in the following studies.

Section 2 – Experimental: Method Development

This section will examine the experimental setup used for NH_3 adsorption microcalorimetry and the steps taken to provide the most accurate results in characterizing solid acids as adsorbents and as catalysts (discussed in Chapters 4 & 5).

3.2.1 NH_3 Adsorption Microcalorimetry

3.2.1.1 Gas Handling System

Ammonia is introduced to the sample through a custom-made glass volumetric gas handling system comprising of blown Pyrex glass fittings, connected using Cajon fittings and Rotulex 'ball and socket' joints. The system encompasses two main sections i) the manifold (coloured in red in Figure 28) and ii) the cells (coloured in green in Figure 28). This system allows a dosing volume of ammonia held in the manifold to be presented to the sample in the cells. The calibration bulb is

present to allow for the calibration of the volumes of the manifold and cells, and by keeping the calibration bulb open, it can effectively become part of the manifold and hence the dosage volume is increased.

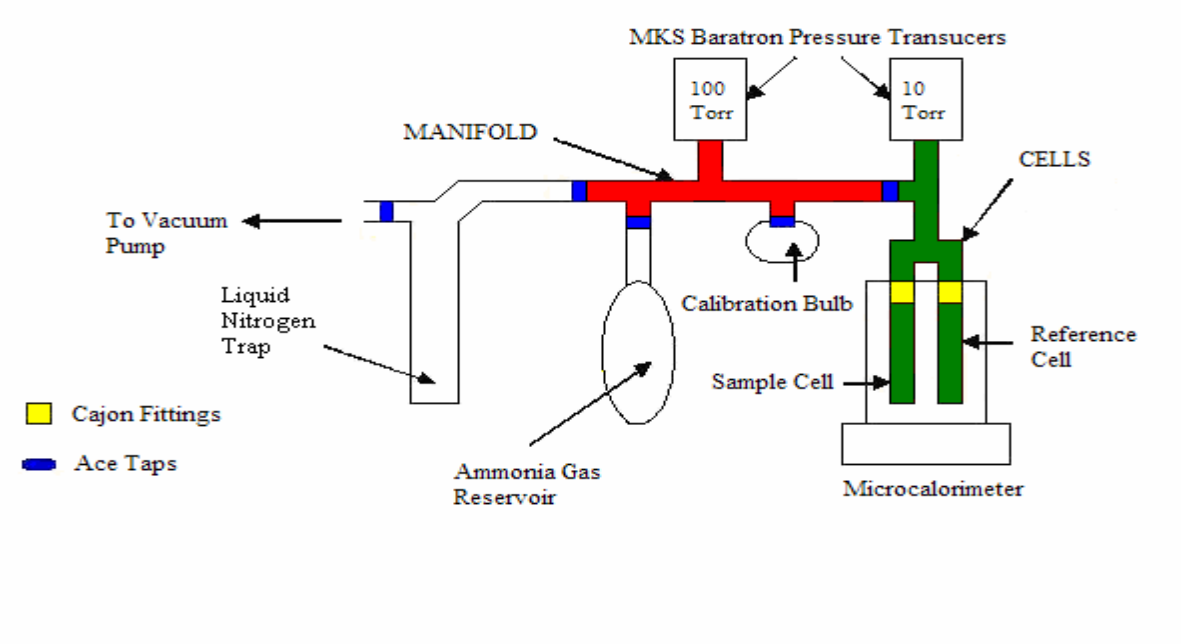

Figure 28: Representation of Setaram C80 microcalorimeter and custom-made volumetric gas handling system.

Pressure is measured using MKS Baratron pressure transducers. The manifold Baratron measures up to 100 torr to one decimal place and the cell Baratron measures up to 10 torr to two decimal places (see Figure 28 above). The cells can be disconnected to add/remove sample. Once a sample is in the sample cell (reference cell empty) the system is evacuated and held under dynamic vacuum of 10^{-2} torr to allow for sample activation. The system is then isolated from the vacuum and ammonia admitted to the manifold and the sample. Doses of ammonia are added until the sample is saturated.

3.2.1.2 Calorimeter

The calorimeter used in this investigation was a Tian-Calvet type differential microcalorimeter Setaram C80. It was electrically calibrated using a Setaram Joule Calibration Cell.

The C80 was connected to a computer using the Setaram Setsoft control software through which data could be acquired. The microcalorimeter measures the differential heat flow of sample vs. reference (mW) against time (s). The heat trace below (Figure 29) gives an example of a typical experiment in which ammonia has been adsorbed as a series of equal sized doses onto a sulfonated polystyrene ion exchange resin.

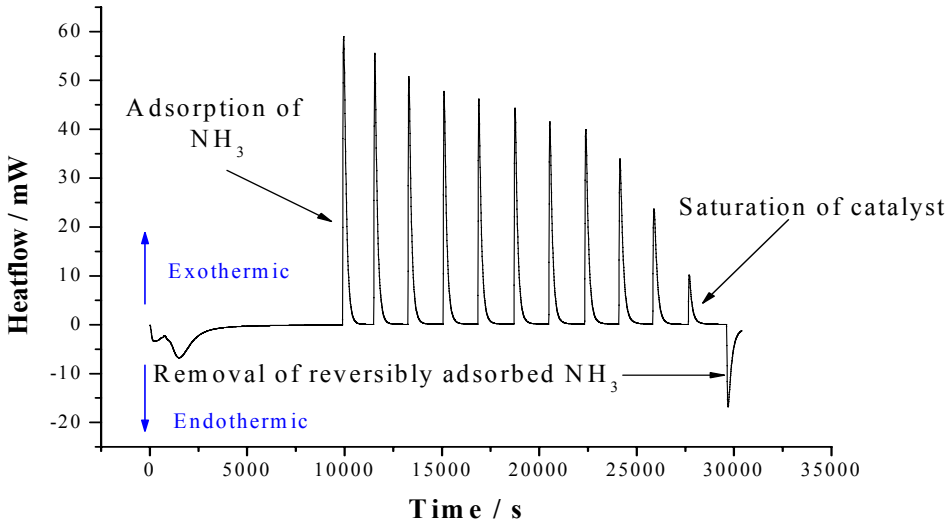

Figure 29: Heat flow trace from the C80 microcalorimeter for ammonia adsorption onto a solid acid catalyst.

Heat flow peaks start off being similar in height and width, but as acid sites became progressively saturated with ammonia and either the amount of ammonia per pulse being adsorbed falls or simply the heat per pulse falls, the peaks become smaller. The endotherm at the end of the experiment is due to desorption of reversibly adsorbed ammonia which occurs when the system is opened to the vacuum pump. Through integration of each peak using the Setsoft software, the energy in joules associated with ammonia adsorption is calculated for each NH_3 injection.

3.2.1.3 Assessing importance of experimental design in adsorption experiments

a) Volume Calibration

To determine the size of ammonia pulses, the volumes of the manifold and cells of the gas handling system detailed in Section 3.2.1.1 were calibrated separately from the calorimeter. To do this the calibration bulb was removed from the gas handling system and weighed at room temperature (~25 °C). It was then weighed again after filling with distilled water. The difference in weight was used to determine the volume of the calibration bulb, assuming the density of water is 0.997 g.cm^{-3} at 25 °C[18]. The volume of the calibration bulb was found to be 17.90 (±0.05) cm^3, after repeating the weighing procedure five times. This will be referred to as $\mathbf{V_1}$.

In the calibration process, a fixed body of gas of known volume and pressure was allowed to expand from the calibration bulb into the previously evacuated manifold, then into the cells. The gas pressure was recorded after the first expansion into the manifold and after the second into the cells. The volume of the manifold ($\mathbf{V_m}$) and the volume of the cells ($\mathbf{V_c}$) were determined using this pressure data and also the known volume of the calibration bulb ($\mathbf{V_1}$). This is described in further detail below.

To obtain calibration graphs, volumes were obtained over a range of gas pressures. To determine the manifold and cell volumes, the gas handling system was firstly evacuated, and then depending on the gas used, either air, ammonia or helium was introduced into the calibration bulb and the manifold until a specific pressure was achieved, this pressure was then recorded as $\mathbf{P_1}$ (the pressure in the manifold and calibration bulb). For calculation of each calibration point, a different initial pressure of gas was used and ranged between 2.5 torr and 100 torr. The calibration bulb was then isolated and the manifold evacuated. After evacuation the manifold was again isolated and the gas in the calibration bulb allowed to expand into the manifold ($\mathbf{V_1} + \mathbf{V_m}$). This pressure was recorded as $\mathbf{P_2}$ (the pressure in the manifold). The tap separating the cells from the manifold was then opened and ammonia allowed to expand into the formerly evacuated cells before being closed again. A third pressure was recorded, $\mathbf{P_3}$ (pressure in the cells). This procedure was carried out with the calorimeter at 30, 100 and 150 °C respectively and the gas handling system at room temperature (25 ± 1 °C). The volumes of the manifold and the cells when calculated using Boyles Law assumes that the entire system was isothermal. Because the system was not isothermal, the

volumes used to calculate the amount of ammonia in the system at any time can be described as 'effective volumes'. Essentially they are the volumes at an effective constant temperature of 25 ± 1 °C.

Knowing the volume of the calibration bulb (V_1), the volume of the manifold, V_m, and the cells, V_c were calculated using equations (1) and (2) shown below.

Manifold volume (**V_m**) determined by:-

$$P_1V_1 = P_2 (V_1+V_m)$$

Rearranging $$V_m = \frac{P_1V_1}{P_2} - V_1 \qquad (\mathbf{3.6})$$

V_m is the manifold volume.

P_1 is the pressure in the manifold + calibration bulb.

V_1 is the volume of the calibration bulb which we already know.

P_2 is the pressure after expansion into the manifold.

Cell volume (**V_c**) determined by:-

$$P_1V_1 = P_3 (V_1+V_m+V_c)$$

Rearranging $$V_c = \frac{P_1V_1}{P_3} - V_1 - V_m \qquad (\mathbf{3.7})$$

V_c is the cell volume.

P_1, V_1, and V_m are shown above.

P_3 is the pressure after expansion into the cells.

Calibration was attempted using helium, air, and ammonia. Helium and air were used as it was expected that there would be relatively little chance of them being adsorbed onto the walls of the gas handling system. Ammonia was used as a calibration gas as this would be the gas being used in all experiments. Calibration data for the manifold and the cells with the calorimeter set at 100 °C is shown below in Figure 30 and Figure 31:

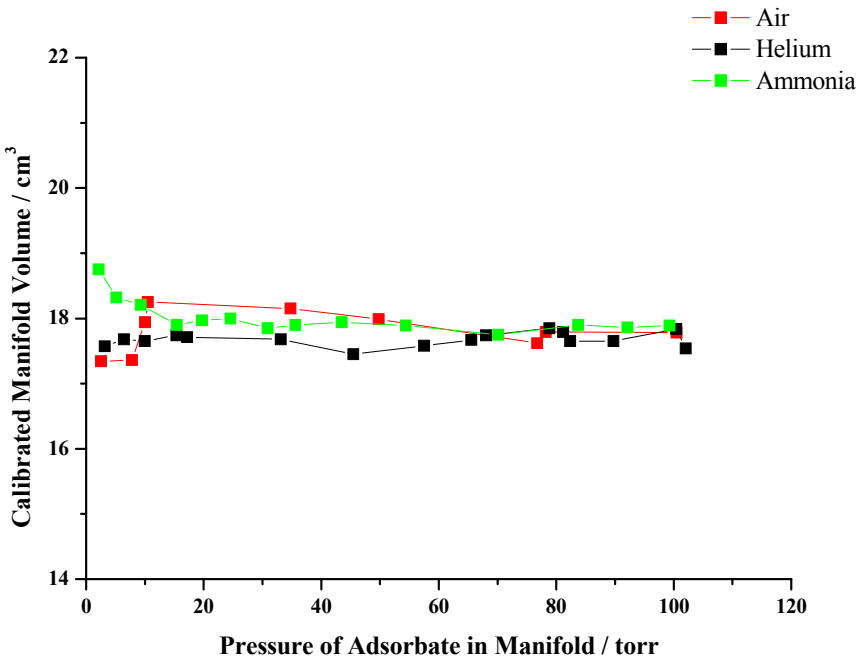

Figure 30: Calibration of the manifold at 100 °C using air, ammonia, and helium.

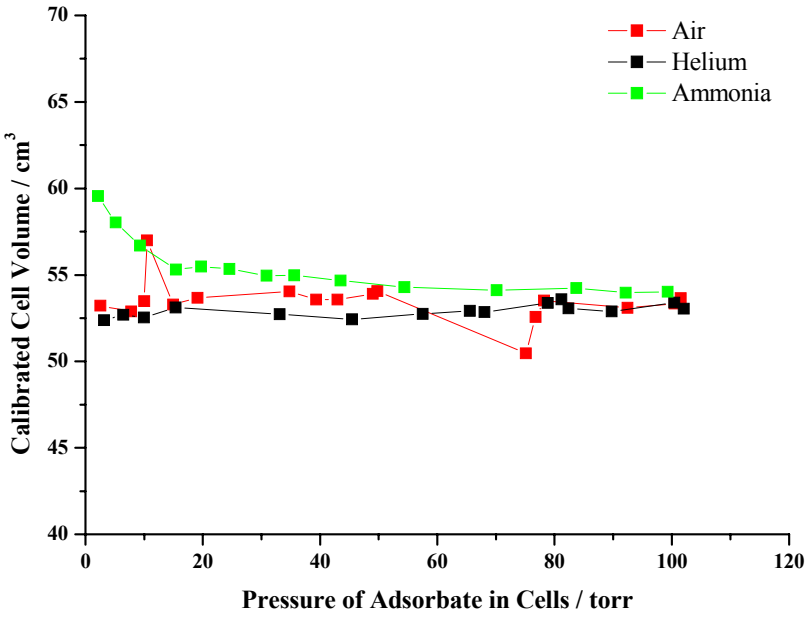

Figure 31: Calibration of the cells at 100 °C using air, ammonia, and helium.

Experiments were performed using air, helium, and ammonia with a range of starting gas pressures in the calibration bulb. The resultant calculated volumes are shown in Figure 30 and Figure 31, which plot volume of either the cells or the manifold versus manifold or cell pressure, it can be seen that both ammonia and to a lesser extent air give different volumes at low pressures, but give similar volumes to helium at high pressure. This could be explained by the adsorption and desorption of ammonia gas on to the glass walls when entering and leaving the manifold and the cells. For the experiments reported later, volumes determined using helium have been used on the assumption that it will adsorb least on to the glass of the gas handling system and volumes are closest to the "real" volumes. The average volumes for the manifold and cells are noted below in Table 19.

	CALORIMETER TEMPERATURE (^{o}C)			
	30	100	150	200
Effective Manifold volume (cm^3)	17.8 ± 0.1	17.8 ± 0.1	17.7 ± 0.1	17.7 ± 0.1
Effective cell volume (cm^3)	59.0 ± 7.4	52.3 ± 7.4	48.7 ± 7.4	46.2 ± 7.4

Table 19: Effective manifold and cell volumes at various temperatures.

(Volume data using helium)

As some solid acids have relatively low concentrations of acid sites it is useful to be able to vary the volume of the ammonia dose. The dose of ammonia could either be in the manifold alone or it could be allowed to enter the calibration bulb as well giving a larger volume of gas. Therefore the volume calibration had to be performed with the tap between the calibration bulb and manifold both open and closed (bearing in mind the volume of the tap barrel). Small differences in manifold volumes were found (Table 20).

Shown below in Table 20 is a comparison of the manifold and cells volumes using helium as an adsorbate when keeping the calibration bulb open and also when it is closed.

	CALORIMETER TEMPERATURE (^{o}C)			
	30	100	150	200
Manifold volume with calibration bulb open (cm^3)	17.8 ± 0.1	17.8 ± 0.1	17.7 ± 0.1	17.7 ± 0.1
Manifold volume with calibration bulb closed (cm^3)	17.4 ± 0.1	17.4 ± 0.1	17.3 ± 0.1	17.3 ± 0.1
Effective cell volume with calibration bulb open (cm^3)	59.0 ± 7.4	52.3 ± 7.4	48.7 ± 7.4	46.2 ± 7.4
Effective cell volume with calibration bulb closed (cm^3)	58.5 ± 7.8	51.4 ± 7.8	47.6 ± 7.8	45.2 ± 7.8

Table 20: Comparison of effective manifold and cell volumes at various temperatures when the calibration bulb is both open and closed.

(Volume data using helium)

Differences in the effective manifold and cell volumes are seen when the calibration bulb is open and closed. This is due to the calibration bulb tap barrel because when the tap is closed, gas is displaced by the tap therefore decreasing the manifold volume. Incidentally, this also applies to the tap between the manifold and the cells, and it was important that the volume of the cells was determined with this tap closed as this configuration was subsequently used in adsorption experiments.

Figure 32 below shows the calibrated volume of the manifold at the calorimeter temperatures in question, and the difference that the calibration bulb being either open or closed makes.

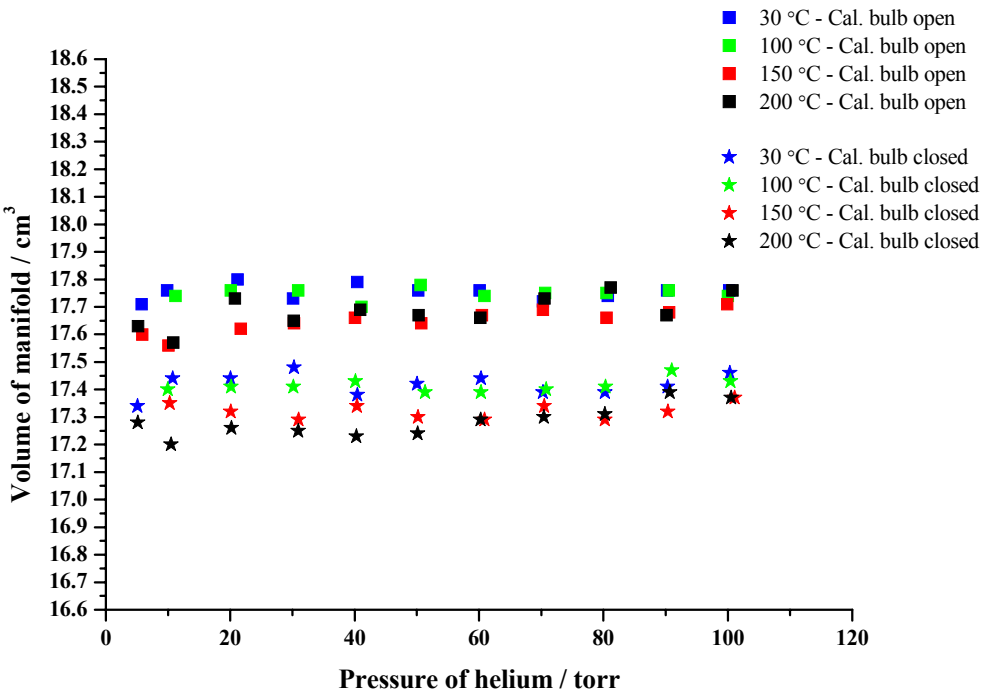

Figure 32: Calibration of the manifold volume at various calorimeter temperatures with the calibration bulb open and closed.

It is important to distinguish volume difference as errors in volumes affect the calculated surface coverage and therefore the molar enthalpies of adsorption. If the value for the volume of the manifold is too low, the calculated molar heats increase and the average surface coverage are erroneously low, and vice versa. For the purposes of this work where ammonia was used as the adsorbate, measures were taken to reduce adsorption on and off the walls of the glass handling system by reducing the necessary time that taps were opened for.

Because calibration (Figure 30 and Figure 31) shows a problem where ammonia adsorbs and desorbs off the walls of the gas inlet system the following procedure was adopted to minimise errors due to this effect. The sequence: "reading pressure ($P_{manifold}$) – opening tap between manifold and cells – closing tap – reading pressure ($P_{manifold}$)" was done as quickly as possible so that the dose could be calculated without error due to NH_3 adsorbing and desorbing on the walls of the glass volumetric system. The "dose" of NH_3 allowed into the cells was calculated from this quickly measured pressure drop in the manifold. To further improve the reproducibility, taps were all opened using the same number of turns for each run.

b) Determining the interval between ammonia pulses

It is essential that the interval between each NH_3 pulse introduced to the catalyst is long enough to allow pressure equilibration and the calorimeter output to return to baseline. A basic experimental procedure is introduced in sections 3.2.1.1 and 3.2.1.2. To determine intervals, an example of a typical Amberlyst 35 run (300 mg), and introducing pulses every 30 minutes was taken and the graph printed showing heat flow (mW) vs. time (s). When this graph was enlarged it showed that the calorimeter signals were returning to baseline more slowly than appeared at first (see Figure 33) and a step effect was beginning to form. It was wondered if this would affect the overall integration of the peaks and therefore it was decided to test this by increasing the interval between pulses from thirty minutes to one hour, two hours, and three hours.

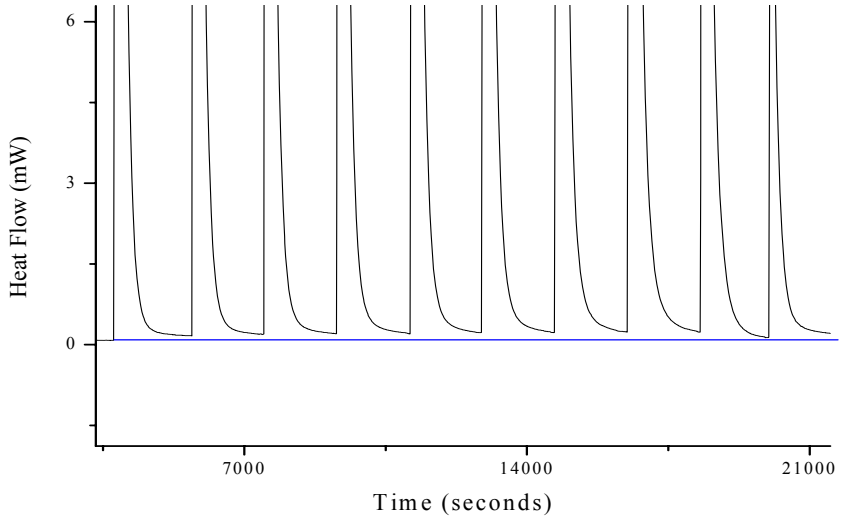

Figure 33: Graph to show step formation during a NH_3 adsorption experiment on the C80 microcalorimeter for a sulfonated polystyrene ion exchange resin.

(interval = 30 minutes)

For the typical run shown above in Figure 33, conditions were as follows:

1. Solid acid: Amberlyst 35 (300 mg as supplied).
2. Activated for 2 hours at 100 °C.

3. 50 torr pulses of ammonia (pressure of dose in the manifold, calibration bulb open).
4. 30 minute interval between each pulse.

For determining the affect of varying interval lengths between NH_3 pulses on the measured heat outputs, conditions were as follows (see Figure 34):

1. Solid acid: Amberlyst 35 (300 mg as supplied).
2. Activated for 2 hours at 100 °C.
3. 50 torr pulse of ammonia (pressure of dose in the manifold, calibration bulb open).
4. 30, 60, 120, and 240 minutes intervals between pulses.

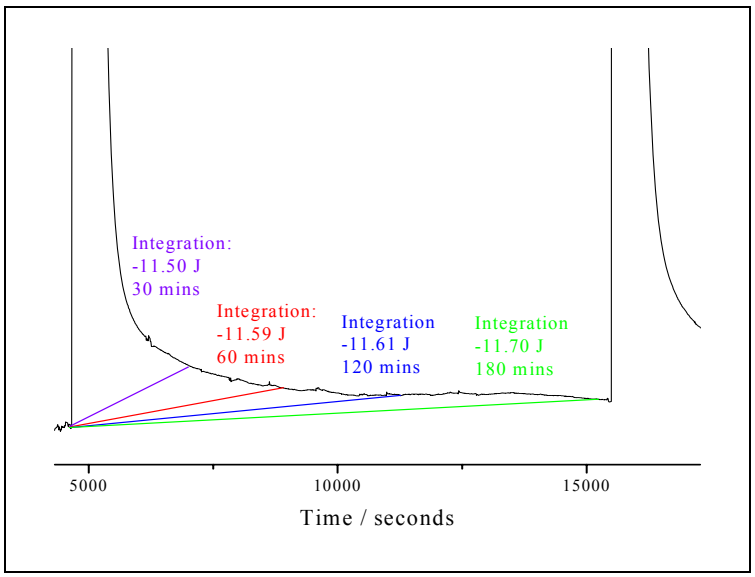

Figure 34: Heat output signals for NH_3 on Amberlyst 35 at 100 °C.

(Integration results for a peak taken at 30 minutes, 1hr, 2hr, and 3hr intervals)

The heat signals were integrated relative to a linear baseline which is drawn from the start of each peak (easily identified) to the start of the next peak. The object of this experiment was to quantify the effect of tailing of the heat output and to establish minimum time required for return to baseline at an acceptable level.

When the above was tested it showed that a pulse time of one hour compared to 30 minutes made less than 0.8 % difference to the enthalpy measured in joules. When the ammonia pulse was extended to two and three hours respectively slight increases in the peak areas was found. Even this made only a 1 % and 1.7 % difference to that of the integration value taken at 30 minutes. The

decision was taken to allow 30 minutes between consecutive pulses. This compromise meant that experiments could be performed in a reasonable time and kept errors due to any system/vacuum instability to a minimum. It was thought that errors incurred as a result of missing residual heat in the tail of each heat signal were less significant than those that would be introduced by prolonging the experiment excessively.

c) *Reproducibility*

The precision of data collected was assessed by making all measurements in triplicate using the same activation conditions and run conditions. The following example shows how reproducible the technique can be (Figure 35).

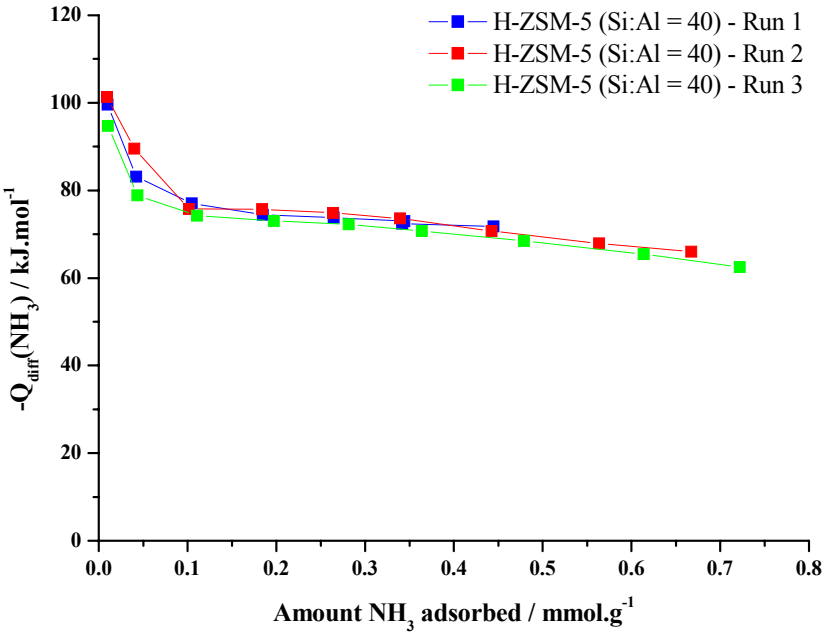

Figure 35: Reproducibility of samples using NH_3 base adsorption microcalorimetry.

The above runs (Figure 35) were obtained on consecutive days, using different samples of the same material from the same batch. All were activated for two hours in-situ at 150 °C, then isolated for 30 minutes so that the baseline could stabilise before introducing the first pulse of ammonia, at 150 °C. For each pulse the amount of ammonia adsorbed at equilibrium was calculated and, using the heat obtained by integrating the calorimeter output, an average molar

enthalpy of adsorption for that pulse determined. These molar enthalpies of adsorption values are plotted against the amount adsorbed. Note that molar enthalpies of adsorption of significantly less than 80 $kJ.mol^{-1}$ are generally assumed to be due to weakly adsorbed (physisorbed) ammonia, so the data plotted here is for a weakly adsorbing sample.

From the work described in this section it has become clear that careful choice of experimental conditions can improve the results whilst using base adsorption microcalorimetry as a technique. Calibration of the volumetric glassware was done using helium as this didn't interact with the glass surface unlike ammonia. Also depending on the temperature of the calorimeter and if the calibration bulb is open or closed, different manifold volumes can be used in calculations of surface coverage to improve precision (see section 3.2.1.3.a, Table 20). Samples were tested in triplicate to verify the results and demonstrate the level of reproducibility of the measurements. Time intervals of 30 minutes were decided on between ammonia pulses, and when integrating the peaks using the Setsoft software it was decided that the straight baseline added to the plots against which to integrate against would be drawn from the same points for each peak to minimise any errors.

[1] R.Sh. Mikhail, E. Robens, "Microstructure and Thermal Analysis of Solid Surfaces", John Wiley & Sons (1983) p. 219.

[2] P.W. Atkins, "The Elements of Physical Chemistry – Third Edition", Oxford University Press (2001) pp. 47-50.

[3] A. Auroux, Topics in Catalysis, 4 (1997) 71-89.

[4] E.M. McCash, "Surface Chemistry", Oxford University Press (2001) pp. 54-56.

[5] P.W. Atkins, "Physical Chemistry - Sixth Edition", Oxford University Press (1999) p. 857.

[6] M.J. Meziani, J. Zajac, D.J. Jones, S. Partyka, J. Rozière, A. Auroux, Langmuir, 16 (2000) 2262-2268.

[7] V. Solinas, I. Ferino, Catal. Today, 41 (1998) 179-189.

[8] A. Auroux, in: Catalyst Characterization: Physical Techniques for Solid Materials, Eds; B. Imelik & J.C. Vedrine, Plenum Press New York (1994) pp. 627-628.

[9] http://thermal-analysis.setaram.com/fichiers/produit/calos-lien3-a200394153164110.pdf- accessed on the 15.05.06.

[10] P.J. Haines, "Principles of Thermal Analysis and Calorimetry", Ed; P.J. Haines, RSC Paperbacks (2002) pp. 136-145.

[11] A. Auroux, "Catalyst Characterization: Physical Techniques for Solid Materials", Eds; B. Imelik & J.C. Vedrine, Plenum Press New York (1994) pp. 632-634.

[12] J.M. Guil, J.A. Perdigon-Melon, M.B. De Carvalho, A.P. Carvalho, J. Pires, Micropor. Mesopor. Mater. 51 (2) (2002) 145-154.

[13] D.R. Brown, A.J. Groszek, Langmuir 16 (2000) 4207-4212.

[14] C.P. Nicolaides, H.H. Hung, N.P. Makgoba, N.P. Sincadu, M.S. Scurrell, App. Catal. A:Gen., 223 (1-2) (2002) 29-33.

[15] B. Boddenburg, G.U. Rakhmatkariev, A. Wozniak, S. Hufnagel, Phys. Chem. Chem. Phys., 6 (2004) 2494-2501.

[16] P.W. Atkins, "The Elements of Physical Chemistry – Third Edition", Oxford University Press (2001) p. 169.

[17] G. Busca, Phys. Chem. Chem. Phys., 1 (1999) 723-736.

[18] 68th CRC handbook of chemistry and physics, CRC Press: Cleveland, Ohio, 1977.

CHAPTER FOUR

SUPPORTED TUNGSTOPHOSPHORIC HETEROPOLY ACIDS AS ADSORBENTS AND CATALYSTS

This chapter will consider the measurement of acidity for carbon and silica supported tungstophosphoric heteropoly acids using the technique of NH_3 adsorption microcalorimetry. Data has been collected at low temperature (30 °C) to determine if the solid acids above are suitable to use as adsorbents in gas separation processes. Acidity data has also been collected at high temperature (150 °C) for catalytic purposes, and compared to distinguish differences in acidity characteristics given by the various supported heteropoly acids. In Chapter 5 the comparison of the high temperature data for supported heteropoly acids will be compared with data obtained for the other solid acids examined.

Section 1 - Theory

4.1.1 Introduction

Keggin type heteropoly acids have been the subject of a large number of studies, and have found several commercial applications as redox and acid catalysts[1]. As the acids themselves are effectively non-porous they need to be supported on a porous solid or altered into microporous insoluble salts to acquire reasonably active heterogeneous catalytic activity[2]. Reports of potential applications of solid acid materials in separation processes are scarce and as separation processes are likely to operate at low temperatures, data on acidity and separation performance need to be determined under these conditions which are rather different from those typically used in catalytic applications. Most adsorption applications of polyoxometalates have dealt with the treatment of toxic organic compounds, the removal of flue gases such as NO_x and SO_2, and the removal of amines and mercaptants[3].

In the work reported here $H_3PW_{12}O_{40}$ supported on silica mesoporous molecular sieve SBA-15, and two synthetic mesoporous carbons has been investigated for potential application in separation processes such as the removal of basic molecular impurities (e.g. ammonia and amines) from air in ultra-pure manufacturing environments[4]. Work has been undertaken to fully characterize the strength and uniformity of acid adsorption sites using microcalorimetric measurements and NH_3 adsorption. Analysis of thermokinetic data has been undertaken to hopefully provide an insight into the rates of processes occurring during the sorption of ammonia and thus provide additional information for interpretation of the heat data for this purpose. The treatment of kinetic data during calorimetry experiments is considerably more developed in the area of reaction calorimetry, where deconvolution of the heat output curves as a function of reaction time using appropriate

models allows insight into the reaction mechanisms[5]. However, these models tend to be based on processes under kinetic control, and are usually not suitable for adsorption processes where mass transfer processes may be rate controlling. Quantitative treatment of the heat output curves in the case of sorption experiments, especially for complex materials, would be significantly more challenging. Therefore in this study rates of adsorption will be compared on the basis of heat peak width and shape, but rigorous modelling is not attempted.

4.1.2 Use of microcalorimetry to determine adsorption characteristics of adsorbents

Base adsorption microcalorimetry is a valuable method for determining solid acid characteristics such as acid strength, and also accessibility of acidic sites using basic probe molecules such as ammonia[6, 7, 8]. It is worth pointing out that for adsorption applications the accessibility and abundance of acid sites may be more important than the strength of acid sites, perhaps in contrast to catalytic applications where acid strength may be crucial.

4.1.3 Definition of thermokinetic parameters: cooling width at half peak maximum (CWHM) and cooling time constant (τ)

The use of thermokinetic parameters allows the judgement of the rates of processes occurring during the sorption of a test molecule. In a differential calorimeter an exothermic event is detected as an increase in the differential signal from the thermopiles which then returns to the baseline as the heat output dies away. Assuming the time constant for the calorimeter is small compared to the rate of heat decay, the rate at which the signal returns to the baseline is dependent on the rate of the process causing the exotherm. In previous similar studies this signal decay has been treated as an exponential decay and the cooling time constant (τ) has been used in the discussion of the diffusion of ammonia as a function of crystal structure of heteropoly acids[9]. Another way of treating the data is to use the peak width at half height (*referred to in this work as CWHM – Cooling Width at Half Peak Maximum*) as a measure of the rate of the process. One reason for using this is that it is easier to measure. The CWHM parameter is not linked to a specific mathematical model. It is somewhat similar to the "width at half height" measurement often used to characterize the width of chromatographic peaks. We believe that for all the data reported in this work, trends in CWHM width are essentially the same as the time constant if each peak is

treated as an exponential decay[10], and when the cooling time constant and the CWHM are compared it can be seen that the functional dependences of both parameters on ammonia uptake are very similar (see Figure 36 and Figure 37).

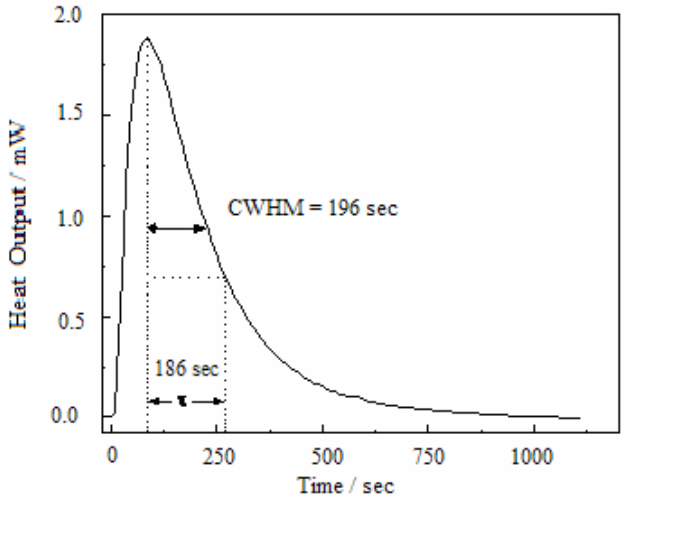

Figure 36: Example of thermokinetic parameter results, cooling constant τ and cooling width half maximum (CWHM).

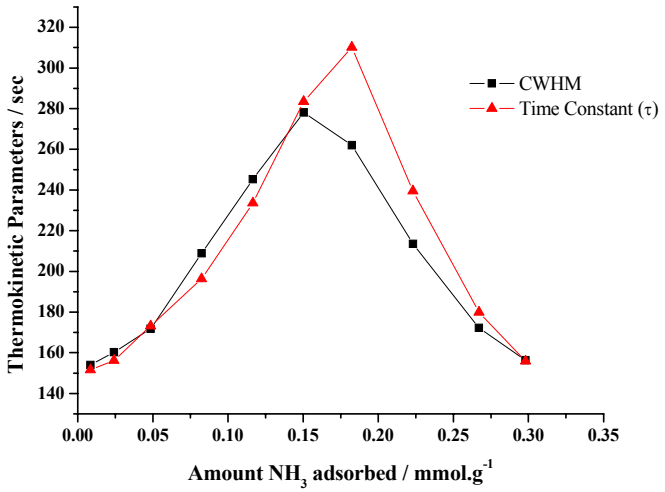

Figure 37: Comparison of thermokinetic parameters for successive microcalorimeter output signals through to saturation for the solid acid HPW/Sibunit (300 mg/g) at 150 °C.

The thermokinetic parameters shown in Figure 37 above represent successive additions of NH_3 to the solid acid Sibunit carbon with a 300 mg/g loading of HPW. From the heat output/time plots for each addition the CWHM and time constant (τ) for each pulse have been determined, as shown in Figure 36. These are plotted in Figure 37 against the amount of NH_3 adsorbed.

Calculation of the cooling time constant (τ) requires the assumption that the experimental cooling curve satisfies the exponential decay model, given by $W = W_0 e^{-t/\tau}$, where W is the power output at a given time, t, and W_0 is the power output at time zero (taken as the peak maximum).

When $t = \tau$ then

$$W = W_0 e^{-1} = \frac{W_0}{e}. \qquad (\mathbf{4.1})$$

So τ is the time taken for the power to decrease to $1/e\,th$ of the maximum value. The assumption that the heat signal decay is exponential is unlikely to be satisfied in the case of complex materials in which several phenomena occur simultaneously such as physical and chemical sorption and diffusion processes, so it seems reasonable that the width at half height (CWHM) be used as an indicator of the rate at which NH_3 diffuses to the adsorption sites, rather than the exponential τ. In order to obtain dimensionless values both parameters (τ and CWHM) can be normalised to the characteristic time constant (30 seconds) obtained during the calibration of this specific instrument. In the following work the normalized CWHM is used and kinetic heat output data shown as a function of the normalized cooling width at half peak maximum.

Section 2 - Experimental

Sample preparation of supported HPW samples has been described in Chapter 2, Section 2.1.1.3.

4.2.1 Activation conditions

For all low temperature adsorption experiments samples were activated externally at 150 °C using a similar experimental set-up to that described in Chapter 3, Section 3.2.1.1. This was done

outside the calorimeter as it was not feasible to heat the calorimeter up to temperature for activation of the samples and then cool it back down to 30 °C. The sample cell containing 150 mg sample was connected using Cajon fittings to the glass volumetric gas handling system linked to the vacuum pump. A supported vertical Lenton tube furnace was then raised up around the sample tube. The temperature of this furnace was controlled by a digital Eurotherm 818P programmer connected to the furnace thermocouple. For the purposes of activation the temperature programmer was set to 150 °C and run for 2 hours under vacuum (10^{-2} torr) prior to adsorption experiments. After activation the sample tube was quickly transferred to the calorimeter with as little exposure to air as possible. Activation occurred at 150 °C for 2 hours prior to NH_3 adsorption experiments at 150 °C.

4.2.2 Microcalorimeter conditions

All low temperature (30 °C) and high temperature (150 °C) NH_3 adsorption microcalorimetry measurements were performed using the Setaram C80 Tian-Calvet microcalorimeter described in Chapter 3 section 3.1.4.1 set at 30 °C and 150 °C respectively. In the experiments ammonia pulse sizes were determined using the calibrated volumes of the volumetric glassware (effective volumes at 25 °C were of course different when the calorimeter was at 30 °C and150 °C), and pressure measured by the MKS Baratron pressure transducer connected to the manifold. The amount of irreversibly adsorbed ammonia was determined via re-adsorption experiments as described below in 4.2.3.

4.2.3 Determination of chemisorbed (irreversibly adsorbed) NH_3

As well as reporting results of the NH_3 adsorption isotherms and distribution of heats of NH_3 adsorption with coverage, an attempt was made to determine the capacity for chemisorbed (irreversibly adsorbed) ammonia of the supported heteropoly acids, using a re-adsorption method. The first adsorption cycle consisted of a series of NH_3 pressure steps for which heat and pressure changes were recorded. When the amount of additional ammonia adsorption had fallen indicating that the adsorption isotherm was almost flat the system was then evacuated at the experimental temperature. This was intended to remove all reversibly adsorbed ammonia and a constant heat baseline used as an indicator that equilibrium was reached. A second adsorption experiment was then performed in a similar way to the first. The difference between the amounts of NH_3

adsorbing in the two experiments was assumed to correspond to the capacity of the sample for irreversibly adsorbed NH_3 as it was assumed that NH_3 adsorbing during the second experiment was all held reversibly on the sample, as shown below in Figure 38.

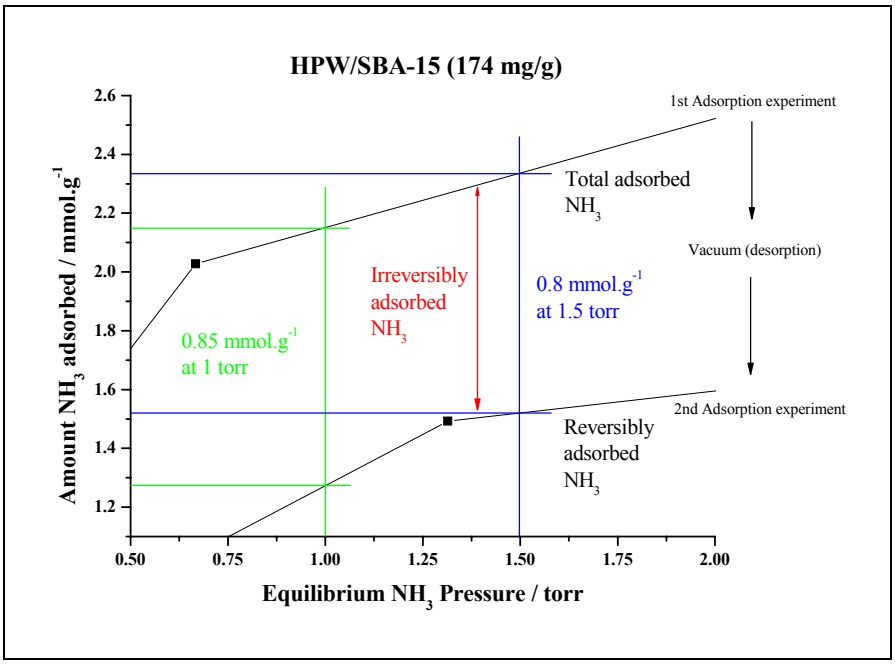

Figure 38: Example of determination of chemisorbed (irreversibly adsorbed) NH_3 from re-adsorption isotherms.

Figure 38 shows a magnified section of part of the isotherm where the isotherms start to level off. The initial isotherm (top line) shows the total adsorbed amount of ammonia whereas the re-adsorption leg is purely the amount of physisorbed (reversibly adsorbed) ammonia. Therefore the difference between the two values can be considered to be the irreversibly adsorbed amount of ammonia adsorbed.

Section 3 – Results & Discussion

A number of supported tungstophosphoric acids were investigated at 30 °C and 150 °C to determine acidity strengths and concentrations under "adsorbent" and "catalytic" conditions. Samples included pure silica SBA-15, SBA-15 supported HPW, the two carbons (Novacarb and Sibunit), and carbon supported HPW all with various loadings of HPW.

For each solid acid a comparison shall be made between low temperature and high temperature NH_3 adsorption isotherms, and using the re-adsorption method described above in Section 4.2.3, the amount of ammonia that is irreversibly adsorbed shall be determined and the stoichiometric ratio of HPW : $NH_{3(irr)}$ adsorption calculated.

Differential heats of NH_3 adsorption versus amount of NH_3 adsorbed for pure HPW and silica and carbon supported HPW samples based on the initial NH_3 adsorption isotherms are also presented. They will be described as distributions of acidity with coverage, as $-Q_{diff}(NH_3)$ can be taken to be representative of the strength of acid sites to which NH_3 is bound and the amount of NH_3 adsorbed is indicative of the concentration of acid sites available. In principle, it would be preferable to determine $-Q_{diff}(NH_3)$ for irreversibly adsorbed NH_3 only, since it is reasonable to assume that it is only this NH_3 which is bound to significantly acidic sites. However, this is not practical and attempts to do this by combining differences between the first and second adsorption isotherms with differences between the heat outputs measured during the collection of the two isotherms result in $-Q_{diff}(NH_3)$ values with a lot of uncertainty from which no conclusions can be drawn. Therefore differential heats of adsorption collected for each pulse of ammonia used to measure the first adsorption isotherm are plotted against the amount of ammonia adsorbed. Even though the measured $-Q_{diff}(NH_3)$ are weighted averages of three separate experiments, it is assumed that the profiles can be used as a rough comparison of acid site strength and concentration between the various supported HPW samples. A comparison will be made between these profiles at 30 °C and 150 °C as at low temperature the effectiveness of solid acids as adsorbents is of interest whereas at elevated temperatures the acid properties are relevant for predicting the catalytic properties of solid acids. Tabulated results are extracted from the profiles to give an indication of the strength of the strongest sites on a sample. To give an indication of the strength of acid sites $-Q_{diff}(NH_3)$ is taken at a coverage of 0.05 $mmol.g^{-1}$. The total surface coverage (irreversibly and reversibly adsorbed NH_3) is measured at the point at which $-Q_{diff}(NH_3)$ falls below 80 $kJ.mol^{-1}$ as this is the heat below which adsorption sites are not considered significantly acidic. This will provide a direct comparison between the various supported HPW samples. As an alternative it is possible to measure initial molar heats of NH_3 adsorption by extrapolating graphs back to zero coverage. Attempts have been made to determine these molar heats at zero coverage for all sample and these are shown in Appendix A. In general variations in these initial molar heat values reflect variations in the heats at 0.05 $mmol.g^{-1}$, with the initial molar heat values generally being 5-10 $kJ.mol^{-1}$ higher than the heats at 0.05 $mmol.g^{-1}$. However, these initial heats are not used in the work

reported here, in part because not all plots of differential heat of NH_3 adsorption versus amount NH_3 adsorbed show linearity, and the justification for making such linear extrapolations is questionable.

For each solid acid the rate of NH_3 adsorption is followed using the thermokinetic parameter, CWHM, with the idea being the smaller the value for CWHM the faster the adsorption and vice versa. Analysis of the heat output curves (ballistic curves) measured at 30 °C and 150 °C has been used to obtain the thermokinetic parameter, CWHM, recorded during the NH_3 adsorption microcalorimetry experiments for supported HPW samples. Results are shown below, and have been based on the first NH_3 adsorption isotherm only.

4.3.1 Pure $H_3PW_{12}O_{40}$ (HPW)

Re-crystallised HPW (from methanol) was used in the following measurements on the pure acid with no support material. Comparing first and second adsorption isotherms at the two temperatures, as shown in Figure 39, shows that the ammonia is nearly all irreversibly adsorbed, with only a small amount of reversibly adsorbed ammonia registered at both low and high temperatures.

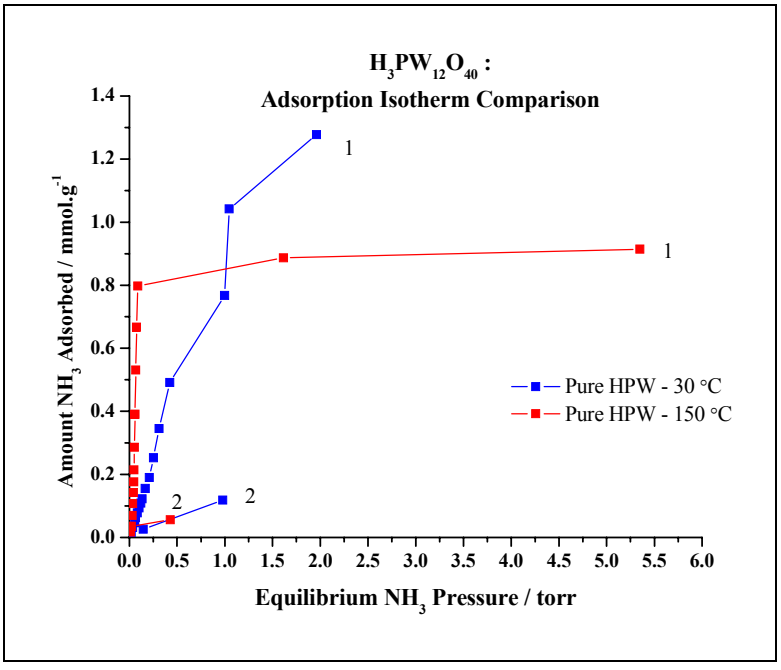

Figure 39: Adsorption - re-adsorption isotherms of NH_3 onto bulk $H_3PW_{12}O_{40}$ at 30 °C and 150 °C. (1= initial isotherm, 2= re-adsorption isotherm)

Shown below in Table 21 is the amount of irreversibly adsorbed NH_3 on pure re-crystallised HPW determined from the isotherms. These values have been determined at specific equilibrium pressure where the total and reversibly adsorbed NH_3 can be compared (as explained in 4.2.3). These values were then used to determine the number of ammonia molecules reacting with each HPW molecule. The maximum chemisorbed amount at 150 °C corresponds to about 2.2 molecules of ammonia per Keggin unit, which is somewhat lower than the expected value of 3 and the values 2.8 – 3.2 measured in earlier microcalorimetry studies[11, 12].

	Pure HPW	
	30 °C	150 °C
Irreversibly Adsorbed NH_3 at 0.25 torr (±0.05 $mmol.g^{-1}$)	0.23	0.75
Mole Ratio $NH_{3(irr)}$:HPW	0.7	2.2
N_2 BET surface area ($m^2.g^{-1}$)	2.3	

Table 21: Re-adsorption data to determine irreversibly adsorbed NH_3 for pure HPW.

The total amount of irreversibly adsorbed NH_3 at 30 °C is lower than at 150 °C when measured at 0.25 torr which is probably due to sorption of reversibly adsorbed NH_3 that is not minimised at this temperature. Significantly, the slope of the initial isotherm is considerably lower than that at 150 °C, which is indicative of the non-equilibrium effect where sorption is much slower and reaction is therefore likely to be incomplete at each pulse therefore explaining the lower mole ratio of 0.7. It needs to be mentioned that when $P \geq 1$torr it is likely that the eventual amount of irreversibly adsorbed NH_3 at 30 °C will give a mole ratio greater than 3 for $NH_{3(irr)}$:HPW. It has been suggested previously that the presence of any traces of water will provide additional proton sites and therefore a higher mole ratio than the theoretical value of 3 per Keggin unit[13].

Shown below in Figure 40 are the distributions of acidity with coverage for pure tungstophosphoric acid (HPW) at both low and high temperatures, based on the initial NH_3 adsorption isotherms. Activation was at 150 °C for two hours prior to adsorption at 30 °C and 150 °C.

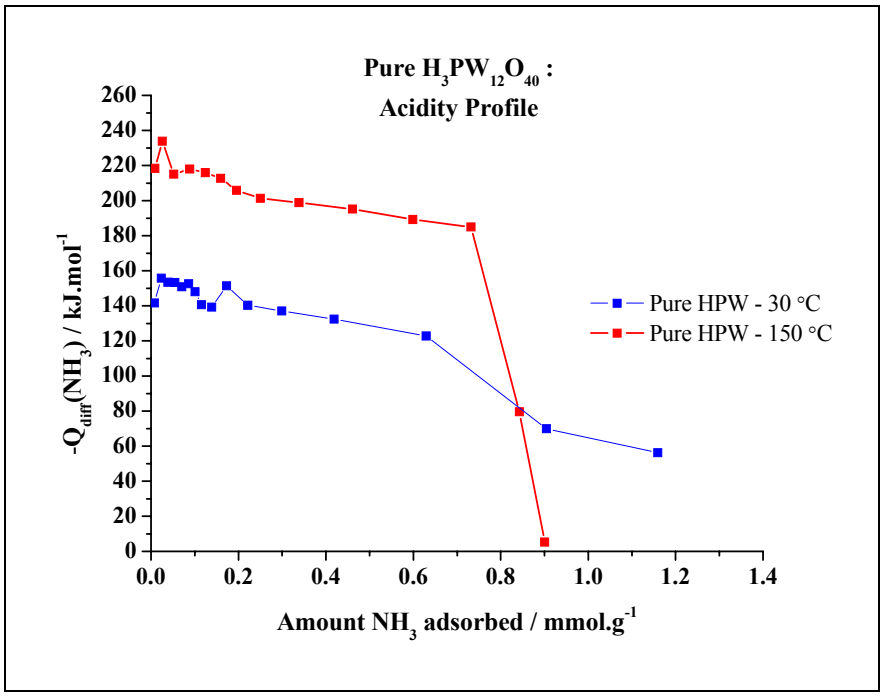

Figure 40: Comparison of differential heat of NH_3 adsorption for $H_3PW_{12}O_{40}$ (HPW) at 30 °C and 150 °C.

Pure HPW shows a relatively high acid strength based on $-Q_{diff}(NH_3)$ and a relatively high concentration of acid sites when ammonia is both adsorbed at 30 °C and 150 °C. It is possible that the high heats seen at low temperature are due to the interaction of HPW with trace water molecules creating further Brønsted acidity[14]. Also there will be a larger contribution from reversibly adsorbed NH_3 at this low temperature explaining the differences in profiles. Looking at the acidity profile for pure HPW at 150 °C shows essentially uniform heats of between 185 – 220 kJ.mol^{-1} and an overall concentration of ca. 0.90 mmol.g^{-1} of acid sites as determined from Figure 40, which is slightly lower than the expected theoretical adsorption of 1.04 mmol.g^{-1} based on 3 NH_3 molecules per Keggin unit[15]. Measurements recorded at 30 °C show that heats are generally uniform but lower (165 kJ.mol^{-1}) but the amount of NH_3 adsorbed on acidic sites is similar. This information is summarised in Table 22.

	Pure $H_3PW_{12}O_{40}$ (HPW)	
Calorimeter Temperature (°C)	30	150
$-Q_{diff}(NH_3)$ at a coverage of 0.05 mmol.g^{-1} (± 5 kJ.mol^{-1})	165	215
Surface Coverage of NH_3 at which $-Q_{diff}(NH_3)$ falls below 80 kJ.mol^{-1} (±0.05 mmol.g^{-1})	0.86	0.84
BET Surface area determined by N_2 adsorption (m^2.g^{-1})	2.3	
Mesopore Volume (ml.g^{-1})	*	
Micropore Volume (ml.g^{-1})	*	

Table 22: Summary of acidity and characterization data for HPW at 30 °C and 150 °C.

**= too low to measure*

The thermokinetic parameter (CWHM) has been measured for each pulse of NH_3 added to the sample and plotted as a function of the amount of NH_3 adsorbed for HPW at both 30 °C and 150 °C. This is shown below in Figure 41. Samples were activated at 150 °C before adsorption.

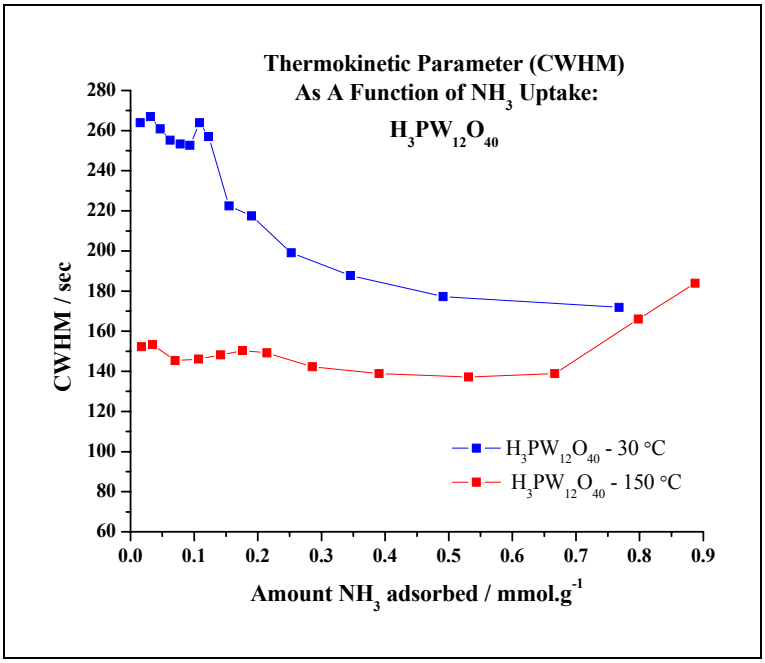

Figure 41: Thermokinetic parameter (CWHM) data for $H_3PW_{12}O_{40}$ at 30 °C and 150 °C.

In an earlier microcalorimetric study, it was observed that the thermokinetic parameter (in this case the time constant, τ) for pure tungstophosphoric acid was effectively independent of the amount of ammonia taken up[9]. This was attributed to the progressive formation of the microporous ammonium salt, which promotes access to the unreacted acid inside the crystalline grains.

Therefore the process of NH_3 reaction with pure HPW can be seen as self-promoting and is accompanied by a gradual change in pore structure. Figure 41 shows the CWHM parameter as functions of ammonia uptake at 150 °C and 30 °C. The rate of sorption is nearly constant at 150 °C until 0.67 $mmol \cdot g^{-1}$ and then increases (an increase in the CWHM parameter or the time constant means a decrease in the rate). It is possible that slow diffusion into the bulk acid crystallites can explain the latter increase and is a possible explanation for the lower than expected stoichiometric ratio of NH_3 molecules per Keggin unit (2.4) obtained in this study (see Table 21).

The corresponding data for pure tungstophosphoric acid at 30 °C is also shown in Figure 41. The rate of sorption at this low temperature is considerably lower than that at 150 °C up to an ammonia loading of 0.15 $mmol \cdot g^{-1}$ and then it gradually increases so that adsorption is actually faster at 30 °C than at 150 °C. This initial slow rate of sorption is consistent with the interpretation of the isotherm data (Figure 39) where equilibrium is not reached and therefore the reaction is likely to be incomplete at each pulse. However, the increase in the rate of sorption also may mean that the contribution of physical sorption is significant: the increase in the rate of sorption coinciding with the decrease in the differential heat of sorption has been attributed in the literature to the transition from chemical (a relatively slow process) to physical (a relatively fast process) sorption[17]. So, in the case of low temperature sorption on tungstophosphoric acid, the slow initial rates of sorption are quite likely due to the slow diffusion of ammonia into the bulk crystalline acid to form the salt, and the higher rate seen for additional NH_3 adsorption is seen because a significant fraction of each NH_3 dose adsorbs weakly on external readily accessible sites.

4.3.2 Supports: Silica (SBA-15) and Carbons (Novacarb, Sibunit)

Adsorption isotherms measured at 30 °C and 150 °C are shown below in Figure 42 for the three supports (no HPW present) used in this work.

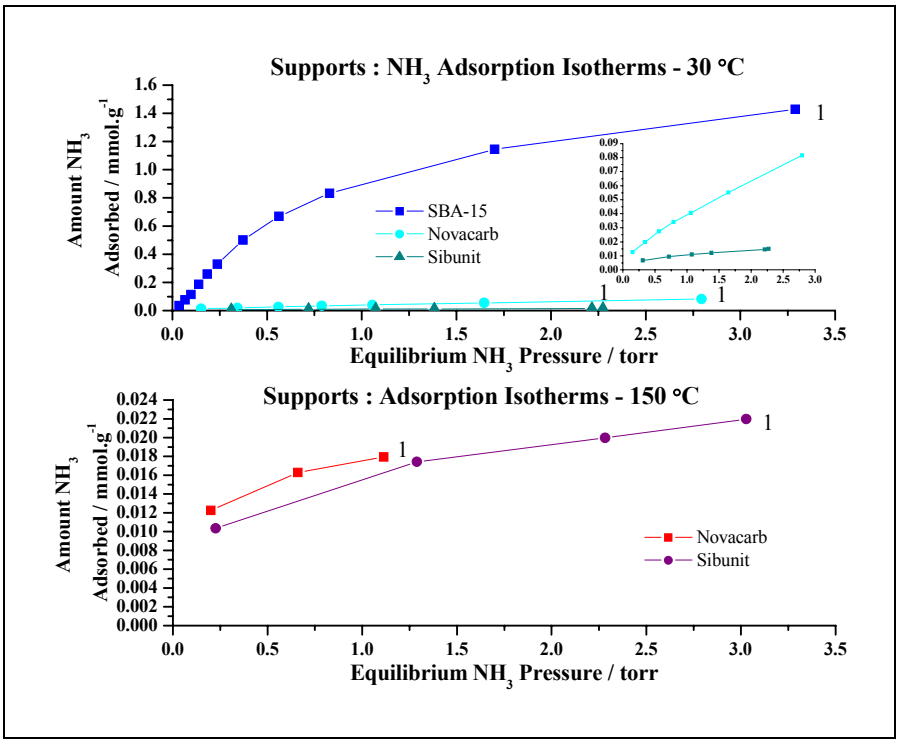

Figure 42: Adsorption isotherms of NH_3 onto supports at 30 °C and 150 °C.

(1= initial isotherm)

(For these materials the re-adsorption isotherm was not performed)

It was not possible to obtain an isotherm for pure SBA-15 at 150 °C as too little NH_3 was adsorbed and saturation was quickly reached. Data obtained at 30 °C and 150 °C for the two carbons show that the NH_3 sorption capacity of Sibunit at 30 °C is considerably lower than that of Novacarb (see inset graph Figure 42a). This is consistent with previous measurements made on these carbons in another laboratory using a custom built set-up equipped with a thermal conductivity detector to measure breakthrough curves of NH_3, in which equilibrium amounts of ammonia adsorption measured at 15.98 Torr ammonia and 30 °C temperature were 0.22 $mmol \cdot g^{-1}$ for Novacarb and only 0.05 $mmol \cdot g^{-1}$ for Sibunit[4]. Variation between the two materials is likely to be due to the different surface chemistries of the two carbon materials. The Novacarb sample differs from Sibunit in that it was activated in CO_2 during preparation, which produces weak surface acid groups and increases the micropore volume of the carbon[5]. Both features would be expected to enhance NH_3 adsorption.

The sorption capacity of SBA-15 at 30 °C measured here (1.4 mmol.g^{-1}) is considerably higher than that reported in the earlier literature (0.89 mmol·g^{-1} at 15.98 Torr ammonia pressure)[4] and considerably higher than the capacity of both carbons. The discrepancy with the earlier data is most likely due to a better structure of the synthesized material, which is indicated by the higher surface area *ca.* 729 m^2·g^{-1} (see Chapter Two, Section 2.3.2.1.a, Table 7) and good hexagonal ordering, see XRD pattern (Chapter Two, Section 2.3.2.1.b, Figure 17). No re-adsorption data was obtained for supports due to the minimal amount of NH_3 adsorbed.

Shown below in Figure 43 are the acidity profiles for the supports in the absence of HPW: pure Novacarb, pure Sibunit and pure SBA-15 at both low (30 °C) and high (150 °C) temperatures, following activation at 150 °C.

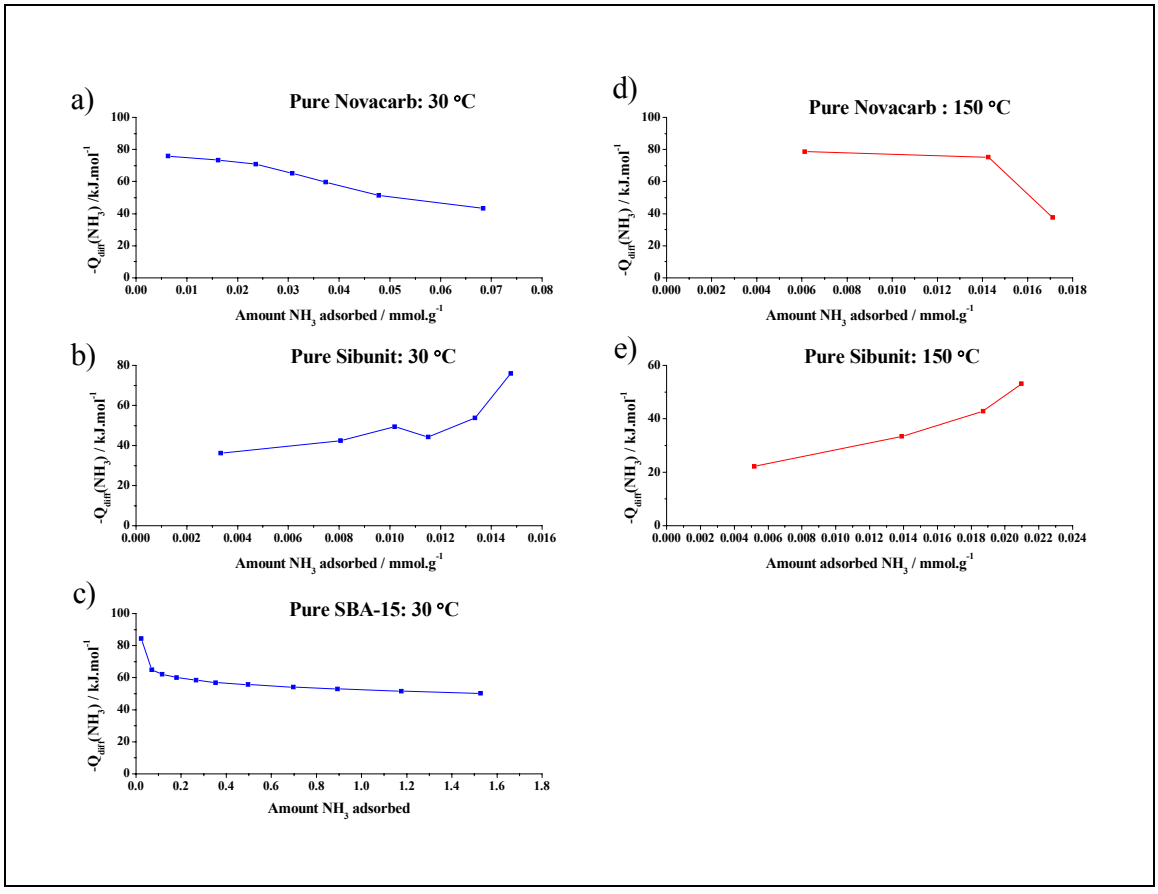

Figure 43: Comparison of differential heat of NH_3 adsorption for pure supports at 30 and 150 °C.

The acidity profiles shown above in Figure 43 show that for all studied supports at both 30 °C and 150 °C only weakly adsorbed NH_3 is measured, with $-Q_{diff}(NH_3)$ below 80 kJ.mol^{-1}. This suggests that there is essentially no intrinsic surface acidity associated with any of the three porous support

materials. It was not possible to obtain a measurement for pure SBA-15 at high temperature due to the amount of NH_3 adsorbed being negligible. At 150 °C for both Novacarb and Sibunit very small amounts of NH_3 are adsorbed so it is likely that large experimental errors exist.

$-Q_{diff}(NH_3)$ / amount NH_3 adsorbed measurements at 30 °C show very different profiles for each of the supports. One significant difference is seen between the carbon supports and SBA-15, as the overall NH_3 uptake is much greater for SBA-15 (ca. 1.5 $mmol.g^{-1}$) than for either Sibunit (ca. 0.006 $mmol.g^{-1}$) or Novacarb (0.07 $mmol.g^{-1}$) carbon (see Figure 43a,b and c). This value also appears considerably higher than previously reported values in the literature (ca. 0.89 $mmol.g^{-1}$ at 15.98 Torr NH_3 pressure[4]). Initial $\Delta H°_{ads}$ for SBA-15 are slightly higher than those of the two carbons (85 $kJ.mol^{-1}$). There is no microcalorimetric data available on SBA-15 at 30 °C or 150 °C though some comparison can be made with the studies of MCM-41 and other ordered template siliceous mesoporous materials, where weakly acidic sites have been associated with silanol hydrogen bonding sites[16]. The presence of weak acid sites native to the support is likely to influence the overall heat output upon adsorption of NH_3 on the acid impregnated materials. Note variation in $\Delta H°_{ads}$ with coverage, especially as saturation is approached, may not be significant because experimental errors are very large under these conditions.

	Pure Novacarb		Pure Sibunit		Pure SBA-15
Calorimeter Temperature (°C)	30	150	30	150	30
$-Q_{diff}(NH_3)$ at a coverage of 0.05 $mmol.g^{-1}$ (± 10 $kJ.mol^{-1}$)	78	79	48	58	75
BET Surface area determined by N_2 adsorption ($m^2.g^{-1}$)	926.0		290.7		728.9
Mesopore Volume ($ml.g^{-1}$)	0.53		0.18		0.63
Micropore Volume ($ml.g^{-1}$)	0.33		0.019		0.09

Table 23: Summary of acidity and characterization data for pure supports at 30 °C and 150 °C.

Shown in Table 23 are the specific heat measurements at a coverage of 0.05 $mmol.g^{-1}$ and also the nitrogen adsorption data for all three support materials. Novacarb shows the highest heats at coverage of 0.05 $mmol.g^{-1}$. This suggests that at both 30 °C and 150 °C weakly acidic sites are more easily accessible in Novacarb, due to Novacarb possessing the highest BET surface area and a high mesopore and micropore volume. It is possible that this weak acidity arises from the

surface chemistry of Novacarb due to its method of preparation. Novacarb is activated in CO_2, which produces weak surface acid groups as well as increasing the micropore volume of the carbon [17]. A further detailed study in the literature of acidic groups on the surface of different Novacarb materials has shown that the CO_2 activated material contains some lactonic or phenolic oxygen groups which may be responsible for very weak acidity, although it does not contain stronger carboxylic acid groups[18,].

4.3.3 SBA-15 Supported $H_3PW_{12}O_{40}$

Adsorption and re-adsorption isotherms are shown below in Figure 44 for SBA-15 supported HPW: HPW/SBA-15 (174 mg/g), HPW/SBA-15 (320 mg/g) and HPW/SBA-15 (420 mg/g) at both 30 °C and 150 °C. Note that a re-adsorption isotherm was not recorded for HPW/SBA-15 (320 mg/g) at 30 °C.

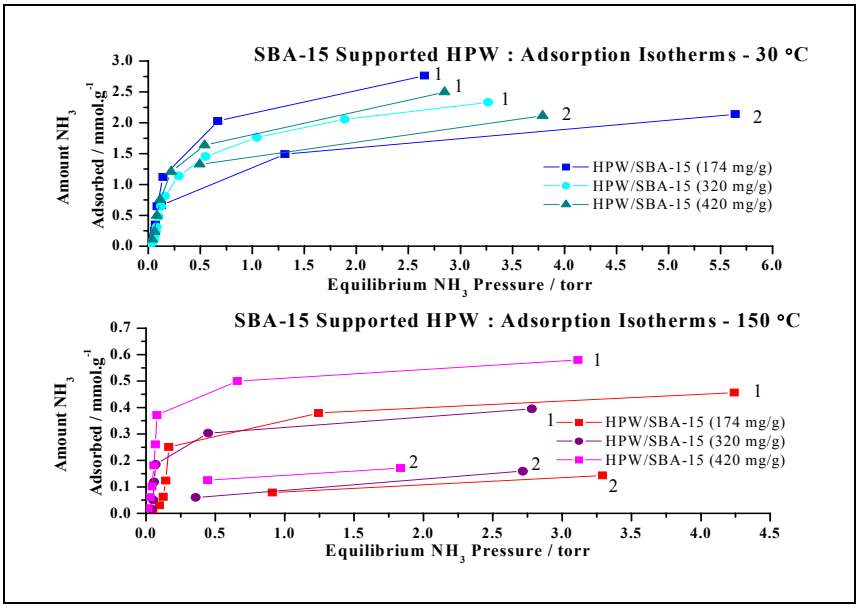

Figure 44: Adsorption - re-adsorption isotherms of NH_3 onto SBA-15 supported HPW at 30 °C and 150 °C. (1= initial isotherm, 2= re-adsorption isotherm)

Sorption at high temperature onto material with high loading of strong acid is expected to be dominated by the chemisorption process whereas, at low temperature, the overall sorption is the sum of irreversibly and reversibly adsorbed NH_3. Adsorption isotherms measured at 150 °C show that as the loading of HPW is increased so does the total amount of NH_3 adsorbed. The overall amount of NH_3 adsorbed is much lower than overall adsorption at 30 °C but is mainly associated

with irreversibly adsorbed NH_3, as can be seen in Figure 44. Isotherms are very similar for HPW/SBA-15 (174 mg/g) and (320 mg/g) at 150 °C suggesting that at lower loadings fewer differences are seen in the amount of NH_3 adsorbed. At 30 °C amount of NH_3 adsorbed does not increase with loading of HPW, as HPW/SBA-15 (174 mg/g) shows the greatest overall amount of adsorbed NH_3.

	HPW/SBA-15 (174 mg/g)		HPW/SBA-15 (320 mg/g)		HPW/SBA-15 (420 mg/g)	
	30 °C	150 °C	30 °C	150 °C	30 °C	150 °C
Irreversibly Adsorbed NH_3 at 1.5 torr ($mmol.g^{-1}$) (± 0.05 $mmol.g^{-1}$)	0.86	0.29	/	0.22	0.45	0.38
Mole Ratio $NH_{3(irr)}$:HPW	16.7	5.6	/	2.6	8.8	7.4
N_2 BET surface area ($m^2.g^{-1}$)	286		/		143	

Table 24: Re-adsorption data to determine irreversibly adsorbed ammonia for SBA-15 supported HPW.

/= not measured

When the ratio of $NH_{3(irr)}$:HPW molecules is studied (Table 24) the ratios at 30 °C are high for HPW/SBA-15 (174 mg/g) and HPW/SBA-15 (420 mg/g). This is probably due to NH_3 adsorbed on non-acidic sites that isn't minimised at such a low temperature. This is most clearly seen for HPW/SBA-15 (174 mg/g) in which the number of NH_3 molecules adsorbed per HPW molecule increases to 16.7, and yet it contains fewer HPW molecules than the higher loadings. At 150 °C the mole ratio decreases for all solid acids. This would be expected as weakly adsorbed NH_3 is only held reversibly at this temperature, and adsorption on non-acidic sites is reduced. Mole ratios are closer to the expected theoretical value of 3 NH_3 molecules per HPW.

Shown below in Figure 45 are the acidity profiles for SBA-15 supported HPW at both low (30 °C) and high (150 °C) temperatures, following activation at 150 °C.

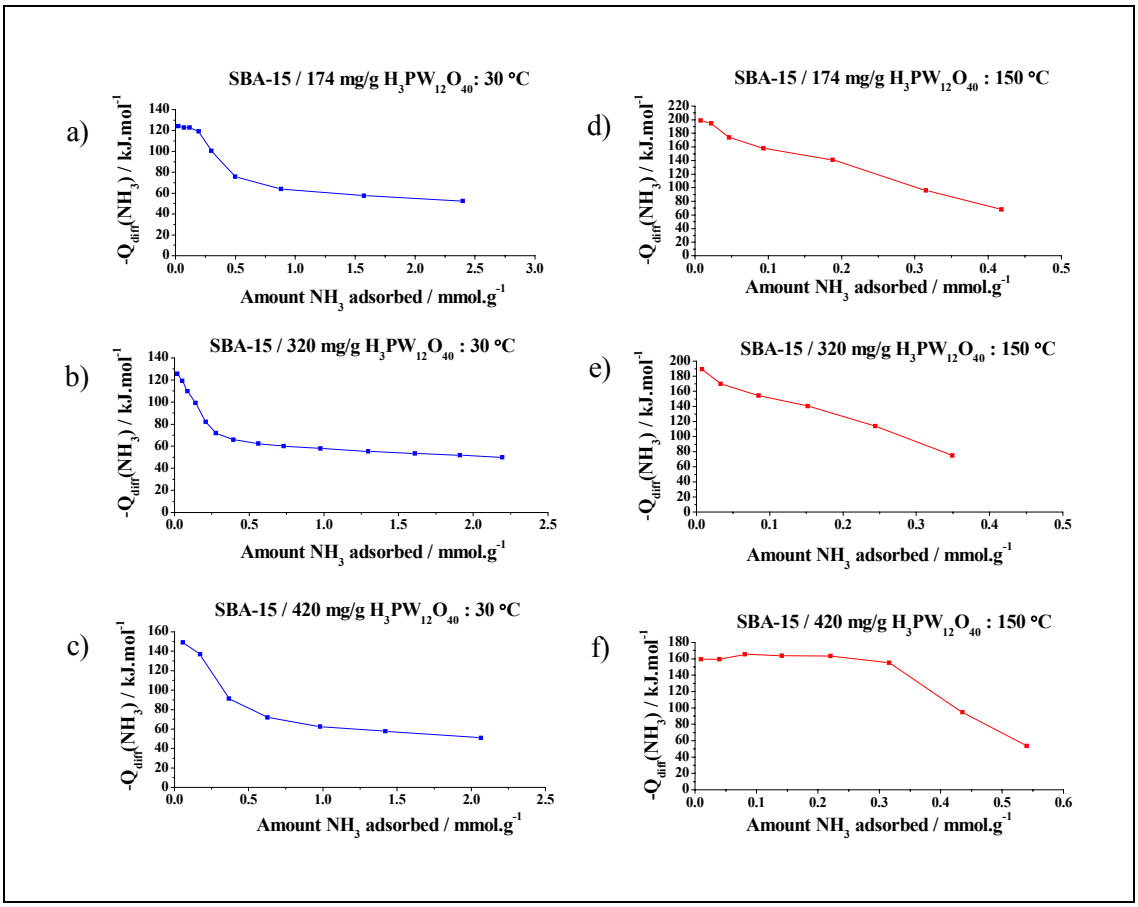

Figure 45: Comparison of differential heats of NH_3 adsorption at 30 °C and 150 °C for SBA-15 supported $H_3PW_{12}O_{40}$.

The difference between the low and high temperature sorption processes for all SBA-15 supported HPWS's is evident from the differential heats of NH_3 sorption data at the two temperatures (see Figure 45). The maximum observed differential heat of sorption at low ammonia coverages in the case of HPW/SBA-15 (420mg/g) measured at 150 °C is about 165 kJ·mol^{-1}. This is lower than the value reported (200 kJ·mol^{-1}) for this acid supported onto Aerosil silica material and measured at the same temperature[9], and lower than the value recorded for pure heteropoly acid (225 – 200 kJ·mol^{-1}), see Figure 40. The decrease in the maximum differential heat of sorption is possibly linked somehow to the strength of interaction between the support material and the heteropoly acid, which may be affecting the acid strength of the HPW and hence the heat output on reaction. The plateau on the differential heat *vs.* surface coverage plot suggests that all the acid sites have similar strengths.

When NH_3 adsorption is carried out at high temperature, as HPW loading is increased, the initial heats of NH_3 adsorption (i.e. the first pulses of NH_3 adsorbed) drop to 190 – 198 kJ.mol^{-1} for both HPW/SBA-15 (174 mg/g) and HPW/SBA-15 (320 mg/g) and the amount of ammonia adsorbed corresponding to strong acid sites ($-Q_{diff}(NH_3)$ above 80 kJ.mol^{-1}) decreases from 0.84 mmol.g^{-1} for pure HPW to 0.33 – 0.50 mmol.g^{-1} up to a loading of 420 mg/g HPW. At a loading of 420 mg/g HPW heats of NH_3 adsorption are reduced to 149 kJ.mol^{-1} but are fairly uniform up to a concentration of 0.3 mmol.g^{-1} (see Figure 45f).

	Pure $H_3PW_{12}O_{40}$ (HPW)		SBA-15 Support	HPW/SBA15 (174 mg/g)		HPW /SBA15 (320mg/g)		HPW/SBA-15 (420mg/g)	
Calorimeter Temperature (°C)	30	150	30	30	150	30	150	30	150
$-Q_{diff}(NH_3)$ at a coverage of 0.05 mmol.g^{-1} (± 5 kJ.mol^{-1})	165	215	75	123	158	117	164	149	160
Surface Coverage of NH_3 at which $-Q_{diff}(NH_3)$ falls below 80 kJ.mol^{-1} (±0.05 mmol.g^{-1})	0.86	0.84	0.03	0.45	0.35	0.28	0.33	0.50	0.50
BET Surface area determined by N_2 adsorption ($m^2.g^{-1}$)	2.3		728.9	286.3		/		143.0	
Mesopore Volume (ml.g^{-1})	*		0.63	0.065		/		0.11	
Micropore Volume (t-plot) (ml.g^{-1})	*		0.09	0.028		/		0.004	

Table 25: Summary of acidity and characterization data for SBA-15 supported HPW at 30 °C and 150 °C.

**= too low to measure /= not measured*

Table 25 above shows that silica support, SBA 15 adsorbs NH_3 relatively weakly and at low concentrations, as described earlier. What little acidity is present is most likely due to very weak acid sites such as silanol hydrogen bonding sites[19]. When HPW is supported on SBA-15, the heats are lower than for pure HPW. The surface areas decrease as HPW loading is increased and the micropore volume in SBA-15 is reduced by the deposition of tungstophosphoric acid (see Table 25). The most significant decrease in pore volume upon supporting the acid is seen in the mesopores suggesting that HPW is deposited in these pores, perhaps blocking them.

For HPW supported on SBA-15 at the highest catalyst loading of 420 mg/g the thermokinetic parameter (CWHM) has been measured as a function of the amount of NH_3 adsorbed at both 30 °C

and 150 °C. The data is compared with that of the pure support material, SBA-15 at low temperature, and is shown below in Figure 46.

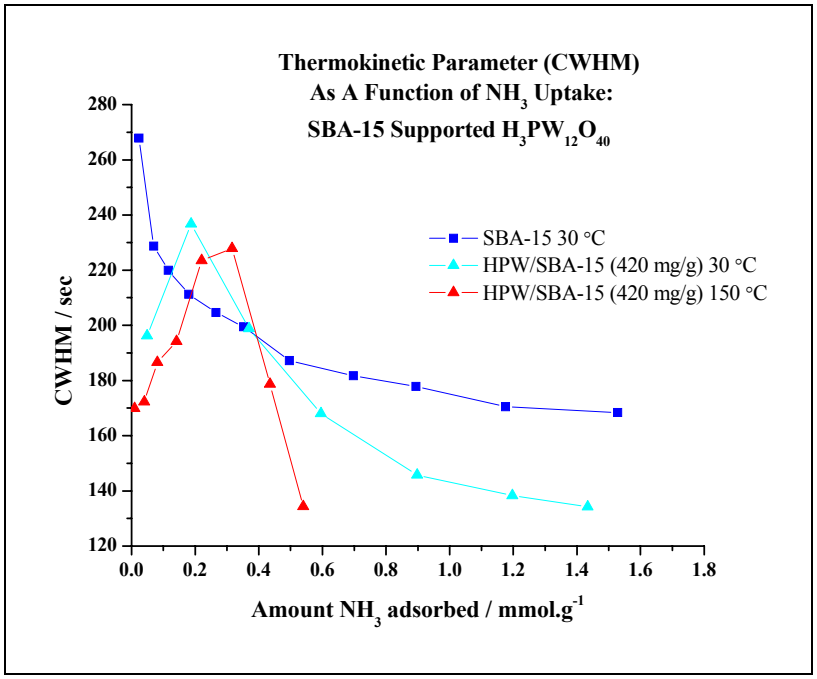

Figure 46: Thermokinetic parameter (CWHM) data for SBA-15 supported $H_3PW_{12}O_{40}$ at 30 °C and 150 °C.

The initial adsorption for SBA-15 at 30 °C shows that up to ~ 0.15 mmol.g^{-1} ammonia coverage, adsorption is very slow possibly due to a limited number of accessible surface acid sites which NH_3 is able to penetrate. This rate then increases possibly as ammonia diffuses into the internal open pore structure and also as it weakly adsorbs as multilayers onto the initial surface acid sites. When the thermokinetic parameter measured as a function of the amount of NH_3 adsorbed for SBA-15 supported HPW is compared to pure HPW a different profile can be seen as the initial reaction is fast then slows down to a minimum before again increasing. The initial adsorption rate for the HPW/SBA-15 (420mg/g) is significantly faster at lower temperatures than that of the bulk HPW (see Figure 41) which shows the advantage of the open pore structure of ordered silica SBA-15, throughout which HPW is well dispersed. It is likely that the adsorption rate is initially very quick because NH_3 is reacting with HPW molecules present on the surface of the SBA-15 support. This rate gradually becomes slower as NH_3 diffuses in to the SBA-15 porous structure until all accessible acidic sites are reacted. Once this occurs the rate again speeds up indicating that NH_3 is reversibly adsorbed onto the solid acid.

4.3.4 Novacarb Supported $H_3PW_{12}O_{40}$

Ammonia adsorption and re-adsorption isotherms are shown below in Figure 47 for Novacarb supported HPW at both 30 °C and 150 °C.

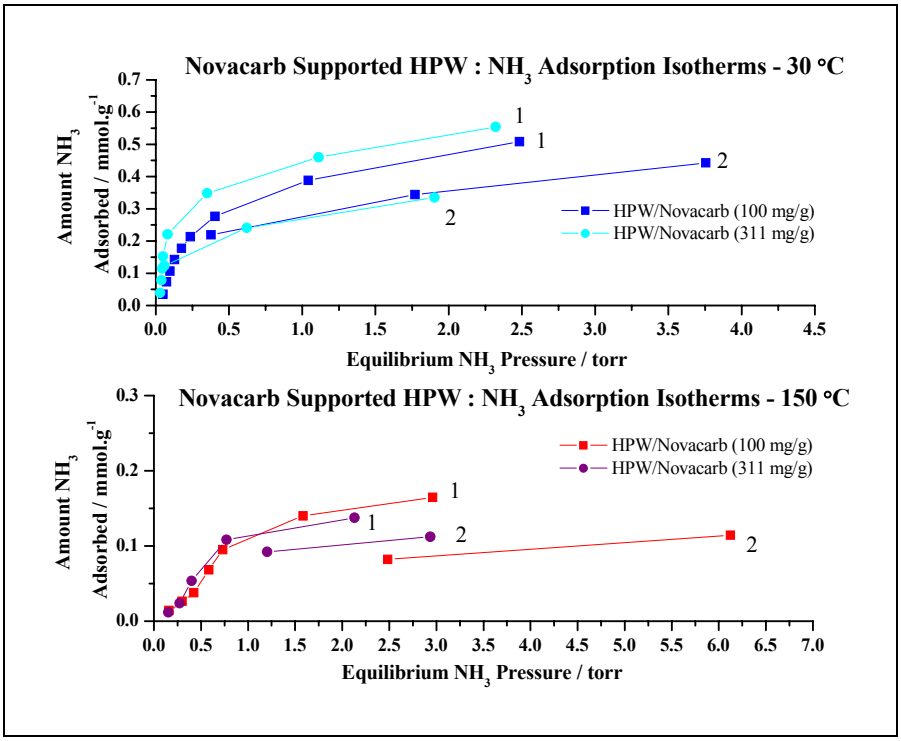

Figure 47: Adsorption - re-adsorption isotherms of NH_3 onto Novacarb supported HPW at 30 °C and 150 °C.

(1= initial isotherm, 2= re-adsorption isotherm)

The first isotherm of each pair is shown in full and the second isotherm (the "reversible" adsorption) is shown only in part, but enough for the differences between the two (equivalent to the amount of irreversibly adsorbed NH_3) to be obtained. The differences are measured at a NH_3 pressure of 1.5 torr for isotherms at 30 °C, and 1.75 torr for HPW/Novacarb (311 mg/g) and 2.75 torr for HPW/Novacarb (100 mg/g) at 150 °C. The total equilibrium ammonia uptake onto HPW impregnated Novacarbs at 30 °C are more than an order of magnitude higher than that of the pure support material. The amount of irreversibly adsorbed ammonia at 30 °C based on the re-adsorption data (see Table 26) for HPW/Novacarb (311 mg/g) is 0.20 $mmol \cdot g^{-1}$, whereas at 150 °C it is 0.07 $mmol \cdot g^{-1}$. The significantly larger irreversibly adsorbed amount of ammonia at low temperature cannot be attributed to strong sorption in micropores or mass transfer effects (non-

equilibrium effects), since the data obtained on pure Novacarb support (see Figure 42, Section 4.3.2.2) show much less adsorption than is recorded here with the supported acid. Again it is possible that any traces of water present in HPW will provide additional proton sites and therefore increase the amount of irreversibly adsorbed ammonia (Section 4.3.1).

	HPW/Novacarb (100 mg/g)		HPW/Novacarb (311 mg/g)	
	30 °C	150 °C	30 °C	150 °C
Irreversibly Adsorbed NH_3 (± 0.05 mmol.g^{-1})	0.16	0.08	0.20	0.07
Mole Ratio $NH_{3(irr)}$:HPW	4.5	2.3	1.8	0.6
N_2 BET surface area (m^2.g^{-1})	423		369	

Table 26: Re-adsorption data to determine irreversibly adsorbed ammonia for Novacarb supported HPW.

Table 26 also shows that in general, less than the stoichiometric number of ammonia molecules are adsorbed per HPW molecule at 150 °C which may suggest that all HPW molecules are not easily accessible. Also the amount of irreversibly adsorbed NH_3 is very similar for the two loadings of HPW again agreeing with the possibility that not all acid sites are easily accessible.

Shown below in Figure 48 are the acidity profiles for Novacarb supported HPW at both 30 °C and 150 °C, following activation at 150 °C.

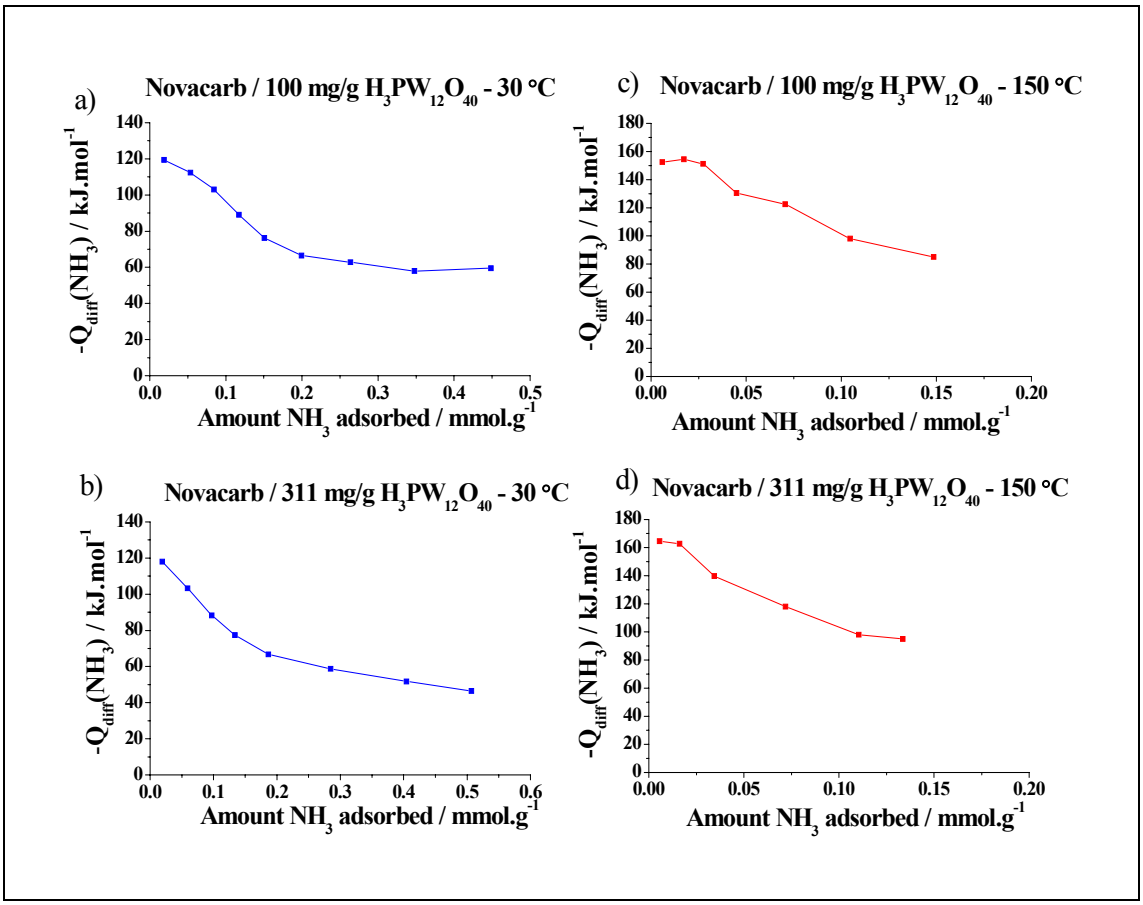

Figure 48: Comparison of differential heats of NH_3 adsorption at 30 °C and 150 °C for Novacarb supported $H_3PW_{12}O_{40}$.

Introducing HPW to the Novacarb support greatly increases the heats and also increases the NH_3 uptake even at low HPW loadings. This suggests that heats produced can be assigned to the addition of the HPW. There is considerable difference between the NH_3 adsorption behaviour at the two temperatures. The initial differential heats of NH_3 adsorption for Novacarb supported HPW at 30 °C are about 120 kJ.mol^{-1} whereas at 150 °C they are around 160 kJ.mol^{-1}. Both of these values are lower than that of pure HPW suggesting quite a strong interaction between the Novacarb support and HPW.

Shown below in Table 27 are the acidity data and N_2 adsorption data for Novacarb supported HPW solid acids.

	Pure $H_3PW_{12}O_{40}$ (HPW)		Novacarb Support		HPW/Novacarb (100mg/g)		HPW /Novacarb (311mg/g)	
Calorimeter Temperature (°C)	30	150	30	150	30	150	30	150
$-Q_{diff}(NH_3)$ at a coverage of 0.05 mmol.g^{-1} (± 5 kJ.mol^{-1})	165	215	78	79	115	150	106	138
Surface Coverage of NH_3 at which $-Q_{diff}(NH_3)$ falls below 80 kJ.mol^{-1} (±0.05 mmol.g^{-1})	0.86	0.84	0.05	0.05	0.13	0.18	0.15	0.18
BET Surface area determined by N_2 adsorption ($m^2.g^{-1}$)	2.3		926.0		423.4		368.7	
Mesopore Volume (ml.g^{-1})	*		0.53		0.37		0.34	
Micropore Volume (ml.g^{-1})	*		0.33		0.15		0.12	

Table 27: Summary of acidity and characterization data for Novacarb supported HPW at 30 °C and 150 °C.

**= too low to measure*

Novacarb support shows weak NH_3 adsorption (see Figure 48). When HPW is supported the surface area of Novacarb decreases, but the heats and NH_3 concentration for both Novacarb supported HPW samples increases. At 150 °C stronger acidic sites are available to adsorb NH_3 than at 30 °C. There is also a contribution from the physical sorption of NH_3 which is evidenced by the lower heat of adsorption at higher ammonia coverage that approaches typical values of physisorption of ammonia.

Shown below in Figure 49 is the thermokinetic parameter (CWHM) which has been measured as a function of the amount of NH_3 adsorbed for Novacarb supported HPW samples at both 30 °C and 150 °C.

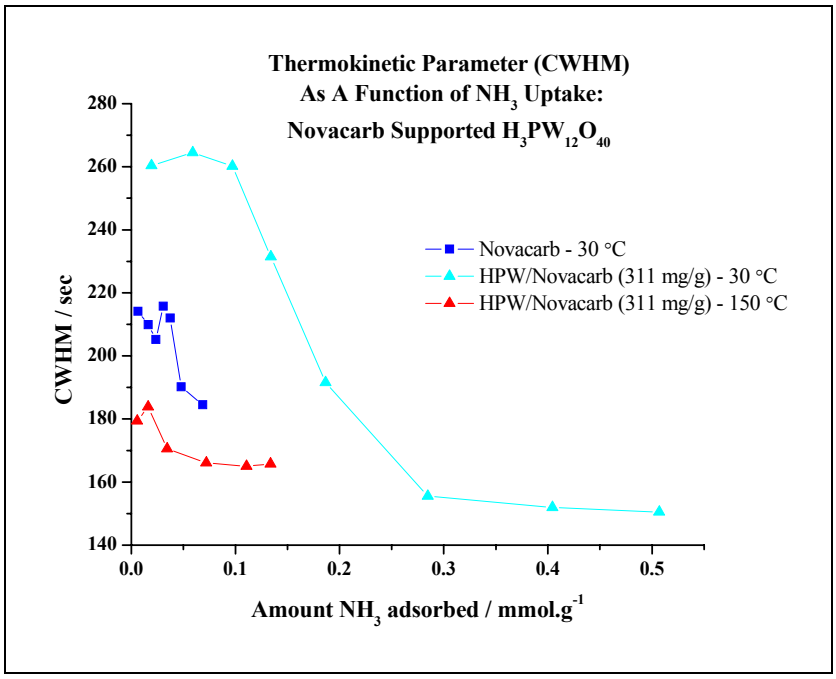

Figure 49: Thermokinetic parameter (CWHM) data for Novacarb supported $H_3PW_{12}O_{40}$ at 30 °C and 150 °C.

The thermokinetic data above in Figure 49 shows that HPW/Novacarb (311 mg/g) has a very slow initial rate at 30 °C which is similar to pure HPW up to a coverage of 0.15 mmol.g^{-1} (see Figure 41), whereas the rate of sorption for pure Novacarb is considerably faster for the relatively small amount of NH_3 that is adsorbed at the same temperature. This suggests that the acid is not well dispersed and the rate of sorption is limited by the same mass transfer effects as in the bulk acid. Also the increase in rate seen at low temperature for HPW/Novacarb (311 mg/g) falls in line with the onset of reversibly adsorbed NH_3 as seen in Figure 48. At 150 °C the rate of adsorption of NH_3 on HPW/Novacarb (311 mg/g) is faster than the pure support but not as quick as pure HPW. This suggests that there is a small contribution from diffusion.

4.3.5 Sibunit Supported $H_3PW_{12}O_{40}$

Shown below in Figure 50 are the NH_3 adsorption and re-adsorption isotherms for Sibunit supported HPW at 30 °C and adsorption isotherms for Sibunit supported HPW at 150 °C.

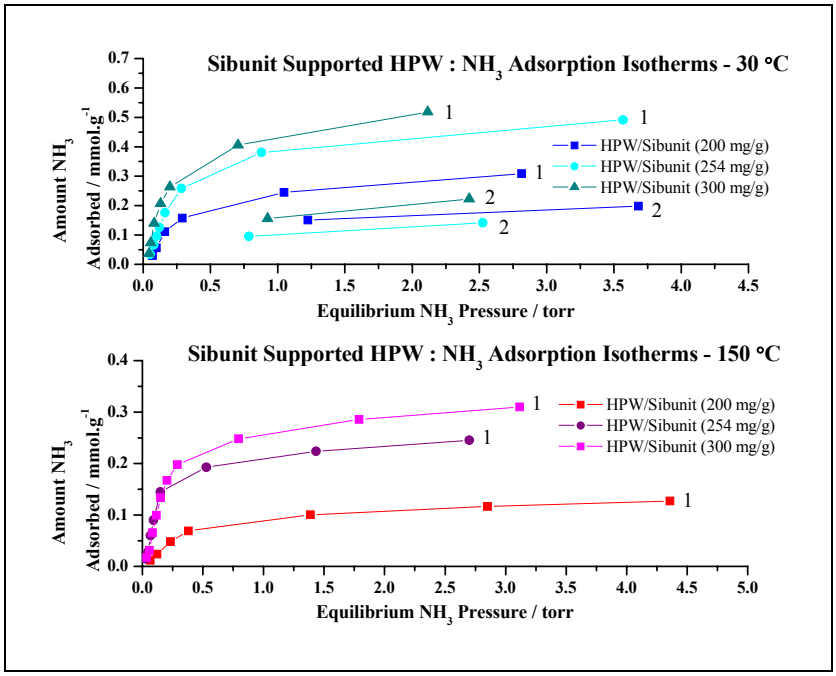

Figure 50: Adsorption - re-adsorption isotherms of NH_3 onto Sibunit supported HPW at 30 °C and 150 °C.

(1= initial isotherm, 2= re-adsorption isotherm)

Similar to Novacarb, the amount of irreversibly adsorbed NH_3 on HPW/Sibunit samples at 30 °C are relatively high for each loadings (see Figure 50 and Table 28). It is apparent that ammonia is reacting mainly with the HPW and not with the support as this adsorbs very little NH_3 (see Figure 42) and also the amount of irreversibly adsorbed NH_3 increases with loading at 30 °C.

	HPW/Sibunit (200 mg/g)		HPW/Sibunit (254 mg/g)		HPW/Sibunit (300 mg/g)	
	30 °C	150 °C	30 °C	150 °C	30 °C	150 °C
Irreversibly Adsorbed NH_3 at 1.5 torr (±0.05 mmol.g^{-1})	0.11	/	0.28	/	0.27	/
Mole Ratio $NH_{3(irr)}$:HPW	2.0	/	3.9	/	3.3	/
N_2 BET surface area ($m^2.g^{-1}$)	133		171		125	

Table 28: Re-adsorption data to determine irreversibly adsorbed ammonia for Sibunit supported HPW.

/= Not measured

Table 28 shows that the mole ratios of $NH_{3(irr)}$:HPW are low for all Sibunit supported HPW at 30 °C in comparison to results obtained for both SBA-15 supported HPW and Novacarb supported

HPW under the same conditions. Their values lie close to the expected stoichiometric value of 3:1 $NH_{3(irr)}$:HPW even though at this low temperature higher values were observed. It is unclear why this is. One possible explanation is that again water is present in HPW molecules providing acidic sites as explained previously for SBA-15 and Novacarb supported HPW.

Shown below in Figure 51 are the acid strength profiles for Sibunit supported HPW at both 30 °C and 150 °C plotting differential heats as a function of ammonia coverage following activation at 150 °C respectively.

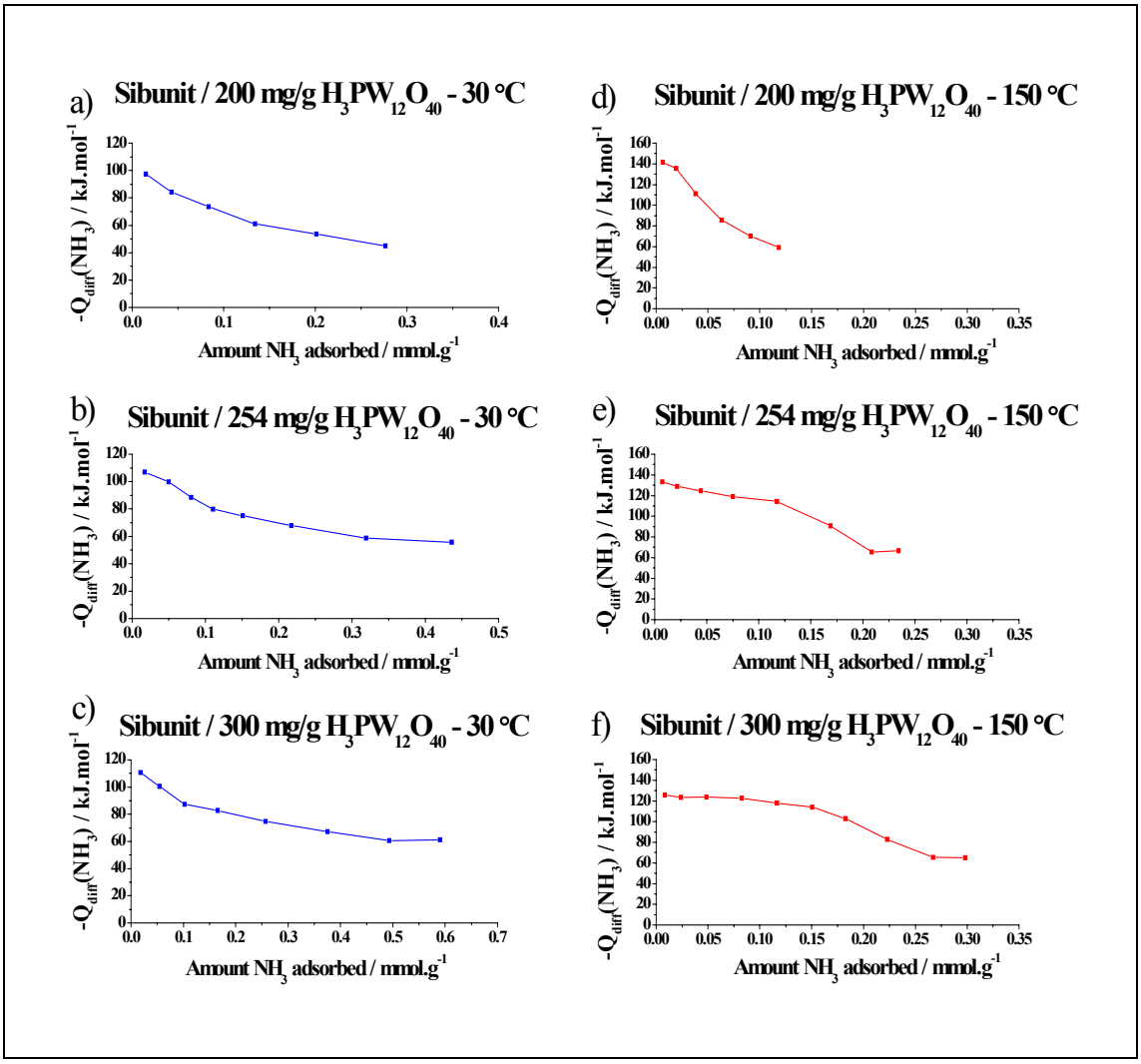

Figure 51: Comparison of differential heats of NH_3 adsorption at 30 °C and 150 °C for Sibunit supported $H_3PW_{12}O_{40}$.

The low acid loading sample (HPW/Sibunit (200 mg/g) is similar to HPW/Novacarb (311 mg/g) as it shows similar behaviour at 150 °C: a rapid decrease in the differential heat of sorption following the initial high value. However, the initial heat of sorption in the case of the 200 mg/g HPW loading Sibunit sample is significantly lower (*ca.* 113 kJ·mol^{-1} at 150 °C) than the corresponding value in the case of the 311 mg/g loading Novacarb sample (160 kJ·mol^{-1}). Based on these -$Q_{diff}(NH_3)$/uptake coverages tungstophosphoric acid supported on Novacarb appears to adsorb more NH_3 at relatively high heats of adsorption than HPW/Sibunit, and might therefore be expected to exhibit higher activity in Brønsted catalysed reactions. The differential sorption heat curve measured on the higher loading sample of Sibunit at 150 °C, where the contribution from reversibly adsorbed NH_3 is assumed to be relatively small, exhibits the behaviour expected from a sample containing a large number of accessible strong acid sites of similar energy, with a characteristic plateau at low ammonia uptake suggesting a uniformity of acid strength.

Shown below in Table 29 of microcalorimetric data for Sibunit supported HPW.

	Pure $H_3PW_{12}O_{40}$ (HPW)		Sibunit		HPW /Sibunit (200mg/g)		HPW /Sibunit (254mg/g)		HPW /Sibunit (300mg/g)	
Calorimeter Temperature (°C)	30	150	30	150	30	150	30	150	30	150
-$Q_{diff}(NH_3)$ at a coverage of 0.05 mmol.g^{-1} (± 5 kJ.mol^{-1})	165	215	48	58	84	102	85	120	100	124
Surface Coverage of NH_3 at which -$Q_{diff}(NH_3)$ falls below 80 kJ.mol^{-1} (±0.05 mmol.g^{-1})	0.86	0.84	0.003	0.05	0.05	0.07	0.10	0.18	0.18	0.23
BET Surface area determined by N_2 adsorption (m^2.g^{-1})	2.3		290.7		132.6		170.9		124.8	
Mesopore Volume (ml.g^{-1})	*		0.18		0.17		0.18		0.15	
Micropore Volume (ml.g^{-1})	*		0.019		0.006		0.013		0.008	

Table 29: Summary of acidity and characterization data for Sibunit supported HPW at 30 °C and 150 °C.

**= too low to measure*

Table 29 shows that on introducing HPW, reduction in the micropore volume is seen, and as loading of HPW increases based on the -$Q_{diff}(NH_3)$/NH_3 uptake profiles at 150 °C the strength of

accessible acid sites also increases. Again there is evidence of an added contribution of reversibly adsorbed / physisorbed NH_3, as heats are extremely low at higher ammonia coverages for all Sibunit solid acids.

The thermokinetic parameter (CWHM) has been measured as a function of the amount of NH_3 adsorbed for Sibunit supported HPW samples at both 30 °C and 150 °C and is shown below in Figure 52.

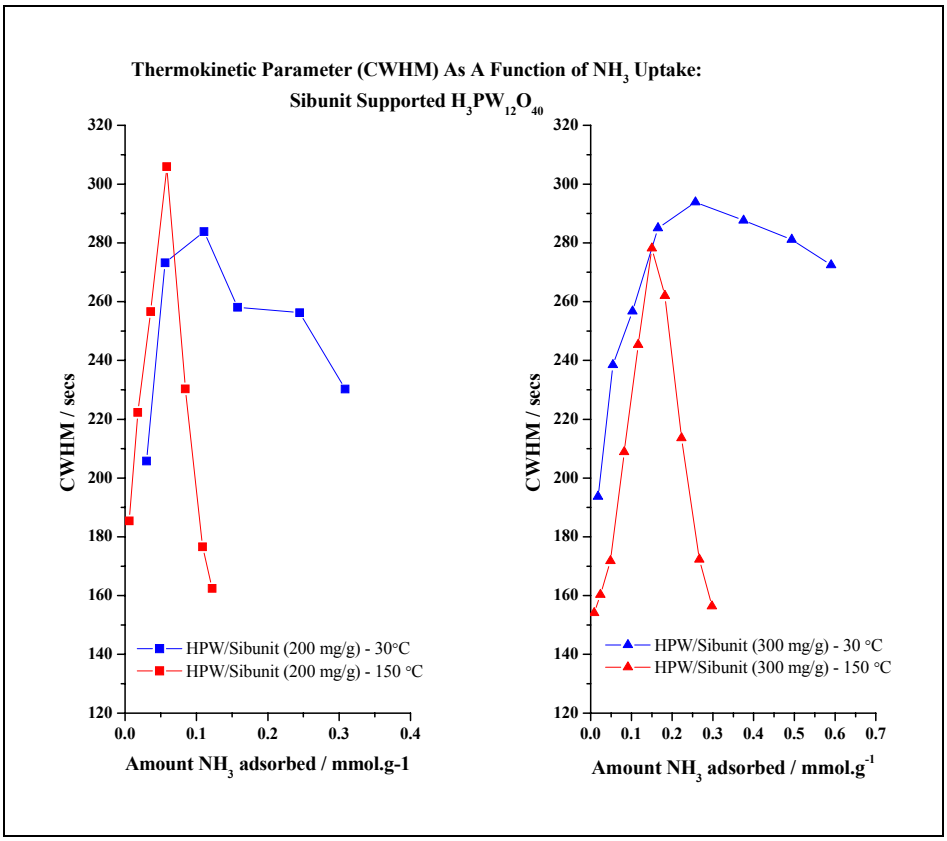

Figure 52: Thermokinetic parameter (CWHM) data for Sibunit supported $H_3PW_{12}O_{40}$ at 30 °C and 150 °C.

The initial sorption rates at 30 °C are significantly higher than that of the bulk acid and are close to the rates observed at 150 °C on the same materials. This suggests that HPW is better dispersed throughout the Sibunit support than in Novacarb supported HPW. Again initial rates are relatively quick at 150 °C which is then followed by a gradual decrease in the rate until a minimum is reached; a gradual increase in the rate of sorption is then seen. Similar behaviour is seen at 150 °C for each of the three supported HPW solid acids though Sibunit shows this behaviour most clearly. The initial rates of sorption in all these materials are only slightly slower than that of the bulk acid

suggesting that there is a small contribution of mass transfer throughout the supports. Sibunit supported HPW shows that the minimum adsorption rates is affected by HPW loading as it shifts to higher coverages as HPW loading is increased. The position of this minimum also correlates with the change in the slope of the differential heat curve that corresponds to completion of the chemisorption process and the onset of physical adsorption. It is not clear why this transition is manifested by a significant decrease and a minimum in the rate of sorption but could possibly be attributed to the increasing contribution of reversibly adsorbed NH_3 and mass transfer effects as it is likely that acid sites located close to the surface will be occupied first by NH_3 molecules. This agrees with the mole ratios of $NH_{3(irr)}$:HPW which are relatively low with values of 2.0 and 3.3 for HPW/Sibunit (200 mg/g) and HPW/Sibunit (300 mg/g) respectively. Also reversibly adsorbed NH_3 becomes more significant as less accessible strong acid sites are being occupied. The slowest rate and the largest difference between maximum and minimum rates are observed for HPW/Sibunit (200 mg/g) (see Figure 52). This is consistent with the above interpretation because Sibunit particles are much larger than either SBA-15 or Novacarb and possesses a less open pore network[4] which could contribute to the slower rate of NH_3 adsorption.

4.3.6 Overall Summary

Bulk tungstophosphoric acid (HPW) and supported HPW onto three different mesoporous solids: SBA-15, Sibunit, and Novacarb (which also contains a significant volume of micropores), have been studied by static NH_3 adsorption microcalorimetry. To measure surface acidity of solid acids by NH_3 adsorption microcalorimetry follows the basic principle that the enthalpy of NH_3 adsorption, referred to in this work as $-Q_{diff}(NH_3)$ is a measure of the strength of available acid sites and the amount of NH_3 adsorbed is equivalent to the concentration of available acid sites (see Chapter1, section 1.1.6.6). It is clear that for the purposes of either adsorbent or catalytic applications that HPW needs to be supported because although HPW has high acid strength and concentration of acid sites, its surface area is extremely low (see Table 30).

Shown below in Table 30 is a comparison of NH_3 adsorption data for all supported HPW samples investigated.

	BET SA determined by N_2 adsorption ($m^2.g^{-1}$)	Micropore Volume ($ml.g^{-1}$)	Mesopore Volume ($ml.g^{-1}$)	Calorimeter temperature (°C)	$-Q_{diff}(NH_3)$ at a coverage of 0.05 $mmol.g^{-1}$ (± 5 $kJ.mol^{-1}$)	Surface coverage of NH_3 at which $-Q_{diff}(NH_3)$ falls below 80 $kJ.mol^{-1}$ (± 0.05$mmol.g^{-1}$)	Irreversibly adsorbed NH_3 ($mmol.g^{-1}$)*	Mole Ratio $NH_{3(irr)}$: HPW #
Pure $H_3PW_{12}O_{40}$ (HPW)	2.3	*	*	30	165	0.86	0.23	0.7
				150	215	0.84	0.75	2.4
SBA-15 Support	728.9	0.09	0.63	30	75	*	/	/
HPW/SBA15 (174 mg/g)	286.3	0.028	0.065	30	123	0.45	0.86	16.7
				150	158	0.35	0.29	5.6
HPW/SBA15 (320 mg/g)	/	/	/	30	117	0.28	/	/
				150	164	0.33	0.22	2.6
HPW /SBA-15 (420 mg/g)	143.0	0.004	0.11	30	149	0.5	0.45	8.8
				150	160	0.5	0.38	7.4
Novacarb Support	926.0	0.33	0.53	30	78	*	/	/
				150	79	*	/	/
HPW/Novacarb (100mg/g)	423.4	0.15	0.37	30	115	0.13	0.16	4.5
				150	150	0.18	0.08	2.3
HPW/Novacarb (311 mg/g)	368.7	0.12	0.34	30	106	0.15	0.20	1.8
				150	138	0.18	0.07	0.6
Sibunit Support	290.7	0.019	0.18	30	48	*	/	/
				150	58	*	/	/
HPW/Sibunit (200 mg/g)	132.6	0.006	0.17	30	84	0.05	0.11	2.0
				150	102	0.07	/	/
HPW/Sibunit (254 mg/g)	170.9	0.013	0.18	30	85	0.1	0.28	3.9
				150	120	0.18	/	/
HPW/Sibunit (300 mg/g)	124.8	0.008	0.15	30	100	0.18	0.27	3.3
				150	124	0.23	/	/

Table 30: Acidity data and other solid acid characteristics for pure HPW and all supported HPW samples.

Activation temperature = 2hrs at 150 °C for 30 °C experiments
Activation temperature = 2hrs at 150 °C for 150 °C experiments
 # based on 2-cycle re-adsorption NH_3 isotherms
**= too low to measure, /= not measured*

Nitrogen adsorption data shows that all three supports materials have relatively high surface areas, but as HPW loading increases these fall. This is as expected because HPW is being deposited in the pores and can be clearly seen in the nitrogen adsorption data above. Table 30 shows that Novacarb retains the greatest surface area in comparison to SBA-15 and Sibunit, even at high HPW loading. This is possibly due to Novacarb being the only support investigated that contains a significant volume of micropores which may not be fully accessible to HPW. On the basis of the sorption data obtained with the unsupported acid at 30 °C it is clear that the rates of sorption when HPW is supported at 30 °C show that mass transfer seen for pure HPW is reduced due to the dispersion of HPW onto the high surface area supports.

When comparing CWHM as a function of the amount of NH_3 adsorbed differences can be seen between pure bulk HPW and supported HPW materials. Supported HPW materials especially Sibunit and SBA-15 show a clearer transition from chemical to physisorption at 150 °C. The position of the minimum in the rate of sorption corresponds to the completion of chemisorption and the onset of physical adsorption. This is not seen so clearly for Novacarb supported HPW and is possibly related to the microporous nature of Novacarb.

Comparisons can be drawn between the two carbon supports Novacarb and Sibunit. Ammonia adsorption data shows that NH_3 is weakly adsorbed onto both support materials (i.e. heats below 80 kJ.mol^{-1}). The sorption capacity of Sibunit appears to be considerably lower than Novacarb, and previously it has been reported that for Novacarb weak acidity arises from its surface chemistry as it is activated in CO_2 during manufacture which produces weakly acidic phenolic and lactonic oxygen groups, which may be responsible for very weak acidity and thus an increase in NH_3 sorption capacity[18]. On the addition of HPW to both Novacarb and Sibunit, the differential heats of NH_3 adsorption increase. Novacarb supported HPW samples show higher $-Q_{diff}(NH_3)$ than Sibunit supported HPW at both 30 °C and 150 °C which suggests less interaction between HPW and Novacarb, and therefore Novacarb should exhibit higher activity in Brønsted catalysed reactions. The differential heat versus coverage plots for Sibunit supported HPW (254 mg/g and 300 mg/g) at 150 °C suggest that acid sites are distributed uniformly and have a similar strength where as Novacarb supported HPW samples do not show this trend. The shapes of the CWHM versus ammonia loading curves for Novacarb and Sibunit supported HPW show very different trends. For Sibunit supported HPW the dynamics of sorption show a clear transition from chemical to physisorption especially at 150 °C whereas this is not clearly seen with HPW/Novacarb (311 mg/g).

When the two mainly mesoporous supports SBA-15 and Sibunit are compared the advantages of the large open pore structure of SBA-15 can be seen. The amount of NH_3 adsorbed is much greater than either of the two carbon supports suggesting that HPW is well dispersed and the most active sites are easily accessible at both 30 °C and 150 °C, and the strength of these sites is much greater indicating that there is less interaction between SBA-15 and HPW than carbon. Also both mesoporous supports show a clear minima in the rates of sorption as a function of NH_3 loading though the difference between the maximum and minimum rates of NH_3 adsorption are considerably smaller for SBA-15 supported HPW when compared with Sibunit supporting the idea that a large degree of acid sites are easily accessible.

NH_3 adsorption data at 150 °C shows that SBA-15 supported HPW have the strongest acid sites even at low HPW loadings when heats are measured at coverage of 0.05 $mmol.g^{-1}$ compared to the carbon supports. This accessibility of strong acid sites is most likely due to the ordered pore structure of SBA-15 and is also evidenced in the surface coverage data showing the concentration of acid sites with heats greater than 80 $kJ.mol^{-1}$ increasing with HPW loading. Other evidence to support the presence of strong acid sites is shown in the 2 cycle adsorption isotherms which show that a high concentration of NH_3 is irreversibly adsorbed in comparison to Novacarb and Sibunit. Note that strongly acidic sites for all supported HPW catalysts are provided purely by the tungstophosphoric acid.

Among the three support materials, SBA-15 shows the most promising performance for both potential high and low temperature industrial applications, due to (i) better retention of acid strength, (ii) good dispersion of acid and (iii) good accessibility of the acid sites.

[1] T. Okuhara, M. Mizuno, M. Misono, App. Catal. A:Gen., 222 (1-2) (2001) 63-77.

[2] L.R. Pizzio, C.V. Cacers, M.N. Blanco, App. Catal. A:Gen., 167 (1998) 283-294.

[3] D.E. Katsoulis, Chem. Rev., 98 (1998) 359-387.

[4] A. Lapkin, B. Bozkaya, T. Mays, Catal. Today, 81 (2003) 611-621.

[5] C. Leblond, J. Wang, R.D. Larsen, C.J. Orella, A.L. Foreman, R.N. Landau, J. Laquidara, J.R. Sowa, D.G. Blackmond, Y.K. Sun, Thermochim. Acta, 289 (1996) 189-207.

[6] Lj. Damjanovic, V. Rakic, U.B. Mioc, A. Auroux, Thermochim. Acta, 434 (2005) 81-87.

[7] M.P. Hart, D.R. Brown, J. Mol. Catal. A:Chem., 212 (2004) 315-321.

[8] D. Meloni, S. Laforge, D. Martin, M. Guisnet, E. Rombi, V.Solinas, Appl. Catal. A :Gen 215 (1-2) (2001) 55-66.

[9] F. Lefebvre, F.X. Liu-Cai, A. Auroux, J. Mater. Chem., 4 (1994) 125-131.

[10] M. O'Neill, J. Phillips, J. Phys. Chem., 91 (1987) 2867-2874.

[11] E.F. Kozhevnikova, I.V. Kozhevnikov, J. Catal., 224 (2004) 164-169.

[12] F. Lefebvre, B. Jouget, A. Auroux, React. Kinet. Catal. Lett., 53 (1994) 297-302.

[13] E.F. Kozhevnikova, I.V. Kozhevnikov, J. Catal., 224 (2004) 164-169.

[14] L.C. Jozefowicz, H.G. Karge, J.B. Moffat, Micro. Mat., 1 (1993) 313-322.

[15] F.X. Liu-Cai, B. Sahut, E. Faydi, A. Auroux, G. Herve, App. Catal. A:Gen., 185 (1999) 75-83.

[16] R.S. Drago, S.C. Dias, M. Torrealba, L. D. Lima, J. Am. Chem. Soc., 119 (1997) 4444-4452.

[17] S.R. Tennison, Appl. Catal. A:Gen., 173 (1998) 289-311.

[18] A. Pigamo, M. Besson, B. Blanc, P. Gazellot. A. Blackburn, O. Kozynchenko, S. Tennison, E. Crezee, F. Kapteijn, Carbon, 40 (2002) 1267-1278.

[19] R.S. Drago, S.C. Dias, M. Torrealba, L.D. Lima, J. Am. Chem. Soc., 119 (1997) 4444-4452.

CHAPTER FIVE

SOLID ACID CATALYSTS STUDIED BY MICROCALORIMETRY

In this chapter the experimental parameters for each catalyst and the results obtained from measuring their surface acidity using ammonia adsorption microcalorimetry will be shown and discussed.

Section 1 – Sample Preparation

Using the experimental set-up described in Chapter 3 each catalyst was subjected to an in-situ activation period before adsorption of ammonia, and each solid acid was run in triplicate. Single examples of results are presented here. The experimental conditions used shall be described below for each catalyst type.

Supported tungstophosphoric heteropoly acid (HPW) samples (150 mg) were used in their as-received state and were activated in-situ under dynamic vacuum for 2 hours at 150 °C before NH_3 adsorption at 150 °C.

Clay samples (150 mg) were used in their as-received powdered state except for Al^{3+} and Fe^{3+} exchanged versions of Fulcat 200 and Al^{3+} exchanged Fulcat 240 whose preparation is described in 2.1.1.2.a. All samples were activated under dynamic vacuum for two hours at 150 °C and 200 °C for two separate series of experiments prior to adsorption at temperatures of 150 °C and 200 °C respectively.

The zeolites (150 mg) were activated under dynamic vacuum for two hours at 150 °C before NH_3 adsorption at 150 °C.

Sulfonated polystyrene ion exchange resins (300 mg) in their as-received state were placed under dynamic vacuum to activate for two hours at 100 °C before NH_3 adsorption at 100 °C.

Section 2 – Results & Discussion

Based on the assumption that $-Q_{diff}(NH_3)$ is a measure of the strength of acid sites and that the amount of NH_3 adsorbed when $-Q_{diff}(NH_3)$ is ≥ 80 kJ.mol^{-1} gives a measure of the concentration of

strong acid sites, acidity data measured at high temperature (100 – 200 °C) for all studied solid acids shall be reported and discussed. Ammonia adsorption measurements were obtained at 200 °C for both clay series and the exchanged Fulcats, as Lewis acid sites are believed to be generated at higher thermal activation temperatures than Brønsted acid sites and also the strength of Lewis acidity is associated with exchangeable cations[1]. Workers have shown that clays exchanged with Fe^{3+} cations exhibit some of the strongest Lewis acid sites[2]. Each solid acid has been run in triplicate, the reproducibility of which has been discussed in 3.2.1.3.c. Graphs presented will plot the differential molar heats of NH_3 adsorption, $-Q_{diff}(NH_3)$ vs. amount of NH_3 adsorbed ($-Q_{diff}(NH_3)$/coverage profiles) and also the NH_3 adsorption isotherms for each solid acid based on these profiles. Simple numerical data taken from the $-Q_{diff}(NH_3)$/coverage plots showing acid strengths (as $-Q_{diff}(NH_3)$) taken at a specific coverage (the same for all catalysts) and also concentration of acid sites with heats above 80 $kJ.mol^{-1}$ shall be shown. This is to allow for ease of comparison between each solid acid.

5.2.1 Supported Tungstophosphoric Acid ($H_3PW_{12}O_{40}$)

The NH_3 adsorption microcalorimetric results obtained at 30 °C and at 150 °C have been shown and discussed in Chapter 4 comparing acidity data for pure HPW and supported HPW on SBA-15, and the two carbons: Novacarb and Sibunit. A comparison will be made in section 5.2.5 between their acidity and other solid acids examined here in this chapter.

5.2.2 Clays

Ammonia adsorption isotherms and acidity data recorded at 150 °C and 200 °C will be shown for the 'Fulcat 200 series' (Rockwood) and the 'K-series' (Süd-Chemie).

5.2.2.1 'Fulcat 200 series' montmorillonite clays

Microcalorimetric NH_3 adsorption results were obtained at 150 °C and 200 °C for the 'Fulcat 200 series' clay catalysts and typical $-Q_{diff}(NH_3)$/coverage profiles and NH_3 adsorption isotherms at 150 °C are shown below in Figure 53.

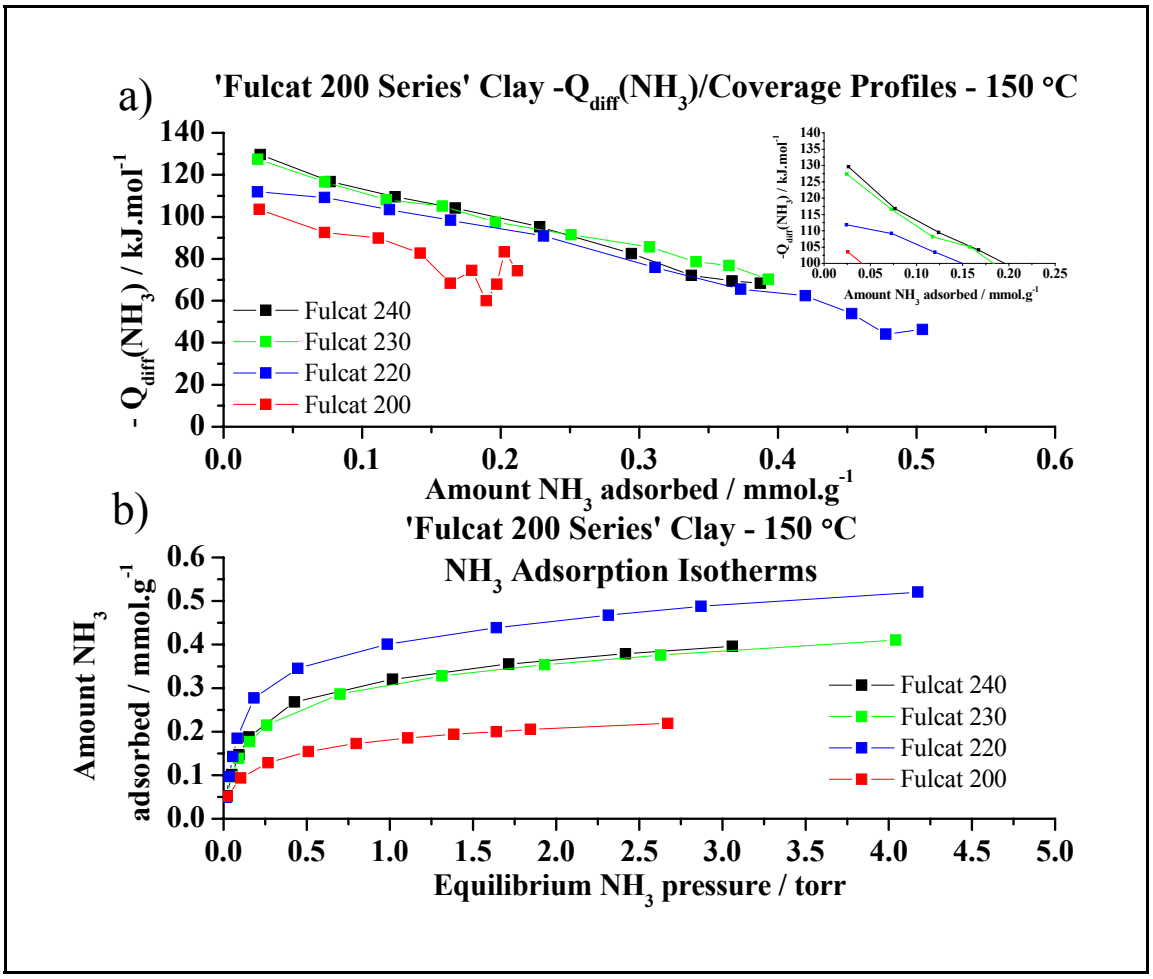

Figure 53: a) -$Q_{diff}(NH_3)$/coverage profiles for 'Fulcat 200 series' clays b) NH_3 adsorption isotherms for 'Fulcat 200 series' clays at 150 °C.

The -$Q_{diff}(NH_3)$ vs. amount NH_3 adsorbed recorded at 150 °C (Figure 53a) are interpreted as -$Q_{diff}(NH_3)$/coverage plots. The NH_3 adsorption isotherms (Figure 53b) were measured as a single cycle for each catalyst and no attempt was made to differentiate between NH_3 irreversibly adsorbed on the catalyst and more weakly held NH_3 which may have been adsorbed reversibly. A comparison between the -$Q_{diff}(NH_3)$/coverage profiles and NH_3 adsorption isotherms for Fulcat 230 and Fulcat 240 (the two most extensively acid treated Fulcats) shows little variation in the molar heats and amount of NH_3 adsorbed, with initial heats of ca.130 kJ.mol^{-1} and NH_3 concentration of 0.40 mmol.g^{-1} when the heats of adsorption fall below 80 kJ.mol^{-1}. A more detailed inset graph is shown in Figure 1a showing the minimal difference between the two clays when only molar heats above 100 kJ.mol^{-1} are shown. Within experimental error no significant difference can be identified. Fulcat 220 would appear to lack the strongest sites exhibited by Fulcat 230 and 240 as it has a lower initial heat of adsorption even though its profile appears to

merge with the two other acid treated clays at higher NH_3 concentrations. The NH_3 adsorption isotherms show that Fulcat 220 adsorbs a greater overall amount of ammonia than either Fulcat 230 or 240 although from the profiles in Figure 53a it appears that the "extra" adsorbed by this clay over Fulcat 230 and 240 is relatively weakly held, and it is possible that it is due to proportionally more reversibly held NH_3 on Fulcat 220 (possibly on non-acidic sites) resulting in a lower overall differential enthalpy. If the concentration of acid sites is related to the C.E.C. it is of no surprise that Fulcat 220 possesses a higher concentration, as C.E.C. data in 2.3.2.1.c shows that the C.E.C.'s for Fulcat 230 and 240 are lower than for Fulcat 220. A distinct difference is seen between the non-acidified parent clay Fulcat 200 and its acid treated counterparts as it adsorbs relatively little NH_3 and differential heats of adsorption are all relatively low. It should be noted that for Fulcat 200 the value of $-Q_{diff}(NH_3)$ shows excessive scatter and has large associated errors because so little of each pulse of NH_3 was adsorbed. Fulcat 200 is in its Ca^{2+} form and therefore would not normally be expected to generate high concentrations of strongly acidic sites. An important feature of the $-Q_{diff}(NH_3)$ vs. amount NH_3 adsorbed profiles exhibited by the Fulcat clays, differentiating them from some other solid acids, is that they do not show uniformity in their acid strength as molar heats of adsorption rapidly drop off. This suggests that variations in acid site strength exist, as might be expected given the non-uniform structure of acid treated clays.

As well as studying acidity data at 150 °C for both series of clays, it was also thought useful to determine $-Q_{diff}(NH_3)$/coverage profiles following activation at 200 °C. Figure 54a below shows $-Q_{diff}(NH_3)$ vs. amount NH_3 adsorbed and the corresponding NH_3 adsorption isotherms for the 'Fulcat 200 series' measured at 200 °C following activation at 200 °C.

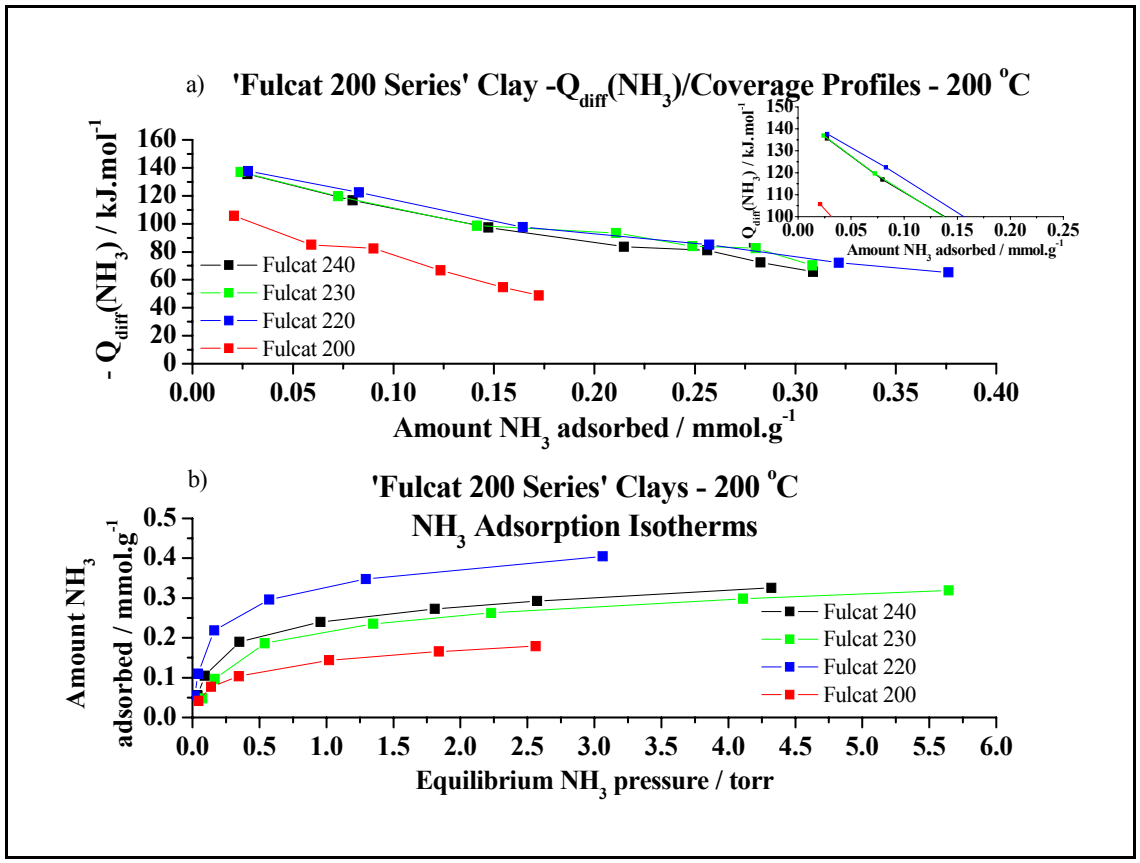

Figure 54: a) -$Q_{diff}(NH_3)$/coverage profiles for 'Fulcat 200 series' clays b) NH_3 adsorption isotherms for 'Fulcat 200 series' clays at 200°C.

It is anticipated from previous work that strength of Brønsted acid sites are maximised at an activation temperature of 100 - 150 °C, and that strength of Lewis acid sites is maximised at activation temperatures of 200 – 250 °C[1]. When -$Q_{diff}(NH_3)$ vs. amount NH_3 adsorbed is measured at 200 °C, molar heats of adsorption for the first pulse of NH_3 increase by ca.10 kJ.mol^{-1} for both Fulcat 230 and Fulcat 240 compared to measurements at 150 °C, and there is a significant increase in initial heats for Fulcat 220 from 115 kJ.mol^{-1} to 140 kJ.mol^{-1}. Again Fulcat 230 and 240 give similar acidity profiles to each other. Therefore, increased -$Q_{diff}(NH_3)$ after 200 °C activation suggests that there is at least a contribution to overall acidity from Lewis acid sites. The amount of adsorbed ammonia judged from the plateau region of the NH_3 adsorption isotherm shown in Figure 54b decreases by about 0.1 mmol.g^{-1} for Fulcat 220, 230 and 240, but Fulcat 220 still adsorbs the highest concentration of NH_3. It is reasonable to expect that at 200 °C the contribution from reversibly adsorbed ammonia would decrease, and the reduced concentration of NH_3 adsorbed is probably due to this factor rather than any decrease in acid site concentration.

	Calorimeter Temperature (°C)	Fulcat 200 (Rockwood)	Fulcat 220	Fulcat 230	Fulcat 240
		Parent Montmorillonite	Progressively acid activated montmorillonite		
$-Q_{diff}(NH_3)$ at a coverage of 0.05 mmol.g^{-1} (± 2 kJ.mol^{-1})	150	98	110	122	124
	200	90	131	128	128
Surface Coverage of NH_3 at which $-Q_{diff}(NH_3)$ falls below 80 kJ.mol^{-1} (± 0.02 mmol.g^{-1})	150	0.15	0.29	0.31	0.32
	200	0.10	0.28	0.29	0.26
BET Surface Area ($m^2.g^{-1}$)		108	271	363	364
Mesopore Volume (ml.g^{-1})		0.145	0.233	0.365	0.635
C.E.C. based on Mg content (± 5 meq 100 g^{-1})		90	68	53	33

Table 31: Comparison of NH_3 adsorption data, N_2 adsorption data, and C.E.C. data for the 'Fulcat 200 series' at 150 °C and 200 °C.

Table 1 above shows a comparison of acidity data determined for the 'Fulcat 200 series' at both 150 °C and 200 °C. An increased initial $-Q_{diff}(NH_3)$ value of 110 kJ.mol^{-1} from 100 kJ.mol^{-1} at a coverage of 0.05 mmol.g^{-1} for Fulcat 200 is seen at 200 °C and is in keeping with some Lewis acidity being present (see Figure 53a and Figure 54a). This would suggest that defect sites described previously are resulting in Lewis acid behaviour because if the same acid sites are responsible for initial adsorption at 150 °C and 200 °C, then the fact that differential heats of NH_3 adsorption are higher at higher temperature would be consistent with a greater degree of Lewis acidity. Allowing for the reduced amount of reversibly adsorbed NH_3 at the higher temperature, it seems likely that the concentration of acid sites on the clays following activation at the two temperatures is more or less the same. The acid treated Fulcat clays 220 - 240 all show a general increase in the strength of available acid sites (as measured by $-Q_{diff}(NH_3)$) when measured at 200 °C, with Fulcat 220 showing the largest increase of 21 kJ.mol^{-1}. One possible reason for this is that Fulcat 220 has a greater percentage of Fe_2O_3 present in its structure as shown in 2.1.2.2, providing high charge to radius Lewis acidic Fe^{3+}, and as explained above the increased level of dehydration is thought to favour Lewis acidity. Generally Lewis acid sites adsorb NH_3 with higher $-Q_{diff}(NH_3)$ than Brønsted acid sites[6]. So if a clay has high concentrations of Lewis sites, it might be expected that increases in $-Q_{diff}(NH_3)$ would be seen. As well as this there is the complication that contribution to $-Q_{diff}(NH_3)$ from reversibly adsorbed NH_3 will be less at the higher

temperature. On comparing Fulcat 230 and 240 it can clearly be seen that there is little difference between them in terms of their acidity and concentration of acid sites.

To determine the effect of cation exchange on the acidity of montmorillonites the parent clay Fulcat 200 (thought to be in the Ca^{2+} form) and the "most" acid treated Fulcat 240 were ion exchanged with the acidic cation Al^{3+}, and Fulcat 200 was also exchanged with Fe^{3+}. This was done with a view to modifying the acidic properties. Typical $-Q_{diff}(NH_3)$/coverage profiles and NH_3 adsorption isotherms are shown below in Figure 55,
Figure *56* and Figure 57 comparing these ion-exchanged varieties with the unmodified versions.

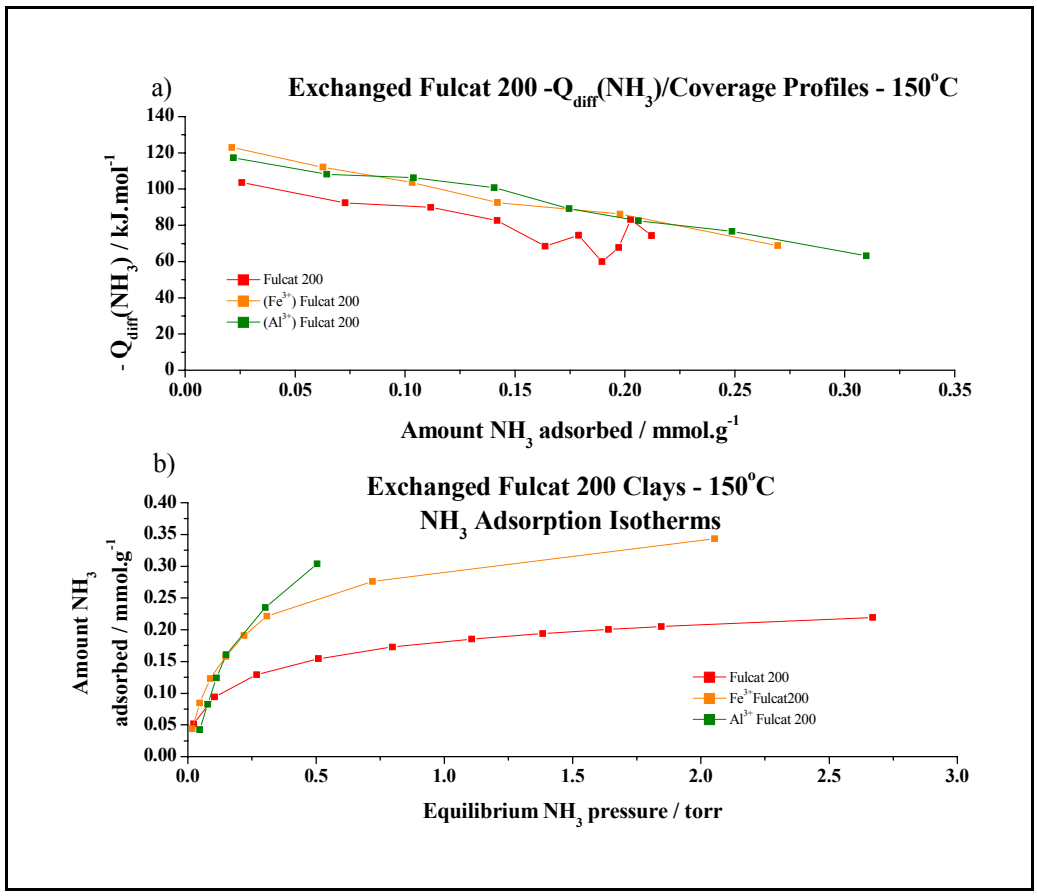

Figure 55: a) Acidity profiles for ion-exchanged Fulcat 200 clays and b) NH_3 Adsorption isotherms for ion-exchanged Fulcat 200 clays at 150 °C.

The $-Q_{diff}(NH_3)$ vs. NH_3 adsorbed plots (Figure 55a) show that the exchangeable cation is a major source of acidity at 150 °C for Al^{3+} and Fe^{3+} exchanged Fulcat 200 clays as strengths and concentrations of acid sites are significantly increased over the parent clay for ion-exchanged

clays. This would be expected as Fulcat 200 is in the Ca^{2+} form, and would not normally generate acid sites. The few acid sites that are measured in Fulcat 200 are almost certainly associated with non-exchangeable sites and probably defect sites within the clay lattice. Results show that Al^{3+} and Fe^{3+} exchanged parent clay are very similar in terms of the strength of acid sites as measured by heats of NH_3 adsorption, and also in the concentration of acid sites, following activation at 150 °C.

Shown below in

Figure *56* are $-Q_{diff}(NH_3)$/coverage profiles and NH_3 adsorption isotherms for exchanged Fulcat 200 clays at a NH_3 adsorption (and activation) temperature of 200 °C.

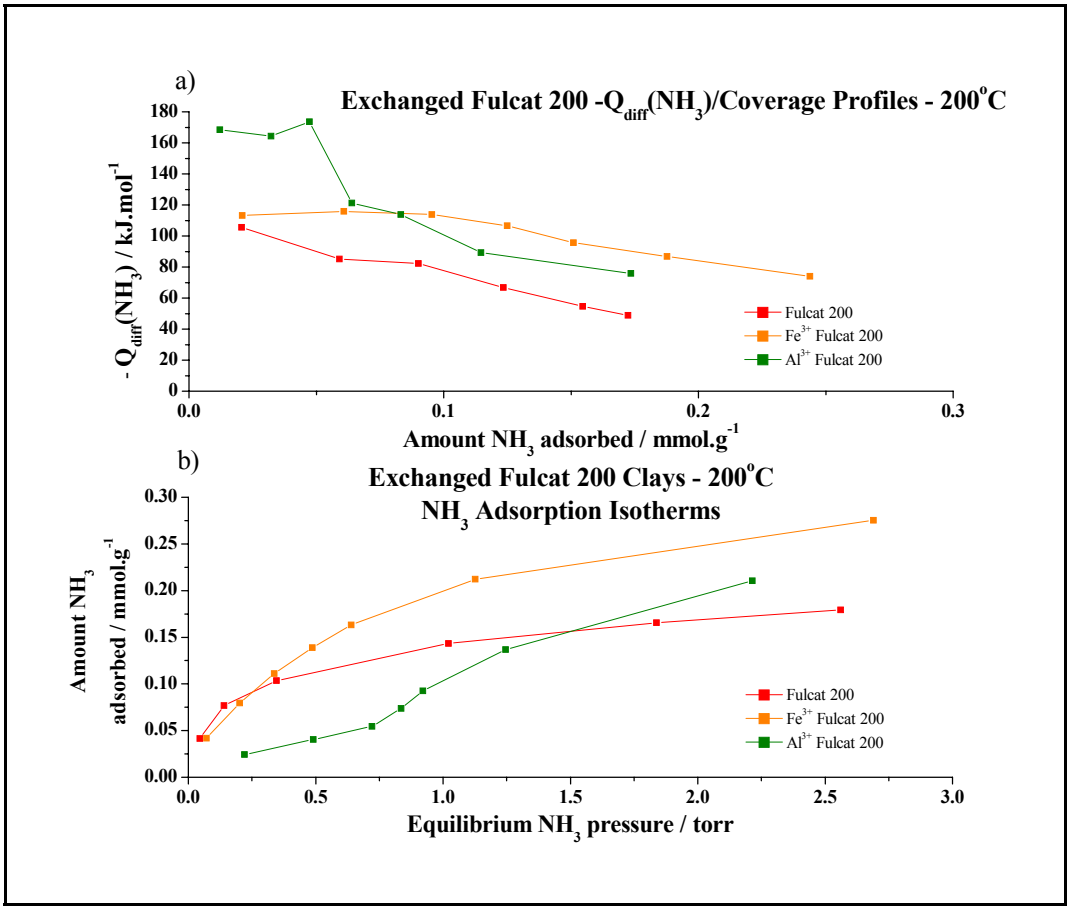

Figure 56: a) $-Q_{diff}(NH_3)$/coverage profiles for ion-exchanged Fulcat 200 clays and b) NH_3 adsorption isotherms for ion-exchanged Fulcat 200 clays at 200 °C.

At 200 °C the uptake of ammonia on Al^{3+} and Fe^{3+} exchanged Fulcat 200 rises more slowly than at 150 °C as shown by the NH_3 adsorption isotherms in

Figure *56*b. The $-Q_{diff}(NH_3)$ vs. amount NH_3 adsorbed is quite surprising in that Al^{3+} exchanged clay shows high initial heats of ~ 170 $kJ.mol^{-1}$ compared to Fe^{3+} exchanged clay that has a heat of 115 $kJ.mol^{-1}$ (

Figure *56*a). This does not agree with previous reports that have indicated that Fe^{3+} exchanged clays, which exhibit high Lewis acidity on activation at 200 °C adsorb NH_3 with higher heats than Al^{3+} exchanged clays for which Lewis acid strength is lower. Previous work based on acidities and catalytic activities in Brønsted acid catalysed and Lewis acid catalysed reactions has shown that on activation at 150 °C the acidity of ion-exchanged clays is mainly Brønsted and Al^{3+} gives much higher activity than Fe^{3+}. Activation at 200 °C results in very little Brønsted acidity and Lewis acidity dominates. Under these conditions the Fe^{3+} form is more active than the Al^{3+} form[3, 4]. Furthermore, it might be expected that anhydrous Fe^{3+} would be able to coordinate to more NH_3 molecules than just one per acid site since it is capable of forming a six co-ordinate complex with NH_3, whereas Al^{3+} does not normally form stable complex ions with NH_3.[5]

	Calorimeter Temperature (°C)	Fulcat 200 (Rockwood)	Al^{3+} Fulcat 200	Fe^{3+} Fulcat 200
$-Q_{diff}(NH_3)$ at a coverage of 0.05 $mmol.g^{-1}$ (± 2 $kJ.mol^{-1}$)	150	98	112	115
	200	90	165	115
Surface Coverage of NH_3 at which $-Q_{diff}(NH_3)$ falls below 80 $kJ.mol^{-1}$ (± 0.02 $mmol.g^{-1}$)	150	0.15	0.23	0.23
	200	0.10	0.16	0.22
Surface Area ($m^2.g^{-1}$)		108	81	95
Mesopore Volume ($ml.g^{-1}$)		0.145	0.134	0.163

Table 32: Comparison of acidity and N_2 adsorption data for ion-exchanged Fulcat 200 (150 °C & 200 °C).

A comparison between the exchanged Fulcat 200 clays is shown above in Table 32 for the NH_3 microcalorimetric acidity data and nitrogen adsorption data. Again the amount of NH_3 adsorbed falls when acidity is measured at 200 °C presumably as reversibly adsorbed NH_3 is reduced. As was mentioned above there is an anomaly in the results for Al^{3+} exchanged Fulcat 200 as this shows exceptionally strong acid sites at a coverage of 0.05 $mmol.g^{-1}$ at 200 °C It is not clear why this is so as reproducibility was also very poor. If this result is set aside then Fe^{3+} exchanged

Fulcat 200 shows that strengths of acid sites do not decrease on activation at the higher temperatures since this will almost certainly dehydrate the cation the result implies that significant Lewis acidity must be present following 200 °C activation.

The most acid treated clay, Fulcat 240, was also exchanged with Al^{3+} and results are shown below for microcalorimetric data obtained at both 150 °C and 200 °C.

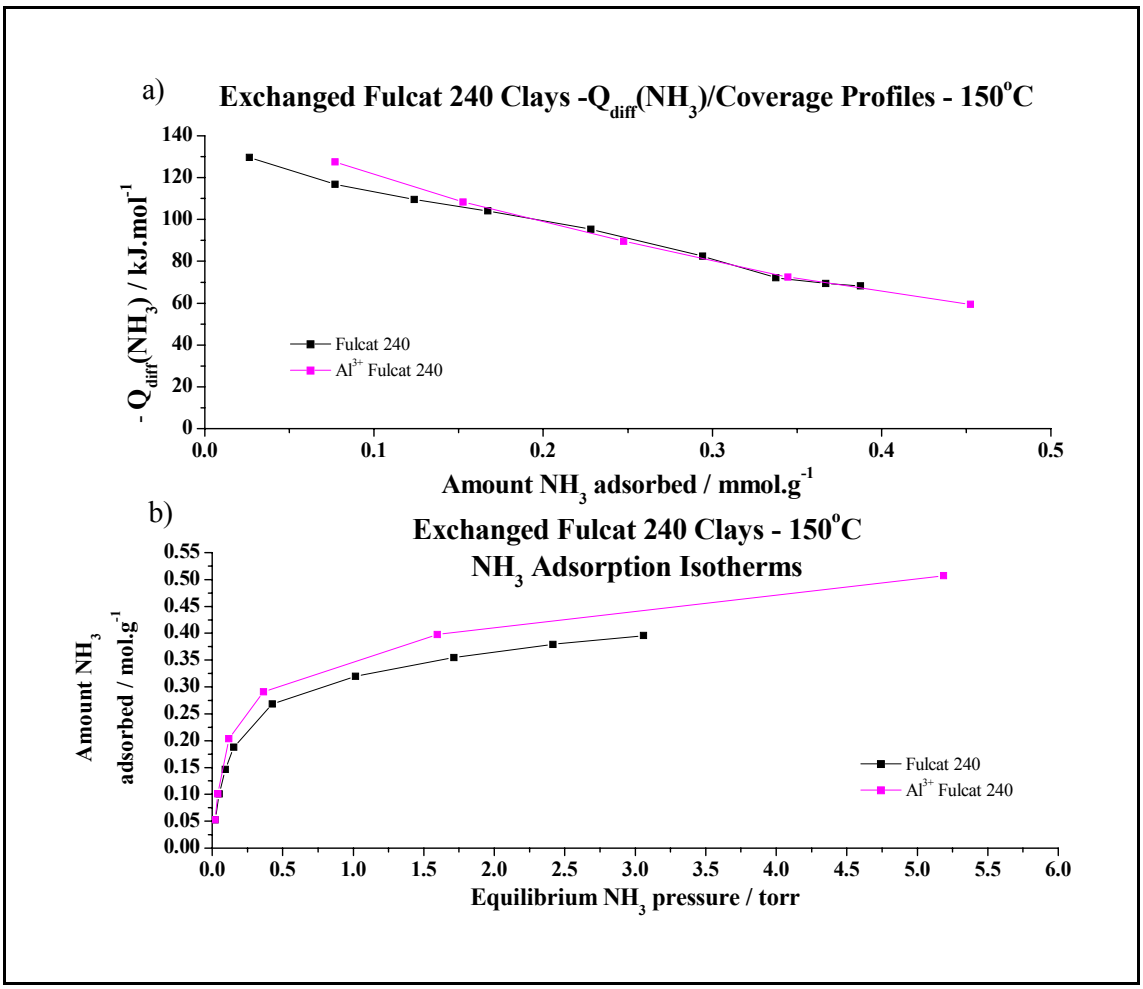

Figure 57: a) -$Q_{diff}(NH_3)$/coverage profile for Al^{3+} exchanged Fulcat 240 clay and b) NH_3 adsorption isotherm forAl^{3+} exchanged Fulcat 240 clay at 150 °C.

When the acid treated clay Fulcat 240 is exchanged with Al^{3+} the amount of ammonia adsorbed increases very slightly as shown by the adsorption isotherm (Figure 57b). This increase is within experimental error and is shown below in Table 33. It can be concluded from Figure 57a that further Al^{3+} exchange does not really alter the strength of acid sites present. These results are not

unexpected and are consistent with the idea that acid-activated montmorillonite clays are largely in the Al^{3+} exchanged form in their as received state[6], and that the process known as auto-transformation has occurred to the acid treated clay in which the H^{+} exchanged form of the clay converts to the Al^{3+} form as aluminium slowly leaches from the lattice as the clay is stored[7].

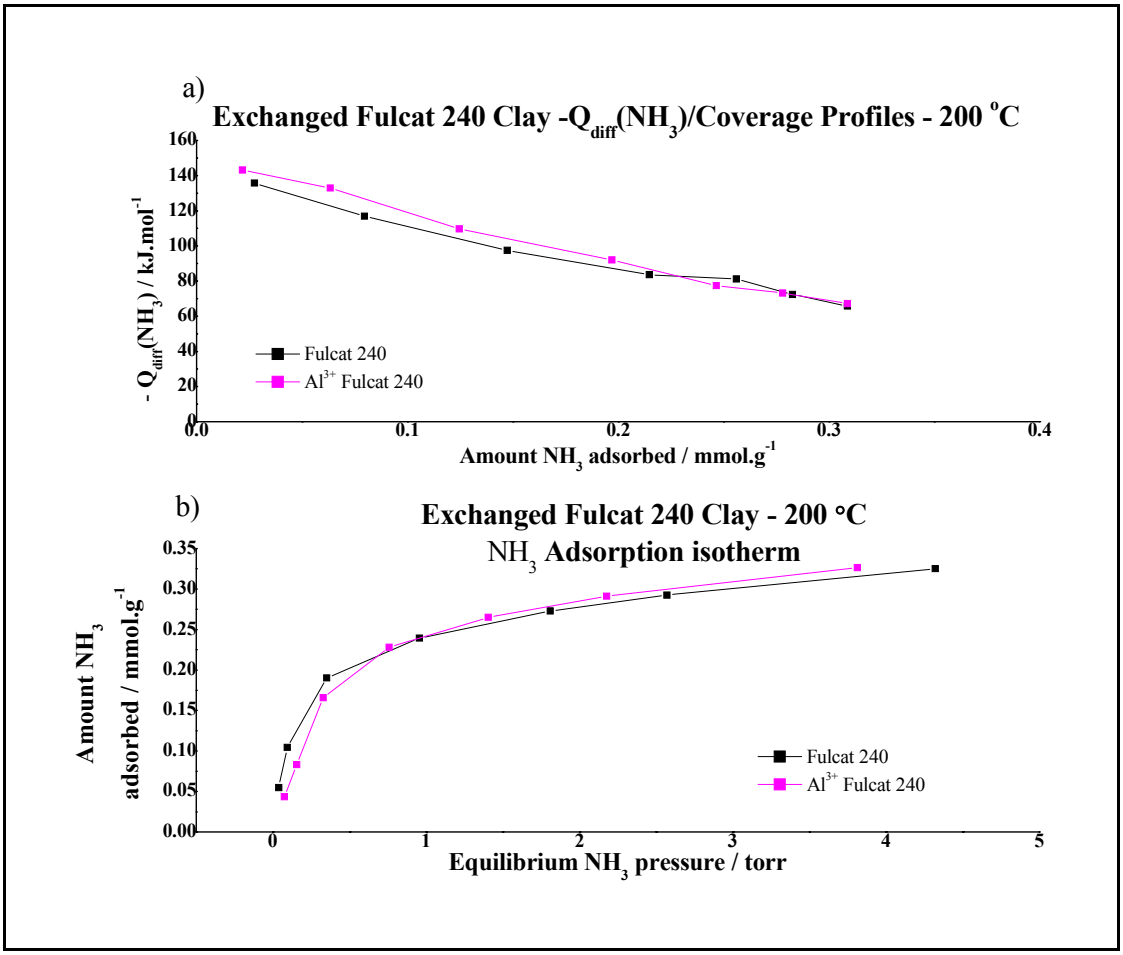

Figure 58: a) -$Q_{diff}(NH_3)$/coverage profile for Al^{3+} exchanged Fulcat 240 and b) NH_3 adsorption isotherm for Al^{3+} exchanged Fulcat 240 clay at 200 °C.

When Fulcat 240 is exchanged with Al^{3+} the 200 °C NH_3 adsorption isotherm does not show any significant variation in either heats or in the amount of ammonia adsorbed compared to the un-exchanged Fulcat240. Again this is consistent with the assumption that Fulcat 240 is already in the Al^{3+} form.

	Calorimeter Temperature (°C)	Fulcat 240	Al^{3+} Fulcat 240
$-Q_{diff}(NH_3)$ at a coverage of 0.1 mmol.g^{-1} (± 2 kJ.mol^{-1})	150	114	123
	200	112	119
Surface Coverage of NH_3 at which $-Q_{diff}(NH_3)$ falls below 80 kJ.mol^{-1} (± 0.02 mmol.g^{-1})	150	0.32	0.31
	200	0.25	0.23
Surface Area ($m^2.g^{-1}$)		364	335
Mesopore Volume (ml.g^{-1})		0.635	0.605

Table 33: Comparison of acidity and N_2 adsorption data for exchanged Fulcat 240 (150 °C & 200 °C).

When this data is compared to data obtained at 150 °C (see Table 33 above) it can be seen that $-Q_{diff}(NH_3)$ increases by ca. 10 kJ.mol^{-1} and the amount of NH_3 adsorbed decreases by 0.1 mmol.g^{-1}. Again it would appear that the same sites are responsible for initial adsorption at both 150 °C and 200 °C and the fact that heats of adsorption are higher at the higher temperature are consistent with a greater degree of Lewis acidity at 200 °C.

5.2.2.2 'K-series' montmorillonite clays

Shown below in Figure 59 are typical $-Q_{diff}(NH_3)$/coverage profiles and NH_3 adsorption isotherms for the 'K-series' montmorillonite clays. Each clay was activated at 150 °C for two hours prior to NH_3 adsorption microcalorimetric measurements at 150 °C.

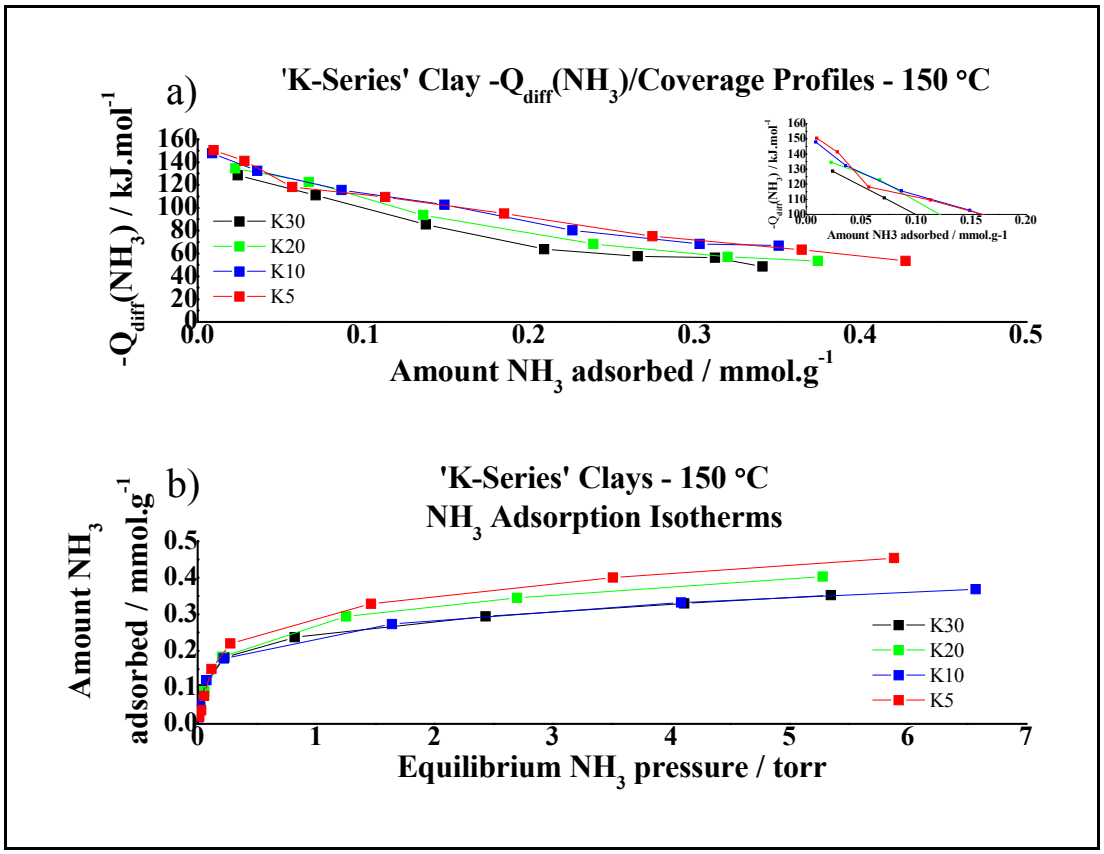

Figure 59: a) -$Q_{diff}(NH_3)$/coverage profiles for 'K-series' clays b) NH_3 adsorption isotherms for 'K-series' clays at 150 °C.

Figure 59a above shows that both acidity profiles and NH_3 adsorption isotherms are similar for all members of the 'K-series', and that the 'K-series' do not follow the expected trend of heats increasing as the amount of acid treatment the clay receives increases. This is shown by K30 the most acid treated clay, as this has the lowest initial heat of NH_3 adsorption whilst the least acid treated member K5 shows the strongest sites with a heat of NH_3 adsorption for the first pulse of ~ 150 kJ.mol^{-1}. This is followed by K10 and K20 and finally K30 all having initial heats between 130 – 135 kJ.mol^{-1}. The heats for all clays decrease relatively quickly with increasing NH_3 coverage and between a coverage of 0.10 and 0.15 mmol.g^{-1} all heats have dropped below 100 kJ.mol^{-1}. This is consistent with the idea of non-uniformity of acid strength in clay structures. The NH_3 adsorption isotherms at 150 °C also show this same trend in terms of the amount of NH_3 adsorbed, with K30 adsorbing the least and K5 adsorbing the most. The overall conclusion is that all 'K-series' clays are very similar to each other. On the basis that increasing acid treatment time improves strength of acid sites K20 would appear to have had less acid treatment and agrees with the higher C.E.C. and powder XRD results as the concentration of acid sites is also greater.

Again microcalorimetric NH_3 adsorption experiments were undertaken at 200 °C. NH_3 adsorption isotherms and $-Q_{diff}(NH_3)$/coverage profiles for the 'K-series' are shown in Figure 60 below.

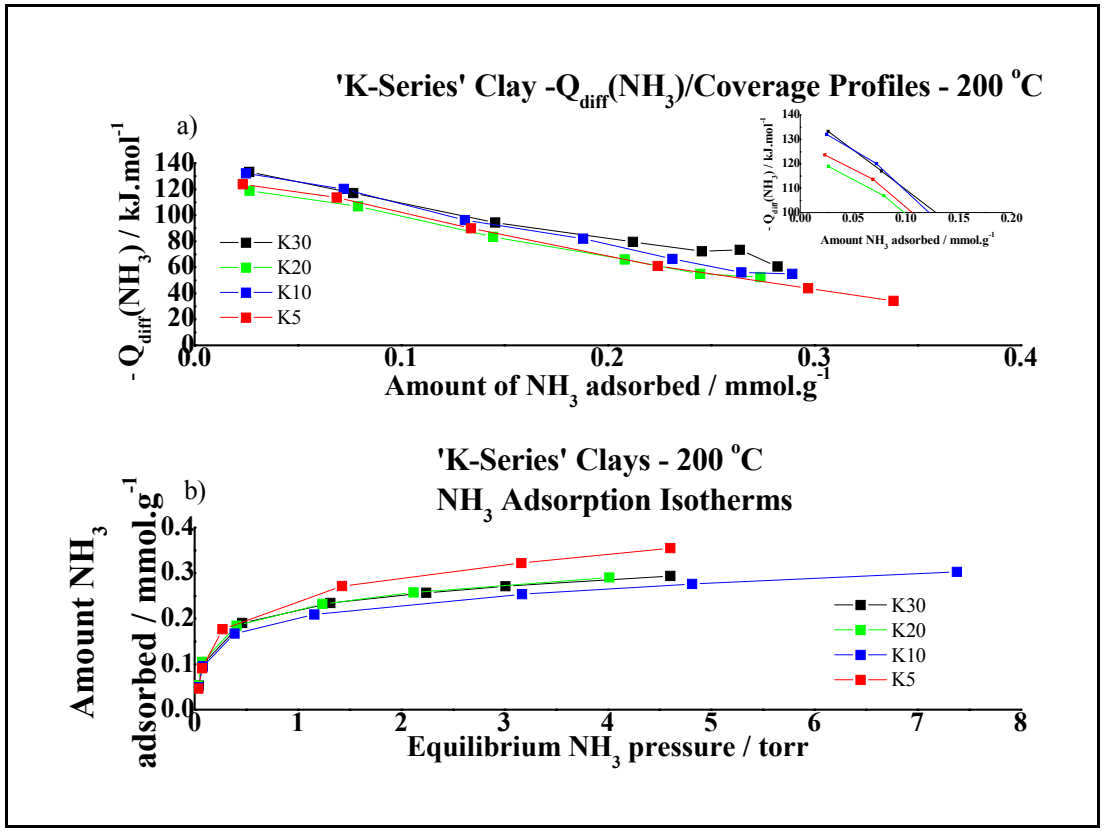

Figure 60: a) $-Q_{diff}(NH_3)$/coverage profiles for 'K-series' clays b) NH_3 Adsorption isotherm comparisons for 'K-series' clays at 200 °C.

At 200 °C the order of the 'K-series' clays differ slightly compared to acidity profiles obtained at 150 °C, with K30 showing the highest heats of NH_3 adsorption. This indicates that K30 has more Lewis acidic sites present over K5, and is followed by K10 and K20. K5 still adsorbs the highest concentration of NH_3, as shown by the NH_3 adsorption isotherms in Figure 60b, and also in agreement with C.E.C. data.

A comparison of microcalorimetric acidity data and nitrogen adsorption data is shown below in Table 34 at 150 °C and 200 °C.

	Calorimeter Temperature (°C)	K5	K10	K20	K30
$-Q_{diff}(NH_3)$ at a coverage of 0.05 mmol.g^{-1} (± 3 kJ.mol^{-1})	150	119	127	129	118
	200	118	126	114	126
Surface Coverage of NH_3 at which $-Q_{diff}(NH_3)$ falls below 80 kJ.mol^{-1} (± 0.03 mmol.g^{-1})	150	0.26	0.23	0.19	0.16
	200	0.17	0.20	0.16	0.21
Surface Area ($m^2.g^{-1}$)		108	181	253	282
Mesopore Volume (ml.g^{-1})		0.375	0.319	0.349	0.402
C.E.C. based on Mg content (± 5) (meq 100 g^{-1})		60	28	30	25

Table 34: Comparison of acidity, N_2 adsorption data, and C.E.C. data for the 'K- series' (150 °C & 200 °C).

Comparison of microcalorimetric NH_3 adsorption data and nitrogen adsorption data for the 'K-series' when acidity data is compared at 150 °C and 200 °C is shown in Table 34 above. It would be expected that progressive acid treatment would destroy the clay's laminar structure and therefore it would be expected that if the cation exchange site is the main source of acidity there would be approximately one acid site per exchange site, and on this basis it would be expected that differential molar heats of NH_3 adsorption (strength of acid sites) would be fairly uniform. In fact they are not uniform suggesting that the strength of the acid sites is somewhat inhomogeneous. Typically 43 – 82 % of acid sites are probed at 150 °C whereas a lower percentage of acid sites are probed at 200 °C.

If the NH_3 microcalorimetric data and other physical characteristics are compared for the two montmorillonite clay series as shown below in

		Fulcat 200 Rockwood	F200 (Al3+)	F200 (Fe3+)	F220	F230	F240	F240 (Al3+)	K5 Sud Chemie	K10	K20	K30
	Temperature (°C)	Parent montmorillonite			Progressively acid activated montmorrillonites				Progressively acid activated montmorillonites			
-Qdiff(NH3) at a coverage of 0.05 mmol.g-1 (± 3 kJ.mol-1)	150	98	112	115	110	122	124	123	119	127	129	118
	200	90	165	115	131	128	128	119	118	126	114	126

Surface coverage of NH3 at which – Qdiff(NH3) falls below 80 kJ.mol-1 (± 0.03 mmol.g-1)	150	0.15	0.23	0.23	0.29	0.31	0.32	0.31	0.26	0.23	0.19	0.16
	200	0.10	0.16	0.22	0.28	0.29	0.26	0.23	0.17	0.20	0.16	0.21
Surface area (m2.g-1)		108	81	95	271	363	364	335	108	181	253	282
Mesopore volume (ml.g-1)		0.15	0.13	0.16	0.23	0.37	0.64	0.61	0.38	0.32	0.35	0.40
C.E.C based on Mg content (± 5 meq 100 g-1)		90	/	/	68	53	33	/	60	28	30	25

Table 35, a number of points can be made.

		Fulcat 200 Rockwood	F200 (Al^{3+})	F200 (Fe^{3+})	F220	F230	F240	F240 (Al^{3+})	K5 Sud Chemie	K10	K20	K30
	Temperature (°C)	Parent montmorillonite			Progressively acid activated montmorrillonites				Progressively acid activated montmorillonites			
-$Q_{diff}(NH_3)$ at a coverage of 0.05 $mmol.g^{-1}$ (± 3 $kJ.mol^{-1}$)	150	98	112	115	110	122	124	123	119	127	129	118
	200	90	165	115	131	128	128	119	118	126	114	126
Surface coverage of NH_3 at which – $Q_{diff}(NH_3)$ falls below 80 $kJ.mol^{-1}$ (± 0.03 $mmol.g^{-1}$)	150	0.15	0.23	0.23	0.29	0.31	0.32	0.31	0.26	0.23	0.19	0.16
	200	0.10	0.16	0.22	0.28	0.29	0.26	0.23	0.17	0.20	0.16	0.21
Surface area ($m^2.g^{-1}$)		108	81	95	271	363	364	335	108	181	253	282
Mesopore volume ($ml.g^{-1}$)		0.15	0.13	0.16	0.23	0.37	0.64	0.61	0.38	0.32	0.35	0.40
C.E.C based on Mg content (± 5 meq 100 g^{-1})		90	/	/	68	53	33	/	60	28	30	25

Table 35: Comparison of acidity, N_2 adsorption data, and C.E.C. data for the 'Fulcat 200 series' and 'K-series' (150 °C & 200 °C).

Neither the 'K-series' nor the 'Fulcat 200 series' show uniformity in the strength of their acid sites. At 150 °C the strongest sites based on differential molar heats are exhibited by the 'K-series' but this is reversed when activated at 200 °C as Fulcats show the highest heats. If it is assumed that concentration of acid sites is related to the ion exchange capacity and that substituted Mg for Al in the octahedral lattice layer of the clay is the predominant source of the lattice negative charge which is neutralised by the exchangeable cations, it is not surprising that Fulcat acid activated clays have a higher concentration of acid sites. Elemental analysis data shows that Fulcat clays retain a higher percentage of Mg within the lattice throughout acid treatment. The other obvious difference between the 'Fulcat 200 series' and the 'K-series' based on elemental analysis is that the former has a much higher iron content than the latter. On the basis that Fe(III) centres could under anhydrous conditions, give rise to relatively high Lewis acidity, it is possible that the iron content of the Fulcats is responsible for the higher acid strength detected for this series following dehydration at 200 °C. There is no obvious reason why the 'K-series' clays exhibit stronger acid sites than the Fulcats at 150 °C. One possible explanation for this is that differences arise in the preparation and acid treatment of the two clay series.

5.2.3 Zeolites

Shown below in Figure 61 are the $-Q_{diff}(NH_3)$/coverage profiles and NH_3 adsorption isotherms for zeolite β and two H-ZSM-5 zeolites with different Si:Al ratios. In-situ activation of catalysts and NH_3 adsorption experiments were carried out at 150 °C, followed by NH_3 adsorption at 150 °C.

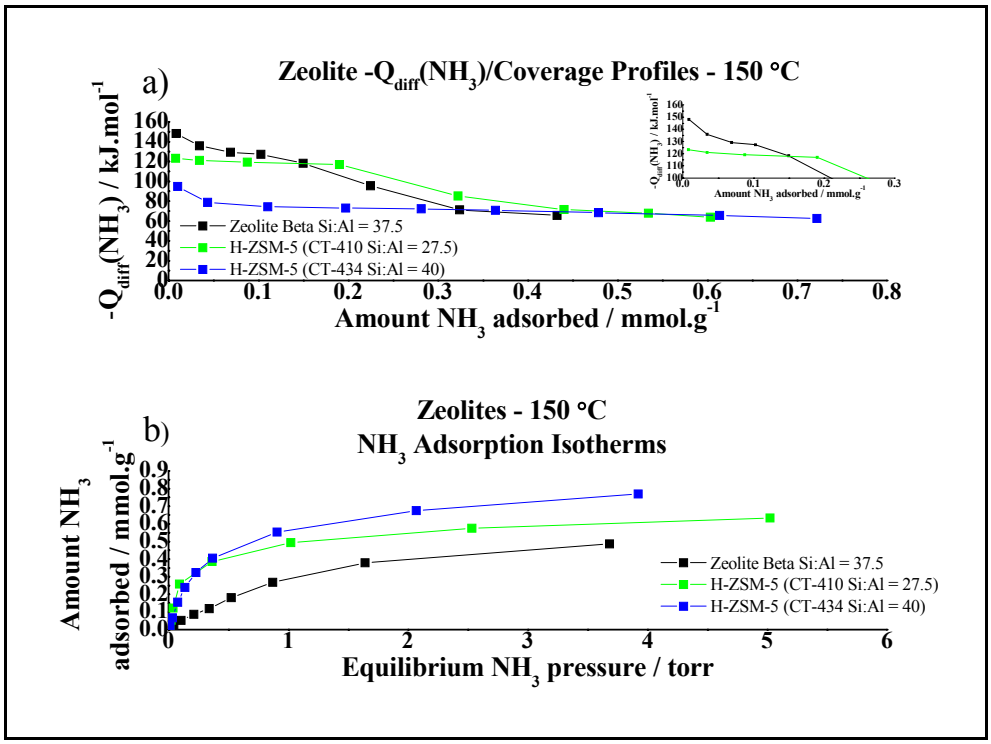

Figure 61: a) -$Q_{diff}(NH_3)$/coverage profiles for zeolites b) NH_3 adsorption isotherms for zeolites at 150 °C.

The -$Q_{diff}(NH_3)$ vs. amount of NH_3 adsorbed plots in Figure 61a above show that relative homogeneity of acid site strength exists for all three zeolites at coverages up to 0.2 mmol.g^{-1}, which agrees with previously reported studies[8, 9]. It appears that very much less NH_3 is absorbed by H-ZSM-5 (40) than would be predicted if each exchange sites accounts for one acid site. This uniformity of heats and therefore acid strength was not seen for the montmorillonite clays and is presumably due to the zeolites having a more ordered and uniform structure. Zeolite β with an Si:Al ratio of 37.5 exhibits the greatest initial heats of NH_3 adsorption . This is closely followed by H-ZSM-5 (27.5) which also shows the highest concentration of acid sites at which -$Q_{diff}(NH_3)$ lies above 80 kJ.mol^{-1}. H-ZSM-5 with an Si:Al ratio of 40 seems to have relatively little acidity and is quickly saturated with ammonia as shown by the nearly constant low heat of adsorption after the first NH_3 pulse, characteristic of reversible adsorption. This is an odd result as previous workers have measured significantly higher initial heats of NH_3 adsorption[10]. It is difficult to explain this but it is conceivable that the zeolite was not in fact in the H^+ form, and since it was used in the as-supplied form, this might explain the limited extent of reaction with NH_3. The NH_3 adsorption isotherms shown in Figure 61b show that zeolite β adsorbs significantly less NH_3 than the H-ZSM-5 solid acids.

	Zeolite Beta Si:Al = 37.5	H-ZSM-5 CT410 Si:Al = 27.5	H-ZSM-5 CT434 Si:Al = 40
Calorimeter Temperature (°C)	150	150	150
$-Q_{diff}(NH_3)$ at a coverage of 0.05 $mmol.g^{-1}$ (± 2 $kJ.mol^{-1}$)	140	119	82
Surface Coverage of NH_3 at which $-Q_{diff}(NH_3)$ falls below 80 $kJ.mol^{-1}$ (± 0.02 $mmol.g^{-1}$)	0.35	0.45	0.04
BET Surface area determined by N_2 adsorption ($m^2.g^{-1}$)	541	353	281
Theoretical acidity ($mmol.g^{-1}$)	0.44	0.61	0.42

Table 36: Comparison of acidity data, N_2 adsorption data, and theoretical acidity for zeolites H-ZSM-5 and Zeolite β at 150 °C.

In theory the amount of NH_3 adsorbed by zeolites can be predicted if it is assumed that Brønsted acid sites are present in a concentration equal to the framework Al concentration. These theoretical values are shown above in Table 36, and when compared with the overall amount of NH_3 adsorbed (Figure 61a) it can be seen that on this basis zeolite β and H-ZSM-5 (27.5) show an 80 % and 74 % occupancy of acid sites by NH_3 respectively.

5.2.4 Sulfonated Polystyrene Ion Exchange Resins

5.2.4.1 Amberlyst resins (Rohm & Haas)

Shown below in Figure 62 are the $-Q_{diff}(NH_3)$/coverage profiles and NH_3 adsorption isotherms for the Rohm & Haas Amberlyst resins which were activated in-situ and run at 100 °C.

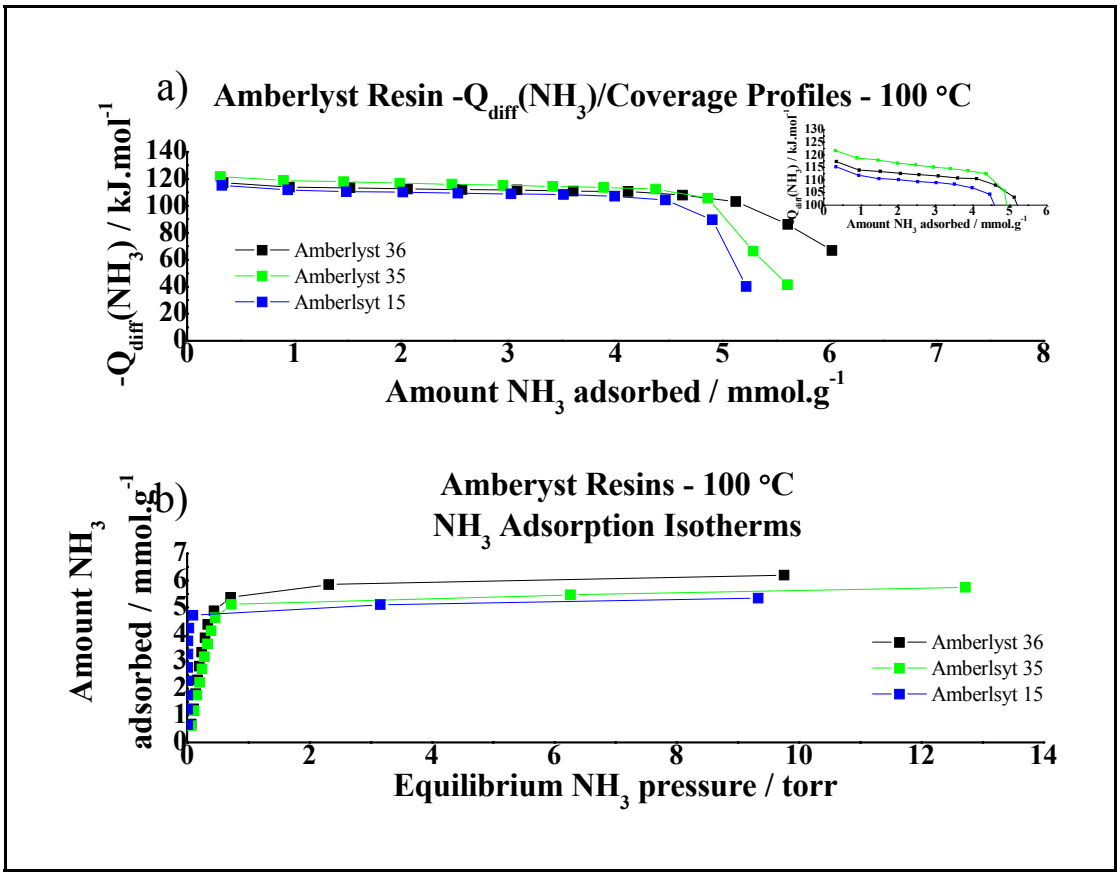

Figure 62: a) -$Q_{diff}(NH_3)$ profiles for Rohm & Haas resins b) NH_3 adsorption isotherms for Rohm & Haas sulfonated polystyrene resins at 100 °C.

The -$Q_{diff}(NH_3)$ vs. amount NH_3 adsorbed (Figure 62a) show very distinctive profiles as they show a constant -$Q_{diff}(NH_3)$ that suddenly decreases. The coverage at which this occurs corresponds well with similar profiles obtained in previous work[11]. NH_3 adsorption isotherms shown in Figure 62b show a sharp increase in the amount of NH_3 adsorbed at very low pressure. The isotherm levels off at a point corresponding to the rapid fall in -$Q_{diff}(NH_3)$. Shown below in Table 37 is an overall comparison of the data for the Amberlyst range of strong acidic cation exchange resins. It can be seen that Amberlyst 35 shows the strongest sites. This is followed by Amberlyst 36 and finally Amberlyst 15. The series of resins follows the expected path with respect to the overall concentration of acid sites and falls in line with increasing persulfonation throughout the range.

	Amberlyst 15	Amberlyst 35	Amberlyst 36
		Persulfonated	
Calorimeter Temperature (°C)	100	100	100
$-Q_{diff}(NH_3)$ at a coverage of 0.05 $mmol.g^{-1}$ (± 2 $kJ.mol^{-1}$)	115	118	117
Surface Coverage of NH_3 at which $-Q_{diff}(NH_3)$ falls below 80 $kJ.mol^{-1}$ (± 0.02 $mmol.g^{-1}$)	5.03	5.30	6.07
Acid-base Titration C.E.C. (± 0.1 $mmol.g^{-1}$)	5.29	5.36	6.19
Manufacturers C.E.C. ($mmol.g^{-1}$)	4.80	5.30	5.50

Table 37: Acidity data, N_2 adsorption data and C.E.C. for Rohm & Haas sulfonated polystyrene resins at 100 °C.

If Table 37 is examined it shows that there is a 2.5 % difference in relative strengths of acidic sites as shown by $-Q_{diff}(NH_3)$ above 80 $kJ.mol^{-1}$ (relating to irreversibly held NH_3) between Amberlyst 15 and Amberlyst 35 indicating that strength of acid sites is similar. This would be expected as the sulfonic acid groups in all cases are essentially the same. Only the concentration of sites is different. Both Amberlyst 35 and Amberlyst 36 have been persulfonated and therefore show higher C.E.C.'s. Amberlyst resins results show that when comparing concentration of acid sites above 80 $kJ.mol^{-1}$ with the acid base titration C.E.C. values, over 95 % of sites are accessible to ammonia. This is most likely due to accessibility of the macroporous structure and associated cation exchange capacities as shown by Amberlyst 35 and 36. Note that, although concentration of acid sites measured by NH_3 adsorption and by aqueous acid-base titration agree quite well, the values for A15 and A36 are higher than the manufacturers' claimed C.E.C.'s. There is no clear explanation for this but results reported here do show the essential trend that Amberlyst 15 (accepted as a "normally" sulfonated polymer) has the lowest concentration of acid sites and Amberlyst 35 and 36 have higher concentrations of acid sites (consistent with claim that they are sulfonated at a level above one sulfonic group per styrene unit i.e. persulfonation).

5.2.4.2 'CT-Series' Resins (Purolite)

NH_3 adsorption isotherms and $-Q_{diff}(NH_3)$/coverage profiles are shown below in Figure 63 for Purolite ion exchange resins CT-175 and CT-275 activated and run at 100 °C.

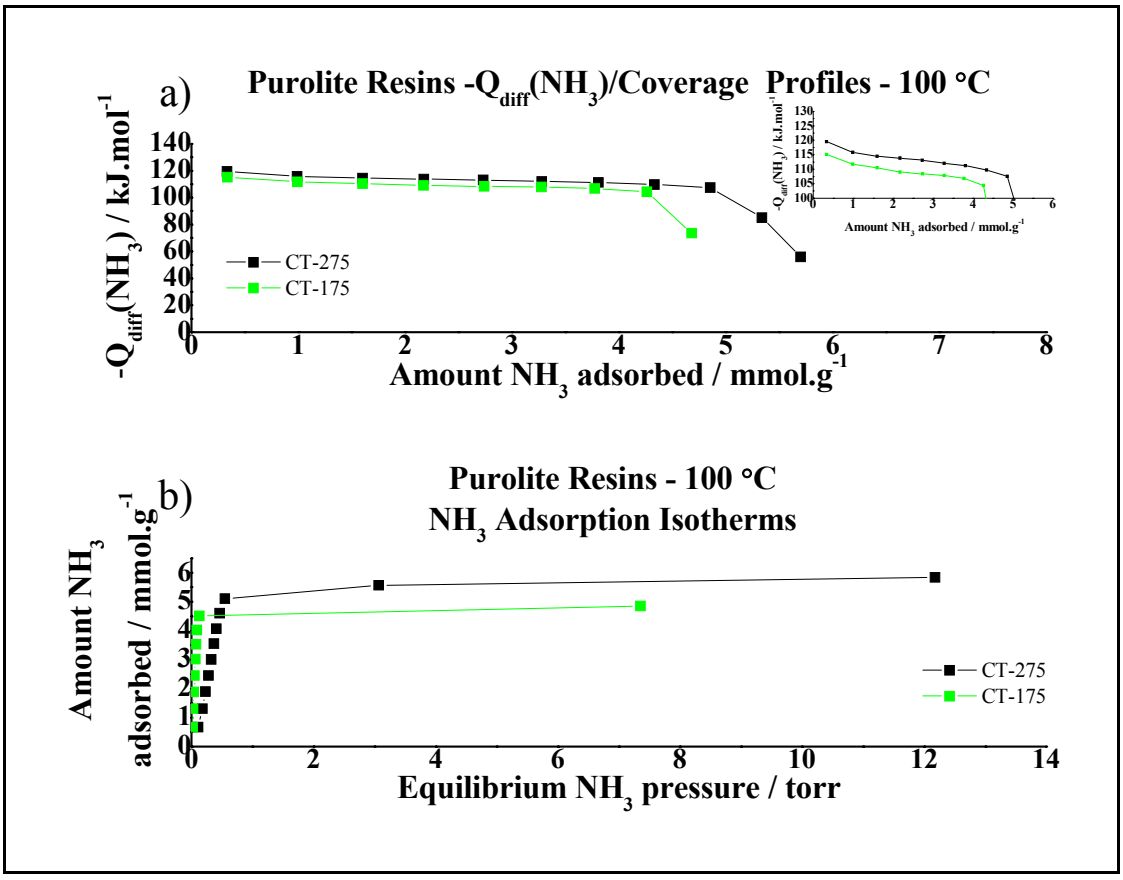

Figure 63: a) $-Q_{diff}(NH_3)$ profiles for Purolite resins b) NH_3 adsorption isotherms for Purolite sulfonated polystyrene resins at 100 °C.

The $-Q_{diff}(NH_3)$ vs. amount of NH_3 adsorbed plots shown in Figure 63a above show that CT-275 has a greater concentration of acid sites and also has slightly stronger acid sites than CT-175, for the same reasons as explained for the Amberlyst series, as CT-275 has been persulfonated and therefore has a greater than stoichiometric loading of sulfonate groups per phenyl ring. Also the 'CT-series' shows the same uniformity in acid strength, and similar NH_3 adsorption isotherms (Figure 63b) with a steep increase at relatively low pressure followed by a plateau. The C.E.C. values for each resin as determined by acid/base titration and by NH_3 adsorption lie close to the manufacturers' stated values, shown in Table 38 below. This good agreement tends to support the view that the differences between measured and claimed C.E.C. with Amberlyst sulfonated polystyrene ion exchange resins described earlier are real.

	CT-175	CT-275
Calorimeter Temperature (°C)	100	100
$-Q_{diff}(NH_3)$ at a coverage of 0.05 mmol.g^{-1} (± 2 kJ.mol^{-1})	114	116
Surface Coverage of NH_3 at which $-Q_{diff}(NH_3)$ falls below 80 kJ.mol^{-1} (± 0.02 mmol.g^{-1})	4.60	5.43
Acid-Base Titration C.E.C. (± 0.1 mmol.g^{-1})	4.94	5.33
Manufacturers C.E.C. (mmol.g^{-1})	4.90	5.20 (min)

Table 38: Acidity data and C.E.C. data for Purolite sulfonated polystyrene ion exchange resins at 100 °C.

An overall comparison of the Amberlyst and 'CT' series is shown below in Table 39.

	CT-175	CT-275	Amberlyst 15	Amberlyst 35	Amberlyst 36
Calorimeter Temperature (°C)	100	100	100	100	100
$-Q_{diff}(NH_3)$ at a coverage of 0.05 mmol.g^{-1} (± 2 kJ.mol^{-1})	114	116	115	118	117
Surface Coverage of NH_3 at which $-Q_{diff}(NH_3)$ falls below 80 kJ.mol^{-1} (± 0.02 mmol.g^{-1})	4.60	5.43	5.03	5.30	6.07
Acid-Base Titration C.E.C. (± 0.1 mmol.g^{-1})	4.94	5.33	5.29	5.36	6.19
Manufacturers C.E.C (mmol.g^{-1})	4.90	5.20 (min)	4.80	5.30	5.50

Table 39: Acidity data and C.E.C. data for Purolite and Rohm & Haas sulfonated polystyrene ion exchange resins at 100 °C.

From the work carried out, it can be seen that the Amberlyst resins are very similar to Purolite resins, although Amberlyst 15 and 36 show slightly higher acidity concentrations than the Purolite resins. Based on $-Q_{diff}(NH_3)$ Amberlyst 35 has the strongest sites. There is generally good agreement between the results obtained via acid-base titration and those by static NH_3 adsorption microcalorimetry to show the concentration of "strong" acid sites for all resins. It has been proposed that the formation of sulfone bridges is partially responsible for controlling acid strength of sulfonic acid groups through networks of neighbouring sulfonic acid groups.[12]

Both of the above mentioned resins belong to the family of strong acid catalysts, with both having a similar number of active sites at ~ 4.8/5.2 eq/kg respectively for CT-175 and Amberlyst 15 and a

similar degree of water retention (between 54-55%). In respect of the degree of sulfonation and acidity, CT-175 and Amberlyst 15 are similar. However, there are structural differences and these are illustrated by the data provided by the manufacturers for surface area and porosity. CT-175 has a lower surface area at 20-40 m^2/g compared to an area of 45 m^2/g for Amberlyst 15, which in comparison has a smaller pore diameter at 250 Å compared to 500-700 Å for CT-175. Differences in the extent of polymer cross-linking (with DVB) may also exist and could conceivably affect acid strength. The DVB contents have not been provided by the manufacturer however so no comment can be made on this.

In terms of results given by the NH_3 adsorption microcalorimetry, CT-175 showed that the initial heat of ammonia adsorption lay at 115±2 $kJ.mol^{-1}$ and had a total average surface coverage of ~ 4.8 $mmol.g^{-1}$. Amberlyst 15 has a similar initial heat that lies at ~116±2 $kJ.mol^{-1}$ but has a higher average concentration of acid sites at 5.19 $mmol.g^{-1}$. We conclude that Amberlyst 15 and CT-175 are very similar.

On comparison of persulfonated resins Amberlyst 35, 36 and CT-275 very few variations can be seen, as $-Q_{diff}(NH_3)$ measurements all lie within experimental error, and both CT-275 and Amberlyst 35 adsorb similar concentrations of NH_3. Amberlyst 36 appears to contain more sulfonated groups per phenyl ring than either Amberlyst 35 or CT-275 as not only does it have the greatest C.E.C determined from acid-base titration but also the coverage at which $Q_{diff}(NH_3)$ falls below 80 $kJ.mol^{-1}$ is much higher than the other two persulfonated polystyrene ion exchange resins.

5.2.5 General Discussion

When an overall comparison is made between the solid acids, sulfonated polystyrene ion exchange resins and zeolites are similar in terms of their degree of uniformity of acid sites and relate to their pore networks. This is shown by powder XRD diffraction patterns for the zeolites, and we know that for sulfonated polystyrene ion exchange resins, a permanent macroporous network is produced by the use of an inert organic solvent such as xylene(see 1.1.4.1.b). On the other hand the clays and supported heteropoly acids show a more pronounced inhomogeneity of acid strengths possibly more related to accessibility of acid sites. Although a recent publication has shown that HPW supported on SiO_2 has shown highly uniform acid strength from loading as low as 26 % weight loading HPW when studied by NH_3 adsorption flow calorimetry[13].

It also shows that the concentration of acid sites in sulfonated ion exchange resins are ten times greater than the zeolites, heteropoly acids, or clays. This is of course a major advantage in their use as solid acid catalysts although their low thermal stability does limit use. It should also be pointed out that NH_3 uptake on sulfonated polystyrene ion exchange resins appears only to bind with strong acid sites (those above 80 $kJ.mol^{-1}$) as there is no sign of reversible adsorption (physisorption) or adsorption onto non-acidic sites. This facilitates the measurement of acidity in these solid acids which are typically Brønsted. A significant difference is seen between persulfonated and stoichiometrically sulfonated materials and is in line with expectations. It is not possible to distinguish if the relatively low differential heats seen for sulfonated polystyrene ion exchange resins mean that only weak acid sites exist. It may be beneficial to probe acid sites using a weaker base in the gas phase.

From NH_3 experiments at 150 °C, pure HPW and SBA-15 supported HPW have been shown to possess the highest $-Q_{diff}(NH_3)$ heats and therefore possess stronger sites than other solid acids measured. It is possible that even though zeolite β and H-ZSM-5 provide strong acidic sites and that they also have a higher concentration of acid sites than clays and carbon supported HPW that their catalytic activity imparted may be low due to pore size restrictions for larger bulkier molecules than NH_3.

When examining clays and zeolites (both siliceous materials), clays show less homogeneity of acid sites which could mean that a range of strengths exist or could mean that it is difficult to differentiate between weakly held NH_3 and strongly held NH_3 in zeolites. It would be reasonable to assume that acid strength distribution is real as would not expect acid strength to vary in zeolites due to uniform pore structure and non-acidic sites exist within montmorillonite clays. Inhomogeneity of acid strength present in acid treated clays therefore could possibly be related to the need for NH_3 to diffuse throughout the clay especially for less acid treated clay members where structure remains intact. Concentration of acid sites for clays increases in line with the C.E.C. so therefore we can conclude that the majority of acid sites exist at C.E.C. sites most probably at a level of one acid site per exchange site.

Ammonia adsorption microcalorimetry gives a useful insight into the concentration and strength of acid sites within solid acids. Although it is not easy to compare certain solid acid catalysts as for instance difficulties arise in comparing sulfonated polystyrene ion exchange resins and HPW

catalysts with other solid acids such as zeolites and acid treated clays, as they possess purely Brønsted acidity, which is not easy to differentiate using NH_3 adsorption microcalorimetry as a stand-alone technique. Also the presence of physisorbed NH_3 (confinement factors) affects differential heats of adsorption, and it has been suggested that it may represent up to 40 % of the adsorption heat in high silica zeolites[14] and must be considered in other micro- and mesoporous materials.

Acid Treated Clays	Fulcat 200 Rockwood	F200 (Al^{3+})	F200 (Fe^{3+})	F220	F230	F240	F240 (Al^{3+})	K5 Süd-Chemie	K10	K20	K30
Calorimeter Temperature (°C)	150	150	150	150	150	150	150	150	150	150	150
$-Q_{diff}(NH_3)$ at a coverage of 0.05 mmol.g^{-1} (± 3 kJ.mol^{-1})	98	112	115	110	122	124	123	119	127	129	118
Surface Coverage of NH_3 at which $-Q_{diff}(NH_3)$ falls below 80 kJ.mol^{-1} (± 0.03 mmol.g^{-1})	0.15	0.23	0.23	0.29	0.31	0.32	0.31	0.26	0.23	0.19	0.16
BET Surface Area ($m^2.g^{-1)}$	108	81	95	271	363	363	335	108	181	253	282
Zeolites	Zeolite β Si:Al = 37.5	H-ZSM-5 Si:Al = 27.5	H-ZSM-5 Si:Al = 40	Sulfonated Polystyrene Ion Exchange resins			Amberlyst 15	Amberlyst 35	Amberlyst 36	CT-175	Ct-275
Calorimeter Temperature (°C)	150	150	150				100	100	100	100	100
$-Q_{diff}(NH_3)$ at a coverage of 0.05 mmol.g^{-1} (± 2 kJ.mol^{-1})	140	119	82				115	118	117	114	116
Surface Coverage of NH_3 at which $-Q_{diff}(NH_3)$ falls below 80 kJ.mol^{-1} (± 0.02 mmol.g^{-1})	0.35	0.45	0.04				5.03	5.30	6.07	4.60	5.43
BET Surface Area ($m^2.g^{-1)}$	541	353	281				45	45	35	30	20-35
Supported Heteropoly Acid	Pure HPW	HPW/SBA-15 174 mg/g	HPW/SBA-15 320 mg/g	HPW/SBA-15 420 mg/g		HPW/Novacarb 100 mg/g	HPW/Novacarb 300 mg/g		HPW/Sibunit 200 mg/g	HPW/Sibunit 254 mg/g	HPW/Sibunit 300 mg/g
Calorimeter Temperature (°C)	150	150	150	150		150	150		150	150	150
$Q_{diff}(NH_3)$ at a coverage of 0.05 mmol.g^{-1} (± 5 kJ.mol^{-1})	215	158	164	160		150	138		102	120	124
Surface Coverage of NH_3 at which $-Q_{diff}(NH_3)$ falls below 80 kJ.mol^{-1} (± 0.05 mmol.g^{-1})	0.84	0.35	0.33	0.5		0.18	0.18		0.07	0.18	0.23
BET Surface Area ($m^2.g^{-1}$)	2.3	286		143		423	369		133	171	125

Table 40: Comparison of acidity data at for acid treated clays, zeolites, sulfonated polystyrene ion exchange resins and supported HPW samples.

[1] M.P. Hart, D.R. Brown, J. Mol. Catal. A:Chem., 212 (2004) 315-321.

[2] T. Cseri, S. Bekassy, F. Figueras, S. Rizner, J. Mol. Cat. A:Chem., 98 (1995) 101-107.

[3] B.A. Williams, S.M. Babitz, J.T. Miller, R.Q. Snurr, H.H. Kung, Appl. Catal. A:Gen., 177 (1999) 161-175.

[4] A.I. Biaglow, D.J. Parrillo, G.T. Kokotailo, R.J. Gorte, J. Catal., 148 (1994) 213-223.

[5] D.F. Shriver, P.W. Atkins, "Inorganic Chemistry – Third Edition", Oxford University Press (1999) pp. 216-217.

[6] D.R. Brown, C.N. Rhodes, Catal. Lett., 45 (1997) 35-40.

[7] C.N. Rhodes, D.R. Brown, J. Chem. Soc. Faraday Trans., 91 (6) (1995) 1031-1035.

[8] D.J. Parrillo, R.J. Gorte, Catal. Lett. 16 (1992) 17-25.

[9] C.P. Nicolaides, H.H. Kung et al., App. Catal. A:Gen, 223 (2002) 29-33.

[10] I.V. Mishin, T.R. Brueva, G.I. Kapustin, Adsorpt, 11 (2005) 415-424.

[11] M. Hart, G. Fuller, D.R. Brown, J.A. Dale, S. Plant, J. of Mol. Catal. A:Chem., 182-183 (2002) 439-445.

[12] R. Thornton, B.C. Gates, J. Catal., 34 (1974) 275-287.

[13] A.D. Newman, D.R. Brown, P. Siril, A.F. Lee, K. Wilson, Phys. Chem. Chem. Phys., 8 (2006) 2893-2902.

[14] E.G. Derouane, C.D. Chang, Micro. Meso. Mat., 35-36 (2000) 425-433.

CHAPTER SIX

CATALYTIC ACTIVITY MEASUREMENTS OF SOLID ACIDS IN RELATION TO THEIR ACIDITY

To determine the suitability of a solid acid catalyst for catalysing a reaction, catalytic data needs to be obtained. This is important as each catalyst type has specific advantages over other catalysts for catalysing different reactions, for example their pore size, their ability to swell and their ability to be selective. An attempt will be made to compare catalytic activity for two chosen reactions with surface acidity data obtained from NH_3 adsorption microcalorimetry along with other structural properties such as their surface areas and C.E.C. For this purpose two Brønsted acid catalysed reactions have been chosen where the use of polar and non-polar solvent has been investigated to see how solvent type affects the catalytic activities of solid acids. This allows the effects of various characteristics of the chosen catalysts to be probed, i.e. clays have layered structures, resins swell in polar solvents, and supported heteropoly acids have relatively rigid structures. The measurements will allow the relationship between catalyst structure, acidity, and activity to be examined.

Section 1 – Model Reactions & Types of Catalysis

The model reactions used to obtain catalytic activity data will be introduced.

6.1.2 Isomerisation of α-Pinene

This reaction has been used by workers[1,2] to measure the catalytic activities of many solid acids, and clays in particular. The reason for using this reaction is that it is almost certainly Brønsted acid catalysed. Because both reactant and products are non-polar the reaction is representative of many important liquid phase reactions in industry, involving hydrophobic and relatively large molecules. Access to catalytic sites can be markedly different in different solvents, especially for clay based catalysts and sulfonated polystyrene resins which are able to swell. The solvent system in this reaction is clearly only going to give access to surface acid sites that would be accessible in non-polar solvents.

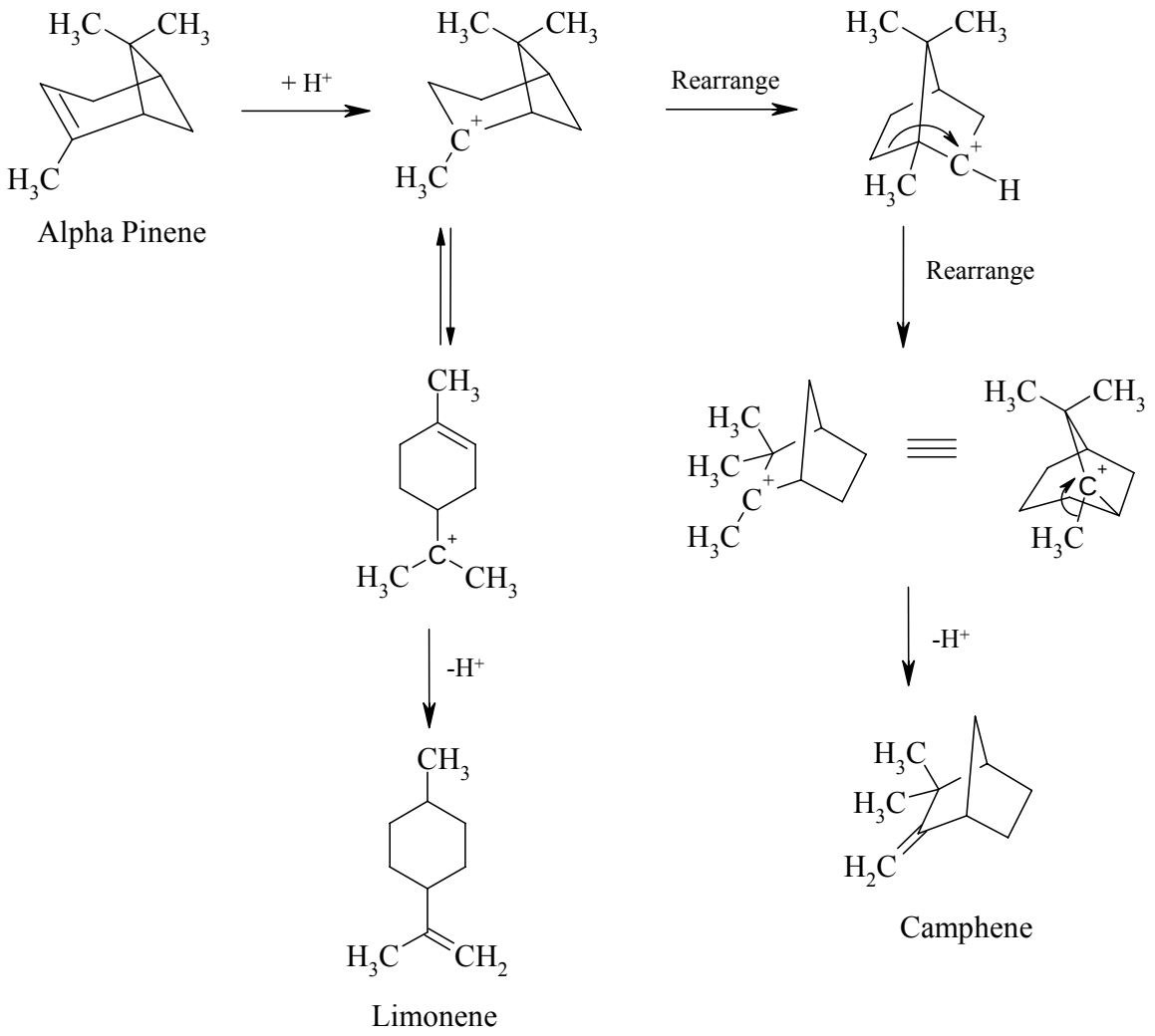

Figure 64: Conversion of α-pinene to camphene and limonene.[3]

The reaction shown above in Figure 64 involves an alteration in the carbon skeleton of the molecule in a 1, 2 – migration known as the Wagner-Meerwein rearrangement. The first step in the reaction is the protonation of the less substituted end of the double bond, and it is also the rate determining step. The resulting carbocation then rearranges to alleviate ring strain and further steps lead to the production of camphene, and other side products such as limonene. As camphene has a less strained structure this provides the primary driving force for the rearrangement. Previous work refers to relative yields of limonene and camphene being dependent on acid strength of sites on solid acid catalysts[4], but in this work activity will be measured in terms of conversion of α-pinene only, as it has not been possible to relate the reaction selectivity to any properties of the catalyst.

6.1.2 Hydrolysis of Ethyl Acetate

This reaction is undertaken in water where difficulties arise in the use of solid acids because severe poisoning of acid sites occurs, and in fact most solid acids lose their catalytic activities in aqueous solutions or have their acid strength levelled to that of the H_3O^+ ion[5]. Aqueous reaction types include hydrolysis, esterification, and hydration. In liquid phase acid catalyzed reactions especially in reactions where water and/or lower alcohols participate, cationic ion exchange resins have been applied successfully, though problems arise when reaction temperatures exceed 100 °C, and also when reactions require high acid strength[6]. It has been reported previously that some heteropoly acids are excellent water tolerant solid acids[7], and when 12-tungstophosphoric acid (HPW) was converted into an acidic caesium salt $Cs_{2.5}H_{0.5}PW_{12}O_{40}$ it was found to be a widely applicable water tolerant solid acid catalyst[8], zeolites (Si:Al ratios > 8.7) have also shown appreciable activity in the hydrolysis of ethyl acetate at 60 °C[9].

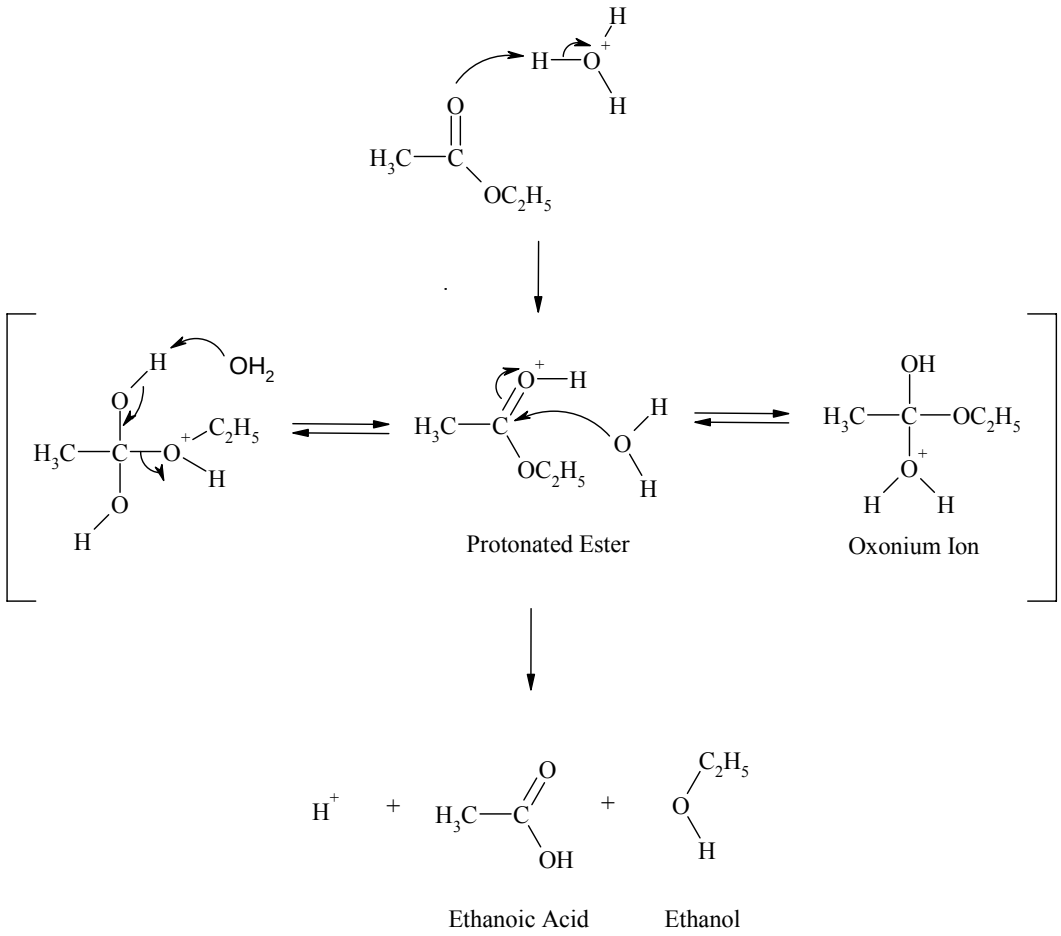

Figure 65: Mechanism for hydrolysis of ethyl acetate.[10]

However, an advantage of using water is that with catalysts for which accessibility to "internal" acid sites depends on hydration, such as clays and sulfonated polystyrene ion exchange resins, accessibility to acid sites is maximised. The mechanism of hydrolysis of ethyl acetate is shown above in Figure 65. The rate determining step for this reaction is again the initial addition of a hydronium ion to form a protonated ester.

6.1.3 Types of Catalysis

Eight different types of catalysis have been demonstrated in relation to solid heteropoly acids[11], some of which could also be used to help explain catalytic results for other types of solid acid such as sulfonated ion exchange resins, acid treated clays, and zeolites. These are shown below in Figure 66, where the two main types of catalysis are: 1) Surface type (Figure 66a) 2) Pseudo-liquid bulk type (I) (Figure 66b).

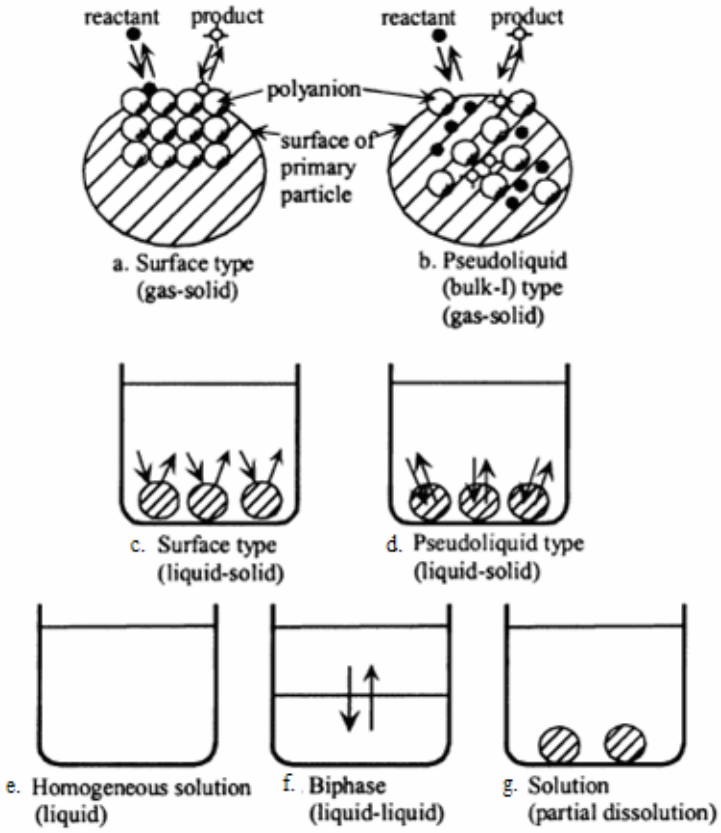

Figure 66: Classes of catalysis demonstrated for heteropoly compounds relevant to other solid acids.[11]

Surface type catalysis (Figure 66a and Figure 66c) is where the catalytic reaction takes place on the outer surface and pore walls "two-dimensional surface" of the catalyst, and the reaction rate is proportional to the catalyst surface area. Figure 66b and Figure 66d represent bulk catalysis "three dimensional surfaces" where catalysis occurs within the bulk of the solid acid. For pseudo-liquid bulk type (I) catalysis with typical heteropoly compounds the reactant molecules are adsorbed between the polyanions in the ionic crystal by replacing water of crystallization or expanding the lattice, and reaction occurs in these interstitial sites[12]. When the diffusion of reactant molecules in the solid is faster than the reaction, the solid bulk can form a pseudo-liquid phase in which a catalytic reaction can proceed. In the pseudo-liquid phase such catalysts appear as solids but behave like liquids (solvent). Sulfonated polystyrene ion exchange resins are also similar in this respect, as when they are solvated molecules are able to gain access to the internal bulk acid sites[13]. It needs to be noted that the contribution of the solid HPW bulk to catalysis varies, and depends on the relative rate of diffusion to the rate of reaction thus giving rise to intermediate cases between surface and bulk catalysis[14]. Both zeolites and acid clays do not have the ability to form pseudoliquid phases and it is assumed that catalysis will take place only on the available surfaces of these solid acids.

Section 2 - Experimental

6.2.1 Apparatus Setup

6.2.1.1 Thermal activation of catalysts for the isomerisation of α-pinene

All catalysts were activated in a vertical Lenton tube furnace, where the temperature was controlled by a digital Eurotherm 818P programmer connected to the furnace thermocouple. The catalyst (50 mg) was held in a quick-fit boiling tube, which was purged with pumped air dried by passing through dehydrated silica gel. The boiling tube was placed in the furnace with the base as close to the thermocouple as possible to ensure the sample was at the furnace temperature. Dry air was maintained at a flow rate of 1 L/min with a 'Hy-Flo' air piston pump (Figure 67). After activation the sample was allowed to cool under a flow of dry air.

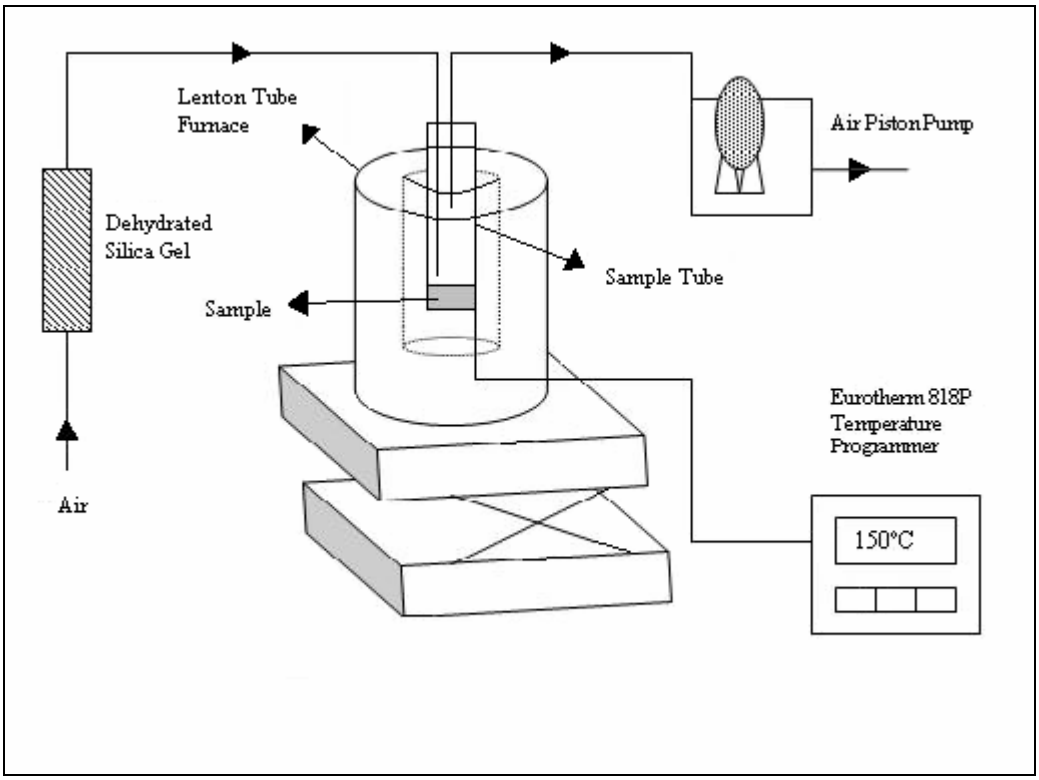

Figure 67: Apparatus set-up for the activation of catalysts in the α-pinene rearrangement.

All clays, zeolites, and supported tungstophosphoric acid samples were activated at 150 °C for one hour prior to use in the α-pinene reaction. Ion exchange resins were activated at 100 °C for one hour (to avoid thermal decomposition of the catalyst). Due to the presence of excess water in reaction mixtures for the hydrolysis of ethyl acetate no thermal activation was considered necessary, but all catalysts were conditioned at room temperature under flowing dry air for one hour before reaction.

6.2.1.2 Reaction vessel and experimental set-up

a) α-pinene rearrangement

The boiling tube used for activation of catalysts (50 mg) was also used as the reaction vessel. This had a connector attached comprising a stopper and a water cooled condenser to which a drying tube was fixed. The boiling tube was immersed in an oil bath at 80 ± 1 °C using an IKA hotplate controlled by a digital controller and thermocouple (ETS-D4 Fuzzy). A stirring magnet in the oil bath ensured that a homogeneous temperature was maintained throughout, and the reaction mixture was stirred using a 1 cm stirring magnet placed in the boiling tube.

A weighed reagent/internal standard mixture containing 0.060 mol dried α-pinene (98 % Aldrich) and 0.010 mol of decane (99 % Aldrich) was heated up to the reaction temperature (80 °C) before adding to the activated 50 mg catalyst in the boiling tube. No additional solvent was used. Samples of the reaction mixture were taken for gas chromatography (GC) analysis using a graduated pipette to remove 0.2 ml to a sample vial via a 0.2 μm syringe filter to remove catalyst. Control experiments showed that the reaction stopped once the activated catalyst was removed via filtration. Reaction mixture was removed every 5 minutes for the first 30 minutes and every 30 minutes thereafter. The mixture was analysed using GC as explained in section 6.2.1.3 normalising the α-pinene peak against that for the internal standard decane. Experiments were repeated in triplicate for each catalyst.

b) Hydrolysis of ethyl acetate

The reaction set-up was slightly modified by using a three-necked round bottomed 50 ml flask and the drying tube was removed from the top of the condenser. The catalyst (50 mg) was placed in the flask with the internal standard acetonitrile (0.40 ml) and 30 ml of distilled water. This was heated to the reaction temperature of 70 °C before adding 16.9 mmol ethyl acetate and starting the reaction. Aliquots (0.2 ml) of reaction mixture were removed every 15 minutes for the first hour then every 30 minutes using a graduated pipette and filtering through a 0.2 μm syringe filter. These samples were again analysed using GC. To follow the reaction, the area of the peak assigned to the product ethanol was normalised against the internal standard acetonitrile, and experiments were repeated in triplicate for each catalyst.

6.2.1.3 Gas Chromatography

For the α-pinene rearrangement reaction a Perkin Elmer 8600 gas chromatograph was used which was modified from pressure-regulated pneumatics to a flow controlled system so that wide bore capillary columns could be used. In this study a SGE 25QC2/BP5 0.25 μm column was used. This is a 25 metre length non-polar column with a 0.25 μm film thickness. The detector was a flame ionisation detector (FID) which used a hydrogen/air flame. GC conditions were set for this reaction by investigating oven, injector, and detector temperatures to obtain optimum peak separations, and a helium flow of 5 ml/min was chosen. Peaks were assigned by injecting pure

samples and determining retention times for the chosen GC conditions. Manual injections of 0.01 µl were used.

For the hydrolysis of ethyl acetate reaction a Carlo Erba Strumentazione GC with FID detector again using hydrogen/air was utilized, and included the following modules: a Fractovap Series 4160 module to control helium flow as well as injection, detection and oven temperatures, and a EL490 control module. A Spectra Physics integrator model SP4270 was attached to the instrument. For this study a 25m/BP20 0.5 µm diameter column was used. This is a 25 metre length polar column with a film thickness of 0.5 µm. Peaks were again assigned by injecting pure samples and determining retention times for the chosen GC conditions. Manual injections of 0.05 µl were used.

6.2.2 Reproducibility and confidence limits for kinetic data

In this section possible sources of error in the results have been considered.

6.2.2.1 Validation of the use of an internal standard

As the precise measurement of concentration or relative concentrations using GC is difficult, largely due to establishing good reproducibility of the size and nature of the sample injection, a known amount of internal standard is incorporated. An internal standard has to meet certain requirements, the main ones being that it should exhibit a separate peak that does not overlap with any other peaks and it should not react with any of the other compounds in the sample mixture.

A repeat injection experiment was followed to assess the use of n-decane as an internal standard in the α-pinene rearrangement reaction. A single solution was taken from a typical run in which the reaction was halted after 1 hr 45 minutes and further injections made. The results are shown below in Table 41.

	Reactant α-pinene Peak Area / Arbitrary Units	Internal Standard Decane Peak Area / Arbitrary Units	Reactant (α-pinene normalised to internal standard peak area) Peak Area / Arbitrary Units
	10731	4.32	2485
	10109	3.95	2557
	11414	4.25	2684
	13126	5.64	2327
Average	11273 (± 1564) (≡ ± 14 %)		2513 (± 186) (≡ ± 7 %)

Table 41: GC results for the rearrangement of α-pinene after reaction was halted after 1 hour 45 minutes.

The average values shown above in Table 41 include a ± value which covers the range around the mean from the lowest to the highest value. Use of an internal standard for this reaction can be seen to considerably reduce range in the peak area of the reactant, and because of this the decision was taken to include decane as an internal standard in the treatment of all results for this reaction.

Again a repeat injection experiment was performed to assess the use of acetonitrile as an internal standard in the hydrolysis of ethyl acetate reaction. A typical experiment was used for this and the reaction halted after 15 minutes. Results for repeat injections of a single solution are shown below in Table 42.

	Product Ethanol Peak Area / Arbitrary Units	Internal Standard Acetonitrile Peak Area / Arbitrary Units	Product (Ethanol normalised to internal standard peak area) Peak Area / Arbitrary Units
	14085	9.23	1527
	14196	9.35	1518
	13958	9.11	1532
	14472	9.40	1539
Average	14178 (± 294) (≡ ± 2 %)		1529 (± 11) (≡ ± 0.7 %)

Table 42: GC results for the hydrolysis of ethyl acetate.

Deviations in the area of the product peak can again be reduced by including an internal standard, as range is reduced from a 2 % to a 0.7 % variation. There is less variation in the normalised area for ethanol than there is for the normalised area of α-pinene. It is not clear why this is the case. It may be related to the condition of the BP column used for pinene analysis which has subsequently been shown to have been old and with below specification performances in terms of peak tailing.

6.2.2.2 Establishing Reaction Conditions Which Lie Outside the Diffusion Limitation Region

The overall rate of a reaction is generally controlled by the following five basic steps, any one of which can be rate determining.

1. Transport of the reactants to the catalyst.
2. Adsorption of the reactants on the catalyst.
3. Reaction on the catalyst involving one or more adsorbed reactants.
4. Desorption of products from the catalyst.
5. Transport of products away from the catalyst.

Steps 2-4 are chemical in nature, and may be regarded as jointly constituting the catalytic reaction whereas steps 1 and 5 involve no chemical change. Step 1 is a physical process in which reactants are brought through the liquid phase to the active sites on the surface of the catalyst and step 5 is the removal of the products away from the catalyst surface. When either steps 1 or 5 are slower than the catalytic rate itself, the rate is determined by the rate of arrival of reactants or the removal of products. If this occurs the rate is said to be 'diffusion limited'. Experiments were undertaken to ensure that conditions in the catalytic experiments carried out did not lead to reactions being under diffusion control by measuring the reaction rate as a function of reaction mixture stirrer speed. A reaction whose rate is governed by a truly chemical step should not have a reaction rate that is affected by improving agitation. Using a magnetic stirrer for both reactions, as described in the experimental section, conversion over a 2 hour reaction period was measured using sulfonated polystyrene ion exchange resin catalyst with the stirrer motors on settings from lowest to maximum. In both reactions at the lower stirrer speeds there was a dependence of conversion on stirrer speed but at between roughly 80 % and 100 % maximum stirrer speed there was no

dependence. It was decided to run all subsequent experiments using maximum mixing speed, using the apparatus described earlier.

Section 3 – Results

In this section, results from catalytic activity measurements for all catalysts will be given. Discussion of these results will then follow in Section 4. To treat the data, the area of the relevant peak was normalised against the area of the internal standard. For the α-pinene rearrangement the α-pinene peak area was normalised against the internal standard, decane so that the extent of reactant conversion was measured. A typical conversion plot of α-pinene is shown below in Figure 68.

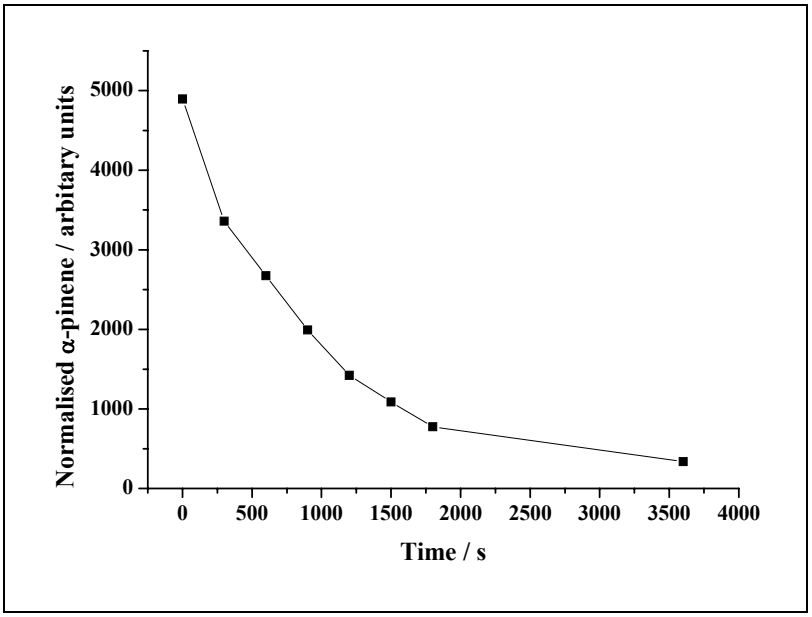

Figure 68: A typical normalised plot for the rearrangement of α-pinene at 80 °C.

An example of a first order natural log plot for the rearrangement of α-pinene over K30 at 80 °C is shown below in Figure 69.

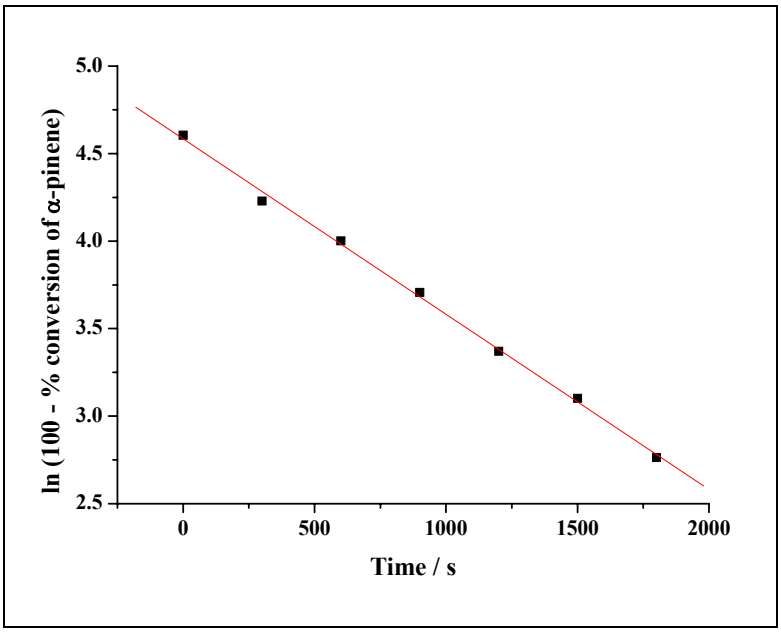

Figure 69: Typical first order plot of ln (100 - % conversion of α-pinene) for K30 at 80°C.

The first order rate constant is taken as the gradient of the line of best fit of points up to 1800 s. This is used as non-linearity is often observed after this time. The alternative way of comparing initial reaction rates from plots like that shown in Figure 68 have not been used as it is difficult to measure enough points at the beginning of the reaction to get reliable values for rates at the start of the reactions.

For the hydrolysis of ethyl acetate the production of ethanol was followed and normalised against acetonitrile. The gradients of the tangent of the curves at time zero were used as initial rates of the reaction and then converted to rates per gram of catalyst. An estimated 95 % confidence limit (as a ± figure) is given for each rate based on the observed plots for each reaction, and results from replicate runs. A typical example is shown below in Figure 70.

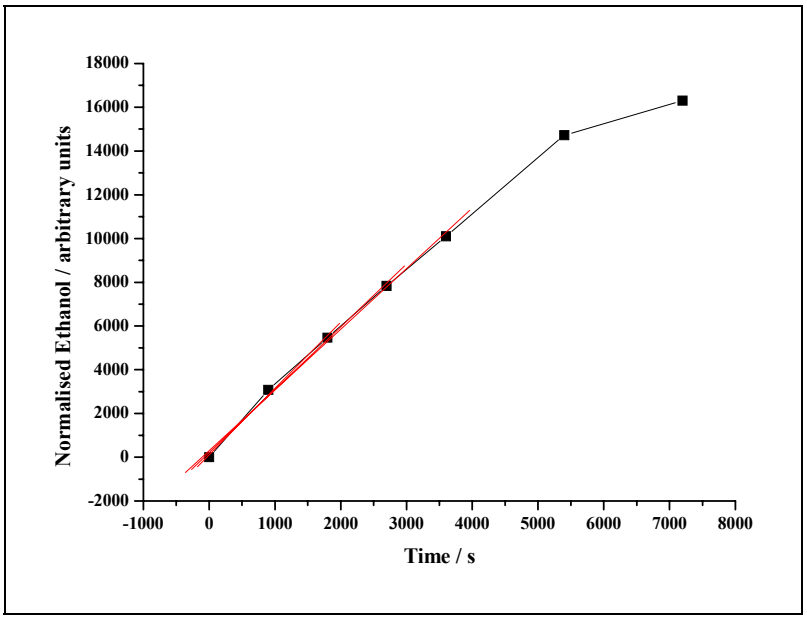

Figure 70: A typical normalised plot for the hydrolysis of ethyl acetate at 60 °C.

It was assumed that both reactions followed either first order or pseudo first order kinetics.

6.3.1 Catalytic Activity of Heteropoly Acid ($H_3PW_{12}O_{40}$)

Shown below in Table 43 and Table 44 are the catalytic activity results for both pure $H_3PW_{12}O_{40}$ (HPW) and supported HPW on silica and carbon supports at a loading of ca. 300 mg HPW per gram support. This was to allow ease of comparison between the supported HPW catalysts in the two test reactions. The same weight of catalyst or supported catalyst (50 mg) was used in each experiment. Rates reported are based on per gram of catalyst (column 1), per gram HPW (column 2) and per mole H^+ (column 3). Rates per mole H^+ have been calculated based on 3 x H^+ ions per mole HPW (for pure HPW this has been calculated on surface H^+ only). It needs to be mentioned that for the hydrolysis of ethyl acetate it is possible that homogeneous catalysis by dissolved HPW is occurring. For this reason no attempt shall be made to compare these results with the heterogeneous catalysis by clays and zeolites.

a) α-pinene rearrangement

Activation of HPW catalysts was achieved at 150 °C for 1 hour prior to catalytic measurements run at 80 °C.

	1st order rate constants k / x 10^{-3} s^{-1} g^{-1} (Cat)	1st order rate constants k / s^{-1} g^{-1} (HPW)	1st order rate constants k / s^{-1} mol^{-1} (H^+)
Pure $H_3PW_{12}O_{40}$ (HPW)	0.18 ± 0.11	0.00018	22.7#
HPW/SBA-15 (320 mg/g)	5.02 ± 0.07	0.016	15.4
HPW/Novacarb (300 mg/g)	6.52 ± 0.45	0.022	21.1
HPW/Sibunit (300 mg/g)	0.40 ± 0.18	0.0012	1.2

Table 43: Catalytic activity results for pure HPW and supported HPW in the re-arrangement of α-pinene.
 # Based on per surface H^+ assuming a cross-section of 144 $Å^2$ for HPW molecule.

Table 43 shows that HPW/Novacarb (300 mg/g) has the greatest activity with respect to overall HPW and mol H^+ catalytic activity. As this reaction is taking place in a non-swelling solvent it would appear that accessibility to Brønsted acid sites on HPW is more limited when HPW is supported on SBA-15 and Sibunit compared to Novacarb. Its larger pore size and more open pore morphology appears to be beneficial in this reaction. Pure HPW has a very low rate constant perhaps consistent with a very low BET surface area (2 - 5 $m^2.g^{-1}$).

b) Hydrolysis of ethyl acetate

The hydrolysis reaction was undertaken at 60 °C and first order rates are shown below in Table 44.

	1st Order Rates / s^{-1} g^{-1}	1st Order Rates / s^{-1} g^{-1} (HPW)	1st Order Rates / x 10^3 s^{-1} mol^{-1} (H^+)
Pure $H_3PW_{12}O_{40}$ (HPW)	6.6 ± 2.8	6.6	6.3
HPW/SBA-15 (320 mg/g)	0.76 ± 0.1	2.4	2.3
HPW/Novacarb (300 mg/g)	1.74 ± 0.6	5.8	5.6
HPW/Sibunit (300 mg/g)	3.38 ± 0.8	11.3	10.8

Table 44: Catalytic activity results for pure HPW and supported HPW in the hydrolysis of ethyl acetate.

In contrast to the results for α-pinene rearrangement, pure HPW is the most active catalyst for ethyl acetate hydrolysis when first order rates are compared but also it produces the largest range around the mean in both reactions. When specific activity relating to HPW is compared Sibunit

supported HPW imparts the highest activity. Discussion of these results is to follow in section 6.4.1.

6.3.2 Catalytic Activity of Montmorillonite Clays

Results are shown below for the 'Fulcat 200 series' and 'K-series' clays where 50 mg catalysts were used in the α-pinene rearrangement and in the hydrolysis of ethyl acetate. Rate constants are reported as per gram of catalyst and also per mole H^+ based on C.E.C. value assuming there is one H^+ for every cation exchange site.

a) α-pinene rearrangement

The rates obtained at 80°C for all studied Fulcat and 'K-series' clays are shown below in Table 45.

	1st order rate constants k / x 10^{-3} s^{-1} g^{-1}	1st order rate constants k / s^{-1} mol^{-1} (H^+)
Fulcat 200 (Parent Clay)	/	/
Fulcat 200 (Fe^{3+})	3.9 ± 0.2	*
Fulcat 200 (Al^{3+})	3.6 ± 0.3	*
Fulcat 220	12.4 ± 2.8	18.2
Fulcat 230	10.1 ± 0.3	19.1
Fulcat 240	19.4 ± 4.7	58.8
K5	2.8 ± 0.3	4.7
K10	14.8 ± 1.7	52.9
K20	16.9 ± 0.2	56.3
K30	18.6 ± 1.4	74.4

Table 45: Rate constants for the rearrangement of α-pinene at 80°C for montmorillonite clays.

*/= no measurable activity, *= no C.E.C. data available.*

Strength of acid sites appears to be beneficial for this catalytic reaction as the 'K-series' show more activity and they generally have stronger acid sites. When overall rate constants for the two clay series are compared the 'K-series' show that rate constants improve with acid treatment level

whereas the 'Fulcat 200 series' show varied rate constants and can only loosely be described as improving with increasing acid treatment. A large rate increase is seen between both Al^{3+} and Fe^{3+} exchanged parent clay Fulcat 200 and Fulcat 200, which in its as-supplied form shows no measurable activity. The general trend is that going through each series in order of the extent of acid treatment received by the clay, catalytic activity increases both in terms of the overall and specific activity per mole H^{+}. It can be seen that Fulcat 240 is the most active catalyst in this reaction, closely followed by K30. Both K10 and K20 have very similar first order rate constants which are slightly higher than both Fulcat 220 and Fulcat 230. The parent clay, Fulcat 200 shows negligible activity but when this is exchanged with Al^{3+} and Fe^{3+} its activity is increased although it is still not as active as the majority of acidified clay samples. In comparison K5 shows low activity similar to that of the Al^{3+} and Fe^{3+} exchanged Fulcat 200. It seems likely that these low activities might reflect the relatively poor accessibility of acid sites in these clays, all three of which retain either all or much of the laminar structure of the parent montmorillonites.

b) Hydrolysis of ethyl acetate

Rate constants were obtained at 60 °C and are shown below in Table 46.

	1st Order Rates / s^{-1} g^{-1}	1st Order Rates / x 10^3 s^{-1} mol^{-1} (H^{+})
Fulcat 200 (Parent Clay)	/	/
Fulcat 200 (Fe^{3+})	0.80 ± 0.1	*
Fulcat 220	2.96 ± 1.1	4.35
Fulcat 230	0.54 ± 0.1	1.02
Fulcat 240	1.44 ± 0.6	4.36
Fulcat 240 (Al^{3+})	0.94 ± 0.3	-
K5	0.50 ± 0.1	0.83
K10	0.46 ± 0.1	1.64
K20	0.36 ± 0.1	1.20
K30	0.34 ± 0.1	1.36

Table 46: Rate constants for the hydrolysis of ethyl acetate at 60°C for 'K-series'.

*/= no measurable activity, *= no C.E.C. data available.*

Results for the hydrolysis of ethyl acetate show the clays to have little activity in this reaction compared to the heteropoly acids described earlier, and no overall trend is seen with increasing acid treatment in either clay series. It is clear that acid treating the clays and delaminating the structure does improve their activity as this can be seen by the improvement in activity of acid treated Fulcat clays in comparison to the parent clay (Fulcat 200) which shows no measurable activity. Another point to be made is that swelling of the clay structures might be expected to make all H^+ accessible. The fact that the specific activity (per H^+) varies so much especially given that all H^+ would be expected to be H_3O^+ and therefore the same, is odd. Possibly there could be some form of internal diffusion control. In fact, relatively poor reproducibility of catalytic data was seen in these systems and first order plots tended to show poor linearity. This is reflected in the large errors associated with tabulated rate constants. Strength of acid sites both Brønsted and Lewis, do not appear to be relevant in this reaction.

6.3.3 Catalytic Activity of Zeolites

For each reaction 50 mg catalyst was used, and for the rearrangement of α-pinene catalysts were activated at 150 °C for 1 hour prior to reaction.

a) α-pinene rearrangement

This reaction was carried out at 80 °C, and rate constants are shown per gram of catalyst and also per mole H^+ in Table 47.

	1st order rate constants k / x 10^{-3} s^{-1}	1st order rate constants k / s^{-1} mol^{-1} (H^+)
Zeolite β	2.5 ± 0.7	5.63
H-ZSM-5 CT 410 (Si:Al = 27.5)	0.20 ± 0.04	0.33
H-ZSM-5 CT 434 (Si:Al = 40)	/	/

Table 47: Rate constants for the rearrangement of α-pinene at 80 °C for zeolites.

/= no measurable activity.

H-ZSM-5 zeolites show very little activity in this reaction with results for H-ZSM-5 (Si:Al = 40) being too low to be measured. Zeolite beta shows the greatest overall activity and specific activity per mole H^+ which is probably due to its 12 member channels and larger pore size (0.7 nm) compared to the 10 membered channel ZSM-5 with a pore size of 0.5 nm.

b) Hydrolysis of ethyl acetate

Both H-ZSM-5 zeolites and zeolite beta were investigated and results are shown in Table 48.

	1st Order Rates / s^{-1} g^{-1}	1st Order Rates / x 10^3 s^{-1} mol^{-1} (H^+)
Zeolite β	2.1 ± 0.3	4.75
H-ZSM-5 CT 410 (Si:Al = 27.5)	1.6 ± 0.4	2.66
H-ZSM-5 CT 434 (Si:Al = 40)	/	/

Table 48: Rate constants for the hydrolysis of ethyl acetate at 60 °C for zeolites.

/= no measurable activity.

Results were not very reproducible especially in the case of H-ZSM-5 (Si:Al = 40) and conversion vs. time plots were erratic. Again activity for H-ZSM-5 (Si:Al = 40) is too low to be measured and zeolite beta still proves to be the most active zeolite of those examined.

These zeolites show very low activity in both reactions compared to the other catalysts tested. It is suspected that the microporous nature of these materials puts diffusion limitations on their use in liquid phase reactions such as these.

6.3.4 Catalytic Activity of Sulfonated Polystyrene Ion Exchange Resins

a) α-pinene rearrangement

For this study the spherical beads were crushed and sieved to give particles of ≤ 125 μm diameter using a mortar and pestle, and ~ 200 mg dry catalyst was used in each reaction. Results are shown below in Table 49. Rate constants are presented per gram catalyst and per mole H^+ based on their C.E.C.'s.

	1st order rate constants k / x 10^{-3} s^{-1} g^{-1}	1st order rate constants k / s^{-1} mol^{-1} (H^+)
ROHM & HAAS		
Amberlyst 15	0.40 ± 0.1	0.09
Amberlyst 35	2.6 ± 0.5	0.49
Amberlyst 36	0.60 ± 0.1	0.11
PUROLITE INTERNATIONAL		
CT-175	0.20 ± 0.05	0.04
CT-275	2.5 ± 0.1	0.48

Table 49: Rate constants for the rearrangement of α-pinene at 80°C for sulfonated ion exchange resins.

The stoichiometrically sulfonated ion exchange resins, Amberlyst 15 and CT-175 show relatively low activity whereas the two persulfonated resins Amberlyst 35 and CT-275 show much higher activity, both giving rate constants around ten times higher than the stoichiometrically sulfonated resins. Surprisingly, Amberylst 36 shows lower activity even though it is also persulfonated. It is unclear why this is the case. Overall all the sulfonated polystyrene ion exchange resins show low activity compared to the other catalysts studied.

b) Hydrolysis of ethyl acetate

Again all resins studied were crushed and 200 mg catalyst was used in each case. Results reported per gram of catalyst and per mole H^+ are shown below in Table 50.

	1st Order Rates / s^{-1} g^{-1}	1st Order Rates / x 10^3 s^{-1} mol^{-1} (H^+)
ROHM & HAAS		
Amberlyst 15	14.5 ± 0.5	2.74
Amberlyst 35	10.6 ± 0.6	1.98
Amberlyst 36	14.3 ± 0.9	2.31
PUROLITE INTERNATIONAL		
CT-175	7.7 ± 0.3	1.56
CT-275	6.5 ± 1.2	1.22

Table 50: Rate constants for the hydrolysis of ethyl acetate at 60°C for sulfonated ion exchange resins.

The catalytic activity measurements for the sulfonated resins showed high reproducibility in this reaction (unlike the clays). All rate constants are the average of triplicate measurements. The activity differences observed between the resins in Table 50 are rather surprising for the Amberlyst series and the 'CT-series' as Amberlyst 35 and CT-275 show the lowest overall and specific activities in their respective ranges even though they are persulfonated and are generally believed to have stronger acid sites than those resins sulfonated at lower levels. By way of contrast, both these resins show the greatest activity in their respective series for the α-pinene rearrangement. Variations are possibly due to the different mechanisms involved as the α-pinene reaction is undertaken in a non-swelling solvent where acid site accessibility is bound to be limited. As α-pinene is unable to swell the resins many of the internal acid sites are assumed to be inaccessible. Also macroporous Amberlyst resins are known to contain a high percentage of divinylbenzene (15 – 30 %) that limits swelling which could help to explain the relative order of activities seen in the hydrolysis of ethyl acetate. It is possible, for example that Amberlyst 35 contains a higher percentage of DVB than the others, and, if this is so, it would explain the particularly low catalytic activity of Amberlyst 35. Another surprising result is the consistently lower activity of the Purolite resins compared to the Rohm & Haas resins. One possible explanation for this is that they have lower surface areas than the Amberlyst resins, which would be important in a non-swelling solvent.

Section 4 – Discussion

Results from Section 3 will be discussed in further detail and the activity of each catalyst will be related to its acidity and other structural properties, described in Chapters Two and Five.

6.4.1 Heteropoly Acids

Shown below in Table 51 is a comparison of catalytic activity data, acidity measurements and BET surface areas for the heteropoly acid compounds used for catalytic activity testing.

CATALYTIC ACTIVITY	Pure $H_3PW_{12}O_{40}$ (HPW)	Sibunit/ 300mg HPW	Novacarb/ 311mg HPW	SBA-15/ 320mg HPW
Rearrangement of α-Pinene (80 °C) 1st Order Rate Constant (k) / 10^{-3} $s^{-1}g^{-1}$	0.18	0.40	6.52	5.02
Rearrangement of α-Pinene (80 °C) 1st Order Rate Constant (k) / $s^{-1}mol^{-1}$ (H^+)	22.7#	1.2	21.1	15.4
Hydrolysis of ethyl acetate (60 °C) 1st Order Rates / $s^{-1}g^{-1}$	6.6	3.38	1.74	0.76
Hydrolysis of ethyl acetate (60 °C) 1st Order Rates / x 10^3 $s^{-1}mol^{-1}$ (H^+)	6.3	10.8	5.6	2.3
ACIDITY				
Temperature of microcalorimeter (°C)	150	150	150	150
$-Q_{diff}(NH_3)$ at a coverage of 0.05 $mmol.g^{-1}$ (± 5 $kJ.mol^{-1}$)	215	124	138	165
Surface Coverage of NH_3 at which $-Q_{diff}(NH_3)$ falls below 80 $kJ.mol^{-1}$ (± 0.05 $mmol.g^{-1}$)	0.84	0.23	0.18	0.33
Acid site concentration per g HPW ($mmol.g^{-1}$)	1.04	0.25	0.26	0.27
MORPHOLOGY				
BET Surface area determined by N_2 adsorption ($m^2.g^{-1)}$	2.3	124.8	368.7	215*
Mesopore Volume ($ml.g^{-1}$)	0.0098	0.15	0.34	No results available
Micropore Volume ($ml.g^{-1}$)	-	0.0083	0.12	No results available

Table 51: Comparison of acidity, nitrogen adsorption, and catalytic activities for supported HPW.

** Estimated BET surface area from measured BET surface areas for other SBA-15 supported HPW solid acids. # Based on per surface H^+ assuming a cross-section of 144 $Å^2$ for HPW molecule.*

Despite its low specific BET surface area, pure unsupported HPW shows an increased first order rate constant in the hydrolysis of ethyl acetate to those of its supported counterparts. This is most likely due to the influence of water, as it has been demonstrated that crystalline HPW behaves like a solution in many respects[15]. This behaviour is due to the fact that HPW contains mobile ionic structures which can absorb a large amount of polar molecules in the catalyst bulk[16]. Therefore not only the surface proton sites but also internal sites of the bulk of the solid heteropoly acid participate in the catalytic reaction when under aqueous conditions. This phenomenon is known by the term "pseudo-liquid phase" as previously explained in section 6.1.3.[17, 18]

On supporting HPW, the overall rate and specific activity per mole H^+ for hydrolysis of ethyl acetate (Table 51) decreases in the following order HPW/Sibunit, HPW/Novacarb and finally HPW/SBA-15. For reactions in polar solvents it was previously established that carbon is an excellent support capable of attaching firmly to HPW so that it is not appreciably dissolved when used as an acid catalyst in water and organic solvents[19]. Kapustin et al previously concluded that the acid strength of supported HPW decreased according to the series SiO_2 > α-Al_2O_3 > carbon and also suggested that significant interaction must exist between HPW and the carbon surface[20]. Acidity data (see Table 11) shows that acid strength based on $-Q_{diff}(NH_3)$ agreed with this series and decreased in the following order: HPW/SBA-15, HPW/Novacarb, and HPW/Sibunit. It is known that on supporting HPW it strongly interacts with silica at low loadings, while the bulk properties of HPW prevail at higher loadings[21]. This could therefore explain why both HPW/Sibunit and HPW/Novacarb have higher first order rates than HPW/SBA-15 as less leaching of HPW from the support is occurring. It is surprising that when leaching of SBA-15 supported HPW occurs it does not impart a similar activity to pure HPW and is possibly related to the idea that when a monolayer of Keggin anions is formed on the silica surface, protons become employed in protonation of the silica surface Si-OH group and therefore do not participate in the catalytic reaction[22].

In contrast the catalytic activity of supported HPW catalysts in the rearrangement of α-pinene reaction shows the following order: HPW/Novacarb (300 mg/g) > HPW/SBA-15 (320 mg/g) > HPW/Sibunit (300mg/g) when overall activity is compared. If specific activity is followed then the same trend is seen for supported HPW. When catalytic activity data for the rearrangement of α-pinene is compared to acidity measurements from NH_3 adsorption data, the catalytic activity for pure HPW based on surface H^+ is consistent with the high concentration and strength of acid sites

shown to be present. The reason for this reversal in catalytic activity order compared to catalytic activity for the hydrolysis of ethyl acetate is most likely related to the accessibility of acid sites as non-polar reactants such as α-pinene are incapable of being absorbed in the HPW bulk and therefore α-pinene can only react with surface acid sites. Evidence of this can be seen in the results table above as there is a good correlation between overall catalytic activity and BET surface area data for supported HPW. Pure HPW which has a very low surface area shows increased catalytic activity when the rate constant is based on surface H^+ and HPW/Novacarb (300 mg/g) which has the highest surface area shows the greatest catalytic activity for its supported counterparts. No nitrogen adsorption data is available for HPW supported on SBA-15 therefore a BET surface area has been estimated as follows. Considering the BET surface area values for SBA-15/174 mg HPW and SBA-15/420 mg HPW were 286 and 143 $m^2.g^{-1}$ respectively (see Table 7, Chapter 2) it would be reasonable to assume that HPW/SBA-15 (320 mg/g) would have a BET surface area ca. 215 $m^2.g^{-1}$. If this were correct this would be consistent with the trend mentioned above. The kinetic data for the rearrangement of α-pinene has shown that accessibility of acid sites is of importance for tungstophosphoric acid. There does not appear to be a strong correlation between strength of acid sites based on $-Q_{diff}(NH_3)$ and catalytic activity for supported HPW samples. As discussed previously, Novacarb supported HPW is the most active of the supported HPW samples even though in contrast to SBA-15 supported HPW it has relatively low strength and concentration of acid sites available. Therefore for this reaction NH_3 adsorption data is a flawed indication of catalytic activity, because it does not account for the accessibility of acid sites and the inability of the larger bulky pinene molecules to diffuse into the secondary structure of HPW.

6.4.2 Montmorillonite Clays

In Table 52 below are the catalytic first order rate constants and acidity and nitrogen adsorption data for both the 'Fulcat 200 series' and the 'K-series' clays.

	Fulcat 200	Fulcat 200 (Al^{3+})	Fulcat 200 (Fe^{3+})	Fulcat 220	Fulcat 230	Fulcat 240	Fulcat 240 (Al^{3+})	K5	K10	K20	K30
CATALYTIC ACTIVITY											
Rearrangement of α-pinene (80 °C) 1st order rate constants k/ $10^{-3}s^{-1}g^{-1}$	/	3.9	3.6	12.4	10.1	19.4	-	2.8	14.8	16.9	18.6
Rearrangement of α-pinene (80 °C) 1st order rate constants k/ $s^{-1}mol^{-1}$ (H^+)	/	*	*	18.2	19.1	58.8	-	4.7	52.9	56.3	74.4
Hydrolysis of ethyl acetate (60 °C) 1st order rates / $s^{-1}g^{-1}$	/	-	0.80	2.96	0.54	1.44	0.94	0.5	0.46	0.36	0.34
Hydrolysis of ethyl acetate (60 °C) 1st order rates / $s^{-1}mol^{-1}$ (H^+)	/	-	*	4.35	1.02	4.36	*	0.83	1.64	1.20	1.36
ACIDITY											
Calorimeter Temperature (°C)	150	150	150	150	150	150	150	150	150	150	150
$Q_{diff}(NH_3)$ at a coverage of 0.05 mmol.g^{-1} (± 3 kJ.mol^{-1})	98	113	112	115	122	124	123	119	127	129	118
Surface coverage of NH_3 at which -$Q_{diff}(NH_3)$ falls below 80 kJ.mol^{-1} (± 0.03 mmol.g^{-1})	0.15	0.22	0.23	0.29	0.31	0.32	0.31	0.26	0.23	0.19	0.16
MORPHOLOGY											
BET surface area determined by N_2 adsorption ($m^2.g^{-1}$)	108	81	95	271	363	364	335	108	181	253	282
Cation exchange capacity (C.E.C.) based on Mg content (mmol.g^{-1})	0.90	*	*	0.68	0.53	0.33	*	0.60	0.28	0.30	0.25

Table 52: Comparison of acidity, nitrogen adsorption, and catalytic activities for 'Fulcat 200 series' and 'K-series' montmorillonite clays.

*/=no measurable activity *=no C.E.C. data available*

Table 52 show a comparison of all data obtained for the 'Fulcat 200 series' and the 'K-series' including overall catalytic activity and specific activity per mole H^+ for the two test reactions; rearrangement of α-pinene and hydrolysis of ethyl acetate, and also NH_3 adsorption data from which acidity measurements have been ascertained. Surface areas and C.E.C. values based on Mg content have also been shown. This is to allow any connection between catalytic activity, surface acidity and other characteristics to be identified.

In the α-pinene rearrangement specific activity per mole H^+ increases as acid treatment is increased for the 'K-series' though K5 is significantly less active. By comparing the activity data for α-pinene rearrangement with the acidity data at 150 °C one possible explanation is that because α-pinene is a large molecule and because K5 retains a more laminar structure than the other K catalysts, only a relatively small fraction of the acid sites (surface acid sites) are accessible to reactants in a non-swelling state.

Again the progressively acid treated 'Fulcat 200 series' show an increased specific activity per mole H^+ similar to the 'K-series', and it is clear that acid treatment is important in relation to catalytic activity for the rearrangement of α-pinene. The parent clay, Fulcat 200 shows no measurable catalytic activity, but when Fulcat 200 is exchanged with Al^{3+} and Fe^{3+}, catalytic activity is on a par with Süd-Chemie's K5 (Table 51). This activity must therefore be related to the exchange of the cations in the structure providing acidic sites. The nature of the exchangeable cation is obviously important as results per gram of catalyst show that Al^{3+} Fulcat 200 imparts a higher activity than Fe^{3+} Fulcat 200 in the rearrangement of α-pinene reaction and suggests that Al^{3+} Fulcat 200generates stronger Brønsted acid sites. One possible explanation for this is that Al^{3+} is very effective at polarising water molecules and also it has a higher charge-to-radius ratio than Fe^{3+} Fulcat 200 (Pauling Radii Al^{3+} = 0.054 nm, Fe^{3+} = 0.065 nm)[23].

To summarise, both the 'Fulcat 200 series' and 'K series' showed very similar trends in the α-pinene rearrangement as specific activity per mole H^+ increased with progressive acid treatment. It does not appear that strength of the few strongest acid sites is indicative of increased catalytic activity as $-Q_{diff}(NH_3)$ at a coverage of 0.05 $mmol.g^{-1}$ for the most acid treated 'K-series' clay K30 shows that the strength of acid sites at this coverage are lower than less acid treated counterparts but it has the highest catalytic activity. Also the concentration of acidic sites probed by NH_3 does

not give a clear picture of catalytic activity in this reaction as exchanged Al^{3+} and Fe^{3+} Fulcat 200 clays show a high surface coverage in comparison to the parent clay and also similar concentration to the 'K-series' but very little overall activity. This leads to the conclusion that accessibility of acid sites is a key factor in this reaction and it is likely that the non-polar conditions prevent both the parent clay Fulcat 200 and the less acid treated clays in each series from swelling. This theory is also supported by the BET surface areas, which increase as the clay structure becomes more delaminated allowing acid sites to be more accessible. It is therefore clear that surface type catalysis is taking place. It has also been shown by other workers that higher activity is observed for acid treated clays in the α-pinene rearrangement reaction with those clays that possess high pore volumes which occur as the clays receive further acid treatment[24]. Another observation is that when the clay is substantially leached the catalyst becomes essentially hydrophobic silica which serves to attract non-polar reagents such as α-pinene.

For the hydrolysis of ethyl acetate no clear correlation can be seen between acidity and catalytic activity for either clay series. Neither series shows an increase in specific activity as they become progressively more acid treated though acid treated Fulcats do show slightly higher specific catalytic activities per mole H^+ than the 'K-series', which could possibly be linked to the surface coverage and BET surface area measurements. Previous workers concluded that short acid treatment times of clays improved catalytic activity because the hydrophilic character of the clay attracted polar reagents to the surface where catalytic protons resided[25]. It follows that for reactions in polar media such as the hydrolysis of ethyl acetate that catalytic activity of acid treated montmorillonite clays would be optimized when the swelling ability of the catalyst was at a maximum.

Ammonia adsorption microcalorimetry data shows strength of acid sites on each clay varies though the actual differences between the clays are relatively minor. The fact that catalytic activities in both Brønsted catalysed reactions also vary suggests that NH_3 adsorption is not a great probe for activity in these reactions and may possibly be due to accessibilities of acid sites to NH_3 being very different to those of pinene and ethyl acetate. Also as NH_3 is adsorbed onto dry clay this does not give real idea indication of how the catalyst will behave in solvent and some properties may alter dramatically. Another reason for lack of catalytic activity is the presence of Lewis acidic sites which would not be active in the chosen reactions as they are catalysed by Brønsted acids.

6.4.3 Zeolites

In Table 53 below are the catalytic rates and acidity and nitrogen adsorption information for the zeolites.

	Zeolite Beta Si:Al Ratio = 37.5	H-ZSM-5 CT410 Si:Al Ratio = 27.5	H-ZSM-5 CT434 Si:Al Ratio = 40
CATALYTIC ACTIVITY			
Rearrangement of α-Pinene (80 °C) Rate k / 10^{-3} s^{-1}	2.5	0.2	/
Rearrangement of α-Pinene (80 °C) Rate k / $mol^{-1}(H^+)$	5.63	0.33	/
Hydrolysis of ethyl acetate (60 °C) 1st Order Rates / s^{-1} g^{-1}	2.1	1.6	/
Hydrolysis of ethyl acetate (60 °C) 1st Order Rates / s^{-1} mol^{-1} (H^+)	4.75	2.66	/
ACIDTY			
Temperature (°C)	150	150	150
$-Q_{diff}$ (NH_3) at a coverage of 0.05 $mmol.g^{-1}$ (± 2 $kJ.mol^{-1}$)	135	119	84
Surface Coverage of NH_3 at which $-Q_{diff}$ (NH_3) falls below 80 $kJ.mol^{-1}$ (± 0.02 $mmol.g^{-1}$)	0.28	0.36	0.04
Theoretical surface coverage ($mmol.g^{-1}$)	0.44	0.61	0.42
Total moles of NH_3 adsorbed (± 0.02 $mmol.g^{-1}$)	0.49	0.61	0.68
MORPHOLOGY			
BET Surface area determined by N_2 adsorption ($m^2.g^{-1}$)	541	353	281
Mesopore Volume ($ml.g^{-1}$)	0.964	0.078	0.042
Micropore Volume ($ml.g^{-1}$)	0.15	0.08	0.12

Table 53: Comparison of acidity, nitrogen adsorption, and catalytic activities for zeolites β and ZSM-5.

/= no measurable activity

A summary of catalytic results shows that ZSM-5 with an Si:Al ratio of 40 shows no appreciable activity in either of the two chosen test reactions, and taking into account the lack of acidity it is most certainly conceivable that it was not in the H^+ form. Zeolite β provides the greatest activity

of all three zeolites in both the rearrangement of α-pinene and the hydrolysis of ethyl acetate. Therefore it appears that access of molecules to acid sites plays an important role in zeolites as well as framework defects and acidity especially for the rearrangement of α-pinene which is a relatively bulky molecule (14.48 nm^3) in comparison to the pores of zeolite β and H-ZSM-5 with pores of 0.67 nm and 0.56 nm respectively[26]. Zeolite β possesses a much higher mesopore volume than H-ZSM-5, and as H-ZSM-5 possesses smaller pore channels than zeolite β could also help explain why zeolite β shows a higher activity than either H-ZSM-5. When comparing these results with the acidity data, zeolite β provides the strongest acid sites and in conjunction with a larger pore size and high BET surface area suggests a reason for its increased activity in both catalytic reactions. The acidity data also suggests that rates are influenced by both the strength and the concentration of acid sites for zeolites in both test reactions although the use of NH_3 as a probe shows its unsuitability for these purposes as NH_3 (0.3 nm) possesses no problem with accessing all acid sites available.

6.4.4 Sulfonated Polystyrene Ion Exchange Resins

Table 54 below shows the overall and specific catalytic activity per mole H^+ for the rearrangement of α-pinene and the hydrolysis of ethyl acetate for sulfonated polystyrene ion exchange resins. Also shown is the NH_3 adsorption data from which surface acidity measurements have been taken to determine strength of acid sites at a surface coverage of 0.5 $mmol.g^{-1}$ and concentrations of acid sites at heats above 80 $kJ.mol^{-1}$. The cation exchange capacities both from acid-base titration and manufacturer's determined values have also been shown.

	CT-175	CT-275 (Persulfonated)	Amberlyst 15	Amberlyst 35 (Persulfonated)	Amberlyst 36 (Persulfonated)
CATALYTIC ACTIVITY					
Rearrangement of α-Pinene (80°C) Rate constants k / 10^{-3} $s^{-1}g^{-1}$	0.2	2.5	0.4	2.6	0.6
Rearrangement of α-Pinene (80°C) Rate constants k / $s^{-1}mol^{-1}(H^+)$	0.04	0.48	0.09	0.49	0.11
Hydrolysis of ethyl acetate (60°C) 1st Order Rates / $s^{-1}g^{-1}$	7.7	6.5	14.5	10.6	14.3
Hydrolysis of ethyl acetate (60°C) 1st Order Rates / $s^{-1}mol^{-1}(H^+)$	1.56	1.22	2.74	1.98	2.31
ACIDITY					
Temperature (°C)	100	100	100	100	100
$-Q_{diff}(NH_3)$ at a coverage of 0.5 $mmol.g^{-1}$ (± 2 $kJ.mol^{-1}$)	113	117	115	120	118
Surface coverage of NH_3 at which $-Q_{diff}(NH_3)$ falls below 80 $kJ.mol^{-1}$ (± 0.02 $mmol.g^{-1}$)	4.60	5.43	5.03	5.30	6.07
Total amount NH_3 adsorbed (± 0.02 $mmol.g^{-1}$)	4.97	5.68	5.23	5.55	6.08
MORPHOLOGY					
Acid-Base Titration C.E.C.	4.94	5.33	5.29	5.36	6.19
Manufacturers C.E.C. ($mmol.g^{-1}$)	4.90	5.20	4.80	5.30	5.50

Table 54: Comparison of acidity, nitrogen adsorption, and catalytic activities for sulfonated polystyrene ion exchange resins.

The catalytic activity of sulfonated polystyrene ion exchange resins is much lower for the rearrangement of α-pinene (non-swelling solvent) compared to catalytic activity in the hydrolysis of ethyl acetate (swelling solvent). A possible explanation for this is the fact that even though macroreticular sulfonated ion exchange resins are able to function in non-swelling solvents (where the reaction is catalyzed by undissociated sulfonic acid groups)[27], many of the internal acid sites are inaccessible to the bulky α-pinene molecules. This could also help explain why a vast improvement is seen in the rate constants obtained for CT-275 and Amberlyst 35 both of which are persulfonated, as there would be a greater number of acid sites available on or close to the surface and the strength of these acid sites are slightly higher than those seen for Amberlyst 15 and CT-175. The extremely low catalytic activity of Amberlyst 36 in the α-pinene reaction is difficult to explain.

Results indicate that the Amberlyst series of sulfonated polystyrene ion exchange resins are much better catalysts in the hydrolysis of ethyl acetate than the Purolite resins, and when activity is

compared to the acid treated clays, sulfonated polystyrene ion exchange resins show increased catalytic activity in the hydrolysis of ethyl acetate. It is uncertain why this is the case as both series have similar levels of sulfonation. This result is unexpected as the 'CT' resins have higher surface areas and pore diameters (see Table 1, 2.1.1.4.a) than the Amberlyst series so diffusion of reactant to acid sites might be more facile for the less active 'CT' resins. Both resins CT-175 and Amberlyst 15 show greater catalytic activity than their persulfonated counterparts CT-275 and Amberlyst 35. This is inconsistent with previous findings[28], and is again unclear why, as in aqueous solution catalytic activity is due to H_3O^+ and it might be expected that when the resins are fully swollen they can form a pseudoliquid phase in the resin bulk in which catalytic reactions can occur similar to HPW, and as CT-275, Amberlyst 35 and 36 all contain a higher degree of sulfonation it would be expected that first order rate constants would also be higher. In relation to their acidity persulfonated resins possess slightly stronger acid sites than either CT-175 or Amberlyst 15 and also a higher concentration of acid sites available. Therefore as a prediction of catalytic activity in the two chosen reactions, surface acidity data from NH_3 adsorption microcalorimetry is not a clear indication of activity. This may be due to the levelling effect of water on acid strength as the persulfonated resins do not necessarily show high catalytic activity even though they have a higher concentration of acid sites and slightly stronger acid sites than monosulfated resins CT-175 and Amberlyst 15. As there are real differences seen in catalytic activity this must either be due to differences in acid strength which bear no correlation with differential heats of NH_3 adsorption as discussed above or are due to differences in the rates of diffusion in the swollen resin gel, which may be linked to porosity, cross-linking or the distribution of sulfonic acid groups across the bead. One possible way to test this theory would be to grind the resins and test catalytic activity in the powder form to see if the reaction is faster.

6.4.5 Conclusion / Summary

When comparing solid acids certain key points can be taken from the data. In terms of catalytic activity certain solid acids are better than others depending on conditions such as pre-treatment, reaction temperature, and solvent type. For instance in the hydrolysis of ethyl acetate sulfonated polystyrene ion exchange resins imparted the greatest activity per mole H^+ followed by zeolites. The reason for this is most likely the ability of sulfonated polystyrene ion exchange resins to act as a pseudoliquid phase catalyst in polar solvents. Also the chosen zeolites possessed a high Si:Al ratio to provide a relatively hydrophobic surface with which to attract ethyl acetate and also to prevent the likelihood of water deactivating the solid acid catalysts. The acid treated clays are not

very active in the hydrolysis reaction and there is no clear correlation between catalytic activities and their surface area or acidity. It follows that maximum activity would occur when the swelling ability of the clays is optimized i.e. at shorter acid treatment times. This is because acid treatment causes delamination and collapse of the clay structure which is then unable to swell therefore making acid sites inaccessible in polar solvents.

For catalytic reactions in non-polar solvents such as α-pinene, sulfonated ion exchange resins are not very active as the solvent is unable to swell the macroporous resin structure and access acid sites. For this reaction acid treated clays have shown the most promise along with zeolite β and H-ZSM-5 (Si:Al = 27.5). This indicates that accessibility as well as strength of acid sites is important because it appears that the size of the channels is important for zeolites.

From NH_3 adsorption microcalorimetric studies HPW has shown to have the strongest available acid sites and sulfonated polystyrene ion exchange resins the lowest with acid treated clays and zeolites providing acid sites of intermediate strength. Although the sulfonated polystyrene ion exchange resins do not possess particularly strong acid sites they have a much higher uniform concentration of acid sites though acid strength does not provide an indication of catalytic activity in either reaction, as Amberlyst 35 and Amberlyst 36 which possess stronger acid sites do not show higher activity than Amberlyst 15 which has slightly weaker acid sites and no clear link can be seen. Also the restrictive pore sizes in ZSM-5 make zeolite β a much better catalyst.

The extent to which NH_3 adsorption data can be used to predict catalytic activities in the chosen reactions appears quite small and is dependent on the properties of the catalysts. For instance NH_3 is able to probe both Lewis and Brønsted acidic sites within solid acids such as montmorillonite clays which are not easy to differentiate between using NH_3 adsorption microcalorimetry as a stand-alone technique. This is of utmost importance for determining catalytic activity for purely Brønsted catalysed reactions. Also the adsorption of NH_3 takes place on a dry solid acid and therefore is not great mimic of how these solid acids perform in a solvent environment. Accessibility of acid sites is probably a crucial factor which is not properly probed by NH_3 as in this case reactants are much larger than NH_3 and are unable to probe all acid sites.

6.4.6 Suggestions for Further Work

The catalytic behaviour of solid acids differs depending not only on solvent type but also the type of catalysis that is taking place. Therefore it would be of interest to modify these solid acids where possible to find a suitable catalytically active catalyst in polar solvents for example, the tethering of alkyl chains to acid montmorillonite clays to produce a more hydrophobic surface. It would also be beneficial to find a material which could be used to support HPW whilst maintaining the acid strength of pure HPW and yet providing increased surface area.

Further study of various probe gases would also be of interest using molecules of varying size to test accessibility within solid acids, and also the use of weaker bases to differentiate between Brønsted and Lewis acid sites. This is of interest especially when using adsorption microcalorimetry to identify solid acid catalysts suitable for either purely Brønsted or Lewis catalysed reactions. The study of pre-treatment temperatures for studied solid acids would also be of interest.

[1] N. Besun, F. Ozkan, G. Gunduz, App. Catal. A:Gen., 224 (2002) 285-297.

[2] O. Akpolat, G. Gunduz, F. Ozkan, N. Besun, App. Catal. A:Gen., 265 (2004) 11-22.

[3] F. Ebmeyer, J. Mol. Struct. – Theochem., 582 (2002) 251-255.

[4] A.D. Newman, D.R. Brown, P. Siril, F. Lee, K. Wilson, Phys. Chem. Chem. Phys., 8 (2006) 2893-2902.

[5] Toshio Okuhara, Chem. Rev., 102 (2002) 3641-3666.

[6] A. Mitsutani, Catal. Today, 73 (2002) 57-63.

[7] M.N. Timofeeva, App. Catal. A-Gen., 256 (1-2) (2003) 19-35.

[8] M. Kimura, T. Nakato, T. Okuhara, Appl. Catal. A-Gen., 165 (1-2) (1997) 227-240.

[9] S. Namba, N. Hosonuma, T.J. Yashima, J. Catal., 72 (1981) 16-20.

[10] J. McMurray, "McMurray Organic Chemistry – 4th Edition", Eds; Brooks/Cole (1995) p.828.

[11] M. Misono, I. Ono, G. Koyano, A. Aoshima, Pure Appl. Chem., 72 (7) (2000) p.1307.

[12] M. Misono, Catal. Rev. Sci. Eng., 29 (2-3) (1987) 269-321; 30 (2) (1988) 339-340.

[13] S. Koujout, D.R. Brown, Catal. Lett., 98 (4) (2004) 195-202.

[14] M. Misono, Chem. Commun., (2001) 1141-1152.

[15] I.V. Kozhevnikov, Russ. Chem. Rev., 56 (9) (1987) 811-825.

[16] T. Okuhara, N. Mizuno, M. Misono, Adv. Catal., 41 (1996) 113-252.

[17] J. Haber, K. Pamin, L. Matachowski, D. Mucha, App. Catal. A:Gen, 256 (2003) 141-152.

[18] M. Furuta, K. Sakata, M. Misono, Y. Yoneda, Chem. Lett., 1 (1979) 31-34.

[19] Y. Izumi, K. Urabe, Chem. Lett., (1981) 663-666.

[20] G.I. Kapustin, T.R. Brueva, A.L. Klyachko, M.N. Timofeeva, S.M. Kulikov, I.V. Kozhevnikov, Kinet. Katal., 31 (4) (1990) 1017-1020.

[21] I.V. Kozhevnikov, J. Mol. Catal. A:Chem., 114 (1-3) (1996) 287-298.

[22] J. Haber, K. Parmin, L. Matachowski, D. Mucho, Appl. Catal. A:Gen., 256 (2003) 141-252.

[23] http://en.wikipedia.org/wiki/Ionic_radius - accessed on 25.06.07.

[24] C. Volzone, O. Masini, N.A. Comelli, L.M. Grzona, E.N. Ponzi, M.I. Ponzi, Appl. Catal. A:Gen., 214 (2001) 213-218.

[25] C.N. Rhodes, D.R. Brown, Catal. Lett., 24 (3-4) (1994) 285-291.

[26] G. Gunduz, R. Dimitrova, S. Yilmaz, L. Dimitrov, M. Spassova, J. Mol. Catal. A:Chem., 225 (2005) 253-258.

[27] A. Chakrabarti, M.M. Sharma, React. Polym., 20 (1993) 1-45.

[28] M. Hart, G. Fuller, D.R. Brown, C. Park et al., Catal. Lett., 72 (3-4) (2001) 135-139.

Appendix A

Shown below are the initial molar heats of NH_3 adsorption at a coverage of zero mmol.g^{-1} for studied solid acids.

Solid Acid	Temperature (°C)	Initial molar heats of NH_3 adsorption at 0 mmol.g^{-1} coverage (kJ.mol^{-1})	Number of points linear plot based on
Supported Heteropoly Acid			
Pure HPW	30	152 ± 2.7	12
	150	221 ± 2.4	12
SBA-15	30	87 ± 8.2	3
Novacarb	30	78 ± 0.5	3
	150	81 ± 0.5	2
Sibunit	30	30 ± 3.5	3
	150	14 ± 2.3	3
HPW/SBA-15 (174 mg/g)	30	125 ± 0.8	4
	150	202 ± 4.0	4
HPW/SBA-15 (320 mg/g)	30	129 ± 1.2	6
	150	189 ± 6.2	3
HPW/SBA-15 (420 mg/g)	30	163 ± 8.4	3
	150	163 ± 2.6	6
HPW/Novacarb (100 mg/g)	30	127 ± 2.9	4
	150	154 ± 2.8	3
HPW/Novacarb (311 mg/g)	30	124 ± 1.3	4
	150	173 ± 6.4	3
HPW/Sibunit (200 mg/g)	30	96 ± 3.8	5
	150	151 ± 3.2	4
HPW/Sibunit (254 mg/g)	30	111 ± 2.4	5
	150	133 ± 1.1	5
HPW/Sibunit (300 mg/g)	30	112 ± 4.0	4
	150	127 ± 1.0	6

Solid Acid	Temperature (°C)	Initial molar heats of NH_3 adsorption at 0 $mmol.g^{-1}$ coverage ($kJ.mol^{-1}$)	Number of points linear plot based on
Acid Treated Clays			
Fulcat 200	150	107 ± 2.4	4
	200	112 ± 2.3	6
Al^{3+} Fulcat 200	150	123 ± 1.9	8
	200	190 ± 17.1	5
Fe^{3+} Fulcat 200	150	126 ± 1.6	6
	200	121 ± 5.6	5
Fulcat 220	150	119 ± 1.9	7
	200	140 ± 3.9	5
Fulcat 230	150	128 ± 1.8	7
	200	136 ± 4.6	6
Fulcat 240	150	132 ± 1.5	6
	200	138 ± 4.6	5
Al^{3+} Fulcat 240	150	141 ± 2.6	4
	200	147 ± 2.5	7
K5	150	142 ± 5.0	7
	200	131 ± 2.2	6
K10	150	141 ± 4.4	7
	200	140 ± 2.4	7
K20	150	134 ± 6.0	6
	200	131 ± 2.2	6
K30	150	127 ± 6.2	7
	200	138 ± 3.1	7

Solid Acid	Temperature (°C)	Initial molar heats of NH_3 adsorption at 0 $mmol.g^{-1}$ coverage ($kJ.mol^{-1}$)	Number of points linear plot based on
Zeolites			
Zeolite β Si:Al = 37.5	150	146 ± 2.9	5
H-ZSM-5 Si:Al = 27.5	150	123 ± 0.7	4
H-ZSM-5 Si:Al = 40	150	86 ± 4.4	6
Sulfonated Polystyrene Ion Exchange Resins			
Amberlyst 15	100	114 ± 0.7	8
Amberlyst 35	100	121 ± 0.4	9
Amberlyst 36	100	116 ± 0.6	8
CT-175	100	115 ± 0.6	8
CT-275	100	119 ± 0.6	8